pennsylvania
DEPARTMENT OF TRANSPORTATION

Flood Mitigation Solutions

FINAL REPORT

August 29, 2022

By Virginia Smith
Villanova University

VILLANOVA UNIVERSITY

COMMONWEALTH OF PENNSYLVANIA
DEPARTMENT OF TRANSPORTATION

CONTRACT # 512001
WORK ORDER # VU WO 003

Technical Report Documentation Page

1. Report No.	2. Government Accession No.	3. Recipient's Catalog No.
FHWA-PA-2022-005-VU WO 003		

4. Title and Subtitle	5. Report Date
Flood Mitigation Solutions Final Report	August 29, 2022
	6. Performing Organization Code

7. Author(s)	8. Performing Organization Report No.
Richard Starkey, Dr. Virginia Smith, Dr. Seri Park, Kyle Fok, Dr. Garrett Clayton, Erin Tammin	VU WO 003 001

9. Performing Organization Name and Address	10. Work Unit No. (TRAIS)
Villanova University Department of Civil and Environmental Engineering Villanova University 800 Lancaster Ave. Villanova, PA 19085	**11. Contract or Grant No.** **440002549**

12. Sponsoring Agency Name and Address	13. Type of Report and Period Covered
The Pennsylvania Department of Transportation Bureau of Planning and Research Commonwealth Keystone Building 400 North Street, 6th Floor Harrisburg, PA 17120-0064	Final Report (7/1/21-9/1/22)
	14. Sponsoring Agency Code

15. Supplementary Notes

16. Abstract
In Pennsylvania DOT District 6 expanding watershed development is increasing demands on roadways and worsening flooding. This research addresses the fundamental question: "How can flood mitigation improve the safety and sustainability of a road network?" While many studies have sought to understand the impacts of hydrologic events on driving conditions and roadway surfaces, this research seeks to understand these impacts from a holistic system approach by applying technological advancements (LiDAR and near IR cameras) and harnessing the data revolution to identify actions that lead to greater resiliency in response to stormwater inundation of roadways. Here we analyze stormwater inundation of the roadway system impacts the safety, maintenance, operation, and ultimately the overall sustainability of a roadway network.

17. Key Words	18. Distribution Statement
Flooding, stormwater, road closures, flood mitigation	No restrictions. This document is available from the National Technical Information Service, Springfield, VA 22161

19. Security Classif. (of this report)	20. Security Classif. (of this page)	21. No. of Pages	22. Price
Unclassified	Unclassified	211	**$180,981.29**

Form DOT F 1700.7 **(8-72)** **Reproduction of completed page authorized**

Flood Mitigation Solutions
5112001 – VU WO 003
Final Report

Villanova University for the Pennsylvania Department of Transportation

August 29th, 2022

Project Team:

- Principal Investigator (PI) - Dr. Virginia Smith
- Co-Principal Investigators (Co-PIs) - Dr. Seri Park & Dr. Garrett Clayton
- Technical Advisor (TA) - Rich Heineman
- Assistant Technical Advisor - George Kapral
- Technical Specialist - Francisco Aguirre
- Project/Contract Manager (PM) - Heather Sorce
- Graduate Research Assistants (GRAs) - Kyle Fok & Richard Starkey

Prepared by Richard Starkey, Dr. Virginia Smith, Dr. Seri Park, Kyle Fok, Dr. Garrett Clayton, Erin Tammin

Executive Summary

In Pennsylvania DOT District 6 expanding watershed development is increasing demands on roadways and worsening flooding. This research addresses the fundamental question: “How can flood mitigation improve the safety and sustainability of a road network?” While many studies have sought to understand the impacts of hydrologic events on driving conditions and roadway surfaces, this research seeks to understand these impacts from a holistic system approach by applying technological advancements (LiDAR and near IR cameras) and harnessing the data revolution to identify actions that lead to greater resiliency in response to stormwater inundation of roadways. Here we analyze stormwater inundation of the roadway system impacts the safety, maintenance, operation, and ultimately the overall sustainability of a roadway network.

This is accomplished by addressing the following research questions:

1. Can points of repeat inundation be identified through environmental spatial statistics? What variables contribute most substantially to stormwater inundation risk? Can priority locations be identified?
2. What methods are efficient for identifying inundated areas? What is the degree and extent of the inundated area?
3. What is the system impact of flood inundation to safety and operation from a network perspective? Can priority locations be identified?
4. What mitigation measures could be effective, and to what degree, in addressing flood mitigation on roadway networks? How can advanced technology enhance the current PennDOT efforts?

These research questions are addressed through the following tasks. The report has been broken into the following Tasks, which describe the findings, as well as outlines (manuals) on how to repeat the analysis.

Task 1: Risk Variable Identification for Flood Inundation

VU will identify points of repeat inundation through environmental spatial statistics and establish the variables that contribute most substantially to stormwater inundation risk. This was accomplished through the following:

1. Create a baseline of analysis techniques used in the field
2. Further holistic spatial analysis by developing preliminary work at VU based on flood inundation data to identify flood inundation-prone locations within metro Philadelphia.
3. Create workflow to repeat this spatial analysis in additional locations.

Task 2: Review Techniques to Deploy LiDAR, near IR, and Drones to Identify Flood Inundation
VU identified how these technologies can be used to map the inundated area and the degree and the extent of the inundated area as well as prioritize the areas to be addressed. This was accomplished by conducting the following:

1. Evaluation of the limitations of deployment using desk and field studies.
2. Establishment of a workflow for different intensities of land use.

Task 3: Assess Impacts of Inundation in Terms of Safety, Network Flow, and Infrastructure Sustainability

VU established the system impact of flood inundation to safety, function from a network perspective, and identify priority locations. This was accomplished by conducting the following:

1. Spatial network analysis to assess the impact of flood inundation from a network safety and network flow prospective.
2. Prioritizing areas of risk based on a network analysis.
3. Work with PennDOT to identify task priority locations, priority issues, and recommendations in a final report, aligning with PennDOT's Asset Management Initiatives (e.g., TAMP, PAMS, etc.).

Task 4: Draft Final Report

Task 5: Final Report

Task 1 Executive Summary

In the Pennsylvania Department of Transportation District 6, like most of the world, expanding watershed development is increasing demands on roadways and worsening flooding. These issues have the potential to be further exacerbated by factors such as urban growth and climate change. This cross-disciplinary research addresses the fundamental research question: "How can flood mitigation improve the safety and sustainability of a road network?"

While many studies have sought to understand the impacts of hydrologic events on driving conditions and roadway surfaces, this study seeks to understand these impacts from a holistic system approach by harnessing the large datasets available and applying spatial analysis to define the areas of risk and the drivers influencing high risk, flood prone areas within the transportation network. Accomplishing this will allow PennDOT to better leverage their data as well as open data sources to identify issues of risk and actions that lead to greater resiliency in response to stormwater inundation of roadways. While this project focuses on Pennsylvania Department of Transportation's (PennDOT's) District 6, the work presented here is designed to be transferable to other PennDOT districts.

In this study, we hypothesize that stormwater inundation of the roadway system impacts the safety, maintenance, operation, and ultimately the overall sustainability of a roadway network. In this task we address part of this hypothesis through identifying the variables that contribute to road network flooding.

This report details three subtasks (1a, 1b, and 1c) to identify points of repeat inundation through environmental spatial statistics and establish the variables that contribute most substantially to stormwater inundation risk. We have accomplished this through the following task:

- Task 1a -- Create a baseline of analysis techniques used in the field
- Task 1b -- Further holistic spatial analysis by developing preliminary work at Villanova University based on flood inundation data to identify flood inundation-prone locations within metro Philadelphia/ PennDOT District 6.
- Task 1c -- Create workflow to repeat this spatial analysis in additional locations.

In completing these tasks, we have created a literature review of the current state of flood prediction for DOTs in the US. We have also created a spatial analysis to identify flood risk hotspots within the District 6 roadway network. And, we have created a multiple regression analysis of environmental, physical, and infrastructure variables to predict bridge closures due to flooding.

The details of these tasks are described in this report and are summarized in the subtask summary documents.

Task 1a Summary

Like Pennsylvania, a critical issue facing departments of transportation (DOTs) across the U.S. is predicting and responding to flooding events. Roadways and bridge flooding have significant economic impacts. State DOTs have implemented integrated flood warning and response systems to mitigate the effects of floods. Support for these efforts is often integrated from items such as internal products, flood inundation mapping using current and projected conditions, turnkey products on the market, the United States Geological Survey (USGS) gaging network and the National Weather Service (NWS) flood forecast system. DOTs and other agencies must determine the flood's extent and severity to effectively work with emergency management and inform the public about road closures and detour routes. A summary of methods used to accomplish these tasks are provided below and detailed in Task 1a report.

Key Findings:

- Urban flooding is an increasingly expensive and pervasive issue in the US. Advancements and integration of relational database systems, real-time data collection tool technologies (e.g., LiDAR, gages etc.), flood prediction models, data process/visualization software (e.g., GIS), and data sharing platforms (e.g., the USGS National Water Information System-NWIS, or the National Weather Service-NWS, River Forecast Center) have made substantial contributions to the effective prediction and forecasting of floods.
- Investments in national programs (NOAA's National Water Model, ASOS, and the USGS NWIS) reflect the importance of effective and accurate flood modeling and management system. Further investment in national datasets such as FEMA floodplain maps and other open access spatial data, allowing deeper insight into flood characteristics.
- There is a board use of national programs such as the use of USGS gages (WaterAlert) and BridgeWatch for flood prediction. Other commonly used tools include HEC-RAS, HEC-HMS, Peek, and Bulletin 17C, and StreamStats/National Streamflow Statistics.
- USGS's NWIS for flood monitoring and federal stream gages as an instrument and tool for flood monitoring are commonly used robust tools for flood monitoring. The other most common instruments and tools used for flood monitoring are federal rain gages and GIS. However, many of the DOTs rely on visual inspection as the most common tool in determining the extent of flooding severity assessment.
- The DOTs provided information on risk thresholds that trigger action. Common responses from DOTs indicated that the NWS issues the warnings and/or parameters that DOTs apply to issue a flood warning. According to a self-ranking, the most important information used in state's flood warning systems is observed stream stage, observed stream inundation, and bridge scour.
- There are a range of studies that investigate approaches and methods relating to flood prediction. Without available and ready-to-use data, exploratory and hypothetical research cannot be executed. Reported challenges and weaknesses to implementing a successful flood monitoring system were state resources (staffing, funding, turnover, etc.), data coverage (e.g., lack of stream gages), and local resources (staffing, funding, turnover, etc.).

Task 1a Report

In the United States (US), like most of the world, expanding watershed development is increasing demands on roadways and worsening flooding. Urbanization results in a steeper hydrograph with higher peaks (Leopold, 1968). More than half of the world's population lives in urban areas, including more than 80% of the U.S. population (U.S. Census, 2010), resulting urban development has a greater impact on natural flow regimes and flooding than ever before. Urban stream management is an increasingly significant and costly issue in the U.S. and the world, as urban hubs support rapidly growing populations (Bernhardt et al., 2005). The rainfall patterns are colliding with urban growth as reflected in flood related losses, which between 2007-2017 cost the US National Flood Insurance Program an average of $2.9 billion annually. Managing the risk of urban flooding is critical to ensuring safe and efficient road networks (Saurez et al., 2005). This research addresses the fundamental question: "How can flood mitigation improve the safety and sustainability of a road network?" This chapter presents an overview of flood risk prediction in the United States. This includes, but is not limited to, relevant initiatives, strategies, and tools.

Urbanization has posed many challenges (Elmqvist et al., 2013). Urban society requires an infrastructure to support its functionality. Infrastructure is considered to promote development. However, the methods and reasoning behind development may not be fully thought out and come with a "cost" (Elmqvist et al., 2013). The "cost" can be interpreted by any means but when considering where development will happen, a large portion of the "cost" is paid by the landscape. Development, more specifically land development, has led to impeding the natural drainage of the environment. Land development reduces the permeability of land, and it forces water to accumulate and pool at the surface level leading to flood inundation (Shade & Kremer, 2019). Additionally, construction in an urban area traditionally involves clearing a landscape, paving, and removing vegetation, decreasing evapotranspiration and infiltration (Du et al., 2015). Addressing flooding becomes more complex when considering variables in addition to the change in land development from urbanization.

Stormwater control has become an essential component of modern infrastructure (Masoner et al, 2019). Stormwater control is a flood mitigation solution that aims to reduce and remove accumulated rainfall. However, stormwater control structures relocate accumulated rainfall to a different location, which can end up being local streams. Introducing the increased volume of water to a local stream can compromise the stream's health (Finkenbine et al, 2000). The stream experiences a greater peak flow, which can encourage erosion (Finkenbine et al, 2000). Additionally, the increased peak flow can influence the degree of scouring around bridge foundations (Melville & Coleman, 2000).

A recent study has explained the shift in the flood mitigation ideology (Schifman et al., 2017). Green infrastructure (GI) is being implemented as an alternative to traditional practices. GI and green stormwater infrastructure (GSI) practices are more conscious of performance in coherence with the larger system. However, optimal decision-making should be made when assessing flooding. Flood mitigation is an essential component of an infrastructure. It is a component of an infrastructure that is relied on and when failure occurs, there are direct and indirect consequences

from a socioeconomic standpoint (Deryugina, 2017). Suggested in the study "Situating Green Infrastructure in Context: A Framework for Adaptive Socio-Hydrology in Cities", current green stormwater infrastructure practices are being implemented with the wrong intent. The study states, "design and implementation of GI usually rely on physical site characteristics and local rainfall patterns, and do not typically account for human or social dimensions" (Schifman et al., 2017). The study suggests considering other variables outside of the traditional variables incorporated in flood mitigation practices.

Climate change has forced the United States to experience changes in precipitation patterns along the coasts (Hayhoe, 2008). The effects of this change differ from place to place, seeing more dry conditions in the west and more wet conditions in the east (Hayhoe et al., 2007). From 1980 to 2020, the U.S. has spent approximately $1.875 trillion on the cost of damages from weather and climate disasters (National Oceanic and Atmospheric Administration, 2021). It can be said that the existing infrastructure is struggling to handle the current weather and climate disasters. A study suggests that hurricane events will increase in intensity by about 5% through the 21st century (Knutson, 2021). If the existing infrastructure cannot handle the current conditions, action must be taken to address the harsher conditions to come (Bates et al., 2008).

Determining the areas that are most susceptible to damage from the weather events can be addressed through flood projection. Flood projection can be utilized to identify places that will flood under certain conditions. However, it is a complex task and existing methods of applying flood projection constitute uncertainty, especially considering urban landscapes (Jung et al., 2011). This study will explore methods used for flood mitigation and flood projection. Flood mitigation solutions are derived from an empirical analysis that involves studying past failures and successes. Flood identification by real-time forecasting involves monitoring real-time data to identify when there is a significant risk of flooding. The benefits and drawbacks associated with each approach will be investigated.

1 Flood Risk Identification Input

To optimize flood mitigation safety measures must be balanced with an effective use of tax money. Therefore, ensuring the constructive use of funds requires directed efforts towards areas most at risk of flooding. There are many approaches and methods for projecting where flooding will occur through flood risk identification (Merz et al., 2010). Method of projecting these floods include analyzing where floods have already happened historically (Hammond et al., 2015), hydrologic and hydraulics modeling (Mignot et al, 2019), and environmental data analysis (Hosseiny et al., 2020). These analyses aim to identify the variables that are the greatest contributors to flooding, accomplishing the ultimate goal of why flooding is happening. This requires datasets that note where flooding has happened, but documentation of the locations and magnitudes of flooding across a landscape is a complex task, and the data is frequently not available. The following section will include processes used to identify flood risk areas.

Types of Analysis and Studies Used for Flood Projection

The current data revolution has changed the way that engineers can view the world (Huang and Fu, 2019). Developing a better understanding of where flooding is happening enables agencies to prioritize and direct their attention to those locations. Methods for determining those locations vary between agencies but the overall awareness for the need to know that information is common. Data that is clear, detailed, and organized can be used to depict the essence of floods within an area.

Different types of data are needed depending on the type of analysis to be completed. Types of data include temporal data, spatial data, and spatiotemporal data. Temporal data describes an attribute at a given time. Spatial data describes an attribute of a specific location. Spatiotemporal data describes an attribute at a given time and a specific location. Understanding what a dataset represents can steer how analysis is completed (Henonin et al., 2013).

As stated, flood projection is a complex task, and the existing approaches to flood projection constitute uncertainty (Jung et al., 2011). Flood inundation is extremely variable (Junget al., 2011). Different flood projection methods use different variables. Commonly used variables among many studies include weather data, stream behavior data, and environmental data. Understanding the conditions of past events can provide insight into the ones to come.

A common method includes multiple linear regression of surface water to determine streamflow for streams where gages are absent from a location or unmonitored (Farmer et al. 2019). This approach leverages gaged locations to estimate flow at ungaged locations. Using multiple linear regression models helps to determine the streamflow frequency statistics. This allows for the analysis and estimation of flood recurrence. Similar approaches are used in the National Water Model (Frame et al., 2020).

Magnitude and frequency of floods can be estimated using the PeakFQ 7.3 Program (Veilleux et al. 2014). The program produces statistical estimates of magnitude and frequency of flood discharges, flood-frequency analysis, data records from stream gages of annual maximum instantaneous peak discharges, which are used in conjunction with the calculation procedures by Bulletin 17C and Expected Moments Algorithm (EMA).

Data Resources

Precipitation and weather data can be incorporated in flood projections. Historical weather data for locations within the US can be accessed through Automated Surface/Weather Observing Systems (ASOS) (ASOS Weather). ASOS stations are located throughout the nation, normally at airports, and collect a wide range of data. Precipitation data recorded at different durations can be obtained. The precipitation data can be manipulated to investigate rainfall intensities or to determine the total rainfall depth during an event. The National Oceanic and Atmospheric Administration (NOAA) is another outlet that can be used to obtain precipitation data (NOAA Weather). Additionally, NOAA Atlas 14 can be used to compare actual events to precipitation frequency estimates (NOAA Atlas 14).

The United States Geological Survey (USGS) contains a plethora of data that can be seen as applicable for flood projection. USGS National Water Information System (NWIS) has stream

gage stations throughout the United States (USGS NWIS). The stream gages normally contain historical data of the gage height and discharge of a stream. USGS's Stream Stats program provides data on historical stream flow at gaged sites.

Data can be retrieved to analyze the behavior of a stream across a weather event. Another outlet to obtain historical stream data is NOAA National Weather Service (NWS) (NOAA NWS). Similar to USGS NWIS, the database contains historical data of the gage height and discharge of a stream. Stream gage data can be used to observe how a stream performed before, during, and after an event.

According to an NCHRP study, most DOTs rely on visual inspection as a tool in determining the extent of flooding severity. Further, DOTs indicated that the NWS issues the warnings and/or parameters that DOTs apply to issue a flood warning. According to a self-ranking, the most important information used in state's flood warning systems is observed stream stage, observed stream inundation, and bridge scour (Park et al., 2021).

Raster data can be used to analyze an environment or landscape. The National Land Cover Dataset (NLCD) contains different datasets pertaining to the land cover of the US (MRLC). Rasters of Land cover classification and urban imperviousness can be obtained and integrated into analysis to develop a better understanding of a study area. The dataset includes raster imagery every two to three years from 2001 to 2019. Raster calculations can be completed to identify shifts in land use or the reshaping of a landscape. Other imagery data that can be deemed useful in flood projection analysis is USGS Landsat (USGS Landsat). The Landsat dataset is useful to provide multispectral imagery and digital elevation models (DEMs).

New sciences and methods are being used to collect multispectral imagery and DEMs. The approach involves using a drone to capture data. Drones can capture LiDAR and multispectral imagery to define variables, such as elevation, flow paths, and land cover types (Anderson et al., 2010). This is a newer technology that can be utilized anywhere that a drone is accessible.

Additionally, states may have spatial data access portals, such as the Pennsylvania Spatial Data Access (PASDA). These portals contain spatial data in the form of shapefiles and rasters that can be utilized. Respective state spatial data access portals allow quick and simplified methods of obtaining data for a concentrated location. The types of data within vary across a wide spectrum including DEMS, Federal Emergency Management Agency (FEMA) flood zones, and flow lines. Enhancing the accessibility of data can promote its use.

There are a range of studies that investigate approaches and methods relating to flood prediction. Without available and ready-to-use data, exploratory and hypothetical research cannot be executed. Reported challenges and weaknesses to implementing a successful flood monitoring system were state resources (staffing, funding, turnover, etc.), data coverage (e.g., lack of stream gages), and local resources (staffing, funding, turnover, etc.) (Park et al., 2021).

2 Flood Modeling

Real-Time Models

At the 2020 TRB meeting of the Hydraulics and Hydrology Committee, new guidelines for flood-frequency analysis and skew maps, titled Guidelines for Determining Flood Flow Frequency, Bulletin 17C, were published by the Advisory Committee on Water Information's Subcommittee on Hydrology, Hydrologic Frequency Analysis Workgroup. Bulletin 17C is a national standard guideline document describing the data and procedures to compute flow frequency, providing a more reliable estimation of flood frequency. Different programs and methods for identifying flooding include the National Streamflow Statistics (NSS) Program is a computer program that compiles all current USGS streamflow data from gaged and ungaged sites and uses regression equations to estimate flood-frequency statistics, including estimation on the magnitude and recurrence intervals for floods in urbanized areas. However, NSS does not have the ability to generate flood frequency plots and flood hydrographs.

The National Water Model (NWM) is a spatial streamflow model that covers the contiguous US. The inter-agency project, led by the National Oceanic and Atmospheric Agency (NOAA), forecasts streamflow using weather forecast, stream forecast, and regression models to predict the full extent of the continuous US hydrography. This breakthrough tool was launched by the National Water Center but is still under development. The large spatial extent of the model makes it difficult to include variable hydraulics, common to urban zones.

Additional methods include the USGS WaterAlert. The WaterAlert provides a water-threshold exceedance notification program that sends out alerts once water quality conditions, water levels, or rainfall amounts meet criteria specified by the user, which is particularly useful in flood monitoring (TRB Report). The program utilizes real-time USGS hydrological data from NWIS, reporting once-a-day or once-per-hour during the duration of the condition. For major flood events, USGS provides hydrological information prior to, during, and after the event with near real-time flood data and summaries available on the internet (e.g., Waterdata and NWIS). Most approaches for flood monitoring and identification include the use of USGS NWIS stream gauge data to forecast the risk of flooding. However, a stream gage needs to be present to have the data input to make the flood risk prediction. There are different approaches taken across the nation to identify flooding in real-time.

BridgeWatch is a web-based software system that monitors real-time stream gage data and relays when limit detections have been breached to the respective party (BridgeWatch). Georgia, Tennessee, Iowa, and Idaho Departments of Transportation (DOT), along with other states, are using the program to monitor bridges that are susceptible to flooding and other adverse environmental conditions (Zirkle et al., 2014). The program monitors gage height data, flow data, and hurricane-induced tidal surge data within a stream. Notifications are sent to the agency responsible for the bridge when thresholds have been surpassed. Georgia DOT is using the program to monitor 76 scour critical bridges aiming to alleviate and potentially avoid hazards tied to emergency response programs (Scannell, 2010).

Implementing the above-mentioned programs can save time, money, and lives (Scannell & Baribault, 2010). These solutions give a larger window to make a proper assessment. Flood management protocols and efforts can be more effectively used to better protect the agency personnel and public travelers (Zirkle et al., 2014). Additionally, the before, during, and after stream gage data can be used to assess the bridges post-event. Overall, flood monitoring and identification is a proactive step to take with respect to flood mitigation.

Alternative Methods for Flood Projection

Flood projection allows for identifying the locations that are prone to flooding. However, there are other options to assess where flood risk is greatest. A source-to-impact analysis to locate flooding areas can be implemented (Vercruysse et al., 2019). The source is defined as the area contributing to flooding, and the impact is defined as the area that floods. A case study used four criteria, total flood extent, maximum flood depths, flooded green spaces and roads, and likelihood of flood, to define a process for identifying which flood mitigation solutions are most practical and efficient with consideration of different infrastructure systems. The results from this analysis state that the modeling process would be most useful for an initial assessment to invite and consider different flood mitigation solutions.

Many DOTs use Geographical Information System (GIS) programs, like Esri's ArcGIS Pro, are used for mapping, displaying, and analyzing spatial and spatiotemporal data, particularly where the hydraulics are non-normal. Illinois, Texas, Minnesota, Florida, Mississippi, and Kentucky are incorporating the tool for assessment and analysis of the landscape, varying from flood risk assessment to locations susceptible to sinkholes. Additionally, Oklahoma, Vermont, and Colorado are using GIS as a platform for communicating information to the public (Park et al., 2021).

Most states are using GIS to improve safety by informing the public of the roads and locations that are vulnerable to flooding. This aligns with efforts from the National Water Model. However, data collection of inundation is often difficult. Increasingly, researchers are going beyond spatial data mining and experimenting with the use of artificial intelligence (AI) to predict flooding (Hosseiny et al., 2020). However, advancements linking AI and physical based models are required to allow AI models transferability.

Modeling programs like the United States Army Corps of Engineers (USACE) Hydrologic Engineering Center's Hydrologic Modeling System (HEC-HMS) can be used to simulate hydrologic processes (Army Corps HEC-HMS). The study "Quantifying the impact of impervious surface location on flood peak discharge in urban areas" states that there is a lack of attention being paid towards the influence that impervious surfaces have on flooding. The study uses HEC-HMS to simulate how the addition of increased impervious surfaces within a watershed affects peak discharge at the outlet of the watershed. The results state that an increase in impervious surfaces upstream constitutes a greater peak discharged compared to an increase of impervious surfaces downstream. The finding suggests that this simulation can be useful to determine the optimal location for new development (Du et al., 2015).

USACE Hydraulic Engineering Center's River Analysis System (HEC-RAS) software is produced by the Army Corps of Engineers for modeling river dynamics. The software allows users to model

one-dimensional and two-dimensional flow, water quality, and sediment transport. Many DOTs across the US (Iowa, North Carolina, South Carolina, Texas, and Maine) reported using HEC-RAS widely to model flooding of transportation systems (Park et al., 2021).

Flood Mitigation Efforts through Green Stormwater Infrastructure

Research in flood mitigation presents new perspectives on the methods that are best at reducing flood risk. The study "The capacity of grey infrastructure in urban flood management: A comprehensive analysis of grey infrastructure and the green-grey approach" compares the performance and efficiency of traditional methods of stormwater control and infrastructure to a combination of traditional methods and GI (Xu et al., 2021). Two types of grey infrastructure, pipe networks and deep tunnels, are analyzed and compared to a combination of grey-green infrastructure. The results state that grey infrastructure can reduce flood severity. However, the pipe networks created more flood hot spots downstream and the deep tunnel would fail if the upstream systems already reached capacity. The grey-green infrastructure proved to be the more stable and effective flood mitigation practice. The grey and green aspects of the grey-green infrastructure appeared to complement each other very well. The GI would perform well at retaining small rainfall, relieving the stress of the grey infrastructure to handle the grey rainfall.

3 Conclusions and Future Work

Similar to much of the U.S. is predicting and responding to flooding events is an increasingly important issue for PennDOT's District 6. To mitigate significant economic impacts on roadways and bridge flooding it is critical to manage flood risk within the District. Across the US DOTs have implemented integrated robust flood management systems; however, challenges still exist for these systems. Advancements and integration of relational database systems, real-time data collection tool technologies (e.g., LiDAR, gages etc.), flood prediction models, data process/visualization software (e.g., GIS), and data sharing platforms (e.g., the USGS National Water Information System-NWIS, or the National Weather Service-NWS, River Forecast Center) have made substantial contributions to the effective prediction and forecasting of floods. This is reflected in national investments made to these programs (specifically, NOAA's National Water Model, ASOS, and the USGS NWIS), which highlights the proven usefulness and importance of managing flood risk, particularly for transportation systems. Further investment in national datasets such as FEMA floodplain maps and other open access spatial data areas allowing deeper insight into flood characteristics.

Some key flood risk management tools include USGS gages (WaterAlert) and BridgeWatch for flood prediction. Other commonly used tools include HEC-RAS, HEC-HMS, PeakFQ, and Bulletin 17C, and StreamStats/National Streamflow Statistics. The other most common instruments and tools used for flood monitoring are federal rain gages and GIS. The DOTs provided information on risk thresholds that trigger action. Common responses from DOTs indicated that the NWS issues the warnings and/or parameters that DOTs apply to issue a flood

warning. According to a DOT across the US the most important information used in state's flood warning systems is observed stream stage, observed stream inundation, and bridge scour.

However, DOTs rely on visual inspection as the most common tool in determining the extent of flooding severity assessment. It is important to note and efforts to manage flood risk cannot be advanced without available and ready-to-use data. Data limitations will hinder exploratory and hypothetical research. Reported challenges and weaknesses to implementing a successful flood monitoring system were state resources (staffing, funding, turnover, etc.), data coverage (e.g., lack of stream gages), and local resources (staffing, funding, turnover, etc.) (Park et al., 2021).

Future work in this field will involve further advancing data quality and feasible coverage, as well as leveraging data to deepen the science and engineering communities' understanding of the parameters impacting and driving flood events. As new data sources become available, through data models, data sharing, and advancements in remote sensing, challenges and opportunities will continue to grow. This will be furthered through hydroinfomatics (Makropoulos and Savic, 2019), but also through the application of artificial intelligence (Miller and Hutchins, 2017).

Task 1b Summary

Task 1B

Further holistic spatial analysis by developing preliminary work at VU based on flood inundation data to identify flood inundation-prone locations within metro Philadelphia

Workflow

Input Data

Variable	Creator	Year(s)
Pennsylvania county boundaries	PennDOT	2022
Pennsylvania local roads	PennDOT	2022
Pennsylvania state roads	PennDOT	2022
PennDOT - Road Closures	PennDOT	2016-2021
Pennsylvania municipality boundaries	PennDOT	2022
Bridges	PennDOT	2022

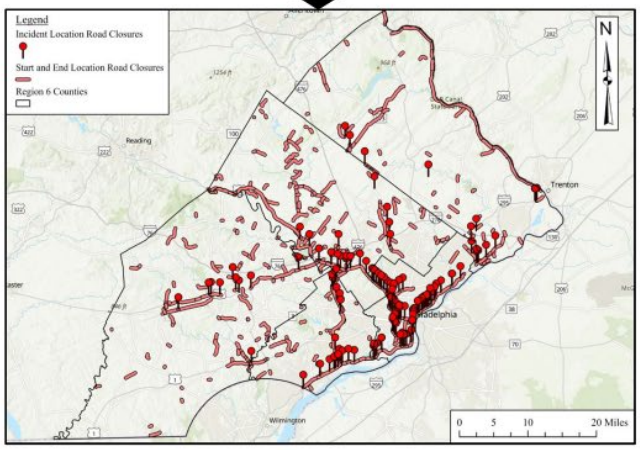

Holistic dataset for the spatial analysis of PennDOT's District 6 flooding risk.

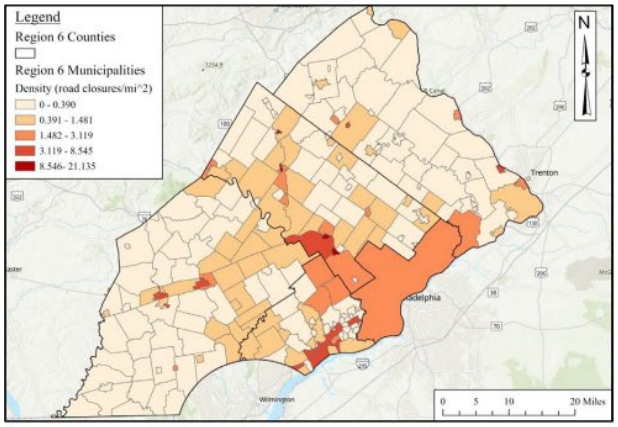

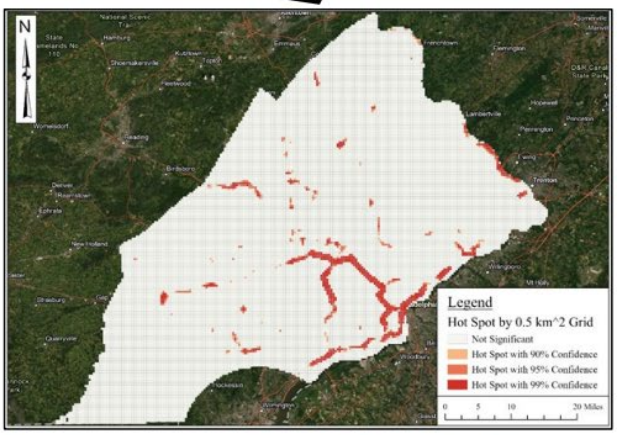

Spatial analysis of road closures based on density of closures per municipality (normalized by municipality square mile area) and road based on a half square km grid.

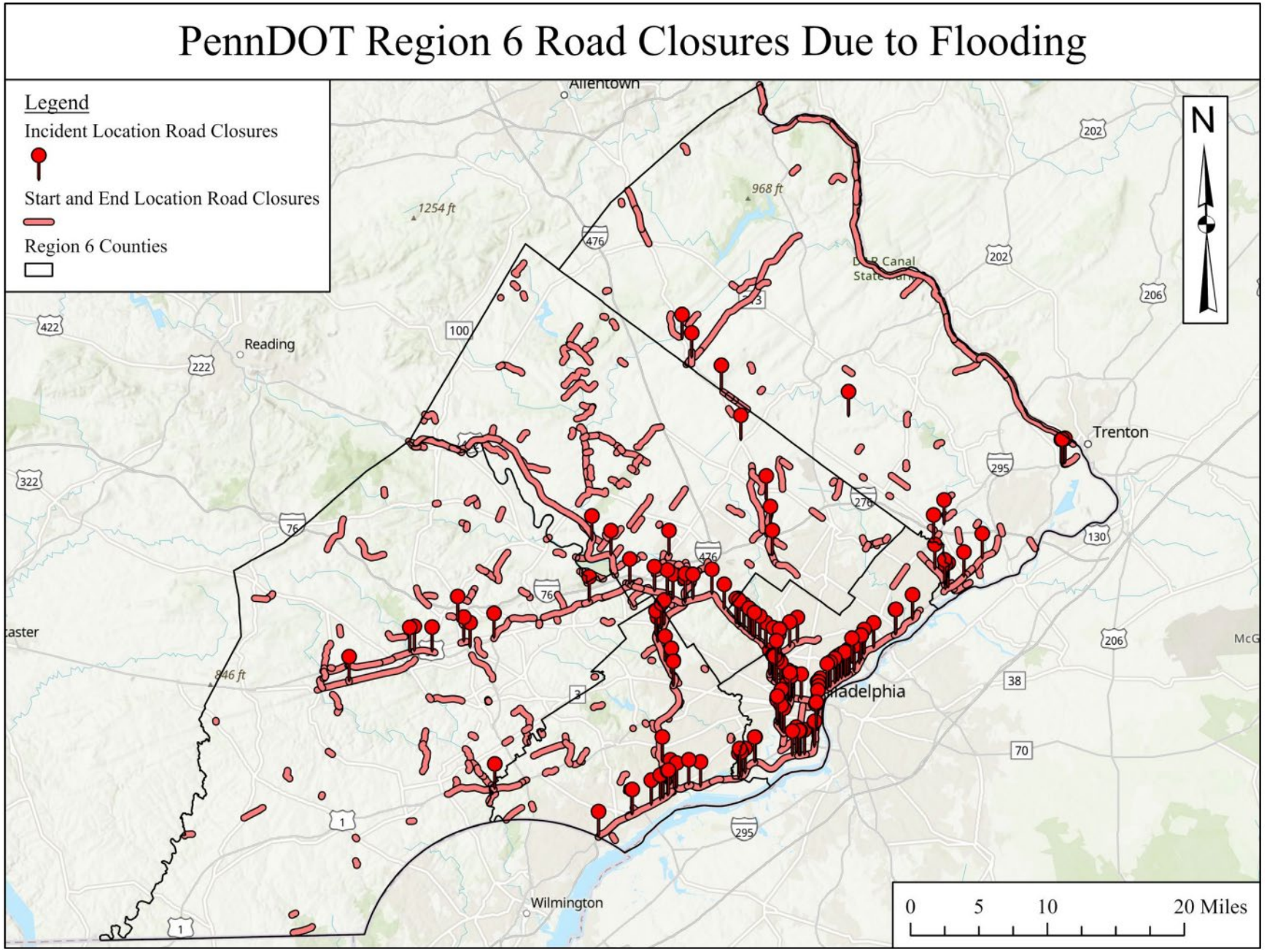
PennDOT Region 6 Road Closures Due to Flooding
Legend
Incident Location Road Closures
Start and End Location Road Closures
Region 6 Counties
N
Allentown
Reading
Trenton
Wilmington
1254 ft
968 ft
846 ft
0 5 10 20 Miles

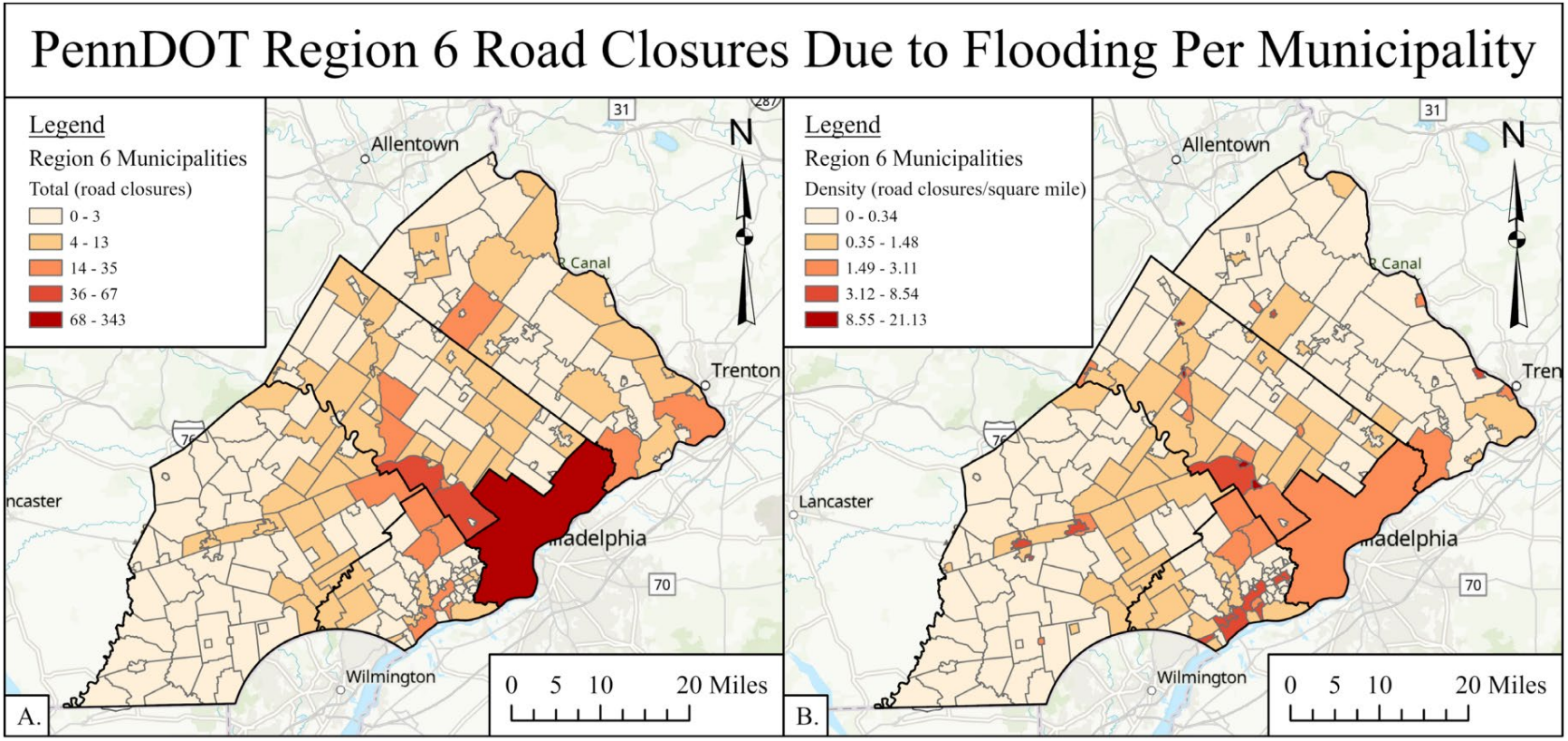
PennDOT Region 6 Road Closures Due to Flooding Per Municipality
Legend
Region 6 Municipalities
Total (road closures)
0 - 3
4 - 13
14 - 35
36 - 67
68 - 343
Allentown
Trenton
Wilmington
Lancaster
N
0 5 10 20 Miles
A.
Legend
Region 6 Municipalities
Density (road closures/square mile)
0 - 0.34
0.35 - 1.48
1.49 - 3.11
3.12 - 8.54
8.55 - 21.13
Allentown
Lancaster
Wilmington
N
0 5 10 20 Miles
B.

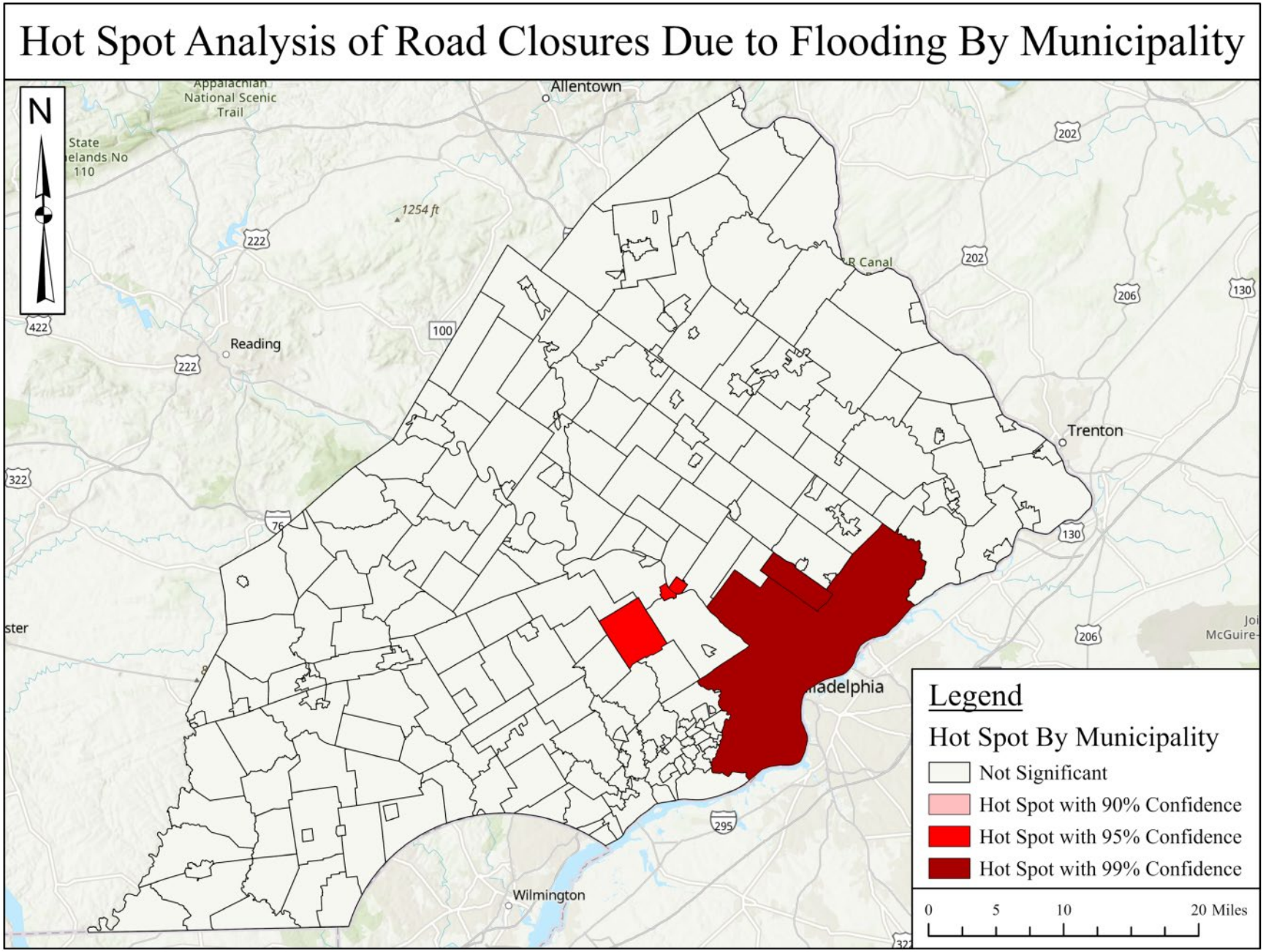
Hot Spot Analysis of Road Closures Due to Flooding By Municipality
N
Appalachian National Scenic Trail
Allentown
State
elands No
110
1254 ft
222
422
Reading
100
202
R Canal
206
130
Trenton
322
76
ster
295
Wilmington
Legend
Hot Spot By Municipality
Not Significant
Hot Spot with 90% Confidence
Hot Spot with 95% Confidence
Hot Spot with 99% Confidence
0
5
10
20 Miles

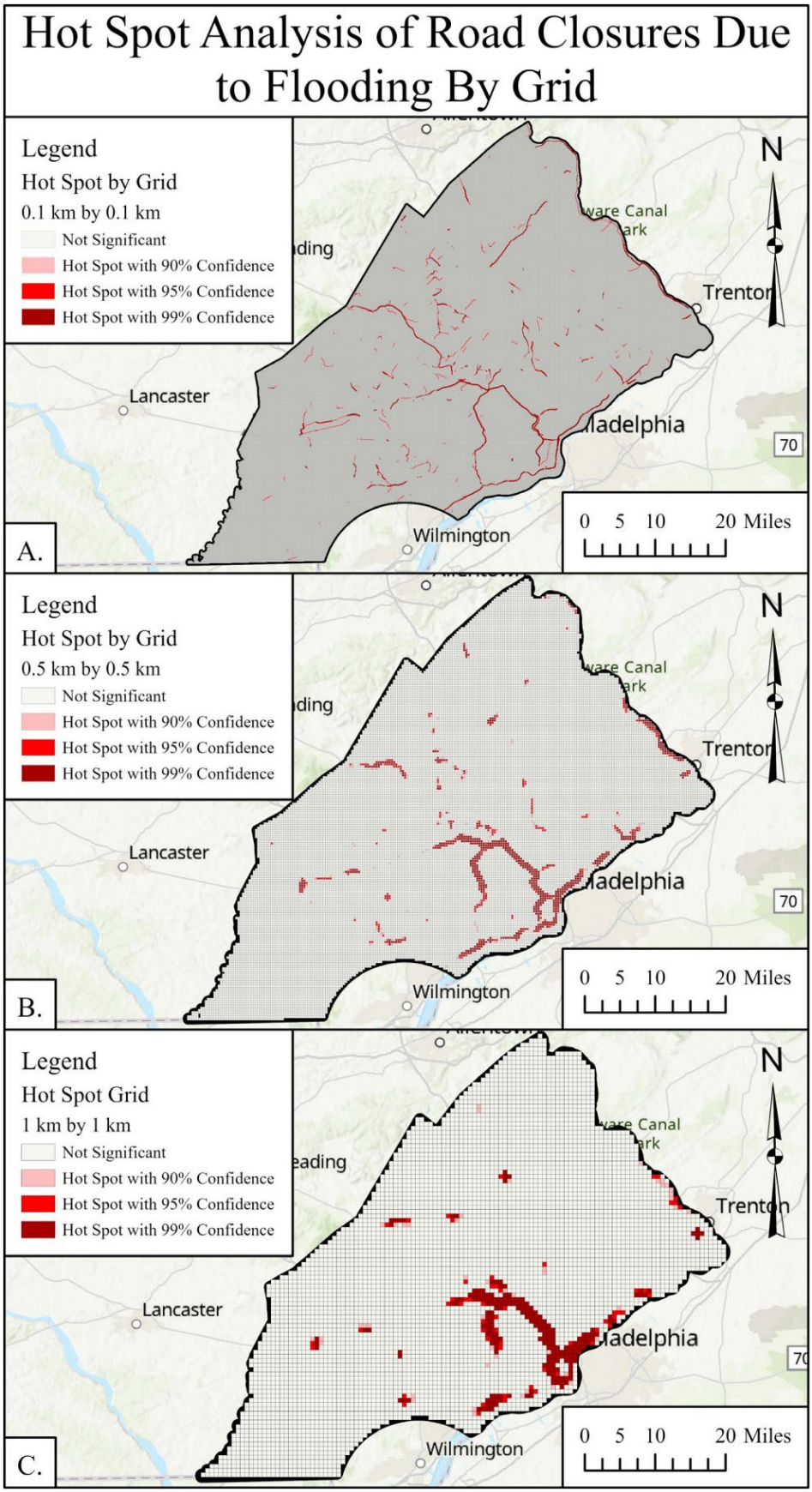
Hot Spot Analysis of Road Closures Due to Flooding By Grid
Legend
Hot Spot by Grid
0.1 km by 0.1 km
Not Significant
Hot Spot with 90% Confidence
Hot Spot with 95% Confidence
Hot Spot with 99% Confidence
N
Lancaster
Wilmington
70
0 5 10 20 Miles
A.
Legend
Hot Spot by Grid
0.5 km by 0.5 km
Not Significant
Hot Spot with 90% Confidence
Hot Spot with 95% Confidence
Hot Spot with 99% Confidence
N
Lancaster
Wilmington
70
0 5 10 20 Miles
B.
Legend
Hot Spot Grid
1 km by 1 km
Not Significant
Hot Spot with 90% Confidence
Hot Spot with 95% Confidence
Hot Spot with 99% Confidence
N
Lancaster
Wilmington
0 5 10 20 Miles
C.

Task 1b Report

1 Introduction

A spatial analysis serves as a powerful method for developing a better understanding of infrastructure data on a spatial scale. A spatial analysis could identify patterns and trends that may not be discovered otherwise. The spatial analysis of traffic crashes is a well-established field with extensive published literature. In recent years several studies have used regression models paired with spatial analysis to analyze and quantify the spatial characteristics of transportation systems (Hanssen et al., 2018; Ismail-Zadeh et al., 2017; Marzochi et al., 2012). Additionally, this approach has been shown to be efficient and effective at analyzing the function of infrastructure systems in response to disasters, such as floods (Crimmins et al., 2021; Godschall et al., 2020).

2 Data and Methods

The following methodology was accomplished primarily using Esri's ArcGIS Pro. Cleaning, organizing, and pre-processing data are necessary steps before any of the input data can be used in the analysis. The preparations include but are not limited to changing the format of the data, alleviating disturbances within the data, and separating or selecting the desired data from a larger dataset. Additionally, a uniform projected coordinate system (PCS) should be used throughout the analysis. NAD 1983 StatePlane Pennsylvania South FIPS 3702 (US Feet) will serve as the project PCS for analysis.

The data used for the analysis in this section is described in Table 2.1, and the specific methods of analysis are described in the following sections.

Table 2.1. Summary of the data sources used in the hot spot analysis.

Variable	Creator	Year(s)/ Date	Source
Pennsylvania county boundaries	Pennsylvania Department of Transportation	2022	Pennsylvania Spatial Data Access
Pennsylvania local roads	Pennsylvania Department of Transportation	2022	Pennsylvania Spatial Data Access
Pennsylvania state roads	Pennsylvania Department of Transportation	2022	Pennsylvania Spatial Data Access
PennDOT - Road Closures	Pennsylvania Department of Transportation	2016-2021	Pennsylvania Department of Transportation
Pennsylvania municipality boundaries	Pennsylvania Department of Transportation	2022	Pennsylvania Spatial Data Access
Bridges	Pennsylvania Department of Transportation	2022	Pennsylvania Spatial Data Access

2.1 Data

Pennsylvania Spatial Data Access (PASDA) Pennsylvania Counties

As stated, District 6 of Pennsylvania will serve as the study area for analysis. Defining the limits of District 6 is necessary to complete later steps of analysis. A polygon shapefile of Pennsylvania's counties is obtained from PASDA and is brought into a new project on AcrGIS Pro. The Project Tool is used to project the shapefile to the project PCS, NAD 1983 StatePlane Pennsylvania South FIPS 3702 (US Feet). The projected shapefile is refined to District 6 counties by using the Select by Attributes Tool. A selection is made by defining a query using the names of the five counties (Fig. 2.1).

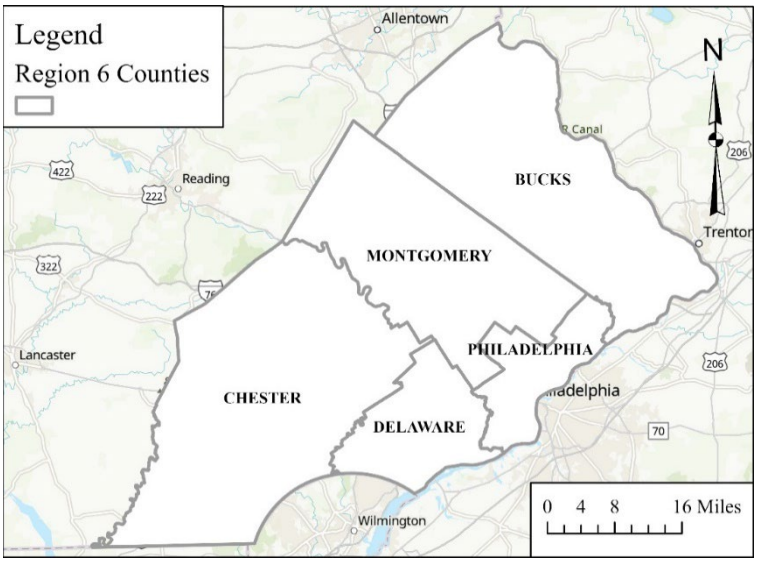

Figure 2.1. District 6 Counties of Pennsylvania.

PASDA Pennsylvania Local and State Roads

The local and state roads will be used for the alignment of the road closures due to flooding. Two datasets, local roads and state roads, are obtained from PASDA and imported to the ArcGIS project. The data is projected to the project PCS using the Batch Project Tool, which allows for multiple shapefiles to be projected at once. The Merge Tool is then used to combine the two shapefiles into one shapefile (Fig. 2.2).

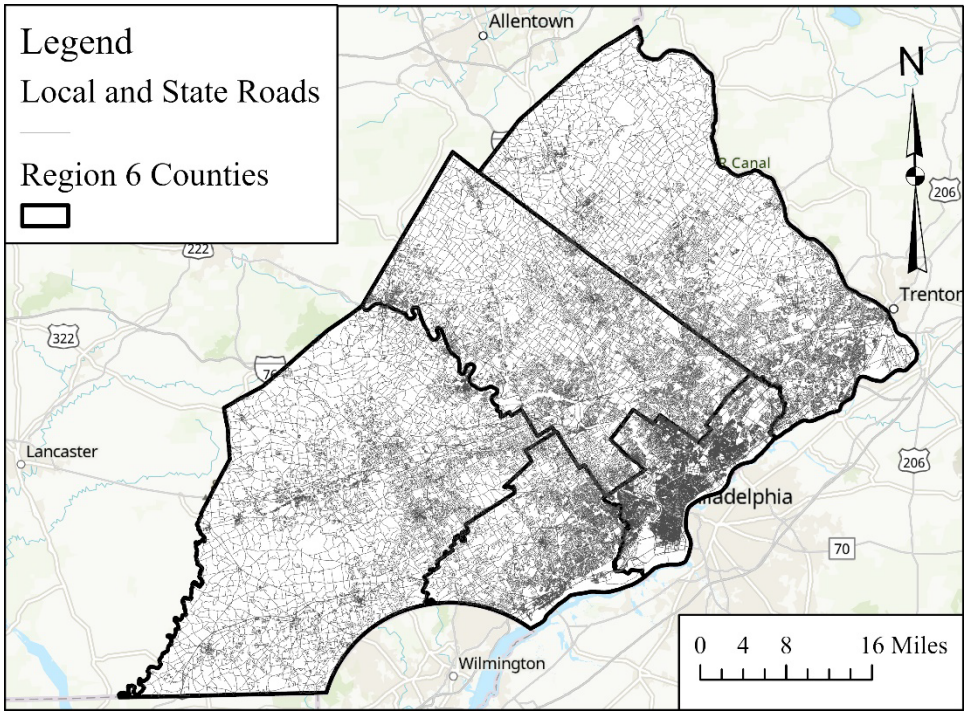

Figure 2.2. Local and State Roads of District 6 PA.

PennDOT Road Closure Due to Flooding Dataset

The road closure due to flooding dataset is in tabular form with a date frame of January 1, 2016, to October 27, 2021. PennDOT uses two methods to record the road closures. The first method is by recording a single incident location. The incident location will have a single set of coordinates that generalizes where the closure occurs. The second method is recording a road closure by a start location and end location. The start location and end location each have their own respective set of coordinates that define the length of the closure. The data is separated into two tables by the method used to record the road closures. The two tables are brought into a new map in ArcGIS Pro (Fig. 2.3).

Incident Location Road Closures Due to Flooding

Considering the method of recording a closure by an incident location, the resulting data will serve as a point. The XY Table to Point Tool is used to generate a point shapefile using the latitude and longitude coordinates within the fields of the data. Additionally, the correct output coordinate

system needs to be assigned before running the tool. The output coordinate system for the road closure due to flooding dataset is the NAD 1983 geographic coordinate system (GCS). Following the incident locations of road closures being displayed as a point shapefile, the Project Tool is used to convert the coordinate system from the recorded GCS to the project PCS. Once projected, the Snap Tool is used to align the incident location points to the nearest roadway.

Start and End Location Road Closures Due to Flooding

For the road closures that are recorded with a start and end location, the resulting data will be displayed as a line. The XY To Line Tool is used to create a line shapefile using the respective start and end sets of coordinates (Fig. 2.3). Similar to the incident location road closures, the same output coordinate system of the NAD 1983 GCS is used. The shapefile is projected to the project PCS. The XY To Line Tool creates a line connecting the start and end locations linearly. The Align Features Tool is used to align the road closures to roadways. The merged local and state roadways shapefile is used as the aligning feature and 300 feet is assigned as the search distance. A portion of the road closures occur at winding roads, or the length of the road closures are great enough for the search distance of 300 feet to be incapable of aligning the road closure to the roadways properly. The remaining road closures that are not aligned after running the Align Features Tool are aligned manually using the built-in edit tools on ArcGIS Pro. The Trace Feature function within the Reshape Tool is used for manual alignment.

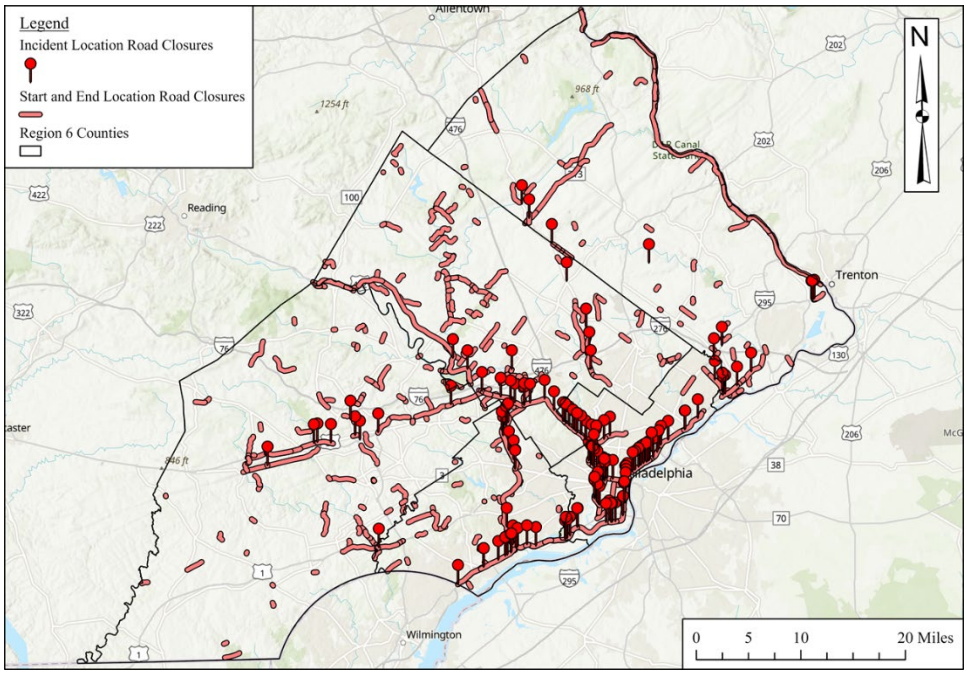

Figure 2.3. Incident location (points) and start and end location (line segments) road closures due to flooding in District 6 PA from January 1, 2016, to November 12, 2021.

2.2 Hot Spot Analysis

As stated, the road closures due to flooding data will serve as a proxy for surface water flooding. A hot spot analysis is completed to identify the locations that experience the most road closures due to flooding across the district 6 landscape. Two approaches are taken to locate the hot spots of road closures. The first is to identify the hot spots by using the municipalities of District 6. The second is to identify the hot spots by using a grid laid across District 6.

PASDA PA Municipalities

A shapefile of all the municipalities of Pennsylvania can be obtained from PASDA. The shapefile is brought into the ArcGIS Pro and projected to the project PCS. The municipalities within District 6 are extracted by using the Select by Attributes Tool. The definition query is arranged to select the municipalities that have the respective county codes for the five counties in District 6. Table 2.2 displays the county codes for the respective counties. The county codes can be found by looking at the attribute table of the already created District 6 county shapefile (Fig. 2.4).

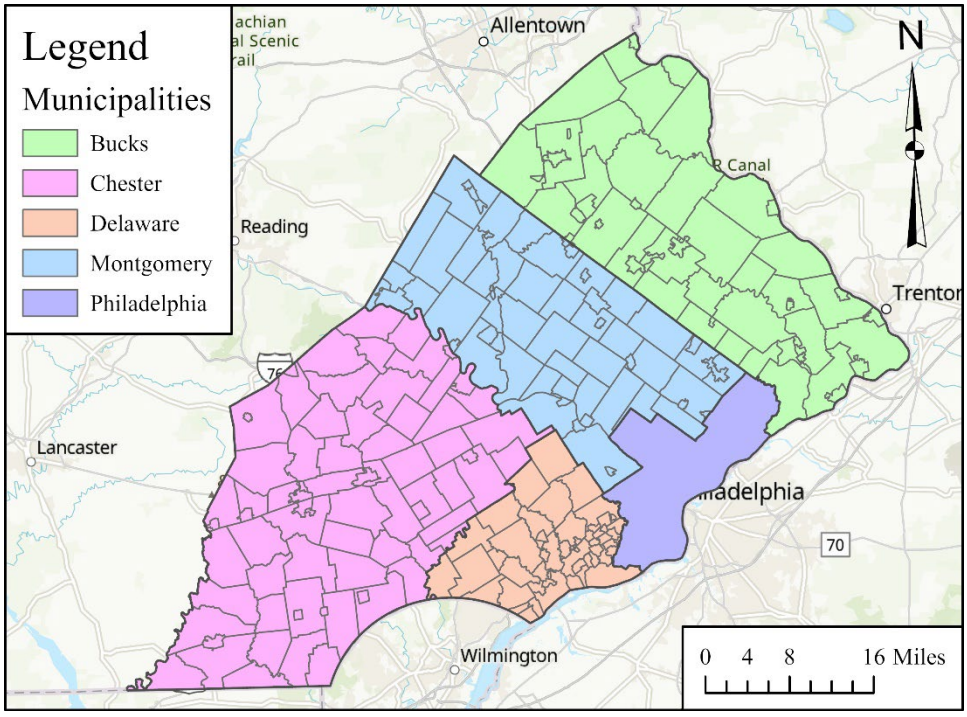

Figure 2.4. Municipalities of District 6 PA.

Table 2.2. County Codes for the respective District 6 PA counties.

County Name	County Code
Bucks County	09
Chester County	15
Delaware County	23
Montgomery County	46
Philadelphia County	67

Hot Spot Analysis of Road Closures Due to Flooding by Municipalities

The road closures due to flooding data are joined with the District 6 municipalities shapefile. The Spatial Join Tool is used to identify the number of road closures within or intersecting the municipalities. Two spatial joins will need to be completed to account for the incident point closures and the start and end line closures. Each spatial join will produce a new shapefile that has a new field to the attribute with the field name "Join_Count". The Join Table tool is used to combine the two tables. The municipality name is used as the unique identifier in the tool. A new field is created in the attribute table of the shapefile that the table join was completed on. The Calculate Field Tool is used to calculate the sum of the two "Join_Count" fields. The new field represents the total number of closures within each municipality. The field will then be used in the Hot Spot Analysis (Getis-Ord Gi*) Tool as the input field. The tool will produce a shapefile with symbology that identifies the road closure hot spots by municipalities.

Hot Spot Analysis of Road Closures Due to Flooding by Grid

A grid is created across District 6 using the Grid Index Features Tool. Three different size grids are used to identify the significance of grid size on the hot spot analysis, which will include a 0.1 km by 0.1 km size grid, a 0.5 km by 0.5 km size grid, and a 1 km by 1 km size grid. The size of the grid is defined in the tool. The District 6 county shapefile is used as the input feature that defines the grid extent. The same process that is used to count the total number of road closures that are within or intersecting each municipality is used to determine the number of road closures that are within or intersecting each grid box. Similarly, the resulting spatially joined shapefile is used as the input feature, and the field identifying the total number of road closures is used as the input field for the Hot Spot Analysis (Getis-Ord Gi*) Tool. The process is repeated for each grid size.

3 Results and Discussion

3.1 Road Closure Due to Flooding

The road closures due to flooding data do not perfectly portray where surface water flooding is happening but still can serve as a proxy for surface water flooding is happening. The road closures identify the general location of where flood inundation is occurring. There were 981 road closures recorded from January 1, 2016, to November 12, 2021. Of those 981 road closures, 287 road closures were recorded as incident locations and 694 road closures were recorded as start and end locations. Figure 2.3 displays the road closures across District 6 of Pennsylvania.

Visualizing the road closures data further develops an understanding of where flooding is happening. Initially, the road closures appear denser towards the center of District 6. The Schuylkill River runs diagonally across District 6, relatively in the center of District 6 as well. Trends and patterns can potentially be identified with further analysis. Also, most of the road closures in Philadelphia County appear to be located along the interstate highways along waterways while there are substantially fewer road closures in the center of the City of

Philadelphia. There is greater contrast when comparing Philadelphia County to the other counties that consist of most road closures appearing to be scattered throughout the entire county.

3.2 Hot Spot Analysis

Hot Spot Analysis by Getis-Ord Gi Statistic*

The Hot Spot Analysis (Getis-Ord Gi*) Tool is used to identify the hot spots of road closures in District 6. The results produce a z-score and a p-value. The z-score represents the standard deviation of the input parameter. Depending on if the standard deviation is positive or negative, the cluster will be considered as a hot spot or cold spot, respectively. The p-value represents the probability, defining the likeliness of an observed pattern. The lower the p-value, the more likely there is a randomness to the clustering. Therefore, pairing a higher z-score and lower p-value results in high confidence in a hot spot.

Road Closures Due to Flooding per Municipality

Before the hot spot analysis is completed, the data is visualized by the number of road closures per municipality, displayed in Figure 4.1A, and the density of road closures per municipality, displayed in Figure 3.1B. The visually displaying the data gives insight into where concentrated road closures due to flooding are happening. Of the 239 municipalities in District 6, 74 municipalities did not have any documented road closures. Seen in Figure 3.1A, road closures due to flooding appear to be concentrated around the City of Philadelphia and the Schuylkill River. Additionally, most of the municipalities without a documented road closure appear to be further from the mentioned concentrated area. However, there may be more documented road closures in a municipality of greater area considering there is more space for a road closure to occur.

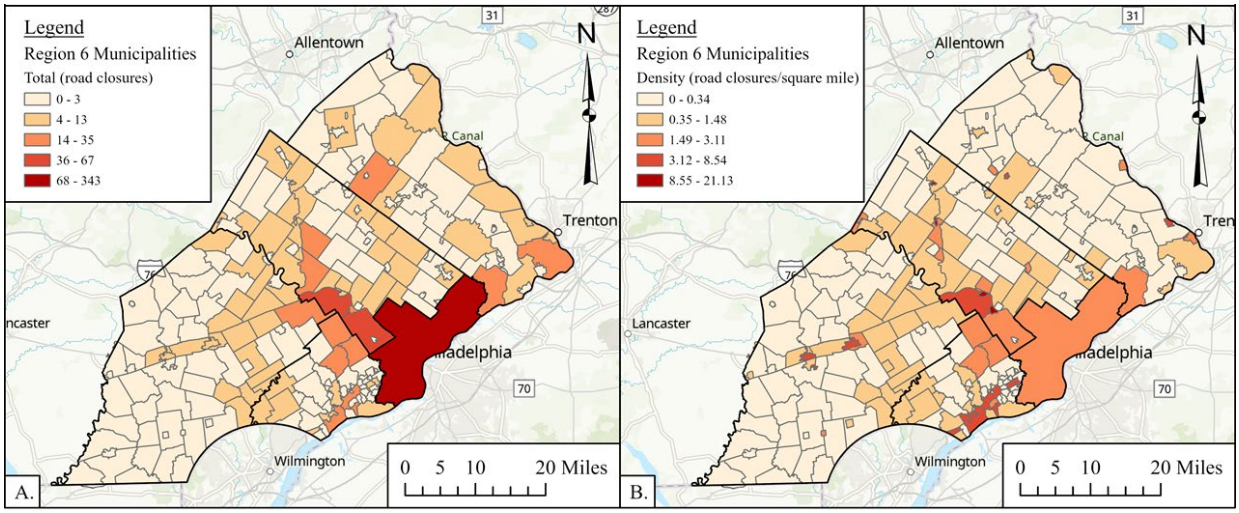

Figure 3.1. A.) Map of the number of road closures due to flooding by municipality created in ArcGIS Pro. **B.)** Map of the density of road closures due to flooding (number of road closures/square miles) by municipality created in ArcGIS Pro.

Figure 3.1B tests this theory displaying the density of road closures. The density of road closures is defined as the number of road closures within a municipality divided by the area in square miles of a municipality. The results, found in Figure 4.1B, are fairly similar to the results found in Figure 3.1A. However, smaller counties appear to be represented better when considering the number of road closures due to flooding for a municipality.

Hot Spot Analysis of Road Closures Due to Flooding by Municipality

Figure 3.1B demonstrates the general locations where road closures due to flooding are happening. The next step of completing a hot spot analysis accomplishes the task of identifying the locations that have a statistically higher likeliness of experiencing road closures. However, using the municipalities as the input feature did not appear to provide significant results. There are five municipalities that are identified as a hot spot with percent confidence greater than 90%; Conshohocken, West Conshohocken, and Radnor Municipal are identified as hot spots with 95% confidence, and Philadelphia and Cheltenham Municipal are identified as hot spots with 99% confidence. The municipalities are focused within the general area of the City of Philadelphia. The results of the hot spot analysis are seen in Figure 3.2.

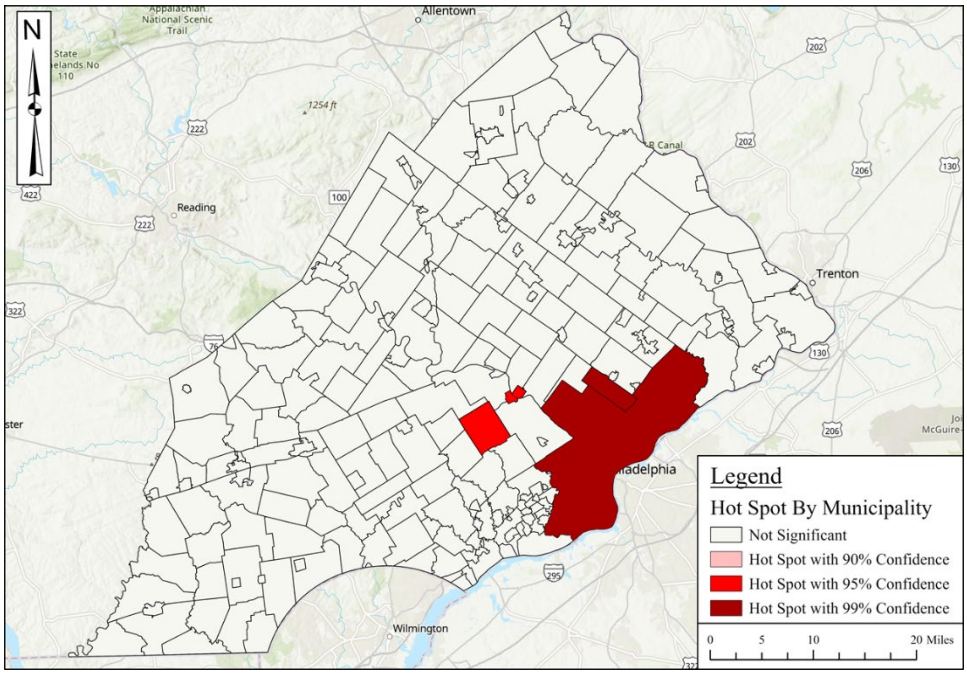

Figure 3.2. Map of the hot spot analysis for road closures due to flooding by municipalities created in ArcGIS Pro.

Considering the spread of road closures across District 6, seen in Figures 3.1, it was expected that the municipalities would mimic this thought, seeing multiple municipalities across District 6 being identified as hot spots. Instead, the results from the hot spot analysis identify five concentrated municipalities being identified as hot spots. To better understand these results, the input data is analyzed.

The municipality of Philadelphia has the most road closures at 343. The second and third municipalities with the most road closures are Lower Merion and Upper Merion with 67 and 66 road closures respectively. The next municipality drops to 35 road closure. The significance behind the number of road closures, in terms of calculating the Getis-Ord Gi* statistic, is that it heavily influences how the hot spots are identified. Especially, when compared to the other parameters that are considered in the calculation, such as the area of the features and the distance to adjacent features. Additionally, the hot spots are identified using an average of the results of all features within the study area, seeing outliers strew the average. Therefore, using the municipalities as the input feature may not be producing the best results for locating the hot spots.

Hot Spot Analysis of Road Closures Due to Flooding by Grid

The goal of the hot spot analysis is to identify the areas where flood inundation is happening. Considering the results of the hot spot analysis using the municipalities as the input feature a different approach is taken aiming to produce better results. As stated, the input value of a feature heavily influences the computation of the Getis-Ord Gi* statistic. Using a grid as the input feature may provide a more equal playing field for identifying hot spot areas since a constant area is used for each grid box. Three different grid sizes are used to complete the hot spot analysis. The grid sizes for the analysis will be a 0.1 km by 0.1 km grid, a 0.5 km by 0.5 km grid, and a 1 km by 1 km. Figures 3.3. displays the results of the hot spot analysis using the different grid sizes.

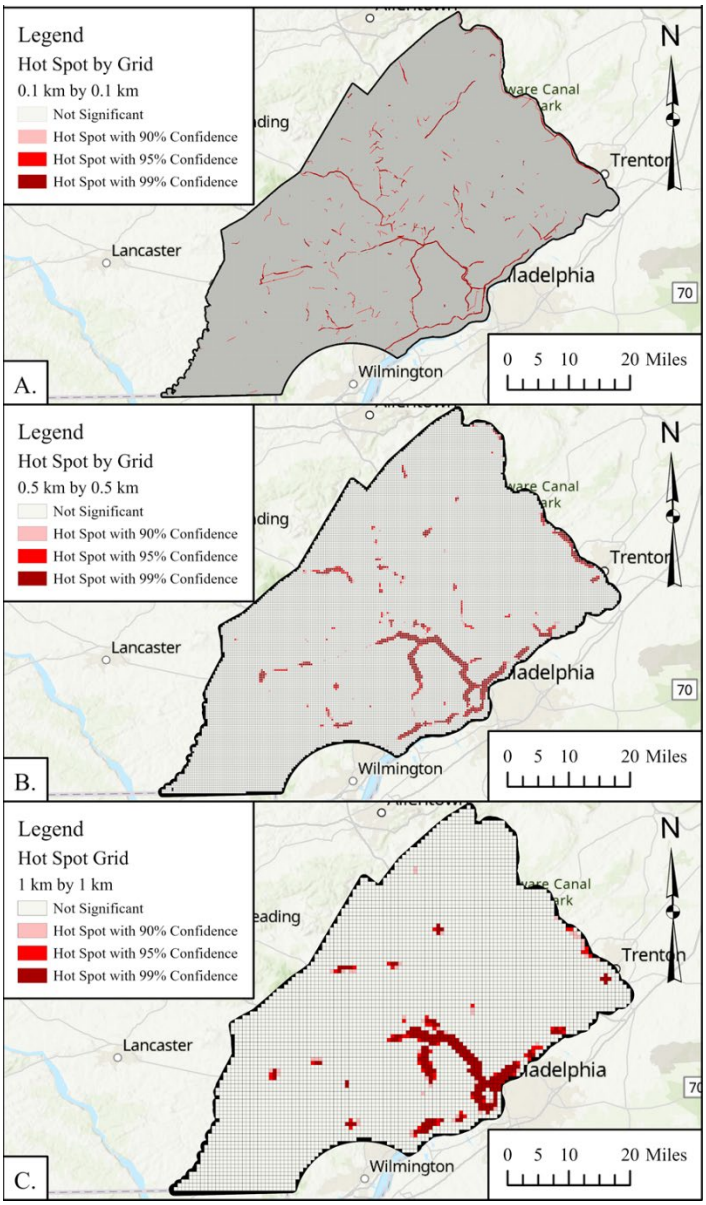

Figure 3.3. A.) Map of the hot spot analysis of road closure due to flooding by a 0.1 km by 0.1 km grid created in ArcGIS Pro. **B.)** Map of the hot spot analysis of road closure due to flooding by a 0.5 km by 0.5 km grid created in ArcGIS Pro. **C.)** Map of the hot spot analysis of road closure due to flooding by a 1 km by 1 km grid created in ArcGIS Pro.

From the results of the hot spot analysis, it appears that reducing the grid size identifies more exact hot spot locations. Using the 0.1 km^2 by 0.1 km grid, seen in Figure 3.3, the hot spots mimicked the relative location of where road closures happened, seen in Figure 3.1. Since the grid size area is fine, the number of closures per grid box is reduced substantially compared to the greater grid sizes. The performance of the hot spot analysis seems to be dependent on the proportioning of the input value of features compared to one another. This idea can be seen when comparing Figures 3.3. When there is more consistency in the input value of features, there are more hot spot areas identified.

The results from the hot spot analysis, when comparing all grid sizes, shared similarities in the areas that are identified as hot spots. The areas that are located as hot spots include along the Schuylkill River near Delaware, Montgomery, and Philadelphia County, the northeast portion of Bucks County along the Delaware River, the eastern coastline of the Philadelphia County, the northern section of I-476 in Delaware County, and along I-95 in Delaware County. These are locations with the greatest area of hot spots. The highest concentrations fall along the Delaware and Schuylkill Rivers, Darby Creek and Perkiomen Creeks.

4 Conclusions

Road closure data was analyzed by a range of geospatial tools to analysis the data by municipality (and normalized by area and analyzed by hot spots) and a range of spatial grid resolutions. Results show areas in District 6 with previous closures, highlighting areas of flood risk. The majority of areas fell along the Delaware and Schuylkill Rivers, Darby Creek and Perkiomen Creek, and other creeks in the District.

It should be noted, since PennDOT records road closures as points and lines, there could be discrepancies in the analysis process. If a point is meant to represent a road closure of greater length, then it would not be accurately represented. Additionally, the road closures may have not reported exactly where water is accumulating, i.e., where flood inundation occurred, if the intention of reporting the road closures were to locate an inaccessible roadway. This issue can be more impactful during analysis linking roadways to closures or grouping them by different types of attributes.

A summary of the workflow and resulting maps can be found in the Task 1b Summary document.

Task 1c Summary

Task 1C
Create workflow to repeat this spatial analysis
Workflow

Input Data

Variable	Creator	Source
NHDPlus HR for 4-digit Hydrologic Unit - 0204 -0206	NHD	USGS/The National Map
Bridges	PennDOT	PASDA
Road Closures	PennDOT	PennDOT
National Flood Hazard Layer	FEMA	PASDA
PAMAP Program - 3.2 ft DEM	DCNR PAMAP Program	PASDA
NLCD Land Cover (CONUS)	National Land Cover Database	National Land Cover Database
Scour-Critical Bridge List	PennDOT	PennDOT

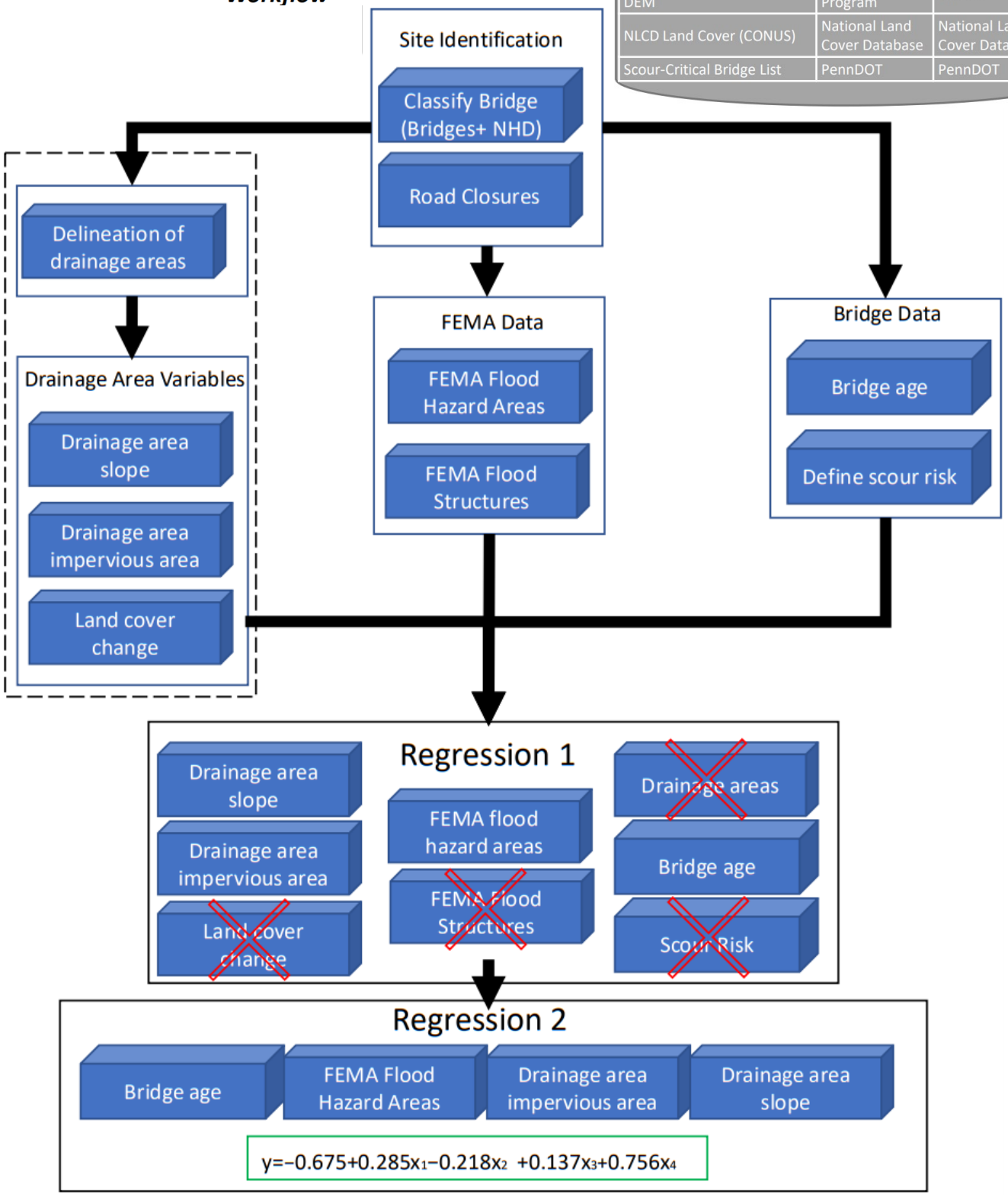

Task 1c Report

1 Introduction

In this subtask we developed a workflow to project areas of flood risk. This was accomplished using a regression analysis. This regression analysis includes criteria that explore the effects that a bridge's attributes, urbanization, stormwater management practices, field-collected data, and natural topography on the associated flooding at bridges. The criteria that will summarize a bridge's attributes are (i) the bridge age and (iii) the location of the bridge within FEMA flood zones. The criteria that summarize the effects of urbanization are (vii) the weighted average of the percent impervious area of the upstream drainage area and (viii) the percent change in land cover of the upstream drainage area. The criteria that summarize the effects of stormwater management practices are (iv) the number of flood control structures within the upstream drainage area and (v) the number of flood obstruction structures within the upstream drainage area, (ix) the scour grade. The criteria that summarize the effects of natural topography are (ii) the upstream drainage area of the bridge and (vi) the average slope of the upstream drainage area. It should be noted that the categorization of the variables is fluid. Each criterion can be summarized by multiple categories. For example, the upstream drainage areas of the bridges can be considered a product of both natural topography and urbanization. Understanding the role that each criterion plays in the analysis is essential. Since flood projection is considered complex and highly variable, incorporating a wide range of variables in the regression analysis aims to identify the variables that contribute most to flood risk.

2 Data and Methods

A regression analysis is completed to locate bridges suspectable to road closures due to flooding considering certain criteria. The criteria used to locate the susceptible bridges are obtained through different datasets and additional spatial analysis completed in ArcGIS Pro. Similar to the process in Task 1b, data cleaning, tidying, pre-processing, and manipulation are exercised to prepare the data for the regression analysis. The project PCS is assigned to NAD 1983 StatePlane Pennsylvania South FIPS 3702 (US Feet). The data used for the analysis in this section is described in Table 2.1. The specific methods of analysis are described in the following sections.

Table 2.1. Summary of the data sources used in the hot spot analysis.

Variable	Creator	Year(s)/Date	Source
USGS NHDPlus HR for 4-digit Hydrologic Unit - 0204	National Hydrology Dataset	2018	United States Geological Survey The National Map
USGS NHDPlus HR for 4-digit Hydrologic Unit - 0205	National Hydrology Dataset	2018	United States Geological Survey The National Map
USGS NHDPlus HR for 4-digit Hydrologic Unit - 0206	National Hydrology Dataset	20018	United States Geological Survey The National Map
PennDOT - Bridges	Pennsylvania Department of Transportation	2022	Pennsylvania Spatial Data Access
PennDOT - Road Closures	Pennsylvania Department of Transportation	2016-2021	Pennsylvania Department of Transportation
National Flood Hazard Layer - Berks County	Federal Emergency Management Agency	2018	Pennsylvania Spatial Data Access
National Flood Hazard Layer - Bucks County	Federal Emergency Management Agency	2019	Pennsylvania Spatial Data Access
National Flood Hazard Layer - Carbon County	Federal Emergency Management Agency	2002	Pennsylvania Spatial Data Access
National Flood Hazard Layer - Chester County	Federal Emergency Management Agency	2021	Pennsylvania Spatial Data Access
National Flood Hazard Layer - Delaware County	Federal Emergency Management Agency	2017	Pennsylvania Spatial Data Access
National Flood Hazard Layer - Lancaster County	Federal Emergency Management Agency	2021	Pennsylvania Spatial Data Access
National Flood Hazard Layer - Lebanon County	Federal Emergency Management Agency	2020	Pennsylvania Spatial Data Access
National Flood Hazard Layer - Lehigh County	Federal Emergency Management Agency	2009	Pennsylvania Spatial Data Access
National Flood Hazard Layer - Montgomery County	Federal Emergency Management Agency	2021	Pennsylvania Spatial Data Access
National Flood Hazard Layer - Northampton County	Federal Emergency Management Agency	2020	Pennsylvania Spatial Data Access
National Flood Hazard Layer - Philadelphia County	Federal Emergency Management Agency	2019	Pennsylvania Spatial Data Access
National Flood Hazard Layer - Schuylkill County	Federal Emergency Management Agency	2021	Pennsylvania Spatial Data Access
PAMAP Program - 3.2 ft Digital Elevation Model	DCNR PAMAP Program	2015	Pennsylvania Spatial Data Access
NLCD 2019 Percent Developed Imperviousness (CONUS)	National Land Cover Database	2019	Multi-Resolution Land Characteristics
NLCD Land Cover (CONUS) All Years	National Land Cover Database	2001-2019	Multi-Resolution Land Characteristics
PennDOT - Scour-Critical Bridge List	Pennsylvania Department of Transportation	2021	Pennsylvania Department of Transportation

2.1 Identifying District 6 Bridges

2.1.1 National Hydrology Dataset (NHD) Flowlines

A shapefile of the NHD flowlines is obtained from Unites States Geological Survey (USGS) The National Map (TNM). The NHD flowlines will enable a selection of bridges that intersect waterways. NHD data is accessible on USGS TNM by a HUC 4 extent. There are three HUC 4s, 0204, 0205, and 0206, that intersect District 6. The three datasets are brought into a new project on ArcGIS Pro (Fig. 3.1). The datasets include a vast amount of data. A flowlines shapefile is attained through the Hydrology folder for each HUC 4. The flowline shapefiles are brought into a

map where the Batch Project Tool is being used to project the shapefiles to the project PCS. The Merge Tool is used to combine the three flowline shapefiles. The NHD flowline dataset includes different types of flowlines. The Select by Attribute Tool is used to select the "StreamRiver", "Coastline", "Artificial Path", "CanalDitch", and "Connector" flowlines from the field named "FType" and create a new shapefile (Fig. 2.1).

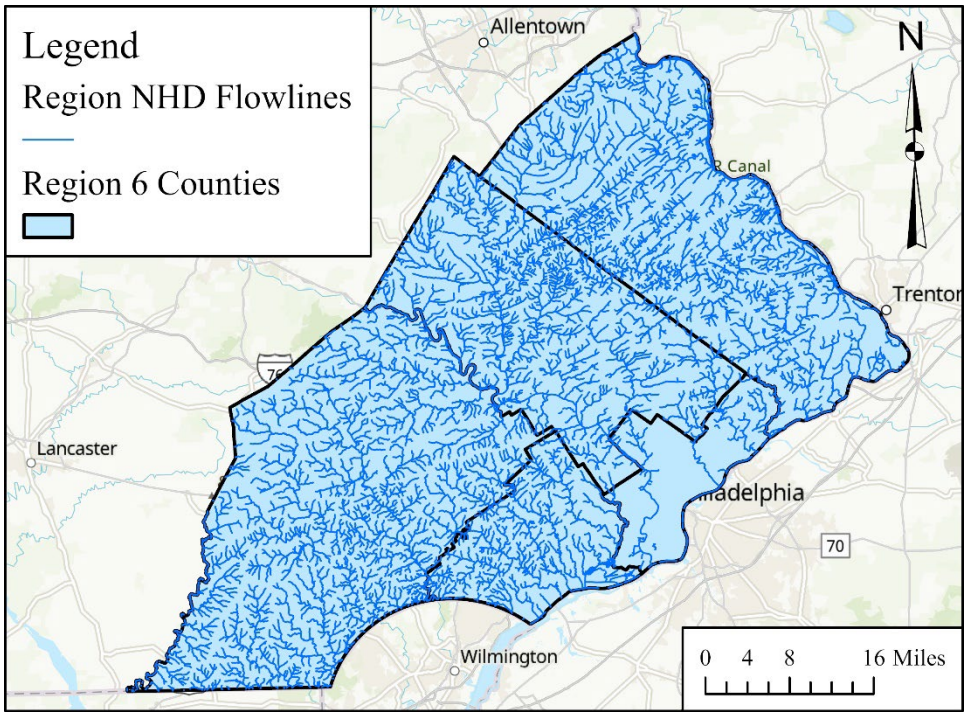

Figure 2.1. NDH flowlines of District 6 PA.

Table 2.2. County Codes for the respective District 6 PA counties.

County Name	County Code
Bucks County	09
Chester County	15
Delaware County	23
Montgomery County	46
Philadelphia County	67

2.1.2 Selection of Bridges Intersecting Waterways

A shapefile of all bridges in Pennsylvania is obtained from PASDA, including bridges that do not intersect waterways. The point shapefile is brought into the ArcGIS Pro project and projected to the project PCS (Fig. 2.2). The respective county codes for each District 6 county are used to select the bridges in District 6 in the "CTY_CODE" field, seen in Table 2.2. The Select by Location Tool is used, with a search extent of 200 feet and assigning the flowlines shapefile as the selecting feature, to select the bridges that intersect waterways. 200 feet is used to consider spatial reference tolerances. A new point shapefile is created containing 3,817 bridges that intersect waterways.

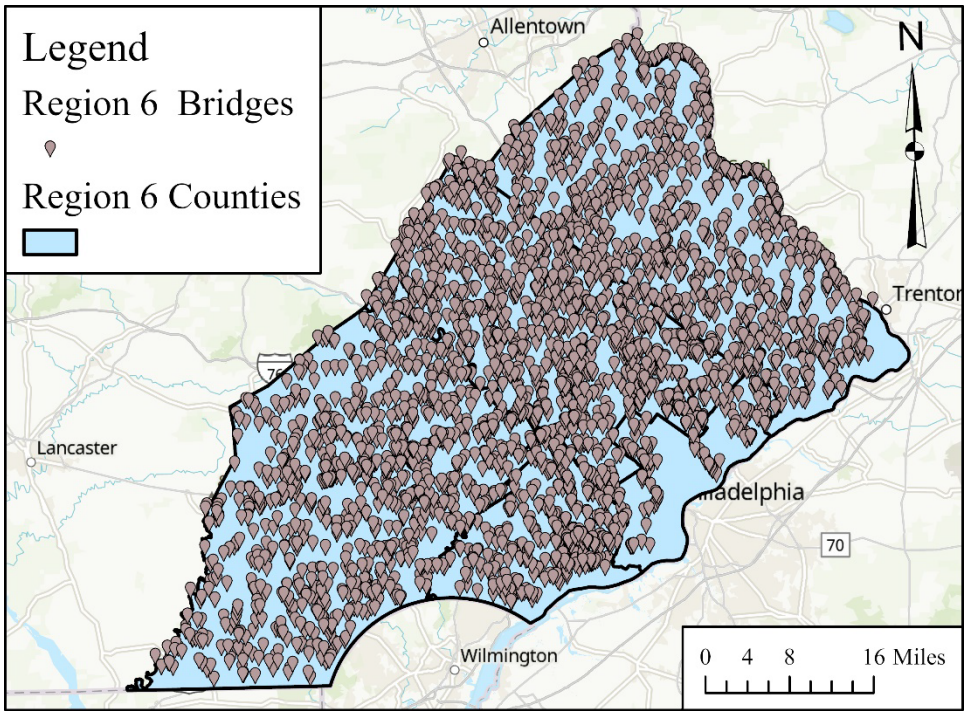

Figure 2.2. Bridges intersecting waterways of District 6 PA.

2.2 Preparations for the Regression Analysis

2.2.1 PennDOT District 6 Road Closures

The road closures shapefiles derived from the hot spot analysis are used to determine the number of road closures due to flooding a bridge experienced. The incident location road closures shapefile, which identifies the exact point of a road closure, and the start and end location road closures shapefile, which identifies the length of a road closure, are spatially joined to the shapefile of the bridges. Two individual spatial joins need to be completed for each road closures shapefile. The incident locations road closures shapefile is joined with the bridges using a search extent of 50 feet. The shapefile produced from the spatial join creates a new field titled "Join_Count", which summarizes the number of incident location road closures at each bridge. The "Join_Count" field is renamed since another join will be completed for the start and end location road closures shapefile, which will also produce a new field titled "Join_Count". The field is renamed to identify the number of start and end location road closures at each bridge.

3.2.2 Delineation of Drainage Areas Upstream of Bridges

ArcGIS Pro has a built-in, ready-to-use Watershed Tool that uses a digital elevation model (DEM), that is stored within the program, to delineate the drainage area of a point feature. The point shapefile on the bridges is used as the input point feature, a snap distance of 200 feet is used, and the bridge ID is assigned as the unique identifier. However, the tool can only handle 1,000 points,

therefore, the 3,817 bridges are separated into four shapefiles and is merged after the tool is run. The Watershed Tool uses a DEM of 30 m by 30 m to produce a polygon shapefile delineating the extent of the upstream drainage area, shown in Figure 2.3. The polygon shapefile produced from the tool is projected to the project PCS. A new field is created, and the Calculate Geometry Tool is used to determine the area in square miles of each drainage area.

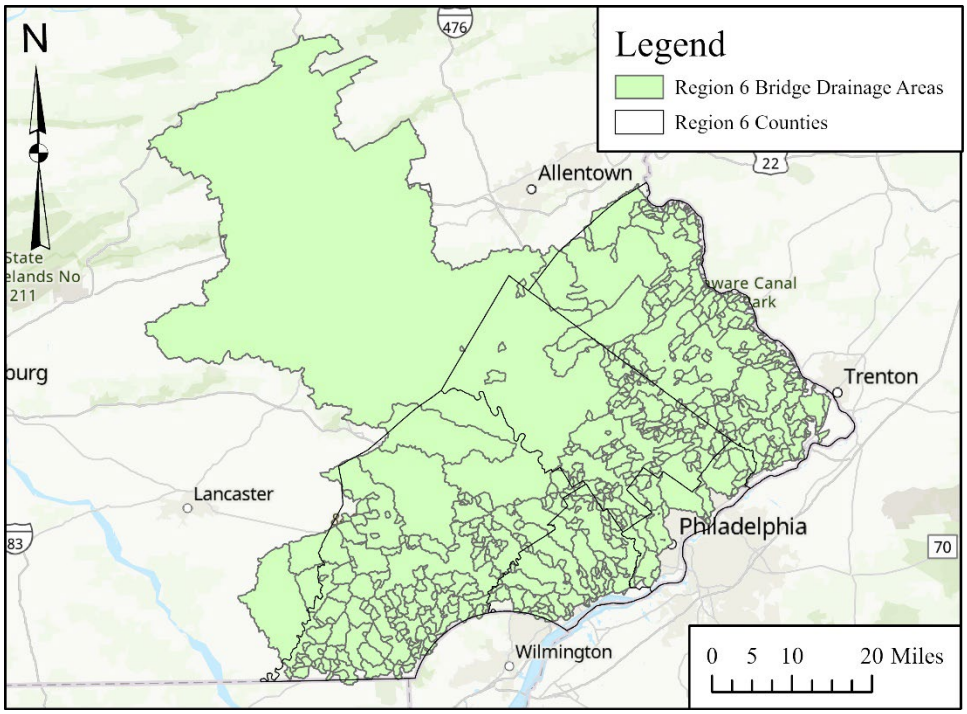

Figure 2.3. Upstream Drainage Area of the bridges in District 6 PA.

2.2.3 Integrating Federal Emergency Management Agency (FEMA) Data

PASDA has a respective FEMA dataset for each county. There are multiple feature classes within the dataset. The regression analysis will consider the flood hazard areas, flood control structures, and flood obstruction structures. The flood hazard areas will be used to identify which flood zone the bridges are within. The flood control and obstruction structures will be used to identify how many of each type of structure is within the upstream drainage area. The point shapefile of the bridges and the polygon shapefile of the drainage areas will be brought into the project.

FEMA Flood Hazard Areas

The flood hazard areas dataset is in the form of a polygon shapefile that classifies areas according to the percent chance of flood hazard titled "S_FLD_HAZ_AR". There are four classifications: area of minimal flood hazard, 0.2% annual chance flood hazard, 1% annual chance flood hazard, and floodway. The FEMA flood hazard areas for the District 6 counties are projected to the project PCS and merged (Fig. 2.4). The Spatial Join Tool is used on the point shapefile of the bridges to identify which flood zone the bridge is located in. The tool creates a new shapefile that includes the flood zone for each bridge, classified in the "ZONE_SUBTY" field.

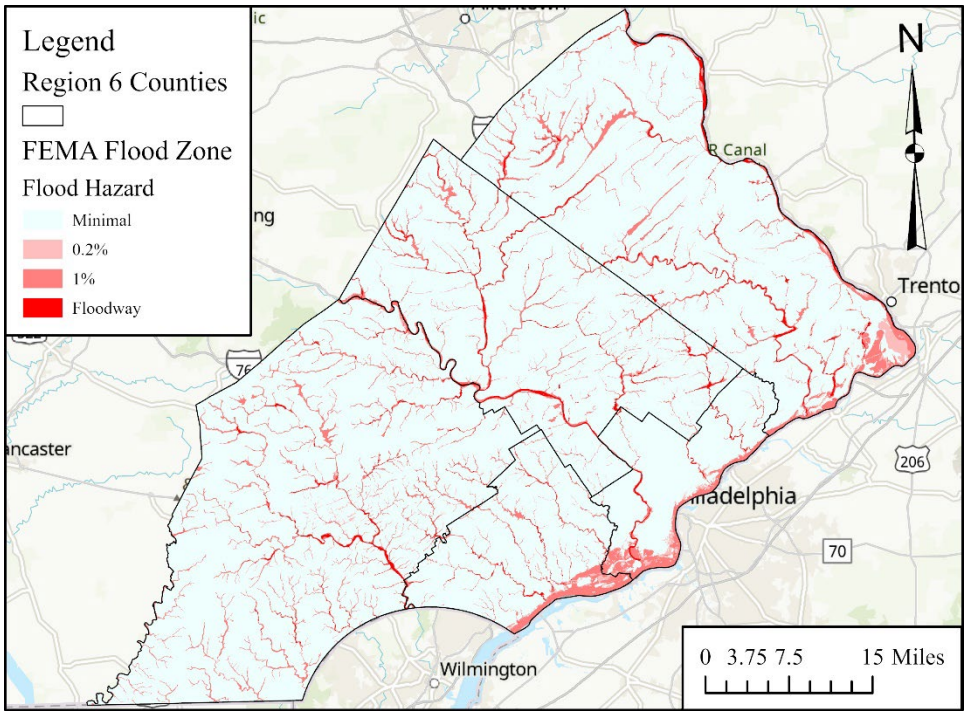

Figure 2.4. FEMA Flood Zones of District 6 PA.

Flood Structures

The drainage areas stretch beyond the District 6 boundaries. Therefore, the FEMA datasets for counties outside of District 6 will need to be obtained. These counties can be determined by importing the PASDA PA Counties shapefile and selecting the counties that intersect the drainage areas. There are twelve counties that are included in the analysis. The counties are Bucks, Berks, Carbon, Chester, Delaware, Lancaster, Lebanon, Lehigh, Montgomery, Philadelphia, and Schuylkill County. After the twelve FEMA datasets are obtained, the shapefile title "S_GEN_STRUCT" for each county is selected bought into the project. The twelve shapefiles are projected to the project PCS and merged (Fig. 2.5).

Table 2.3. Flood structure types separated into controls and obstructions.

Flood Control Structures	**Flood Obstruction Structures**
0.2 PCT Annual Chance Flood Discharge Contained in Structure	Obstruction
1 PCT Annual Chance Flood Discharge Contained in Structure	Canal
Control Structure	Channel
Dam	Culvert
Floodway Contained in Structure	Side Weir Structure
Weir	Wing Wall

Two selections are made to extract different attributes from the field titled "STRUCT_TYP", which represents the structure type. The structure types fall into two categories being flood control structures and flood obstruction structures. Table 2.3 displays the attributes selected for each category. After the selection, the two shapefiles produced from the selection are spatially joined to the polygon shapefile of the drainage area. Two spatial join operations are completed, similar to the process in 3.2.1 PennDOT District 6 Road Closures, to identify the fields that are associated with the number of flood control structures and the number of flood obstruction structures.

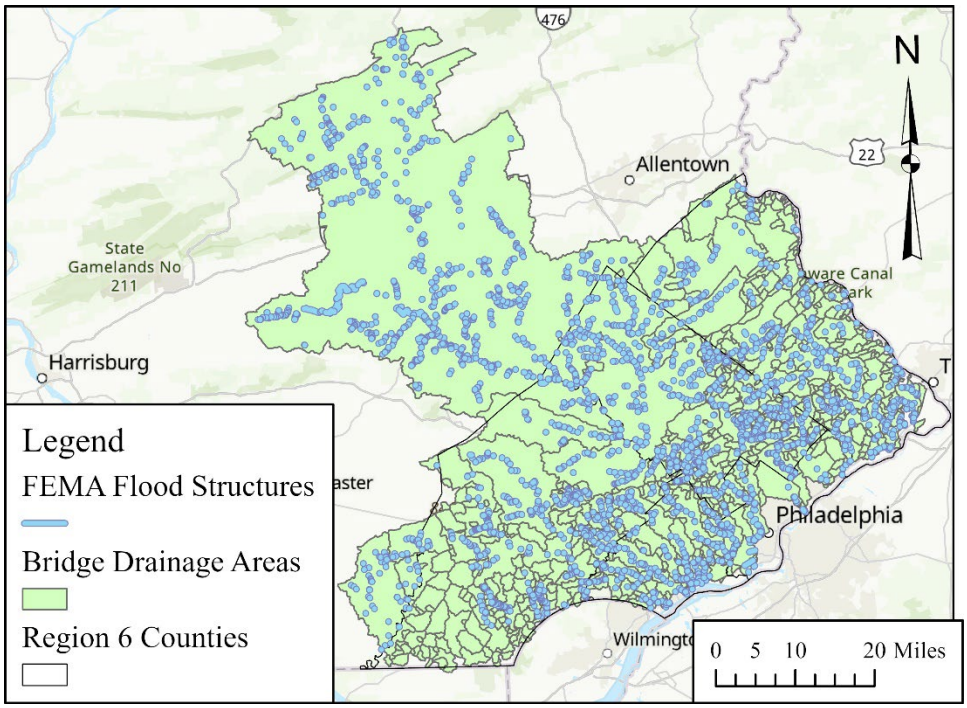

Figure 2.5. FEMA Flood Control Structure in within the upstream drainage areas of bridges that intersect waterways.

2.2.4 Slope of the Upstream Drainage Areas

A 3m-by-3m DEM from 2015 in the form of a raster is available on PASDA. The DEMs can be extracted by county mosaics and have a PCS of NAD 1983 StatePlane Pennsylvania South FIPS 3702 (US Feet) (Fig. 2.6). Mosaic DEMs for the counties listed in 3.2.2.2 FEMA - Flood Structures will be used to cover the extent of all drainage areas. The Mosaic to New Raster Tool is used to merge the rasters of the twelve counties. The mosaic raster is run through the Fill Tool to smooth and remove any disturbances in the raster. Once the raster is cleaned, the Slope Tool will be used to calculate the slope across the raster. The Zonal Statistics to Table Tool is used to summarize the average slope of each drainage area, with an output measurement of percent rise. A table join is completed on the resulting table with the shapefile of the drainage areas.

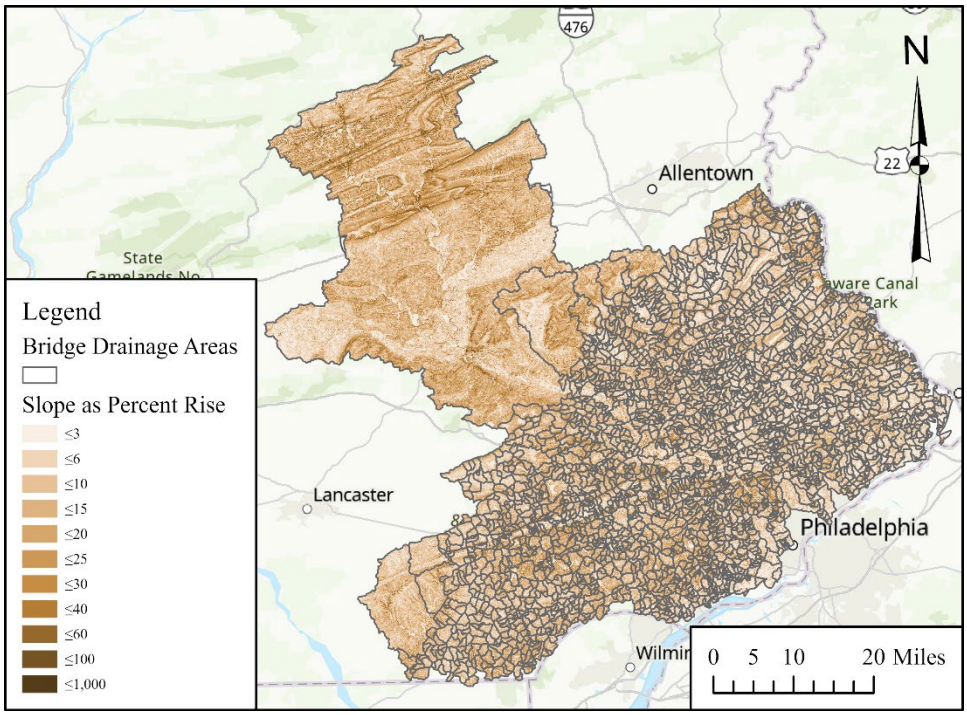

Figure 2.6. Slope raster derived from a 3 m by 3 m DEM of the upstream drainage areas of the bridges that intersect waterways.

2.2.5 National Land Cover Dataset (NLCD)

Raster data obtained from the NLCD is used to incorporate and analyze the effects of urbanization. The analysis will incorporate the 2019 NLCD Percent Impervious raster and 2016 and 2019 NLCD Land Cover rasters and are observed within the upstream drainage area of the bridges. The rasters are obtained from Multi-Resolution Land Characteristics (MRLC) consortium and are brought into the project. The rasters have a resolution of 30 m by 30 m and have a PCS of Albers Conical Equal Area. The rasters are not projected to the project PCS. Projecting rasters can lead to distortions and recalculations of cell value causing discrepancies in results. Therefore, the shapefile of the drainage areas is projected to Albers Conical Equal Area for analysis. The rasters cover the entire United States, so the Clip Raster Tool is used to make the raster more manageable. The projected polygon shapefile of the drainage area is used as the clipping geometry.

2019 NLCD Percent Impervious

Each cell of the percent impervious raster indicates precent impervious area a 30 m by 30 m cell (Fig. 3.7). A weighted average of the percent impervious is found for each drainage area to describe the nature of the upstream drainage area of a bridge. Following the pre-processing of the rasters, the Summarize Categorical Raster Tool is used to produce a table that summarizes the number of cells by its percent of imperviousness, using the polygon shapefile of the drainage areas as the

areas of interest. The Table to Excel Tool is used to export the summarized table to an Excel file. The weighted average is calculated using Equation 1.

$$W = \frac{\sum_{i=0}^{n}(w_i \cdot X_i)}{\sum_{i=0}^{n}(w_i)} \qquad \textbf{Equation 1}$$

The weighted average of percent impervious, W, is calculated for each drainage area, where n represents the number of terms to be averaged, w represents the percent of a group, and X represents the number of pixels per group. The table produced from the tool groups the number of pixels for each percent from zero to 100. The weighted average of percent impervious is assigned to each bridge ID and brought back to the ArcGIS Pro. The Table Join is used with the shapefile of the drainage areas using the bridge ID as the unique identifier.

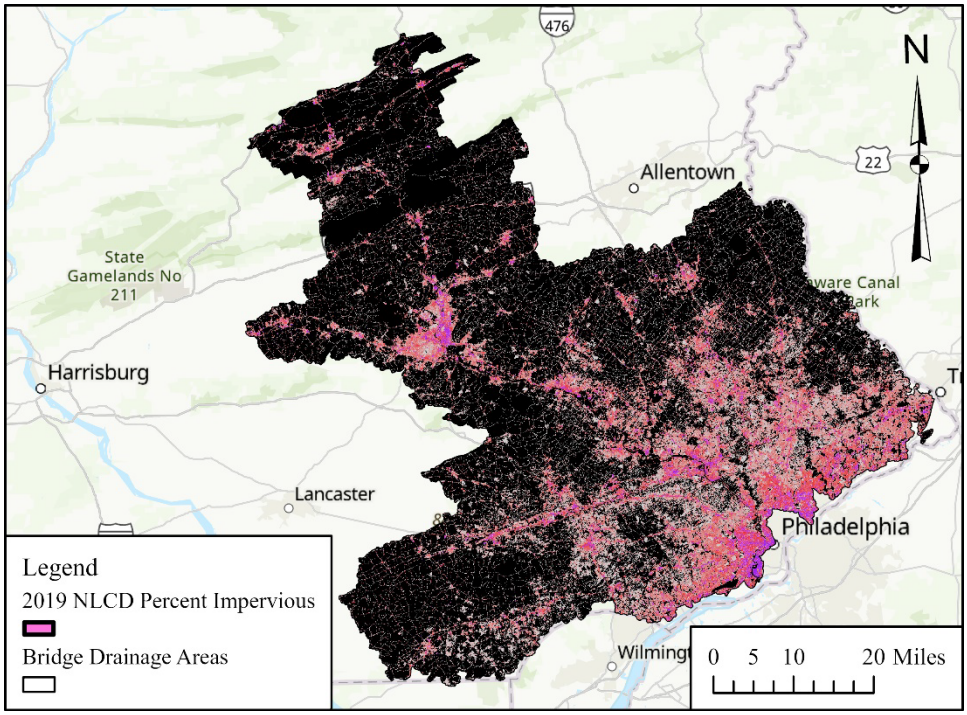

Figure 2.7. 2019 NLCD percent impervious for the upstream drainage areas of bridges that intersect waterways.

2016 and 2019 NLCD Land Cover

The land cover rasters are used to see how the landscape has developed from 2016 to 2019. The rasters for 2016 and 2019 share the same raster properties. The Minus Tool is used on both rasters to identify the cells that changed between the three-year time steps. The raster produced from the Minus Tool assigns a value of zero to the cells that did not change and assigns a value of less than or greater than to the cells that change. The Reclassify Tool is used to reclass a group of cells. The cells that have a value less than or greater than zero are reclassed to have a value of 1 (Fig. 2.8). The Zonal Statistic as Table Tool is used on the raster that experienced the reclass of values. The tool will determine the sum of the cell values and the shapefile of the drainage areas serves as the

feature zone data. Since the values of the cells that changed are reclassed to one, the sum will portray the total number of cells that change.

From the table produced, a new field is created to determine the percentage of cells that change from 2016 to 2019. The Calculate Field Tool is used to compute the percentage. The value of 100 is being multiplied by the "SUM" field, which computes the sum of the number of cells that change, and that is divided by the "COUNT" field, which is the total number of cells. After the percent of land change is calculated, the percent change of land cover table will be joined to the shapefile of the drainage areas. Once the percent change of land cover of each drainage area is added to the shapefile of the drainage areas, a final table join is run to attach all the data relating to the drainage area to the shapefile of the bridges that intersect waterways.

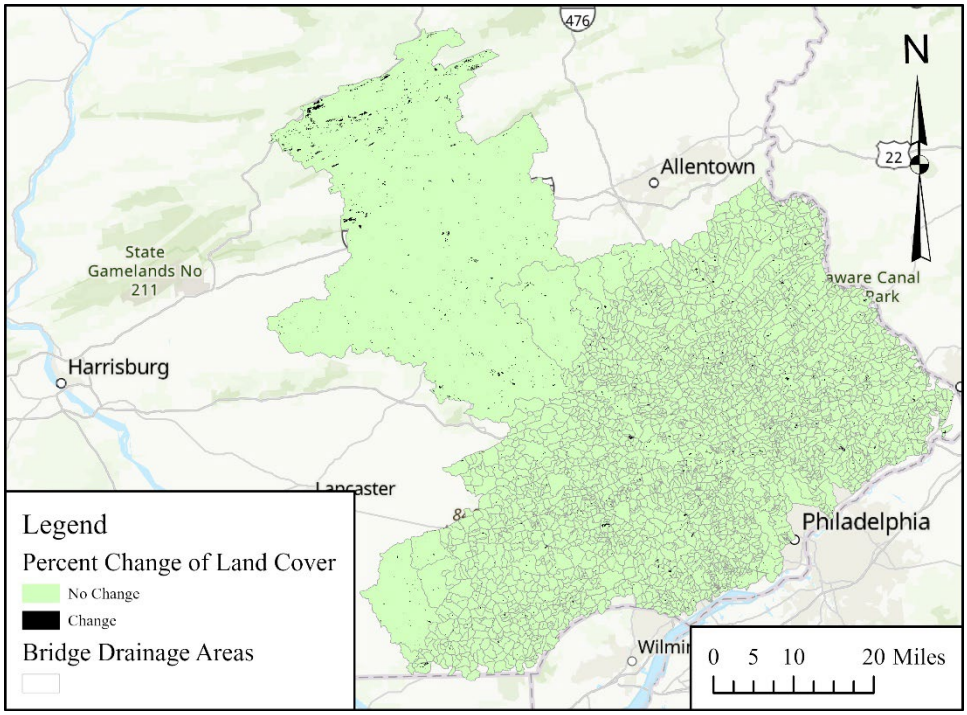

Figure 2.8. 2016 to 2019 percent change of land cover from the NLCD of the upstream drainage areas of the bridges that intersect waterways.

2.2.6 PennDOT Scour-Critical Bridges

PennDOT provided a list of 865 scour-critical bridges from August 2021. The scour critical list includes a grade corresponding to the scour level, determined from inspections and field observations. The bridges on the list include a bridge ID which can be used to join the data with the shapefile of the bridges that intersect waterways (Fig. 2.9).

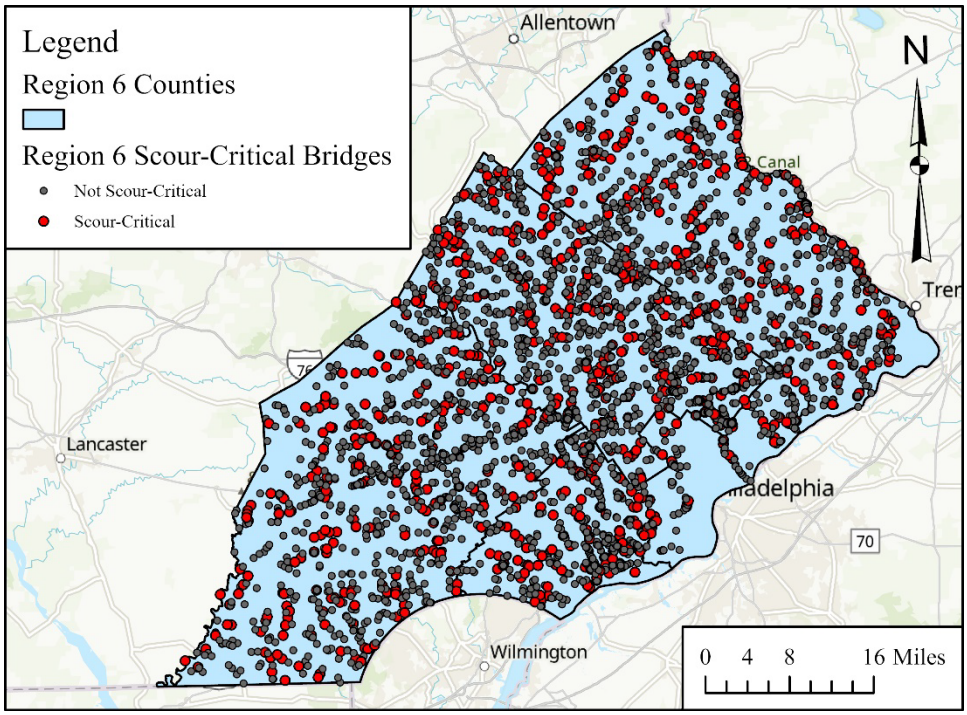

Figure 3.9. Scour-critical bridges in District 6 PA.

2.2.7 PennDOT Bridge Age

The Pennsylvania bridge shapefile from PASDA, includes many attributes to describe each bridge. The construction year of a bridge and most recent year of construction on a bridge will be used to determine the bridge age. From the shapefile of the bridges that intersect waterways, a new field is created. The maximum year of the two attributes is selected, using the Calculate Field Tool, for the new field. Another field is created to define a bridge age, which is the present year minus the maximum year of the two attributes (Fig. 2.10). This action is completed using the Calculate Field tool.

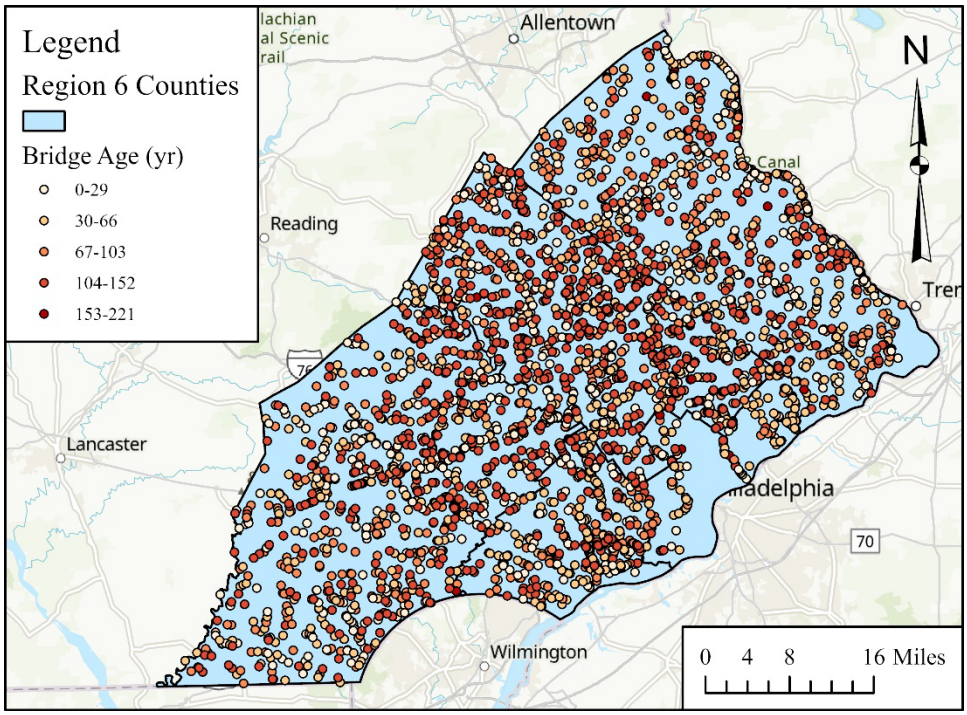

Figure 2.10. Age of the bridges in District 6 PA.

2.3 Regression Analysis

As stated, there are 3,817 bridges within District 6 to be used for the regression analysis. The regression analysis aims to identify which variables of the ten derived variables contribute most surface water flooding at bridges. Since the road closures due to flooding data are serving as a proxy for flooding, the y-variable of the regression is assigned as the number of road closures. The x-variables included are (i) the bridge age, (ii) the upstream drainage area of the bridge, (iii) the location of the bridge within FEMA flood zones, (iv) the number of flood control structures within the upstream drainage area, (v) the number of flood obstruction structures within the upstream drainage area, (vi) the average slope of the upstream drainage area, (vii) the weighted average of the percent impervious area of the upstream drainage area, (viii) the percent change in land cover of the upstream drainage area, (ix) and the scour grade. After spatial analysis is completed to join all the data for each to the shapefile of the bridges that intersect waterways, the Table to Excel Tool is used to extract the table from AcrGIS Pro and format it as an Excel File. Once in excel, additional manipulations are made to the data before the Regression Tool in the Analysis ToolPak can be run.

Table 2.4. Reclass values assigned to data attributes.

	Label	Reclass Value
FEMA Flood Zones	Floodway	1
	1% annual chance flood hazard	0.67
	0.2% annual chance flood hazard	0.33
	Area of minimal flood hazard	0
Scour Grade	A	1
	B	0.67
	C	0.33
	D/ Not included on list	0

2.3.1 Reclass of Data

The data from the location of the bridges within the FEMA flood zones and the scour grade of the bridges are reclassed on a zero to one scale. Table 2.4 defines the values that are assigned to the data for reclassification. For the FEMA flood zones, there is a respective risk of flooding occurring depending on the flood zone. A value of 1 will signify the greatest risk. The floodway is a designated location for water to accumulate, therefore a reclass value of one is assigned. The 1% annual chance flood hazard identifies the areas that will be inundated during a 100-yr storm, which is a lesser risk than the floodway but still a greater risk than the 0.2% annual chance so a reclass value of 0.67 is assigned. The 0.2% annual chance flood hazard identifies the areas that will be inundated during a 500-yr storm, which is a lesser risk than a 1% annual chance but a greater risk than a location designated as an area of minimal flood hazard so a reclass value of 0.33 is assigned. The locations designated as an area of minimal flood hazard are considered to not be inundated for a 500-yr storm, which is assigned a reclass value of zero since it has the least chance of happening.

Table 2.5. PennDOT Scour Grade Legend

Scour Grade	Scour Description
A	Inspect all bridges for flood damage where a significant flooding event was experienced. Bridges in this category that have been closed due to approach roadway or bridge overtopping or pressure flow must be inspected for flood damage before reopening to traffic. Inspect once every 4 hours.
B and C	Inspect all bridges for flood damage where a significant flooding event was experienced or if the bridge has been closed due to either approach roadway or bridge overtopping or pressure flow must be inspected for flood damage before reopening to traffic. B - Inspect once every 12 hours. C - Inspect once every 24 hours.
D	Inspect for flood damage after each significant flooding event or if the bridge has been closed due to overtopping or pressure flow.

Table 2.5 defines the parameters for assigning a scour grade. The reclass values are based on an inspection performance. A bridge with a higher inspection rate will be assigned a higher reclass

value. Scour grade D is grouped with bridges that are not on the list since there is not a required periodic inspection.

2.3.2 Data Distributions

Of the data that is not reclassed, there is a varied range of the data for each criterion. To produce a regression equation that is not too influenced by one variable, distributions are applied to the data.

$$x' = \log(x_i) \qquad \textbf{Equation 2}$$

$$x' = \frac{\max(x) - x_i}{\max(x)} \qquad \textbf{Equation 3}$$

In Excel, two types of distributions are applied to each variable. The log distribution is seen in Equation 2, and the normal distribution is seen in Equations 3. The raw data is represented as xi and the distributed data is represented as *x'*. The function *max(x)* represents a variable's maximum value.

The Histogram Tool in the Analysis Toolpak is used to display the distribution of each variable. The tool produces plots of the frequency of data within assigned bins. The performance of each distribution is visually analyzed and enables identifying which distribution best fits a variable. The variables that are identified to best fit a log distribution are (ii) the upstream drainage area of the bridge, (vi) the average slope of the upstream drainage area, (vii) the weighted average of the percent impervious, and the variables that best fit a normal distribution are (i) the bridge age, (iv) the number of flood control structures within the upstream drainage area, (v) the number of flood obstruction structures within the upstream drainage area, and (viii) the percent change in land cover.

After appropriate distributions are applied to the variables, the Regression Tool in the Analysis ToolPak in Excel is used. The number of road closures is assigned as the y-variable, and the reclassified and distributed x-variables are assigned as the x-variables. A distribution or reclassification is not applied to the number of road closures since it is what is being predicted by the regression analysis. The Regression Tool defines coefficients for each variable to create an equation. The performance of the regression tool can be summarized through two outputs.

The first output that summarizes the performance of the regression is the *Significance F*, which defines the statistical significance. If this value is less than 0.001, then the regression can be considered as reliable. The second output used to gauge the performance of the regression is the *P-Values*, which are assigned values to each x-variable. If the *P-Values* for the associated x-variables are greater than 0.05, then they should not be considered due to lack of correlation within the regression. Multiple iterations of the regression are run removing the x-variables that do not satisfy the *P-Value* limit through each iteration until both performance limits are met.

3 Results and Discussion

The intention of this study is to define a reusable process for predicting a bridge's vulnerability to flooding under given conditions. This is achieved through the regression analysis which produces a linear regression equation. The linear regression equation will predict the number of road closures due to a flooding a bridge will experience. As stated, the road closures due to flooding data serve as a proxy for surface water flooding. Therefore, a bridge predicted to have a greater number of road closures will signify a bridge more susceptible to flooding.

Identifying the conditions that should be considered in the regression relates to the variables that are noted as being the greatest contributors. Those variables are identified through completion of multiple iterations of the regression. It is found that only two iterations are necessary to produce a sufficient *Significance F* and *P-Values*. The variables that remained after the two iterations are (i) the bridge age, (iii) the location of the bridge within FEMA flood zones, (vi) the average slope of the upstream drainage area, (vii) the weighted average of the percent impervious area of the upstream drainage area. The linear regression equation produced from the regression analysis can be seen below in Equation 4.

Table 3.1. The defined coefficients and P-Values of the input variables produced from the regression analysis.

		Coefficients	**P-Values**
b	Intercept	-0.675	1.98 E-11
x_1	Bridge Age	0.285	3.65E-14
x_2	FEMA Flood Zone Score	-0.218	2.05E-09
x_3	Weighted Average of Percent Impervious Area	0.137	2.27E-06
x_4	Average Slope	0.756	5.75E-15

$$y = -0.675 + 0.285x_1 - 0.218x_2 + 0.137x_3 + 0.756x_4 \qquad \textbf{Equation 4}$$

The 3,817 bridges within District 6 are used as the data entries in the regression analysis. The number of road closures due to flooding, a proxy for surface water flooding, is represented in the regression equation as *y*. Table 4.1 displays the coefficients of each variable determined from the regression analysis. The *x* values in the equation are the input values after an applied reclassification or distribution of the respective variables: the bridge age is x_1, the location of the bridge within FEMA flood zones is x_2, the average slope of the upstream drainage area is x_3, the weighted average of the percent impervious area of the upstream drainage area is x_4.

Table 3.1 also lists the *P-Values* of each variable. The *P-Values* are directly related to coefficients. As stated, the *P-Values* describe the associated correlation of a variable to the linear regression equation. Therefore, the lesser *P-Values* will produce a greater positive coefficient or lesser negative coefficient. This behavior is displayed in Table 3.1 when comparing the average slope and weighted average of percent impervious area. Additionally, this concept demonstrates why the variables that have a *P-Value* greater than 0.05 are removed through iterations considering there is seeing slight to no correlation between the variable and results of the linear regression equation. Lastly, this concept helps develop a better understanding of which remaining variables are contributing most to the number of road closures due to flooding after the final iteration has been made.

Table 3.2. Hypothetical values assigned to each parameter for modeling the prediction of number of road closures due to flooding for a bridge.

	Criteria	**Input Values**
x_1	Bridge Age (yr)	6
x_2	FEMA Flood Zone Score	0.00
x_3	Weighted Average of Percent Impervious Area (%)	76.5
x_4	Average Slope (% rise)	16.2
y	Number of Road Closures	0.7771

Using the linear regression equation, a model is created in Excel. The tabular model creates a reusable process to predict the number of road closures due to flooding for any bridge. However, for a proper prediction, the model requires a value for all considered variables. Therefore, the associated data for each variable needs to be collected or available to model it. Table 3.2 displays the tabular model determining the number of road closures for a hypothetical bridge using relative input values for each parameter. Additionally, there are minimum and maximum value limits for each variable. The bridge age and average slope have a minimum value limit of zero but have no maximum value limit. The FEMA flood zone score has a minimum score limit of zero and a maximum score limit of one. The score pertaining to each flood zone is found in Table 3.2. The weighted average of percent impervious area has a minimum value limit of zero and maximum value limit of 100. Data distributions for the bridge age, the weighted average of percent impervious area, and the average slope are integrated in the tabular model.

The performance of the model is assessed through testing different hypothetical values and analyzing the results. The model displayed newer bridges and areas of contained a greater portion of impervious surfaces lead to more road closures due to flooding at bridges. However, the areas

with the greatest average slope contributed most. Additionally, assessing the performance of the model proved that there are capability limits and flaws. The FEMA flood zone input seemed to perform opposite from what was expected. Bridges that are in a more hazardous flood zone are expected to increase the number of road closures due to flooding. Instead, a bridge located in a flood zone, which has a score of one, reduced the likeliness of road closures. The most notable result is the weak maximum output of number of road closures the model can produce under the value limits of the variables. The model is only capable of putting out a maximum of 1.40 road closures. Comparing this value to the actual maximum number of road closures, which is 18 road closures, further outlines the flaws in the model.

4 Conclusion

Of the variables remaining after the final iteration of the regression, the results can signify that urbanization, natural topography, and attributes of bridges are the greatest contributors to flooding at bridges. The polynomial equation, produced by the regression, has an R^2 value of 0.0405. While this is a relatively low correlation, this is unsurprising given the relatively high number of independent variables.

Future work could aid in the further development of the regression analysis. These improvements include applying different distributions that better suit each input allowing for a proper representation of the data. Normal and log distributions were tested on each parameter; however, other parameters may benefit from applying other distributions. Other types of data or parameters could also be tested. Only PennDOT or open data sources were considered. Different variable accuracy and resolution could be tested. Additionally, a different form of regression can be utilized.

In future work on this project the dependent variables will be divided into different classes depending on the type of event leading to the flooding. This will provide further insight into the drivers of flood risk based on physical parameters. It is known that distinct parts of District 6 respond to different types of flood events. Certain neighborhoods flood during intense short rains, while others flood during less intense long rain events, and others rain on snow events. By further breaking down the dependent variables in a regression analysis the physical parameters resulting in flood risk can be better understood.

Task 1 References

Anderson, K., Bennie, J. J., Milton, E. J., Hughes, P. D. M., Lindsay, R., & Meade, R. (2010). Combining LiDAR and IKONOS Data for Eco-Hydrological Classification of an Ombrotrophic Peatland. *Journal of Environmental Quality*, *39*(1), 260–273. https://doi.org/10.2134/jeq2009.0093

Bates, B. C., Kundzewicz, Z. W., Wu, S., & Palutikof, J. P. (2008). *Climate Change and Water*. IPCC Secretariat. http://41.73.194.134/handle/123456789/552

Bernhardt, E. S., Palmer, M. A., Allan, J. D., Alexander, G., Barnas, K., Brooks, S., ... & Sudduth, E. (2005). Synthesizing US river restoration efforts. Science, 308(5722), 636-637.

DCNR PAMAP Program. (2015). *PAMAP Program - 3.2 ft Digital Elevation Model.* Pennsylvania Spatial Data Access. Retrieved January 13, 2021, from https://www.pasda.psu.edu/uci/DataSummary.aspx?dataset=41.

Deryugina, T. (2017). The Fiscal Cost of Hurricanes: Disaster Aid versus Social Insurance. *American Economic Journal: Economic Policy*, *9*(3), 168–198. https://doi.org/10.1257/pol.20140296

Du, S., Shi, P., van Rompaey, A., & Wen, J. (2015). Quantifying the impact of impervious surface location on flood peak discharge in urban areas. *Natural Hazards*, *76*(3), 1457–1471. https://doi.org/10.1007/s11069-014-1463-2

Elmqvist, T., Fragkias, M., Goodness, J., Güneralp, B., Marcotullio, P. J., McDonald, R. I., Parnell, S., Schewenius, M., Sendstad, M., Seto, K. C., Wilkinson, C., & McDonald, R., I. (2013). *Urbanization, Biodiversity and Ecosystem Services: Challenges and Opportunities: A Global Assessment* (2013th ed.). Springer. https://doi.org/10.1007/978-94-007-7088-1

Farmer, W. H., J. E. Kiang, T. D. Feaster, and K. Eng, "Regionalization of surface-water statistics using multiple linear regression," Techniques and Methods 4-A12, U.S. Department of the Interior, 2019.

Federal Emergency Management Agency. (2002). *National Flood Hazard Layer - Carbon County*. Pennsylvania Spatial Data Access. Retrieved January 13, 2021, from https://www.pasda.psu.edu/uci/DataSummary.aspx?dataset=2284.

Federal Emergency Management Agency. (2009). *National Flood Hazard Layer - Lehigh County*. Pennsylvania Spatial Data Access. Retrieved January 13, 2021, from https://www.pasda.psu.edu/uci/DataSummary.aspx?dataset=2290.

Federal Emergency Management Agency. (2017). *National Flood Hazard Layer - Delaware County*. Pennsylvania Spatial Data Access. Retrieved January 13, 2021, from https://www.pasda.psu.edu/uci/DataSummary.aspx?dataset=2309.

Federal Emergency Management Agency. (2018). *National Flood Hazard Layer - Berks County*. Pennsylvania Spatial Data Access. Retrieved January 13, 2021, from https://www.pasda.psu.edu/uci/DataSummary.aspx?dataset=2283.

Federal Emergency Management Agency. (2019). *National Flood Hazard Layer - Bucks County*. Pennsylvania Spatial Data Access. Retrieved January 13, 2021, from https://www.pasda.psu.edu/uci/DataSummary.aspx?dataset=2274.

Federal Emergency Management Agency. (2019). *National Flood Hazard Layer - Philadelphia County*. *Pennsylvania Spatial Data Access. Retrieved January 13, 2021, from https://www.pasda.psu.edu/uci/DataSummary.aspx?dataset=2294*.

Federal Emergency Management Agency. (2020). *National Flood Hazard Layer - Lebanon County*. Pennsylvania Spatial Data Access. Retrieved January 13, 2021, from https://www.pasda.psu.edu/uci/DataSummary.aspx?dataset=2288.

Federal Emergency Management Agency. (2020). *National Flood Hazard Layer - Northampton County*. *Pennsylvania Spatial Data Access. Retrieved January 13, 2021, from https://www.pasda.psu.edu/uci/DataSummary.aspx?dataset=2293*.

Federal Emergency Management Agency. (2021). *National Flood Hazard Layer - Chester County*. Pennsylvania Spatial Data Access. Retrieved January 13, 2021, from https://www.pasda.psu.edu/uci/DataSummary.aspx?dataset=2277.

Federal Emergency Management Agency. (2021). *National Flood Hazard Layer - Lancaster County.* Pennsylvania Spatial Data Access. Retrieved January 13, 2021, from https://www.pasda.psu.edu/uci/DataSummary.aspx?dataset=2289.

Federal Emergency Management Agency. (2021). *National Flood Hazard Layer - Montgomery County*. Pennsylvania Spatial Data Access. Retrieved January 13, 2021, from https://www.pasda.psu.edu/uci/DataSummary.aspx?dataset=2292.

Federal Emergency Management Agency. (2021). *National Flood Hazard Layer - Schuylkill County*. *Pennsylvania Spatial Data Access. Retrieved January 13, 2021, from https://www.pasda.psu.edu/uci/DataSummary.aspx?dataset=2376*.

Finkenbine, J. K., Atwater, J. W., & Mavinic, D. S. (2000). STREAM HEALTH AFTER URBANIZATION. *Journal of the American Water Resources Association*, *36*(5), 1149–1160. https://doi.org/10.1111/j.1752-1688.2000.tb05717.x

Frame, J., Nearing, G., Kratzert, F., & Rahman, M. (2020). Post processing the US national water model with a long short-term memory network. J. Am. Water Resour. As., https://doi. org/10.31223/osf. io/4xhac, in review.

Hammond, M. J., Chen, A. S., Djordjević, S., Butler, D., & Mark, O. (2015). Urban flood impact assessment: A state-of-the-art review. Urban Water Journal, 12(1), 14-29.

Hanssen, F.; May, R.; van Dijk, J.; Rød, J.K. (2018). Spatial Multi-Criteria Decision Analysis Tool Suite for Consensus-Based Siting of Renewable Energy Structures. J. Environ. Assess. Policy Manag. 20, 1840003.

Hayhoe, K., Wake, C., Anderson, B., Liang, X. Z., Maurer, E., Zhu, J., Bradbury, J., DeGaetano, A., Stoner, A. M., & Wuebbles, D. (2007). Districtal climate change projections for the Northeast USA. *Mitigation and Adaptation Strategies for Global Change*, *13*(5–6), 425–436. https://doi.org/10.1007/s11027-007-9133-2

Henonin, J., Russo, B., Mark, O., & Gourbesville, P. (2013). Real-time urban flood forecasting and modelling–a state of the art. Journal of Hydroinformatics, 15(3), 717-736.

Hosseiny, H., Nazari, F., Smith, V., & Nataraj, C. (2020). A framework for modeling flood depth using a hybrid of hydraulics and machine learning. Scientific Reports, 10(1), 1-14.

Ismail-Zadeh, A.T.; Cutter, S.L.; Takeuchi, K.; Paton, D. (2017). Forging a paradigm shift in disaster science. Nat. Hazards, 86, 969–988.

Jung, I. W., Chang, H., & Moradkhani, H. (2011). Quantifying uncertainty in urban flooding analysis considering hydro-climatic projection and urban development effects. *Hydrology and Earth System Sciences*, *15*(2), 617–633. https://doi.org/10.5194/hess-15-617-2011

Knutson, T. (2021, August). *Global Warming and Hurricanes: An Overview of Recent Research Results*. NOAA Geophysical Fluid Dynamics Laboratory. https://www.gfdl.noaa.gov/global-warming-and-hurricanes/#:~:text=However%2C%20using%20the%20CMIP3%20and,general%20agreement%20with%20previous%20studies.

Leopold, L. B. (1968). Hydrology for urban land planning: A guidebook on the hydrologic effects of urban land use (Vol. 554). US Geological Survey.

Makropoulos, C., & Savić, D. A. (2019). Urban hydroinformatics: past, present and future. Water, 11(10), 1959.

Marzocchi, W.; Garcia-Aristizabal, A.; Gasparini, P.; Mastellone, M.; Ruocco, A. (2012). Basic principles of multi-risk assessment: A case study in Italy. Nat. Hazards, 62, 551–573.

Masoner, J. R., Kolpin, D. W., Cozzarelli, I. M., Barber, L. B., Burden, D. S., Foreman, W. T., Forshay, K. J., Furlong, E. T., Groves, J. F., Hladik, M. L., Hopton, M. E., Jaeschke, J. B., Keefe, S. H., Krabbenhoft, D. P., Lowrance, R., Romanok, K. M., Rus, D. L., Selbig, W. R., Williams, B. H., & Bradley, P. M. (2019). Urban Stormwater: An Overlooked Pathway of Extensive Mixed Contaminants to Surface and Groundwaters in the United States. *Environmental Science & Technology*, *53*(17), 10070–10081. https://doi.org/10.1021/acs.est.9b02867

Melville, B. W., & Coleman, S. E. (2000). *Bridge Scour*. Water Resources Publications, LLC.

Merz, B., Hall, J., Disse, M., & Schumann, A. (2010). Fluvial flood risk management in a changing world. *Natural Hazards and Earth System Sciences*, *10*(3), 509-527.

Mignot, Emmanuel, Xuefang Li, and Benjamin Dewals. "Experimental modelling of urban flooding: A review." Journal of Hydrology 568 (2019): 334-342.

Miller, J. D., & Hutchins, M. (2017). The impacts of urbanization and climate change on urban flooding and urban water quality: A review of the evidence concerning the United Kingdom. Journal of Hydrology: Regional Studies, 12, 345-362.

National Land Cover Database. (2001-2019). *NLCD Land Cover (CONUS) All Years*. Multi-Resolution Land Characteristics. Retrieved January 13, 2021, from https://www.mrlc.gov/data/nlcd-land-cover-conus-all-years.

National Land Cover Database. (2019). *NLCD 2019 Percent Developed Imperviousness (CONUS)*. Multi-Resolution Land Characteristics. Retrieved January 13, 2021, from https://www.mrlc.gov/data/nlcd-2019-percent-developed-imperviousness-conus.

National Oceanic and Atmospheric Administration. (2021). *Hurricane Costs*. NOAA: Office for Coastal Management. Retrieved December 14, 2021, from https://coast.noaa.gov/states/fast-facts/hurricane-costs.html

Park, S., Smith, V., & Hyde, A. (2021). Practices for Integrated Flood Prediction and Response Systems (No. NCHRP Project 20-05, Topic 51-10).

Pennsylvania Department of Transportation. (2022). *Pennsylvania county boundaries*. Pennsylvania Spatial Data Access. Retrieved January 13, 2021, from https://www.pasda.psu.edu/uci/DataSummary.aspx?dataset=24.

Pennsylvania Department of Transportation. (2016-2021). *PennDOT - Road Closures*. Pennsylvania Department of Transportation.

Pennsylvania Department of Transportation. (2021). *PennDOT - Scour-Critical Bridge List*. Pennsylvania Department of Transportation.

Pennsylvania Department of Transportation. (2022). *PennDOT – Bridges*. Pennsylvania Spatial Data Access. Retrieved January 13, 2022, from https://www.pasda.psu.edu/uci/DataSummary.aspx?dataset=35.

Pennsylvania Department of Transportation. (2022). *Pennsylvania local roads*. Pennsylvania Spatial Data Access. Retrieved January 13, 2022, from https://www.pasda.psu.edu/uci/DataSummary.aspx?dataset=1038.

Pennsylvania Department of Transportation. (2022). *Pennsylvania state roads*. Pennsylvania Spatial Data Access. Retrieved January 13, 2022, from https://www.pasda.psu.edu/uci/DataSummary.aspx?dataset=54.

Pennsylvania Department of Transportation. (2022). *Pennsylvania municipality boundaries*. Pennsylvania Spatial Data Access. Retrieved January 13, 2022, from https://www.pasda.psu.edu/uci/DataSummary.aspx?dataset=41.

Scannell, J. P., & Baribault, M. K. (2010). *Georgia DOT's Implementation of BridgeWatch*. International Conference on Scour and Erosion (ICSE-5). https://ascelibrary.org/doi/abs/10.1061/41147%28392%2992

Schifman, L. A., Herrmann, D. L., Shuster, W. D., Ossola, A., Garmestani, A., & Hopton, M. E. (2017). Situating Green Infrastructure in Context: A Framework for Adaptive Socio-Hydrology in Cities. *Water Resources Research*, *53*(12), 10139–10154. https://doi.org/10.1002/2017wr020926

Shade, C., & Kremer, P. (2019). Predicting Land Use Changes in Philadelphia Following Green Infrastructure Policies. *Land*, *8*(2), 28. https://doi.org/10.3390/land8020028

Suarez, Pablo, William Anderson, Vijay Mahal, and T. R. Lakshmanan. (2005). "Impacts of flooding and climate change on urban transportation: A systemwide performance assessment of the Boston Metro Area." Transportation Research Part D: transport and environment 10, no. 3: 231-244.

U.S. Census Bureau (2010). Urban-Rural Populations. Retrieved from http://www.census.gov/geo/reference/ua/urban-rural-2010.html.

United States Geological Survey. (2018). *NHDPlus HR for 4-digit Hydrologic Unit – 0204*. USGS The National Map. Retrieved January 13, 2021, from https://apps.nationalmap.gov/downloader/#/.

United States Geological Survey. (2018). *NHDPlus HR for 4-digit Hydrologic Unit - 0205*. USGS The National Map. Retrieved January 13, 2021, from https://apps.nationalmap.gov/downloader/#/.

United States Geological Survey. (2018). *NHDPlus HR for 4-digit Hydrologic Unit - 0206*. USGS The National Map. Retrieved January 13, 2021, from https://apps.nationalmap.gov/downloader/#/.

Veilleux, A. G., T. A. Cohn, K. M. Flynn, R. R. Mason, and P. R. Hummel, (2014). Estimating magnitude and frequency of floods using the PeakFQ 7.0 program, Fact Sheet.

Vercruysse, K., Dawson, D. A., Glenis, V., Bertsch, R., Wright, N., & Kilsby, C. (2019). Developing spatial prioritization criteria for integrated urban flood management based on a source-to-impact flood analysis. *Journal of Hydrology*, *578*, 124038. https://doi.org/10.1016/j.jhydrol.2019.124038

Xu, C., Liu, Z., Chen, Z., Zhu, Y., Yin, D., Leng, L., Jia, H., Zhang, X., Xia, J., & Fu, G. (2021). Environmental and economic benefit comparison between coupled grey-green infrastructure system and traditional grey one through a life cycle perspective. *Resources, Conservation and Recycling*, *174*, 105804. https://doi.org/10.1016/j.resconrec.2021.105804

Zirkle, J., Reese, L., & Claman, D. (2014, January). *Implementation of BridgeWatch™: A Program for Monitoring Scour Critical and Unknown Foundation Bridges; Using*

BridgeWatch to Monitor Road Overtopping [Conference Presentation]. National Hydraulic Engineering Conference 2014, Iowa City, Iowa. https://pubs.lib.uiowa.edu/nhec/article/id/27575/

Task 2 Executive Summary

In the report we present the results from project **Task 2: To review techniques to deploy Lidar, near IR, and drones to identify flood inundation**. This was accomplished by conducting the following:

a. Evaluation of the limitations of deployment using desk and field studies.

b. Establishment of a workflow for different intensities of land use.

In support of these two areas of work, we explored:

1) *The use of drones in stormwater management:* Drones have evolved into turnkey type tools that can easily be obtained, modified, and deployed for a broad range of tasks. Drone based sensing systems provide a way to obtain localized, high-resolution data without the need for relative more expensive and complex airplane or satellite imagery. While drone use for recreation is lightly regulated, any non-leisure use of drones must comply with FAA regulations including that the main Pilot in Command (PIC) holding a current Part 107 certificate (Drone Pilot's License) and that Drones are required to be registered regardless of weight. Based on this study, the use of Drones shows great promise for use in flood management, damage assessment, prediction, etc., especially when coupled with the right sensors.

2) *Multispectral imaging:* Multispectral cameras capture images using several lenses and sensors, allows different ranges of wavelengths of light to be separated into separate images. This provides much more data than typical visible spectrum imaging. With the addition of partially visible or invisible bands, the images can be used to calculate indices for vegetation heath, soil, water and more. In this report, we show that different indices can be applied to aerial multispectral imagery to identify standing water, plant cover/health, and to differentiate between different surface types. This makes multispectral imaging a promising tool for flood mitigation.

3) *Lidar*: Lidar enables the collection of 3D models of physical objects and locations through the use of puled laser light. Lidar systems have found a broad range of application in flood-related disciplines like stormwater management. In this report, examples of both aerial and terrestrial Lidar are discussed that show the potential for Lidar's use in flood mitigation. Of specific interest is the emerging iPhone based Lidar system that enables high resolution digital modeling of physical objects or locations with a device that can fit in your pocket.

All aspects of our use of drones for data collection, the sensors that were used and the processing and visualization methods used are discussed in the report. Data was collected during flights at flood-prone PADOT sites.

Task 2a Summary

In this task we evaluate the limitations of deployment using desk and field studies of drone and drone-based sensors, specifically multispectral cameras and Lidar. Globally, there has been a proliferation of drone use for a broad range of situations, including applications that have direct relevance to the Pennsylvania Department of Transportation (PADOT), such as highway inspection and maintenance, vegetation health monitoring, and, in general, visual inspection of most any site. These systems consist of two primary components, the drone itself and the sensor (which could be a camera) that collects the information. These technologies have evolved into turnkey solutions capable of collecting high-resolution, localized data that can directly be used to support planning decisions. Thus, drone systems should be considered for inclusion in the standard set of tools for maintenance and inspection teams.

Specific technologies on which this report focuses include drones and two sensors that are particularly relevant, multispectral imaging and Lidar. On overview of each subsection is presented below:

In task 2a, a brief literature review covering drones, multispectral cameras, and Lidar is presented, with a specific focus on their use in stormwater management and related fields. This is followed by the results of field studies focused on multispectral imaging and Lidar. The major findings include:

- Drone systems are, indeed, turnkey solutions that can be integrated into field team workflows, although they require official licensing and adherence to FAA regulations.
- Both multispectral cameras and Lidar have a great potential in flood management. This includes both aerial (i.e., drone) and terrestrial use.

Task 2a Report

In this section, a brief literature review of drone systems, multispectral cameras, and Lidar is presented. This is followed by a discussion of all aspects of drone systems, including drone selection, sensor integration, regulations, mission planning, and safety. Next field results that were conducted at flood prone PADOT sites using multispectral cameras and LiDAR systems are presented.

1 Literature Review

1.1 Drone Systems

Although the focus of this report is on the use of drone systems, it is important to note that any unmanned vehicle (ground, surface, underwater, and air) is well suited for monitoring (Dunbabin et al, 2012). Air vehicles, specifically small rotorcraft, commonly referred to as drones, offer the advantage of being able to scan large areas at differing scales with high speed from many vantage points (Favorskaya et al, 2017). This is especially useful for smaller-scale localized applications.

In the United States a person who uses any unmanned air system (UAS) for non-recreation purposes must hold a Part 107 certification. In other words, a commercial unmanned aircraft certification/license is required for the use of any drone that is not used for recreation. Any flight undertaken by PADOT will fall under this category. As a measure for just how much UAS use has grown in the recent pass, FAA data on the number of certified drone pilots can be reviewed[1]. In all of 2019 150,391 pilots were certified. This is compared to 241,567 pilots certified from just, January 1, 2021, to August 16, 2021. An increase of 60% over just 2/3 of the year.

Over the past 15 years, drones have found application across many disciplines because of their broad availability, ease of use, and low cost. Applications of drones to stormwater related fields include broad use in agriculture (Zhang et al, 2012, Arnold et al, 2013, Gay et al, 2013, Duggal et al, 2016, Kaneko et al, 2016, Baluja et al, 2014, Acevo-Herrera et al, 2009, Archer et al, 2004, Soliman et al, 2013, Jenal et al. 2019), forestry (Favorskaya et al, 2017, Sankey et al 2017, Liu et al 2021), lake, river, and steam monitoring (Kontopoulu et al. 2017, Prior et al. 2020, Larson et al. 2018). While the goal in these applications may be slightly different than the flood monitoring focus of this report, their use in these fields have many overlapping and parallel applications. For example plant health monitoring (Zhang et al, 2012, Arnold et al, 2013, Gay et al, 2013, Duggal et al, 2016, Kaneko et al, 2016, Jenal et al. 2019), soil moisture monitoring (Baluja et al, 2014, Acevo-Herrera et al, 2009, Archer et al, 2004, Soliman et al, 2013), vegetation control (Favorskaya et al, 2017), forest inventory (Favorskaya et al, 2017), coastal flooding (Favorskaya et al, 2017), forest fire monitoring (Favorskaya et al, 2017), ground cover identification (both natural and man-made) (Sankey et al 2017, Liu et al 2021), surface temperature and water stress levels (Berni et al. 2009), mapping (Liu et al 2021), Digital surface models (Liu et al 2021, Grant et al 2018), and water quality measurements (Kontopoulu et al. 2017, Prior et al. 2020 and Larson et al. 2018).

[1] http://archive.org

This summary of the literature only scratches the surface of the growing applications of drones in stormwater related fields. One sensing method that is discussed in this report is multispectral imaging. Multispectral imagery has been applied with excellent results for vegetation monitoring and mapping, as discussed above. Interest in these systems can be captured by looking at the number of research papers that have been produced with these sensors over the past 20 years. Using the keywords "Drone" and "Multispectral" on Google Scholar[2] the interest in drone based multispectral imaging can be captured, as shown in Fig. 1.1 as the blue line. As can be seen, interest has grown steadily. Searches for "Multispectral" or "Drone" independently are also included for reference.

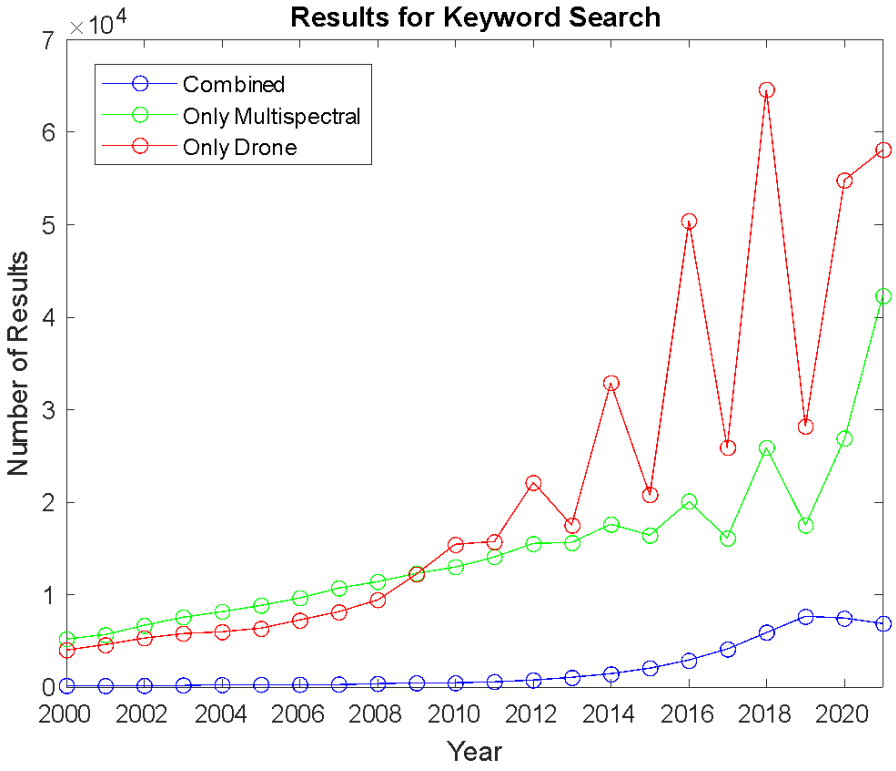

Figure 1.1. Number of Results with Given Keyword and Year.

Operation of drones falls into two potential paradigms: 1) Human-operated and 2) Autonomous. In the immediate future, human-operated drones will dominate drone application. This is strictly regulated by the FAA and determination of whether drone use is allowed depends on FAA regulations, such as restrictions of flying near people or in restricted airspace. A longer-term vision for the use of drones is to have them operate autonomously. The drone could be stored on-site or launched from a hub. It could perform daily monitoring tasks and report back. In contrast to human-operated drones, autonomous drone operation is still not a turnkey system, although they have been broadly studied due to a huge interest in drone delivery (Bamburry, 2015) and associated applications. Thus, completely autonomous flight is yet to be deemed safe and reliable. Regarding

[2] http://scholar.google.com

government oversight, current FAA regulations allow autonomous flight but do not allow for beyond visual line of sight (BVLOS) operation, although it is being considered.

1.2 Multispectral Imaging

Multispectral cameras, like the one shown in Fig. 1.2, use multiple lenses to capture images with different wavelength ranges. These cameras typically include wavelength ranges in the visible spectrum (one sensor each for red, green, and blue color ranges) and infrared spectrum (infrared or thermal, red edge, near infrared). Data from these images can be used in many applications such as mapping, water quality, vegetation health, and more (Yuan et al. 2017, Berni et al. 2009, Goel et al. 2002, Bendig et al. 2015, Robertson et al. 2018, Jenal et al. 2019, Ayad et al. 2020). In the following, In this project, the primary data collected from drone flights are multispectral images of the selected flood prone roads. In the section, a brief literature review of relevant multispectral imaging applications is presented.

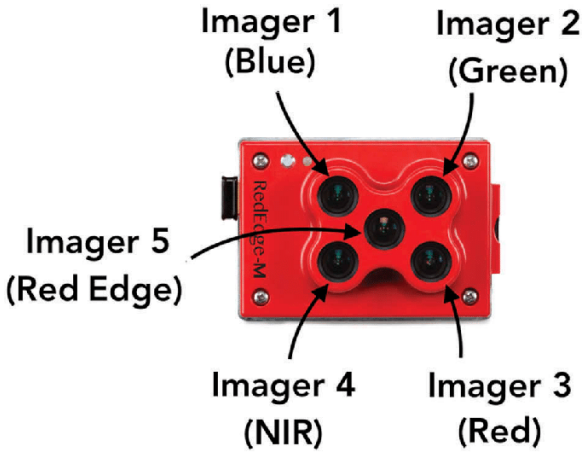

Figure 1.2: Labeled Sensors of a Rededge-M Multispectral Camera
https://www.researchgate.net/figure/The-MicaSense-RedEdge-as-an-advanced-multilens-and-multispectral-camera-specially_fig2_334643258

Different materials and conditions of materials do not reflect all spectrums of light in the same manner. Obviously, surfaces with different colors reflects certain wavelengths of light more. For water, much of surface reflectance is influenced by the substances and particles that are dissolved or suspended in it (Ayad et al. 2020, Prior et al. 2020). This is useful since the more particulates that are present in the water, the more difficult it is for light to pass through the water which can be used to determine the amount and type of particulates present.

Figure 1.3 shows a plot of various spectrum reflectance with different qualities of water are shown. This comes from a recent study by Ayad et al., regarding coastal runoff water quality from the Tijuana River. The images were produced by European Space Agency (ESA) Sentinel 2A/B and United States Geological Survey (USGS) Landsat 8. This study highlights the ability of multispectral imaging for water quality purposes. Of course, the study utilizes satellite images rather than drone images as used in this project. This changes the scale of the collected data, but the concept remains the same. For larger flows of water such as the Tijuana River, satellite images are a better tool than drone imaging due to the manpower needed for drone surveys. For smaller

streams and localized data collection, multispectral drone imaging provides an appealing option when compared to sample collection at multiple points.

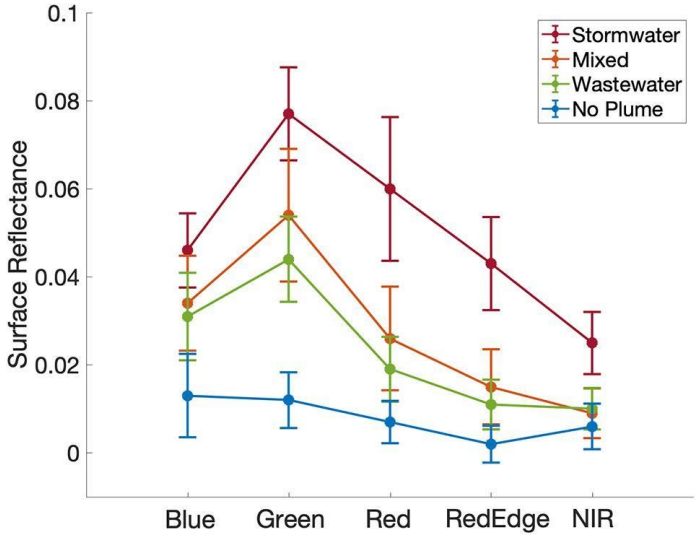

Figure 1.3: Reflectances of Different types of Water at Different Light Bands **(**Ayad et al. 2020**)**

In addition to its use for water, multispectral imaging can also help classify vegetation and plants. For most plants, a deep green color signifies a healthy, thriving plant. A dying, unhealthy plant will display colors such as brown, red, yellow, and straw color instead. Of course, the colors correspond to the concentration of chlorophyll in the plant (Bendig et al. 2015). The more chlorophyll, generally the healthier the plant. By using multispectral imaging, the amount of green reflectance by plants (and therefore the concentration of chlorophyll) can be measured as a factor of plant health (Bendig et al. 2015).

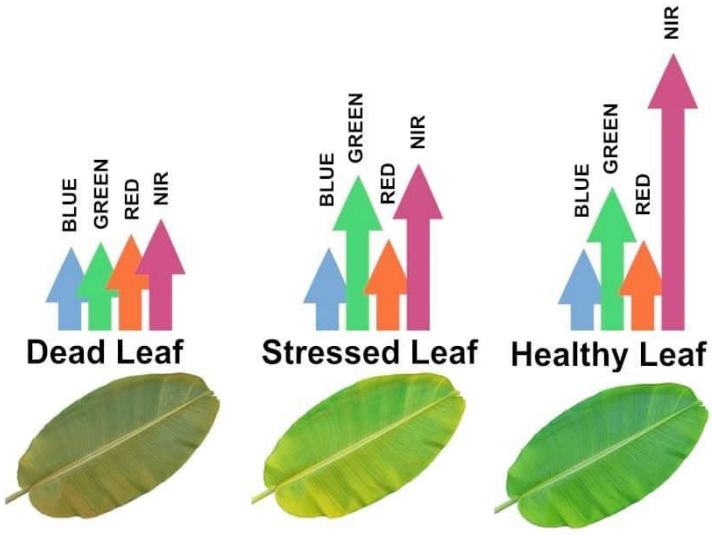

Figure 1.4: Diagram of different Reflectance Levels with Plant Health
https://mydroneservices.com/our-services/agricultural-services/

Near infrared (NIR) and red-edge spectrum reflectance also increase with good plant health (Bendig et al. 2015). These spectrums cannot be seen with the naked eye, but cameras can capture them. By comparing the reflectance of different spectrums, state of a plant can be determined and action can be taken to correct any issues. One of the applications of this reflectance behavior is with vegetation indices.

Indices are formulas and methods to evaluate data by comparing, normalizing, correcting collected data into a form that is easy to understand. Multispectral imaging data can be used to calculate indices for both water and stormwater based applications, and for vegetation. The index used for vegetation in this project is the normalized difference vegetation index(NVDI). According to ArcGIS Pro's Indices Gallery webpage[3], "NVDI is a standardized index allowing you to generate an image displaying greenness, also known as relative biomass. This index takes advantage of the contrast of characteristics between two bands from a multispectral raster dataset—the chlorophyll pigment absorption in the red band and the high reflectivity of plant material in the near-infrared (NIR) band." So, NVDI is a measure of the amount of healthy plant/biomass in an image. To calculate NVDI, the reflectance of NIR and red are used in the formula below.

With the ability to distinguish between different "surface" types, multispectral imaging can also be used as a mapping tool. By utilizing multiple indices, neural networks can use that data to distinguish features in the image.

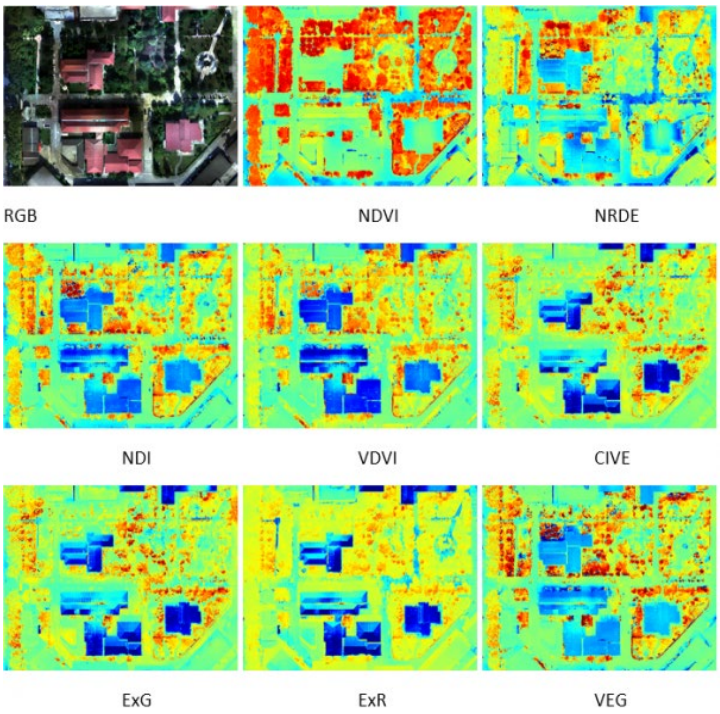

Figure 1.5: Example of Different Image Indices Used for a Single Aerial Image
https://www.gim-international.com/content/article/vegetation-mapping-using-multispectral-uav-images

[3] https://pro.arcgis.com/en/pro-app/2.8/help/data/imagery/indices-gallery.htm

Figure 1.5 shows images of Babol Norshirvani University of Technology (BNUT) with processed image indices. The vegetation, buildings, and pathways can be easily distinguished using the different indices (Parmehr 2021). By training a neural network to recognize the ranges of the different surfaces, an accurate map with specified area types can be created as seen in Fig. 1.6. Applying this method to flood prone streams, data can be collected over multiple months to see the changes in bank surface area, vegetation, and roads.

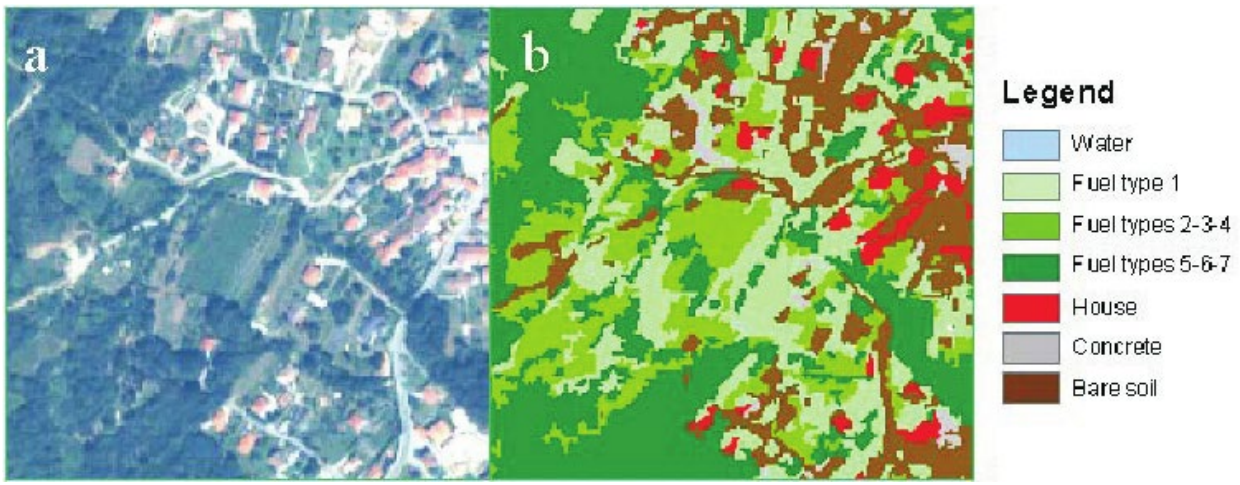

Figure 1.6: Classified Land Using Multispectral Data
https://www.researchgate.net/figure/a-Quickbird-multispectral-image-b-Preliminary-land-use-and-fuel-map-obtained_fig1_228418654

1.3 LiDAR

Lidar is able to measure distance by measures the time it takes for a pulsed beam of light (from a laser) to bounce off an object or surface and return to the sensor, yielding an accurate measurement of distance to the object or surface since the speed of light is known. If this is repeated many times with the laser bouncing off different targets, the resulting data forms a "point cloud" or digital model of the physical objects around the Lidar sensor.

The capabilities of LIDAR have spurred their use in a broad range of applications. Of note are their application in autonomous robotics (Rivai et al, 2020), which has spurred rapid advancement of LIDAR sensors. Sensor packages can include single or multi beam setups. Many use mirrors to direct the beams, some rotate the beams yielding 360 degree information, and emerging solid-state sensors allow for compact packages that are even being included in commercial cellphones[4].

The deployment of LIDAR sensors typically falls into one of three broad categories: Aerial, Stationary Terrestrial and Mobile Terrestrial.

- Aerial LIDAR deployment offers the advantage of being able to scan large areas to differing scales from the vantage of an aircraft (Favorskaya et al, 2017). Furthermore,

[4] https://www.cnet.com/tech/mobile/Lidar-is-one-of-the-iphone-ipad-coolest-tricks-its-only-getting-better/

scanning can be done at high speed, from many vantage points, and using integrated IMU and GPS technology to create elevation models that span wide areas Unmanned aerial vehicles (UAV)are gaining increasing utility for smaller scale applications, which opens the door for many civil applications such as vegetation control, forest inventory, coastal flooding, forest fire monitoring etc. (Favorskaya et al, 2017).

- Terrestrial LIDAR refers to fixed position or handheld applications that cover a relatively small area at once. The dense point clouds produced make it very useful for biomass estimations in forestry (Favorskaya et al, 2017).
- Mobile LIDAR is an emerging application that uses low-cost mobile robot for mapping an environment with a front view. Many studies allow mobile robots to map their environments through SLAM (Simultaneous Localization and mapping) algorithms in unfamiliar locations (Rivai et al, 2020). For example, Rivai et al 2020, use an omnidirectional three wheeled mobile robot for mapping a room using LIDAR.

LIDAR technology has found much utility in both urban and natural environments because of its potential to extract features and provide highly detailed data for modelling and simulation (Garnett et al, 2018). Applications that have direct relevance to PADOT include:

- *Hydrological LIDAR Applications:*
    - UAV based Lidar can be used during or immediately after a storm or flooding event to expedite inspection and can be used to mitigate the impacts by modelling, predicting, and assessing flood damage (Crimmins et al, 2019).
    - LIDAR can be used to identify surface runoff pathways by mapping bare earth (Dabrowska et al, 2018).
    - Breili et al 2020 combine sea level projections, storm surge return height with nationally available high resolution LIDAR data to map coastal flooding in Norway, allowing for flood prediction flood risk classification. LIDAR can be used to augment and improve coastal flooding assessment technique techniques.
    - Baby et al 2021 simulate the waterflow on the ground, in streams and detects accumulation of water in depressions. This provides a tool for identifying areas with flood risk.
    - Hung et al use LIDAR to map building impervious area for hydrological applications.
- Urban Stormwater Management Applications
    - UAV LIDAR can be used to assess standing water height on roadways as it has been shown to play a significant role in pavement deterioration (Crimmins et al, 2019).

  - Urban morphology and green cover analysis deal with identification and classification of surface features, especially in urban areas, that affect stormwater management (Yan et al, 2015).
  - High resolution flood propagation and inundation modelling can be attained by using very high-resolution LIDAR (1-m resolution) (Li et al, 2021).
  - Ivan et al 2018 describe an algorithm to extract surface ponds based on LIDAR digital elevation models.

- *Earth Science*
  - LIDAR enables high resolution mapping of topography, bathymetry and vegetation (Okyay et al, 2019).
  - Grant et al 2018 quantify rainwater harvesting potential using GIS software, aerial photographs and airborne LIDAR data.

- Urban Drainage Delineation
  - Gurganus et al 2017 used mobile LIDAR to measure surface features and develop designs for improved roadside drainage.
  - Lee et al 2020 used mobile LIDAR to inspect roadside channels, calculate channel attributes and evaluate them.
  - Shams et al 2018 developed a methodology for measuring the cross slope of roads using mobile Lidar to enable efficient handling of cross-slope issues.
  - Elmekati et al 2019 used airborne LIDAR to generate a digital terrain model for assessing geotechnical health and stability of a road embankment.
  - With mobile LIDAR, Neupane et al 2019 developed a heuristic based method for automating road surface type identification, from reflected laser intensity measurement, to extract road surface type information.

- Vegetation Health
  - High resolution LIDAR can be used to measure and classify vegetation by measuring individual plant characteristics (Sankey et al, 2017).
  - To measure urban tree canopy cover, LIDAR can be fused with multispectral satellite imagery data. (Parmehr et al 2016)

- Underground monitoring
  - Xie et al 2019 used LIDAR data for non-contact deformation monitoring of stormwater sewage tunnels.
  - Zhang et al 2019 use LIDAR to determine the full ring deformation characteristic of large stormwater sewage tunnels during full-scale loading tests.

- Gaspard et al 2020 combined mobile LIDAR for above ground survey of stormwater assets.

2 Drone Systems

Drone systems provide a platform for localized, high-resolution sensing without the need for the expensive and complex equipment required for airplane or satellite imagery. There are a multitude of design choices and considerations when using sensing packages on a drone as discussed in the following. Details of individual drone subsystems can be found in Appendix A.

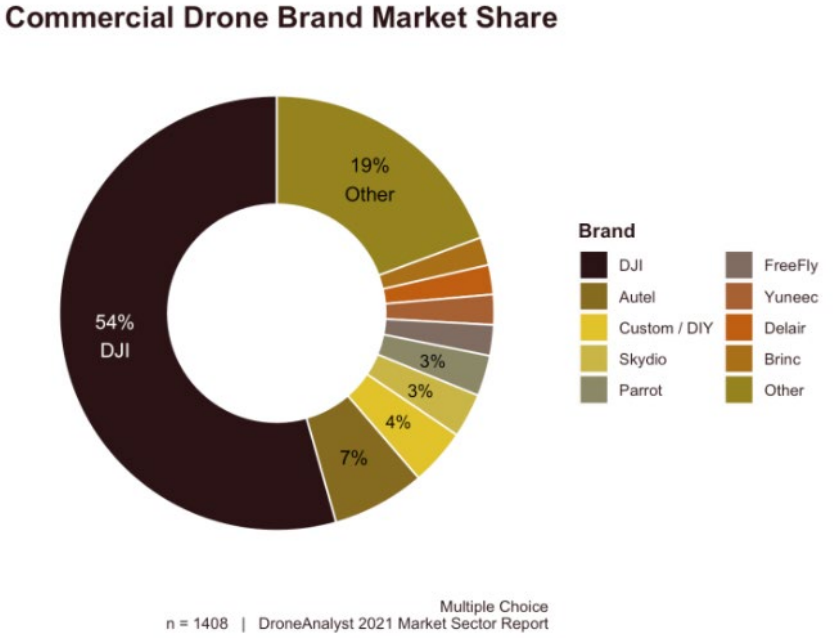

Figure 2.1: Drone Market Share
https://www.thedronegirl.com/2021/09/14/2021-dji-market-share/

2.1 Drone Choice

Commercial Choices: Commercially made drones provide the easiest starting points for all types of users and applications. They provide streamlined workflow and integration for compatible systems and add-ons (like sensors). There are four companies that hold a significant share of the drone market, which is summarized in Fig. 2.1. The most dominant company is DJI[5], which sells both consumer (see Fig. 2.2) and professional (see Fig. 2.3) level drones. Second is Autel Robotics[6] which controls a smaller, but growing market share. These companies are distantly followed by Skydio[7] and Parrot[8]. Products produced by these companies allow for customization. Consumer-level drones have active on-line communities that enable the use of aftermarket components, 3D print files, accessories and more. Products aimed towards the professional market provide controls

[5] http://www.dji.com
[6] https://www.autelrobotics.com/
[7] https://www.skydio.com/
[8] https://www.parrot.com/us

and telemetry within the software ecosystem of the company but have much more space to customize. For example, the drone used in this project is a DJI S900 as seen in Fig. 2.3. Compared to the Mavic 2 Pro shown in Fig. 2.2, the professional drone has more motors, retractable landing gear, and a multitude of attachment points to interface with the drone system. These all contribute to its customizability and utility when compared to a consumer level drone.

Figure 2.2. DJI Mavic 2 Pro, a Commercial Drone Made for a Typical Consumer http://www.dji.com

Figure 2.3. DJI Spreading Wings S900, a Prosumer/Professional Drone http://www.dji.com

Figure 2.4. DIY Drone based on the Generic S550 Frame
https://www.wikdrone.com/powerday-diy-s550-six-axes-hexacopter-pixhawk-px4-flight-controller-7m-gps-ppm-simonk-30a-esc/US_10046

DIY Drones: DIY drones, like the one shown in Fig. 2.4, provide a significant ability to customize at the cost of design and development dollars and time. These drones can be significantly cheaper than commercially built drones but may not provide the same ease of use in flight. Components exist which could provide the lost functionality but can increase costs significantly. DIY drones are a good option for projects that do not require the flight software that is provided to commercial drones but are not necessarily recommended unless the user has time and funds budgeted for starting up the project.

2.2 Drone Specifications

Drones are typically specified by weight, physical dimensions, and flight time. The total weight of the drone and the cargo capacity are important factors to consider. The total weight of the drone is important due to FAA limitations for small unmanned aerial systems (sUAS or drones) that set an upper weight limitation is 55lb. If this limit is reached, a Part 107 Certified Remote Pilot cannot operate the drone unless the drone receives an airworthiness certificate which requires the owner to complete a process proving the drone eligible.

Some of the specifications for the drone used in this student, the DJI S900 are listed below (see: https://www.dji.com/spreading-wings-s900 for a full set of specifications).

Frame

- Diagonal Wheelbase, 900mm
- Frame Arm Length, 358mm
- Frame Arm Weight (Including Motor, ESC, Propeller), 316g
- Center Frame Diameter, 272mm

- Center Frame Weight (with Landing Gear Mounting Base, Servos), 1185g
- Landing Gear Size, 460mm(Length)×450mm(Width)×360mm(Height)

Flight Parameters

- **Takeoff Weight, 4.7Kg ~ 8.2Kg**
- **Total Weight, 3.3Kg**
- Power Battery, LiPo (6S、10000mAh~15000mAh、15C(Min))
- Max Power Consumption, 3000W
- Hover Power Consumption, 1000W (@6.8Kg Takeoff Weight)
- **Hover Time, 18min (@12000mAh& 6.8Kg Takeoff Weight)**
- Working Environment Temperature, -10 °C ~ +40 °C

2.3 Cargo Capacity and Loading

Cargo capacity is the manufacturer specified cargo weight that is valid for "normal" operations. Typically, a drone can carry significantly more weight than the noted cargo capacity by the manufacturer, but it serves as a "baseline" measurement where you can expect safe and good-performance operation. Alterations to this baseline will change the performance of the drone, for example endurance (or flight time). The increased power consumption will drain the battery much faster than if the drone were not loaded as heavily. This may also lead to issues if the battery used cannot supply enough power to the drone. In addition, increased weight leads to increased wear on the drone's motors and speed controllers. To remedy this, more frequent maintenance and pre-flight inspections should be performed if a drone is operated outside the specified cargo capacity.

The performance of a drone corresponds to its ability to move in the air. How well can it move in the air? How long can it move in the air? What humidity and temperature can it move in? There are many more questions to answer. For most drone pilots, general aircraft design considerations can be used to decide on the design of the cargo. The total amount of weight and its distribution on a drone is important to the performance on a drone. In addition to the changes mentioned in the previous paragraph, an uncentered weight and drone movement causes different forces to act on a drone. Uncentered weights cause an additional moment which needs to be corrected by the motors to stay upright. The movement of the drone also requires the motors to work harder.

These are all factors to consider when loading a drone. Although it is possible to load drones past the manufacturer suggested maximum cargo capacity, the factors to consider are significant. Due diligence, calculations, and precautions should be done well in advance of commissioning or modifying any drone system.

2.4 Regulations

The Federal Aviation Administration (FAA) manages the use of drones in the United States. As a general rule, drones heavier than 0.55 pounds but less than 55 pounds or a drone being used commercially should be registered with the FAA[9]. This provides a registration number that is required to be attached to the drone (by label, sticker, etc.). In the future, a system called remote ID will replace the need for labeling the drone with a transponder either attached to the drone or built in with the drone.

A drone pilot can only fly commercially if they hold a part 107 certificate[10]. There are a number of online flight training schools available. After an exhaustive search, we chose to use the pilot institute[11]. Some of the key things to consider when considering regulations are:

- A commercial flight is anything that is not done for leisure or for recreation regardless of whether there is monetary exchange.
- All drones are required to follow airspace regulations and are considered aircraft.
- One important regulation for PADOT to consider is sustained flights over people and roads, which are regulated under Part 107. Four categories of drone flights are described on the FAA website with differing rules regarding each one. Flights performed in this project were not subject to the rule as flights did not occur over non-flight crew members and transitions over roads occurred when no vehicles were present.
- The flight team must maintain visual contact with the drone at all times during the flight, as regulated by the FAA in the regulations shown in Fig. 2.5.

§ 107.31 Visual line of sight aircraft operation.

(a) With vision that is unaided by any device other than corrective lenses, the remote pilot in command, the visual observer (if one is used), and the person manipulating the flight control of the small unmanned aircraft system must be able to see the unmanned aircraft throughout the entire flight in order to:

(1) Know the unmanned aircraft's location;

(2) Determine the unmanned aircraft's attitude, altitude, and direction of flight;

(3) Observe the airspace for other air traffic or hazards; and

(4) Determine that the unmanned aircraft does not endanger the life or property of another.

(b) Throughout the entire flight of the small unmanned aircraft, the ability described in paragraph (a) of this section must be exercised by either:

(1) The remote pilot in command and the person manipulating the flight controls of the small unmanned aircraft system; or

(2) A visual observer.

Figure 2.5. FAA Rules on Visual Line of Sight
https://www.law.cornell.edu/cfr/text/14/107.31

In addition to federal regulations, an individual pilot's set of rules and regulations is important for safe flight. Briefing the crew on the flight, and constant communication are all ways to ensure a

[9] https://faadronezone.faa.gov/#/
[10] https://www.ecfr.gov/current/title-14/chapter-I/subchapter-F/part-107
[11] https://pilotinstitute.com/

safe flight. By following previously agreed on rules with the crew in addition to federal regulation, a flight is not only safer, but will be performed much smoother than with a crew without the knowledge beforehand.

3 Multispectral Imaging Field Studies

During the course of this project, the following multispectral imaging drone flights were undertaken at flood prone PADOT locations:

- Burmont Road, October 22nd 2021.
- Garges Road, January 21st 2022.
- Old Sumneytown Pike, January 28th 2022.
- Radnor Road/Croton Road, April 11th 2022.
- Burmont Road, April 13th 2022.
- Goshen Road, April 20th 2022.

The drone workflow discussed in Task 2b was followed. These flights were done at select flood prone roadways which satisfied the selection requirements mentioned in Task 2b. Particularly, these locations provided adequate take-off and landing space in addition to easily accessible observation points. During these flights data was collected by the multi spectral camera shown in Fig. 1.2. Once the flight was complete, the images from the flight were processed using ArcGIS Pro. Images from all flights for the year have been processed, with selected images shown in the following section to highlight the capabilities of multispectral imaging.

3.1 Multispectral Drone System

The drone used in these field studies was a DJI S900 hexcopter drone[12]. This drone was purchased used with the DJI Zenmuse Z15 gimbal[13] included. The drone and gimbal are controlled by two separate radio controllers. The camera used is the Micasense Rededge MX multispectral camera[14]. The drone and gimbal receives power from a 12000mAh 6S lithium polymer battery while the multispectral camera receives power from two 450mAh 2S lithium polymer batteries connected to a voltage converter which supplies power to the USB hub in which the camera is connected.

In order to mount the camera, an aluminum bracket was cut and drilled to fit the mounting holes on the back of the camera as well as for the mounting screw on the gimbal. For balancing the gimbal, additional weight needed to be mounted as the weight of the camera is insufficient for proper balance. To add weight, packs of tape-bound washers were mounted on various locations of the gimbal. The placement also ensures the gimbal is balanced and will have the least amount of drift possible. See Fig. 7 in Appendix A for an image of the mounted camera.

[12] https://www.dji.com/spreading-wings-s900
[13] https://www.dji.com/zenmuse-z15
[14] https://support.micasense.com/hc/en-us/articles/360011389334-RedEdge-MX-Integration-Guide

3.2 Colorscale Selection

The images in Figs. 3.1, 3.2, and 3.3 show data collected using the multispectral camera flown at the Burmont Road site. Figure 3.1 shows the base red band image, which is similar to a typical black and white photo. Figure 3.2 and 3.3 show the same vegetation index data (NVDI from Sec. 1.2) using different color scales. These images were constructed in ArcGIS using built-in stitching and band-matching tools as described in Task 2b.

To extract useful data out of the resulting layered image, band arithmetic must be applied. Certain indices are built into ArcGIS, which allows you to simply select the index after the mosaic is generated. For a single snapshot, band arithmetic is the easiest method to generate image indices. The two images in Fig. 3.2 and 3.3 are processed using the exact same method and are identical in terms of the data they contain. These two images may be processed the same way but have two different color scales applied to them. These color scales change how the data is presented and can be used for different applications. The green-magenta image would be perfect for separating organic and inorganic objects as the organic objects appear green and contrast well with the magenta car and road (inorganic). The multi-color scale takes this one step further and allows you to observe the density of the foliage. The denser foliage seen in the sample red band image can be compared with the orange, red, and yellow regions of the multicolored image. Also, bare branches can be clearly seen in those images which correspond with the less dense foliage regions.

Figure 3.1. Sample Red Band Image

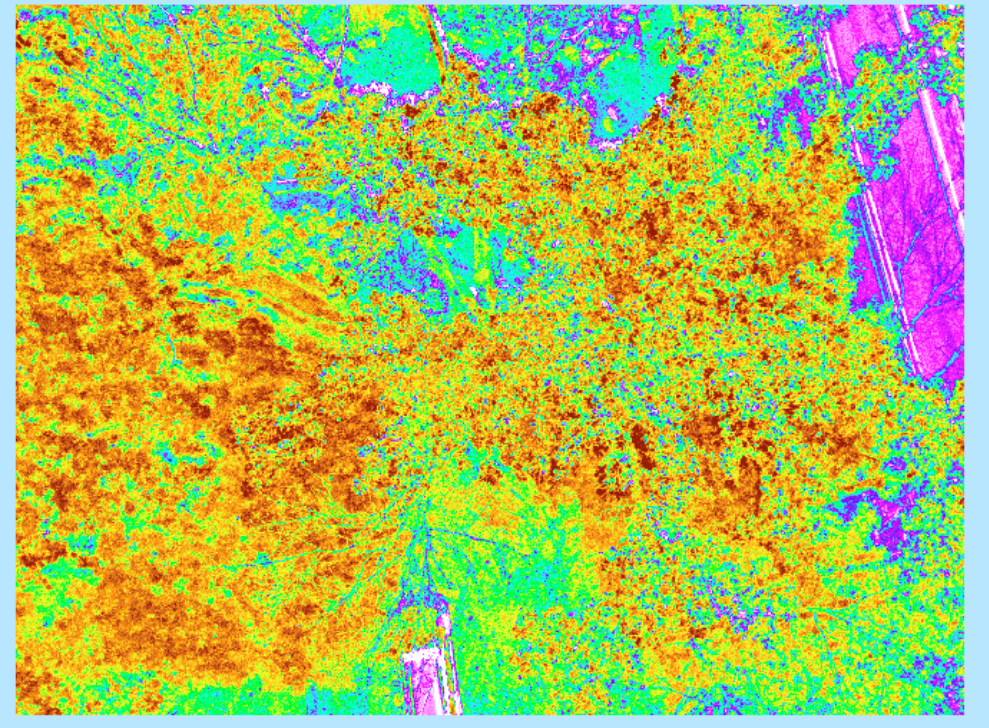

Figure 3.2. NVDI Processed Image Using a Multicolored Scale

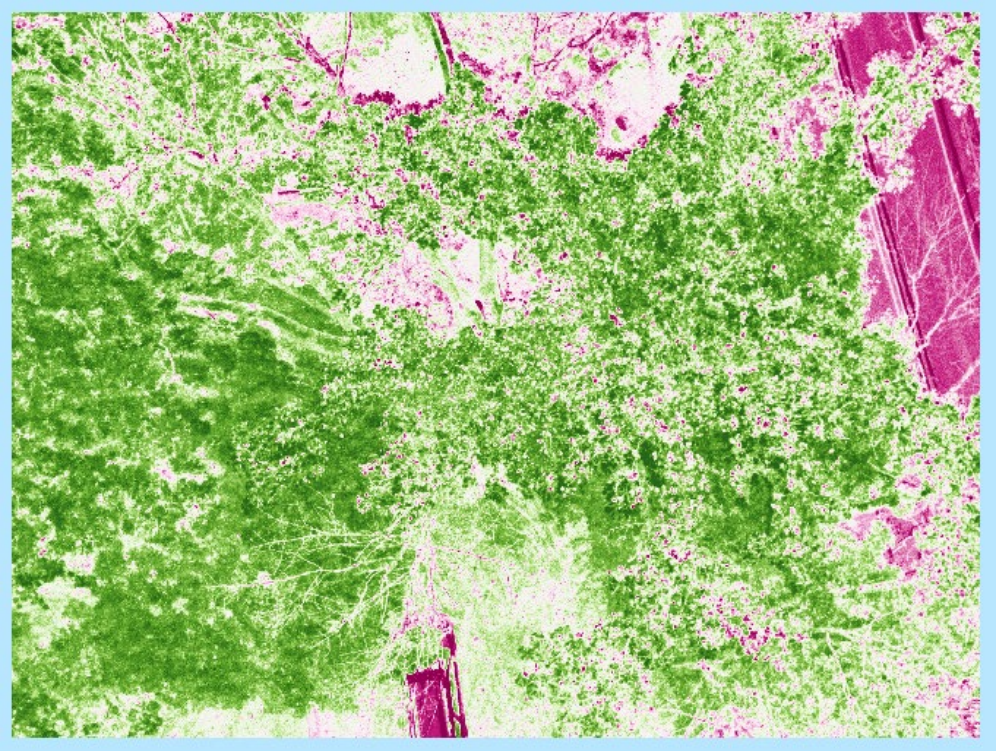

Figure 3.3. NVDI Processed Image Using a Dual Color Scale

3.3 Standing Water Identification

In order to show the efficacy of multispectral imaging to distinguish between flooded and unflooded areas, the multispectral camera was used to capture images of an on-campus rain garden during a rain event and subsequently on a sunny day. Figure 3.4 shows the flooded rain garden on the right and unflooded on the left. Blue band images are on top and NVDI images are on the bottom.

From the blue band images, there are two things to note. First that the rain garden does display standing water, both in the trench and on the bank to the right of the trench. Second, the unflooded rain garden was taken when vegetation had grown.

The sunny day (right) NVDI images has a shadow cast by a parking garage next to the rain garden. The shadows result in less accurate data that is ignored. It is also noted that the rain garden still retains some water due to a previous rain event. Finally, with more sun coverage and less overall moisture, the overall scale of the index values appears to shift towards the lower values (blue), thus the color of the image is darker in the field area.

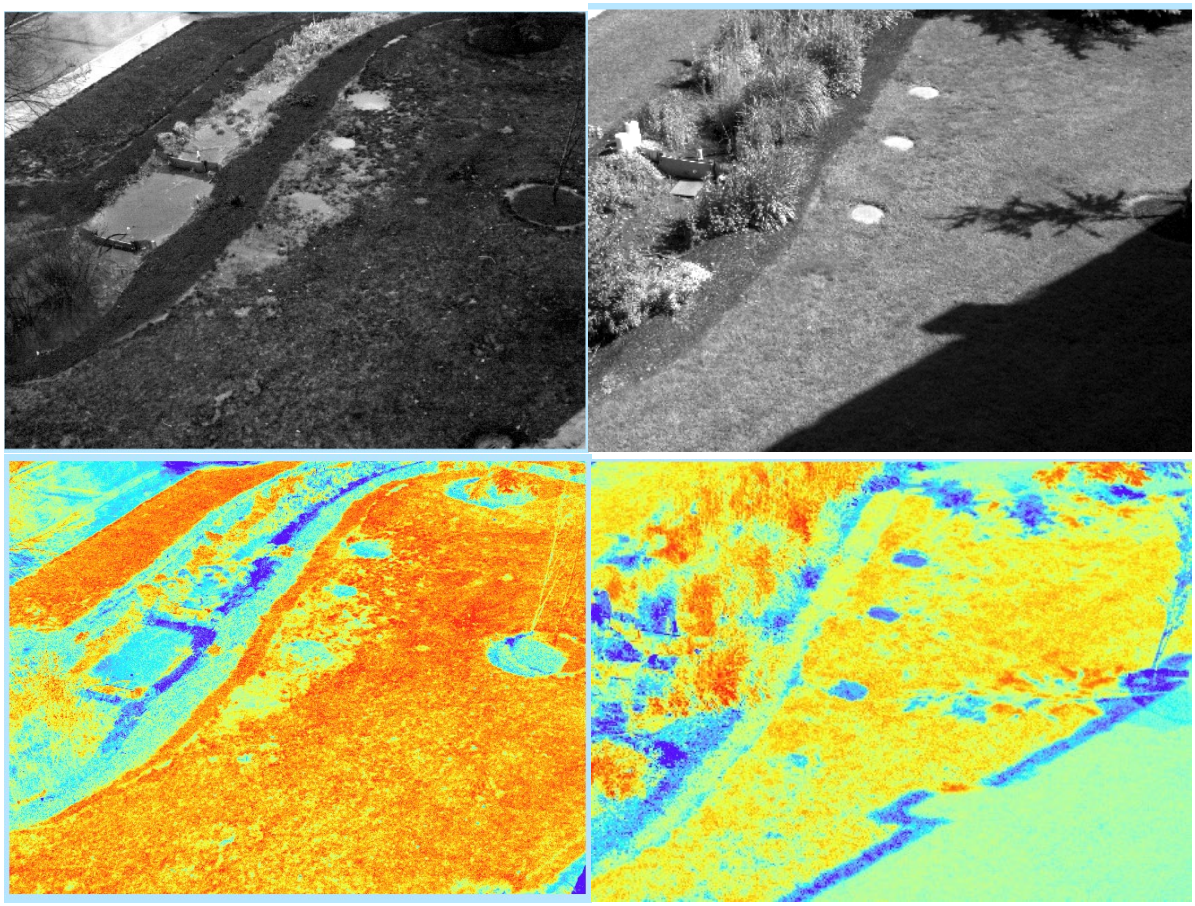

Figure 3.4. The top two images show the blue band image for a rain garden in two states, left: flooded after a rain event and right: in a dry state. The bottom two images show the NVDI images for the same rain garden states.

From comparison between the two NVDI images, the following conclusions are drawn:

- The NVDI images clearly show the healthy plant life in the unflooded image (orange areas in the right image versus blue areas in the left.)
- The NVDI images shows the existence of standing water in the flooded image (blue and yellow area on the right bank of the trench when compared to the right image – boxed in red).

3.4 Groundcover/Water Identification

The images in 3.5 and 3.6 show a different area of the Burmont Road location. The same process from 3.2, with one exception, a wider multicolor scale was used. Using this scale, distinct regions and surface types can be distinguished easily. The yellow surfaces are manmade such as the school bus, car, and roadway. The water appears green, with splotches of yellow most likely due to reflections. The rocky soil of the bank is a lighter blue, with some darker colors from larger rocks. Tree cover can be seen as the purple blotches at the edge of the image. With multiple images stitched together, a neural network can automatically classify these surface types when given the NVDI value ranges of these different types of surfaces. With more indices available to use, the surface predictions of the neural network can be more accurate.

Figure 3.5. Red Band Image of the Creek

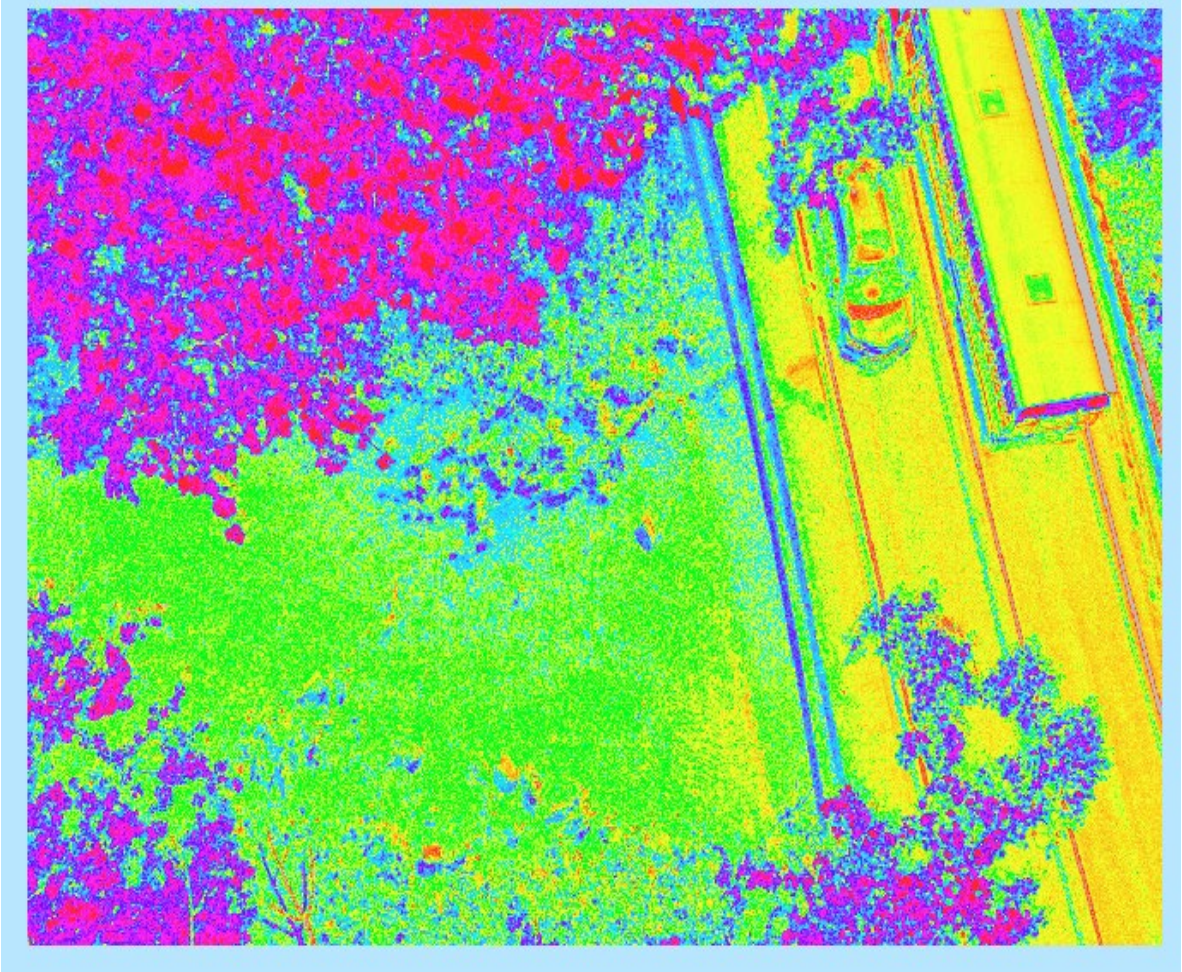

Figure 3.6. NVDI Processed Image with Multicolor Scale

3.5 Image Stitching and Potential Use in Monitoring

The images in Figs. 3.7 and 3.8, taken from Garges Road, show a riverbank where water overflowed and damaged much of the vegetation on the bank. Using the NVDI index (with the brighter orange showing heathier plants), damage to the vegetation can be seen where a dimmer orange color shows regions in which vegetation is unhealthy and which may not have enough strength in the roots to prevent a scour from eroding the bank. With additional long-term imaging of this location, changes in the bank can be monitored as it occurs. Instructions for creating the mosaic can be seen in Task 2b.

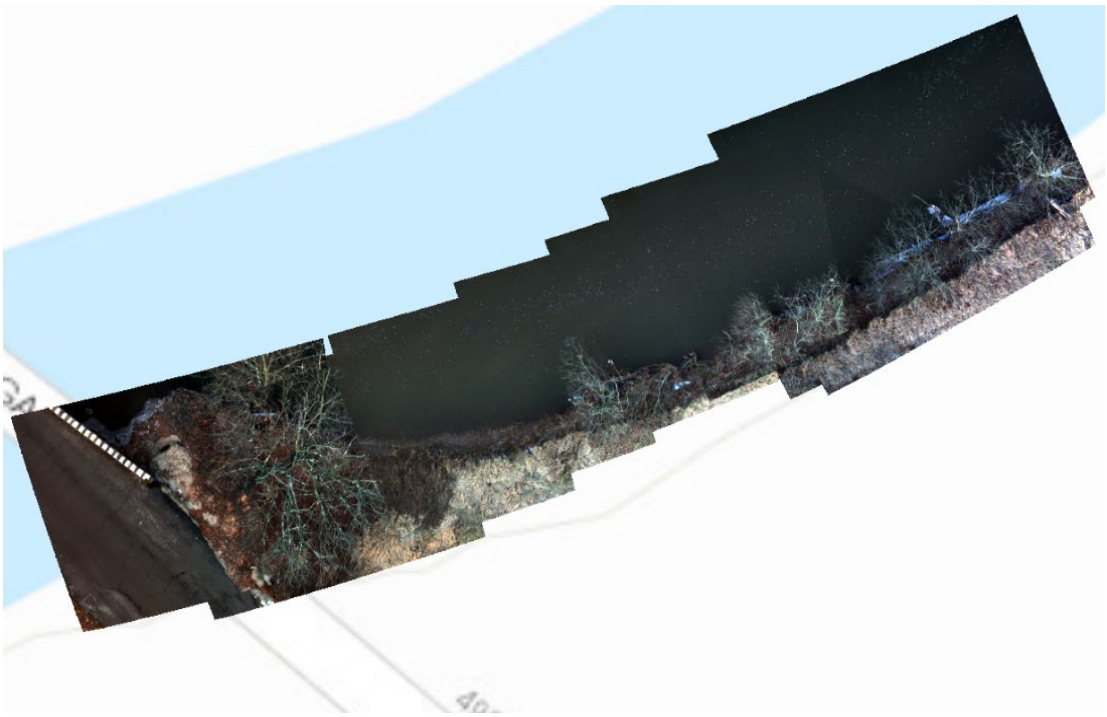

Figure 3.7. Mosaic of the Bank of a Creek

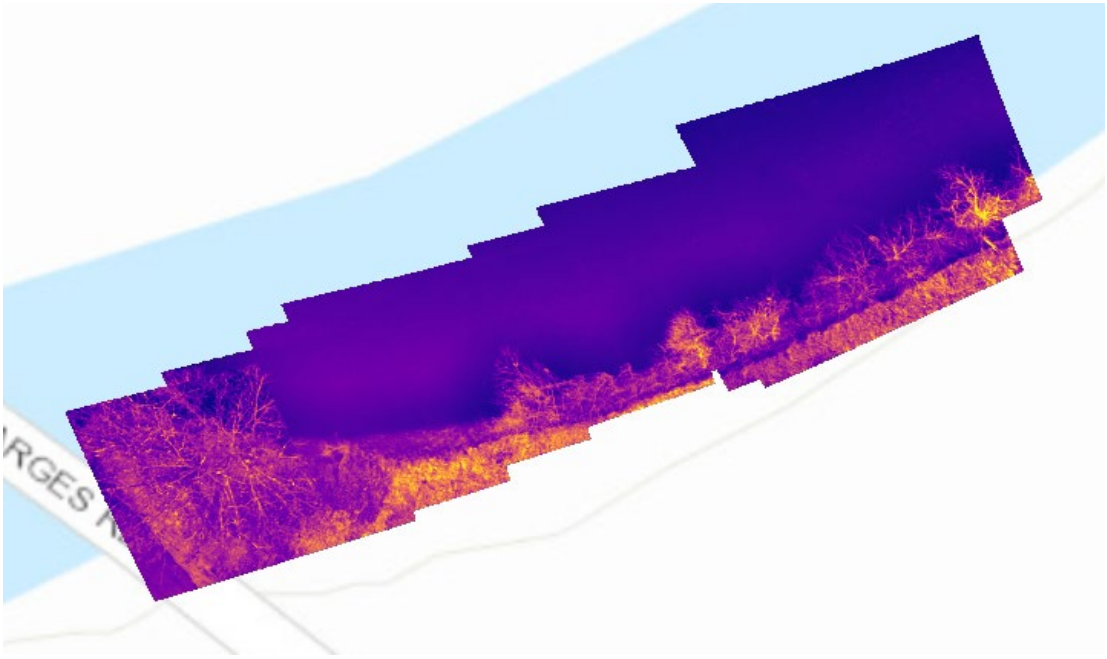

Figure 3.8. NVDI Processed Image from Fig. 3.7.

4 LiDAR Field Data

In the following, we present two examples of field collected Lidar data. One showing data collected from a UAV Lidar unit and one showing a data obtained using a cell phone based Lidar.

4.1 UAV Mounted Lidar

Figure 4.1. shows Lidar data collected from a rain garden on Villanova University's campus. A custom Lidar package (see Appendix B) was flown using the S900 drone discussed in Sec. 1.

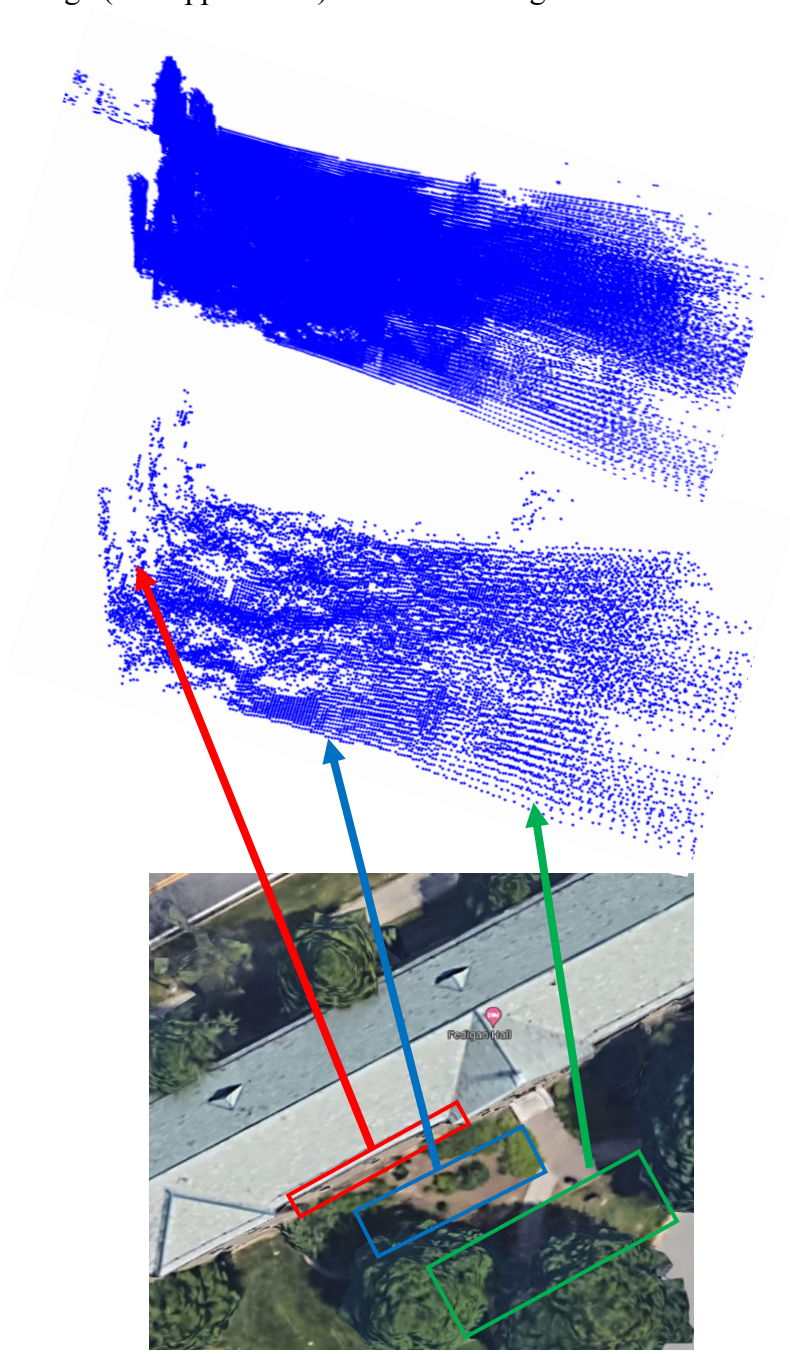

Figure 4.1. Drone collected Lidar data. Top: Raw Lidar data. Middle: Filtered Lidar Data. Bottom: Image of the scanned area. The red box shows a wall, which corresponds to the area called out in the middle figure. The blue and green boxes and arrows correspond to a rain garden and a flat grassy area, respectively.

The top point cloud shows the raw lidar data. From this scan, ground features are not clearly identifiable. After filtering, point cloud in the middle, scanned features become clearer. Note that the features shown in the image correspond to features seen in the site photo shown at the bottom of the figure. The red box highlights a wall, the blue box highlights a rain garden, and the green box highlights a flat grassy area. This study shows the great potential for Lidar to yield digital elevation maps, which can be used in flood management and mitigation as discussed in the literature review.

4.2 Cell Phone Scan

The iPhone 12 Pro models (from Apple Inc.) incorporate a Lidar scanner in the camera cluster. The Lidar scanner acts as a rangefinder for the camera, but can also be used to produce 3D images with the phone by using a 3rd party application. Compared to the Velodyne VLP-16 used in the UAV Lidar discussed above, the iPhone scanner has a much lower range and a smaller field of view. Fig. 4.2 shows a 3D surface obtained using an iPhone Lidar. As can be seen in the image, the resolution is sufficient to identify features, measure their size and locations.

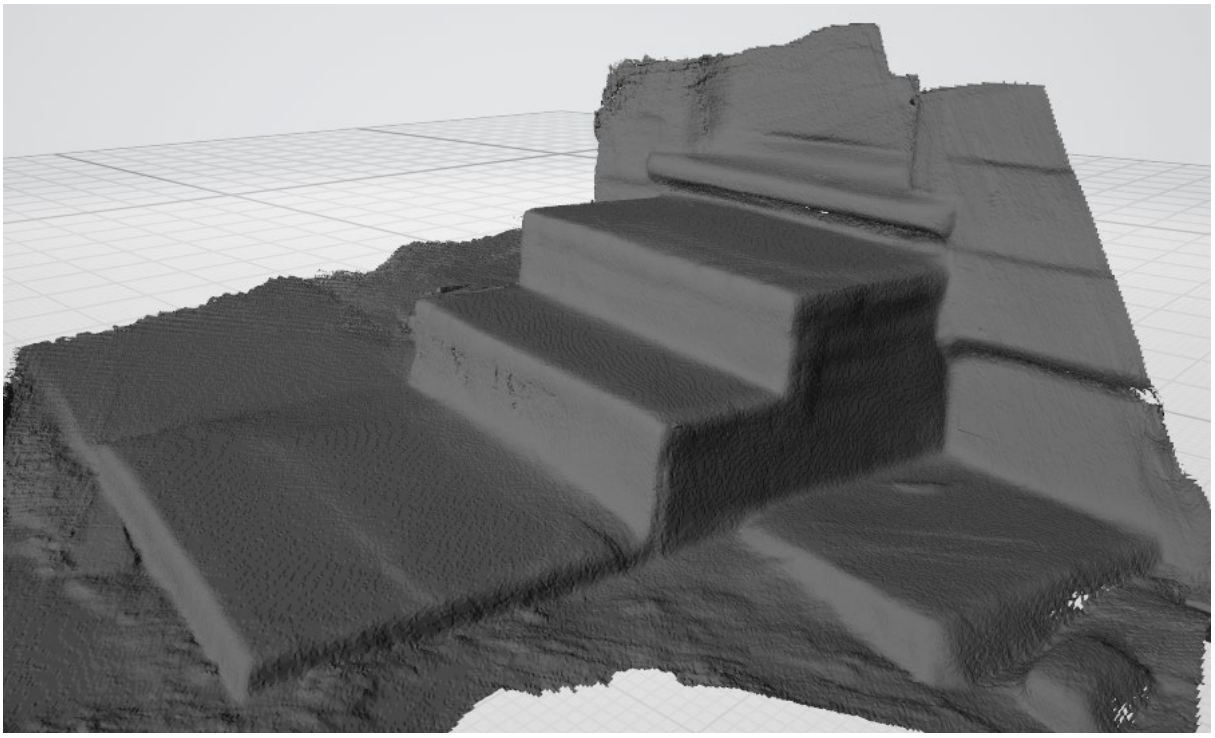

Figure 4.2. Lidar Scan of Steps Using iPhone 12 Pro

5 Conclusions and Future Work

As seen in the literature review and field studies above, drones are clearly shown to be a viable tool for flood monitoring, stormwater management, and related fields.

Based on the field studies presented in this section, multispectral imaging has been shown to be a useful tool in identification and monitoring of flood inundated areas. The following findings are reported:

- Using the NVDI vegetation health index, the following can be identified:
    - Healthy versus unhealthy vegetation
    - Different ground covers (including standing water)
- Drones can be used to collect multispectral imagery over large areas.
- Using the built-in tools from ArcGIS, the data can be geolocated and stitched together to create maps of NVDI, RGB, or other data collected from the multispectral cameras.

Based on the field studies presented in this section, the use of Lidar for floor-related studies is promising. The following findings are reported:

- There is a broad range of work in the application of Lidar to stormwater related fields.
- Both aerial and terrestrial Lidar scans are useful to identify the topography of an area of interest.
- The growing availability of Lidar data, for example in the most recent iPhones, allows this tool to be easily and cheaply deployed.

Future work includes further exploration of the use of Multispectral imagery to identify floods (identification of standing water) both from UAV and using terrestrial imaging and collecting more extensive data sets with the custom Lidar package and further exploration of the use of Lidar in stormwater management.

Task 2b Summary

In this task we present the workflow used for:

1) The drone studies presented in Task 2a: This includes pre-flight, in-flight, and post-flight considerations, including maintenance.
2) The multispectral data analysis shown in Task 2a: This provides a step-by-step methodology to create the multispectral imaging figures using ArcGIS.

Task 2b Report

In this Task, an overview of workflow practices for drone flights is provided. These practices are a simple guide for creating a workflow which matches well with any type of drone survey. Maintenance and upkeep practices are generally described. This is followed by the workflow used to process the multispectral data presented in Task 2a.

1 Drone Workflow

Drone flight can be broken into 3 phases: pre-flight, in-flight, and post-flight. Considerations for each of the sections are discussed below.

1.1 Pre-flight

The following should be done before the flight.

- *Site selection:* Site selection should consider if the site provides:
    - Good launch and landing points for the drone.
    - Enough visibility for the team to maintain visual line of site to the drone. For areas with more visual obstructions, for example, tree cover, multiple visual observers should be used to ensure visual contact is not lost.
    - Flight paths that do not go over roads. If the flight path will cross over a road, care must be taken so the drone does not go over cars traveling on the road.
    - Flight paths that do not go over people. Flights of people that are not a part of the flight team must be done in compliance with FAA regulations.
    - Uncontrolled workspace or airspace in which flight authorization can be easily obtained. This is usually done with the use of Low Altitude Authorization and Notification Capability (LAANC)[15].
    - A time window in which all operations are possible. The duration of the flight should not during any temporary flight restrictions (TFRs), located in special use airspace during restrictive times in a restricted area, or in prohibited areas. Information on these will be listed on Notices to Airmen (NOTAMs)[16].

Site inspection: Tall trees, power lines, road shoulders, private property, accessibility, and anything else that may affect the drone or cause issue with access to the flight mission (for example imaging) must be identified. In addition, anything of note for the survey should be noted.

[15] https://www.faa.gov/uas/programs_partnerships/data_exchange
[16] https://www.notams.faa.gov/dinsQueryWeb/

- *Flight briefing:* After observations have been made, the team should regroup to share their findings with the pilot in command. The pilot will decide on a flight path, flight height, ground control point locations, and desired locations for visual observers. The team will give feedback to the pilot until a final plan is complete.
- *Drone inspection:* Before flight, the drone should be inspected to assure airworthiness (see Sec. 1 Part 5 Inspections and Maintenance).

1.2 In-flight

During flight, the pilot must maintain constant communication with the team and notify the team of any changes to the original plan. Visual observers will notify the pilot if the drone is no longer in their line of sight and of any possible collisions that may occur. In addition, the visual observers will notify the pilot when they are nearing the area to be inspected. Once the mission is complete, the drone will land as specified in the flight plan.

1.3 Post-flight

Once the flight is complete and the drone touches down, the following should be done:

- The team can regroup and debrief with the pilot.
- Collected data can be taken off the drone and uploaded to a computer for post processing. The data should be shared with other involved parties as well as any cloud shared folders for back-up.
- A post-flight report should be written to document the flight. This report should include sections detailing the findings of the data collected and any notes on the condition of the surveyed area. General information should be listed first, such as participants, date, and goals. In addition, any planned deviations from typical procedures should be noted and explained. Any issues or accidents should be discussed along with possible solutions. An example flight report is shown in Appendix C.

1.4 Inspections and Maintenance

Once a drone system has been acquired and tested for airworthiness, the maintenance of a drone mainly consists of visual inspections before, during, and after flight. For the frame of the drone, look for cracks, delamination, deep scratches, and surface bubbles. Anything that seems out of the ordinary should be replaced and inspected carefully. Propellers should be inspected for chips, cracks, stress discoloration, and delamination (for fiber-based propellers). All the connections such as screws and bolts should not be loose and should be rust free. Use thread lock when available and tighten to the proper spec (generally hand tight with the correct tool is fine). If the drone is operating in a high moisture environment, it may be a good idea to coat the screws in a layer of oil to prevent corrosion. It is difficult to inspect electronics without complicated tools and tedious measurements. So, a general system of checks before flights is suggested. Ensure all wireless connections are in good working order. Run the motors without lifting off to make sure the controls work as they should. Listen for any out of the ordinary sounds in the motor. This may be an

oscillating sound, ticking, loud whirring, etc. With the battery unplugged, spin the motors with your hands to make sure there isn't any strong resistance or scraping noises. For motor bearing maintenance, disassemble the motors to take out the bearings. If they are dry, apply some dry lubricant to the ball bearings, bearing cage, and bearing race.

2 Workflow for Image/Data Mosaic in ArcGIS

The images in field collected images in Task 2a were processed using ArcGIS Pro. ArcGIS Pro provides in-software support for the Micasense Rededge multispectral cameras used in this work, which streamlines the process. The workflow to create the stitched image in Fig. 2.1 and apply indices (like NVDI) is presented below.

Figure 2.1. Sample of ArcGIS Adjusted Data

1. Open a new project. Select the type of project or start without a template (Can be added later)

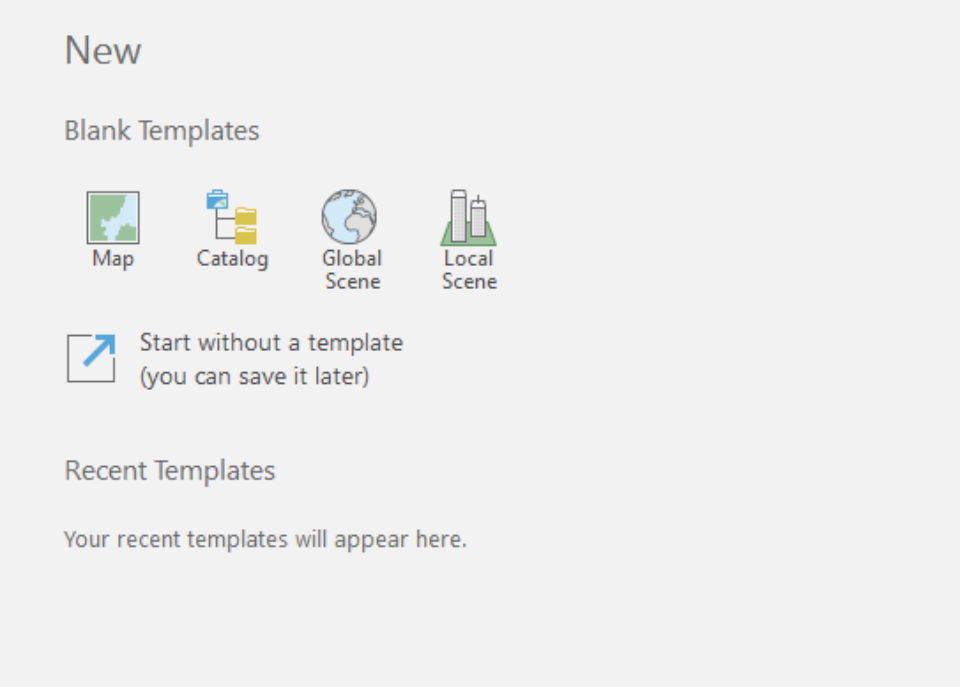

2. Start a new mapping workspace for each set of data.

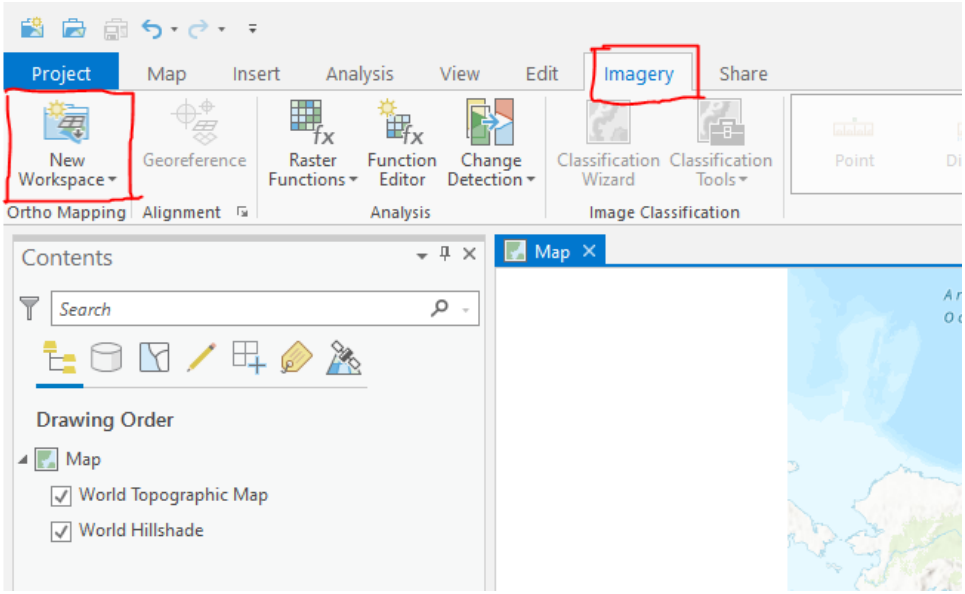

3. Set a name, continue to the next page (may change the basemap to what you like) and select the type of camera used along with the images from the survey. Geolocation and spatial reference should be automatically filled.

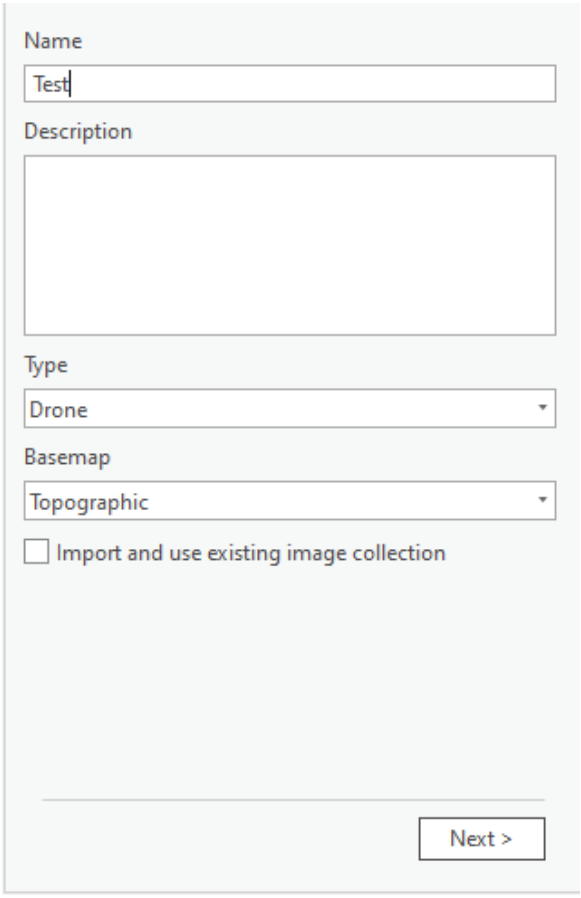

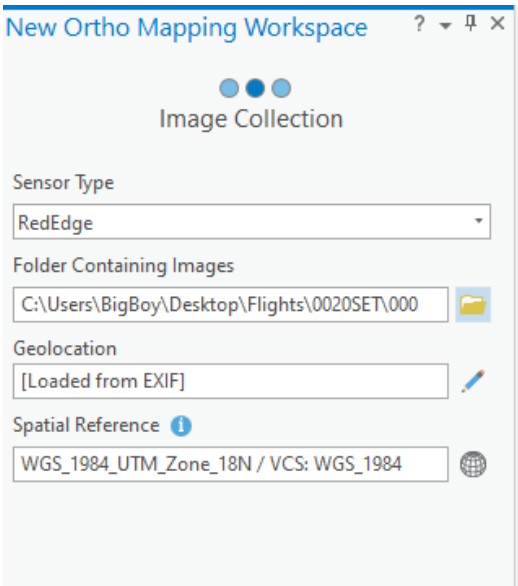

4. Select the elevation source. If the drone flight is at a constant altitude, use the constant elevation option with the approximate altitude. Ensure statistics and pyramids are built. Press finish once all options are set.

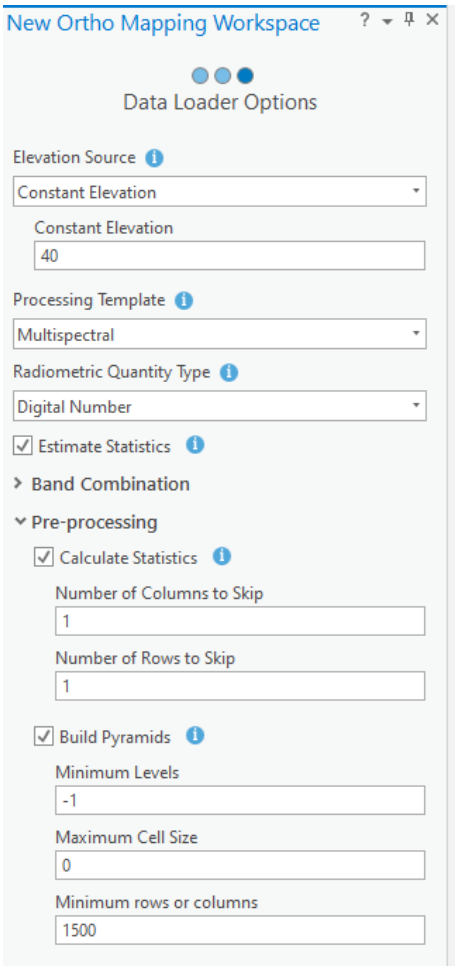

5. The program will place all the images in the correct spot. This may take a couple of minutes depending on the processing power of the computer used.

6. Once the program finishes, select the adjust tool. Change any settings desired and check the high accuracy GPS if GPS signal during the survey was strong.

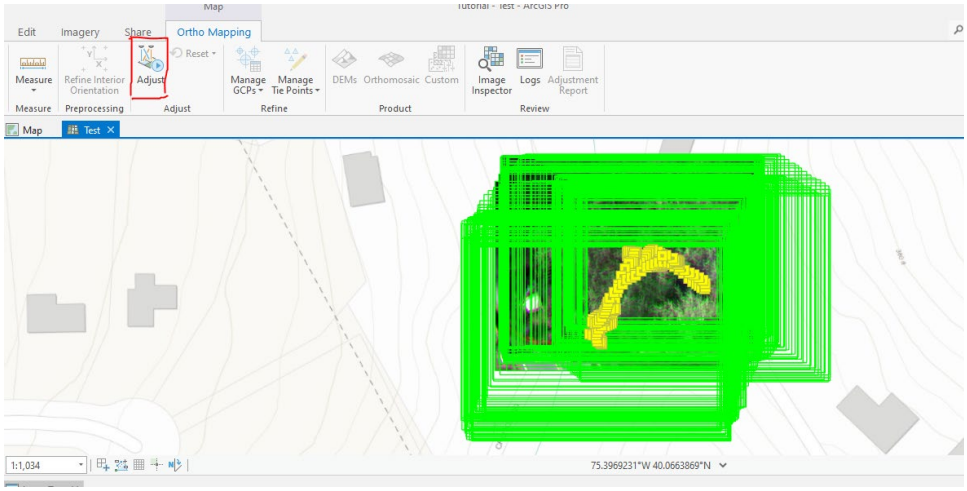

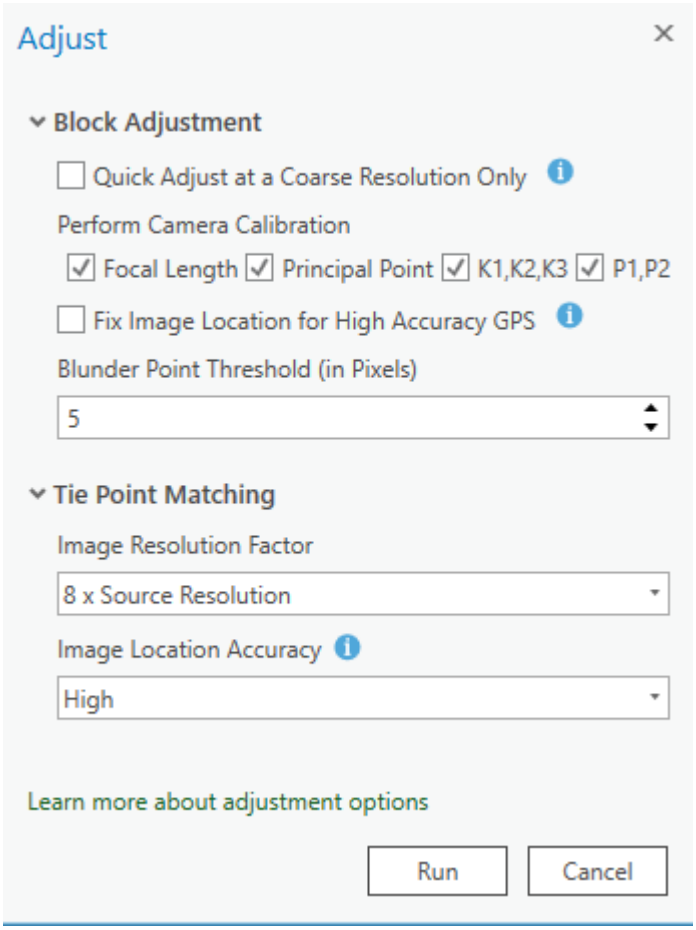

7. The program will align the bands of the camera and adjust the images for possible tilt in the images. Finally, it will place these images together into a rough mosaic.

8. In order to calculate indices for the images, the resulting mosaic has to be processed into an "orthomosaic". Select the orthomosaic tool.

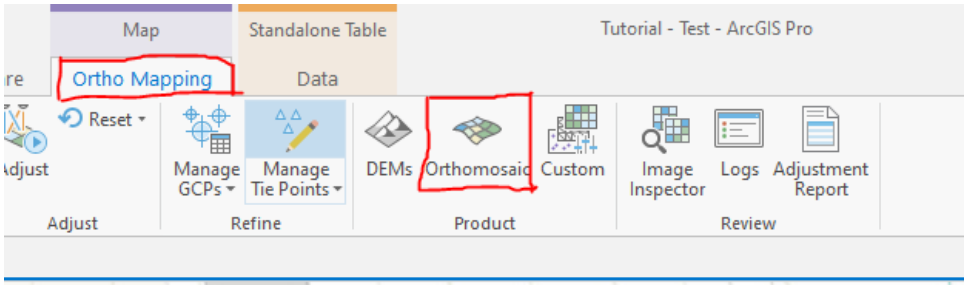

9. Settings can be adjusted if need be. Standard settings will be used for this project. The program will now perform final adjustments to the images.

10. Once the image has been converted to an orthomosaic, indices can be easily calculated using built in imagery tools. Make sure the orthomosaic is selected on the content list to the left.

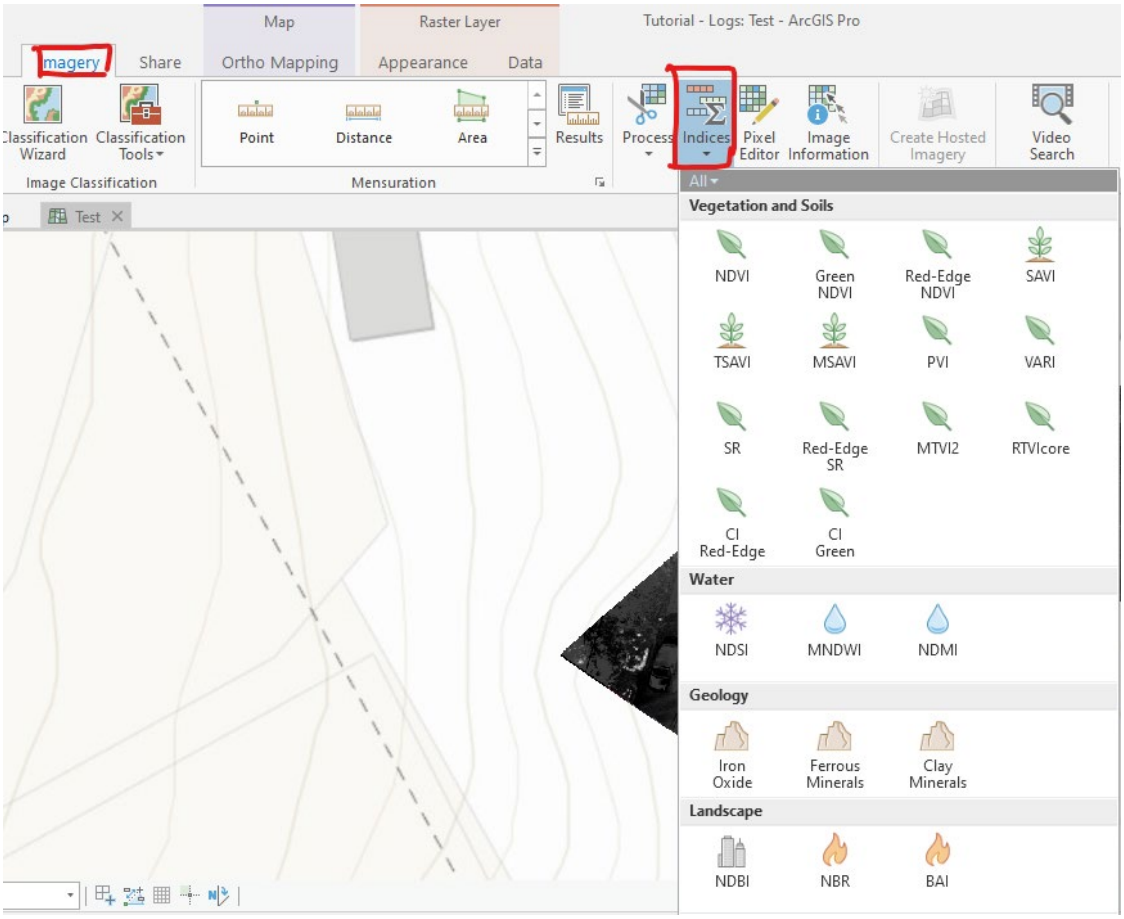

11. The resulting image can now be exported by right clicking its selection on the content list to the left and selecting data and export raster.

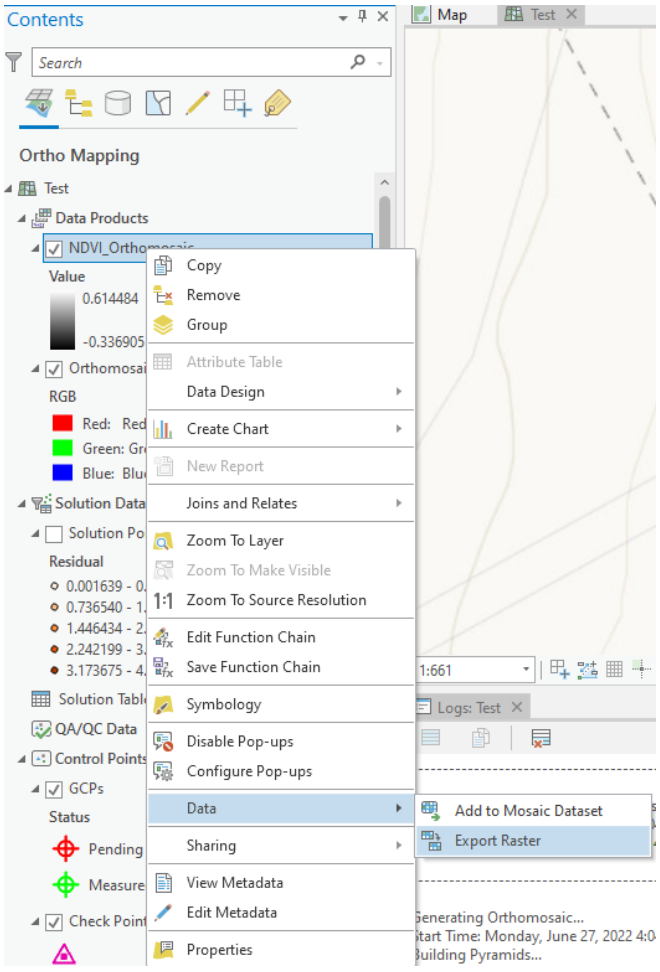

Task 2 References

Acevo-Herrera, R., Aguasca, A., Bosch-Lluis, X. & Camps, A. (2009) On the use of compact band dicke radiometer (ariel) and UAV for soil moisture and salinity map retrieval: 2008/2009 field experiments. In IEEE International Geoscience and Remote Sensing Symposium. 4, 729.

Archer, F., Shutko, A. M., Coleman, T. L., Haldin, A., Novichikhin, E., & and Sidorov, I. (2004). Introduction, overview, and status of the microwave autonomous copter system (macs). International Geoscience and Remote Sensing Symposium. 5, 3574-3576.

Arnold T., De Biasio, M., Fritz, A., & Leitner, R. (2013) Uav-based measurement of vegetation indices for environmental monitoring. In Sensing Technology (ICST), 704-707.

Ayad, M., Li, J., Holt, B., & Lee, C. (2020). Analysis and classification of stormwater and wastewater runoff from the Tijuana River using remote sensing imagery. *Frontiers in Environmental Science*, *8*. https://doi.org/10.3389/fenvs.2020.599030

Baby, S. N., Arrowsmith, C., Liu, G.-J., Mitchell, D., Al-Ansari, N., & Abbas, N. (2021). Finding Areas at Risk from Floods in a Downpour Using the Lidar-Based Elevation Model. Journal of Civil Engineering and Architecture, 15. https://doi.org/10.17265/1934-7359/2021.01.001

Baluja, J., Diago, M. P., Balda, P., Zorer, R., Meggio, F., Morales, F., & Tardaguila, J. (2012). Assessment of vineyard water status variability by thermal and multispectral imagery using an unmanned aerial vehicle (UAV). Irrigation Science, 1-12.

Bamburry (2015), D. Drones: Designed for product delivery. Design Management Review, 26(1), 40-48.

Bendig, J., Yu, K., Aasen, H., Bolten, A., Bennertz, S., Broscheit, J., Gnyp, M. L., & Bareth, G. (2015). Combining UAV-based plant height from crop surface models, visible, and near infrared vegetation indices for biomass monitoring in Barley. *International Journal of Applied Earth Observation and Geoinformation*, *39*, 79–87. https://doi.org/10.1016/j.jag.2015.02.012

Berni, J., Zarco-Tejada, P. J., Suarez, L., & Fereres, E. (2009). Thermal and narrowband multispectral remote sensing for vegetation monitoring from an unmanned aerial vehicle. *IEEE Transactions on Geoscience and Remote Sensing*, *47*(3), 722–738. https://doi.org/10.1109/tgrs.2008.2010457

Breili, K., James Ross Simpson, M., Klokkervold, E., & Roaldsdotter Ravndal, O. (2020). High-accuracy coastal flood mapping for Norway using lidar data. Natural Hazards and Earth System Sciences, 20(2), 673–694. https://doi.org/10.5194/nhess-20-673-2020\

Crimmins, M., Park, S., McCarthy, L., & Smith, V. (2019). Exploring the Application of LiDAR for Flooded Roadway Management. International Conference on Transportation and Development 2019: Innovation and Sustainability in Smart Mobility and Smart Cities -

Selected Papers from the International Conference on Transportation and Development 2019, 36–45. https://doi.org/10.1061/9780784482582.004

Dabrowska, J., Dabek, P. B., & Lejcuś, I. (2018). Identifying surface runoff pathways for cost-effective mitigation of pollutant inputs to drinking water reservoir. Water (Switzerland), 10(10). https://doi.org/10.3390/w10101300

Duggal, V., Sukhwani, M., Bipin, K., Reddy, G. S., and Krishna, K. M. (2016) Plantation monitoring and yield estimation using autonomous quadcopter for precision agriculture. International Conference on Robotics and Automation (ICRA). 5121-5127.

Dunbabin, M & Marques, L. (2012). Robots for environmental monitoring: Significant advancements and applications. IEEE Robotics & Automation Magazine, 19(1)j, 24-39.

Elmekati, A. H., Dannenberg, R., & Ghanem, N. M. (2019). Geotechnical Health Assessment of Roadway Embankment Using Airborne LiDAR. 131–137. https://doi.org/10.1061/9780784482070.013

Favorskaya, M. N., & Jain, L. C. (2017). Overview of Lidar technologies and equipment for land cover scanning. In Intelligent Systems Reference Library (Vol. 122, pp. 19–68). Springer Science and Business Media Deutschland GmbH. https://doi.org/10.1007/978-3-319-52308-8_2

Garnett, R., & Adams, M. D. (2018). LiDAR-A technology to assist with smart cities and climate change resilience: A case study in an urban metropolis. ISPRS International Journal of Geo-Information, 7(5), 161. https://doi.org/10.3390/ijgi7050161

Gaspard, N., Garza, N., Hernandez, M., & Ogidan, O. S. (2020). Developing a Proactive City-Wide Stormwater CCTV Master Plan and Condition Assessment Program San Antonio, TX. Pipelines 2020: Utility Engineering, Surveying, and Multidisciplinary Topics - Proceedings of Sessions of the Pipelines 2020 Conference, 362–371. https://doi.org/10.1061/9780784483213.040

Gay, A. P., Stewart, T. P., Angel, R., Easey, M., Eves, A. J., Thomas, N. J., Pearce, D., A., & Kemp, A. I. (2009). Developing unmanned aerial vehicles for local and flexible environmental and agricultural monitoring. In Proceedings of RSPSoc 2009 Annual Conference. 471-476.

Goel, P. K., Prasher, S. O., Patel, R. M., Smith, D. L., & DiTommaso, A. (2002). Use of airborne multi–spectral imagery for weed detection in field crops. *Transactions of the ASAE*, *45*(2), 443–449. https://doi.org/10.13031/2013.8513

Grant, A. T. J., McKinney, N. L., & Ries, R. (2018). An approach to quantifying rainwater harvesting potential using imagery, geographic information systems (GIS) and LiDAR data. Water Science and Technology: Water Supply, 18(1), 108–118. https://doi.org/10.2166/ws.2017.026

Gurganus, C. F., Gharaibeh, N. G., & Scullion, T. (2017). Case study on the use of mobile lidar to produce a preliminary drainage design. Transportation Research Record, 2655(1), 82–90. https://doi.org/10.3141/2655-11

Hung, C. L. J., James, L. A., & Hodgson, M. E. (2018). An automated algorithm for mapping building impervious areas from airborne LiDAR point-cloud data for flood hydrology. GIScience and Remote Sensing, 55(6), 793–816. https://doi.org/10.1080/15481603.2018.1452588

Ivan, K., Gagacka, D., & Matecka, P. (2018). AUTOMATED TOOL FOR THE EXTRACTION OF THE SURFACE PONDS BASED ON LIDAR DATA. Geographia Technica, 13, 96. https://doi.org/10.21163/GT_2018.132.07

Jenal, A., Bareth, G., Bolten, A., Kneer, C., Weber, I., & Bongartz, J. (2019). Development of a VNIR/SWIR multispectral imaging system for vegetation monitoring with unmanned aerial vehicles. *Sensors*, *19*(24), 5507. https://doi.org/10.3390/s19245507

Kaneko, K. and Nohara, S. (2014). Review of effective vegetation mapping using the UAV (unmanned aerial vehicle) method. Journal of Geographic Information System, 6(6), 733.

Kontopoulou, E., Kolokoussis, P., & Karantzalos, K. (2017). Water quality estimation in Greek lakes from Landsat 8 multispectral satellite data. *European Water*, *58*, 191–196.

Larson, M. D., Simic Milas, A., Vincent, R. K., & Evans, J. E. (2018). Multi-depth suspended sediment estimation using high-resolution remote-sensing UAV in Maumee River, Ohio. *International Journal of Remote Sensing*, *39*(15-16), 5472–5489. https://doi.org/10.1080/01431161.2018.1465616

Lee, C. C. (Barry), & Gharaibeh, N. G. (2020). Automating the evaluation of urban roadside drainage systems using mobile lidar data. Computers, Environment and Urban Systems, 82, 101502. https://doi.org/10.1016/j.compenvurbsys.2020.101502

Li, B., Hou, J., Li, D., Yang, D., Han, H., Bi, X., Wang, X., Hinkelmann, R., & Xia, J. (2021). Application of LiDAR UAV for High-Resolution Flood Modelling. Water Resources Management, 35(5), 1433–1447. https://doi.org/10.1007/s11269-021-02783-w

Liu, H., Xiao, P., Zhang, X., Zhou, X., Li, J., & Guo, R. (2021). Object-based island green cover mapping by integrating UAV Multispectral Image and Lidar Data. *Journal of Applied Remote Sensing*, *15*(03). https://doi.org/10.1117/1.jrs.15.034512

Neupane, S. R., & Gharaibeh, N. G. (2019). A heuristics-based method for obtaining road surface type information from mobile lidar for use in network-level infrastructure management. Measurement: Journal of the International Measurement Confederation, 131, 664–670. https://doi.org/10.1016/j.measurement.2018.09.015

Okyay, U., Telling, J., Glennie, C. L., & Dietrich, W. E. (2019). Airborne lidar change detection: An overview of Earth sciences applications. https://doi.org/10.1016/j.earscirev.2019.102929

Parmehr, E. G., Amati, M., Taylor, E. J., & Livesley, S. J. (2016). Estimation of urban tree canopy cover using random point sampling and remote sensing methods. Urban Forestry and Urban Greening, 20, 160–171. https://doi.org/10.1016/j.ufug.2016.08.011

Peter, D. K., d'Oleire Oltmanns, S., Ries, J. B., Marzol, I., & Hssaine, A. A. (2014). Soil erosion in gully catchments a_ected by land-levelling measures in the souss basin, Morocco, analysed by rainfall simulation and uav remote sensing data. Catena, 113, 24-40.

Prior, E. M., O'Donnell, F. C., Brodbeck, C., Runion, G. B., & Shepherd, S. L. (2020). Investigating small unoccupied aerial systems (SUAS) multispectral imagery for total suspended solids and turbidity monitoring in small streams. *International Journal of Remote Sensing*, *42*(1), 39–64. https://doi.org/10.1080/01431161.2020.1798546

Rivai, M., Hutabarat, D., & Jauhar Nafis, Z. M. (2020). 2D mapping using omni-directional mobile robot equipped with LiDAR. Telkomnika (Telecommunication Computing Electronics and Control), 18(3), 1467–1474. https://doi.org/10.12928/TELKOMNIKA.v18i3.14872

Robertson, J. J., Fletcher, T. D., Danger, A., & Szota, C. (2018). Identifying critical inundation thresholds to maintain vegetation cover in stormwater treatment wetlands. *Ecological Engineering*, *116*, 80–86. https://doi.org/10.1016/j.ecoleng.2018.02.031

Sankey, T., Donager, J., McVay, J., & Sankey, J. B. (2017). UAV Lidar and hyperspectral fusion for forest monitoring in the southwestern USA. Remote Sensing of Environment, 195, 30–43. https://doi.org/10.1016/j.rse.2017.04.007

Shams, A., Sarasua, W. A., Famili, A., Davis, W. J., Ogle, J. H., Cassule, L., & Mammadrahimli, A. (2018). Highway Cross-Slope Measurement using Mobile LiDAR. Transportation Research Record, 2672(39), 88–97. https://doi.org/10.1177/0361198118756371

Soliman, A., Heck, R. J., Brenning, A., Brown, R., & Miller, S. (2013). Remote sensing of soil moisture in vineyards using airborne and ground-based thermal inertia data. Remote Sensing, 5(8), 3729-3748.

Xie, X., Zhao, M., He, J., & Zhou, B. (2019). Automatic and visual processing method of non-contact monitoring for circular stormwater sewage tunnels based on LiDAR Data. Energies, 12(9), 1599. https://doi.org/10.3390/en12091599

Yan, W. Y., Shaker, A., & El-Ashmawy, N. (2015). Urban land cover classification using airborne LiDAR data: A review. In Remote Sensing of Environment (Vol. 158, pp. 295–310). Elsevier Inc. https://doi.org/10.1016/j.rse.2014.11.001

Yuan, J., Dunnett, N., & Stovin, V. (2017). The influence of vegetation on rain garden hydrological performance. *Urban Water Journal*, *14*(10), 1083–1089. https://doi.org/10.1080/1573062x.2017.1363251

Zhang C. & Kovacs, J. M. (2012). The application of small unmanned aerial systems for precision agriculture: a review. Precision agriculture, 1-20.

Zhang, Z., Yin, T., Huang, X., Zhang, F., Zhu, Y., & Liu, W. (2019). Identification and visualization of the full-ring deformation characteristics of a large stormwater sewage and storage tunnel using terrestrial laser scanning technology. Energies, 12(7), 1304. https://doi.org/10.3390/en12071304

Task 2 Appendix List

Appendix A: Drone Subsystems

Appendix B: Custom Lidar Sensor Package

Appendix C: Sample Flight Report

Appendix A: Drone Subsystems

Drones contain a number of subsystems (seen in Fig. 1) that are all important to performance. While many of these components are not directly apparent in commercial drones, industrial and DIY drones require knowledge about these subsystems. A discussion of important subsystems is provided in this appendix.

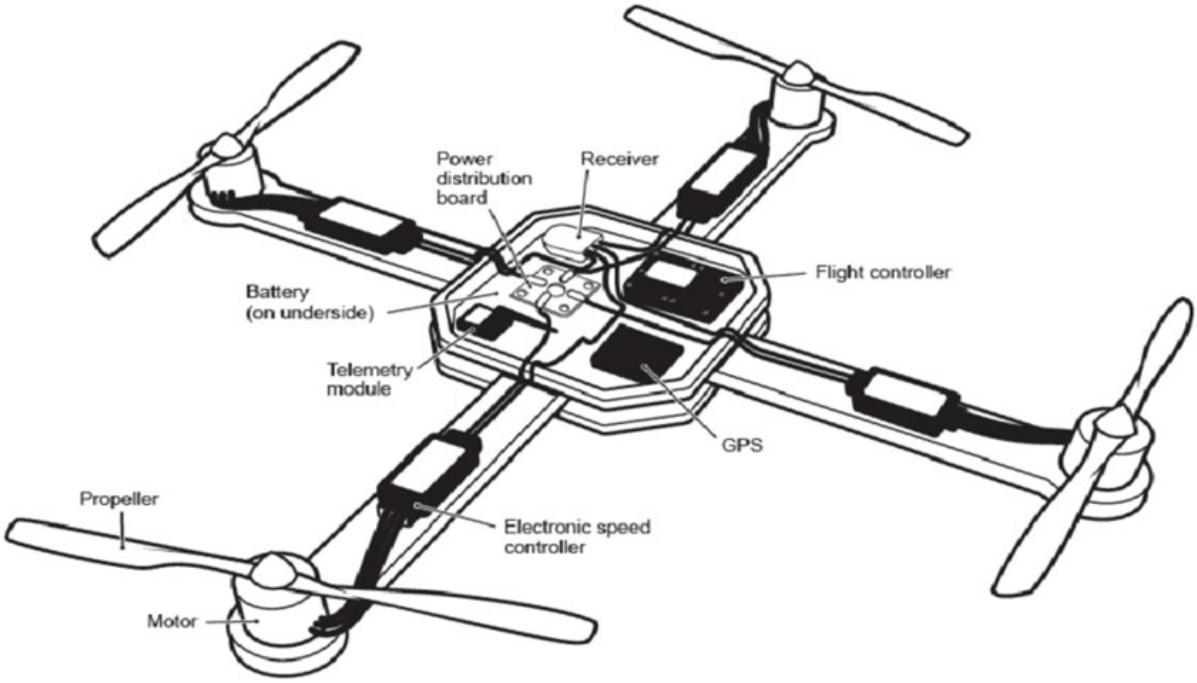

.

Figure 1. Drone Component Diagram
https://www.researchgate.net/figure/Architecture-of-a-drone_fig2_313903813

1 Flight Controller

The flight controller is arguably the most important part of the drone. It handles all of the real time processing and control to make sure the drone can stay in the air. In addition, most flight controllers handle telemetry, audio/video streaming, and radio control. There are 4 streams of data that the flight controller oversees: GPS, inertial measurement unit (IMU), radio, and telemetry. An example flight controller from DJI is shown in Fig. 2.

Figure 2. DJI A2 Flight Controller Package
https://www.dji.com/a2

GPS: For imaging and sensor packages, GPS is extremely important for post processing purposes and automation. Built in GPS allows the drone to fly on its own without the need for human input. For large plots of land, this is extremely useful as a human pilot is not required for the flight which reduces possible errors in image capture. The ideal imaging pattern covers the entire desired area with regularly spaced images. A human pilot would not be able to perfectly fly the path using only manual controls. For surveys without automation, GPS is one of the few sensors used by the flight controller to maintain a steady hover in the wind.

Inertial Measurement Unit: An inertial measurement unit (IMU) is a device that measures the tilt and acceleration of the drone. It is a combination of accelerometers, gyros, and magnetometers. Most drone IMUs only integrate accelerometers and gyros as magnetometers are not that important to flights. The data from the IMU is what is mostly processed by the flight controller in real time. By measuring the tilt and acceleration of the drone in real time, it can ensure the drone does not flip over by automatically increasing or decreasing power to the motors. This adjustment can be relative to the radio control input, to the wind, or to the drone's weight imbalance. Flight controllers for racing drones have an option for a complete manual mode (disabling the IMU system) which allows the drone to power its motors past an easily balanceable limit. This allows the pilot to perform stunts and fast turns, but at the cost of the drone being unable to keep itself in the air without constant input.

Radio: The radio system on a drone typically refers to the radio receiver from the controller. This receiver has enough connections for each motor of the drone and typically some extra connections for other manually controllable subsystems. This may be for lights, camera connections, a parachute, landing gear, gimbal controls and anything else added to the drone. The radio controller chosen for a drone should have enough switches to fly the drone and operate various systems. It is recommended for multiple radio controllers to be used if there are too many systems to be operated.

For example, a drone with a robotic arm attached may have a pilot who controls the movement of the drone and associated systems while an operator uses their own radio controller to control the robotic arm. It is better to have more operators than to risk overloading the pilot and possibly causing an accident.

Telemetry: Telemetry is the two-way connection between the drone and ground station for data. Many flight controllers offer telemetry for only sensors that are integrated into it. It is useful for knowing the state of the drone as it flies and provides useful information such as battery voltage, GPS signal, radio signal and more. For professional use, telemetry is used for automated flying or live streaming of data to the ground station. For that form of telemetry, separate specialized modules are required to be attached to the drone as flight controller telemetry cannot handle the data on its own.

Batteries: Batteries are the source of energy for the entire drone. There can be multiple batteries which are in charge of supplying power to different subsystems of the drone. The motor's speed controllers of the motors will have a specification on the voltage of battery needed. In addition, the battery should be able to supply the maximum current specified by the speed controllers as well as any other components. The maximum current rating can be found as the "C" rating on lithium polymer batteries, which will provide the maximum current when multiplied by the battery's rated capacity in milliamp-hours.

2 Motors and Electronic Speed Controllers (ESCs) and Propellers

The main propelling power of the drone is generated by the motors attached to each arm. Propellers are attached to the ends of the motor which creates the lifting force of the drone. This system is shown in Fig. 3. The electronic speed controller (ESC) supplies the power from battery or distribution board to the input of the motor. Generally, drone motors are brushless direct current (BLDC) motors. This means that instead of direct current supplied to the positive and negative ends of the motors, there is a three-phase input from the speed controller. So, three inputs of alternating current are needed to power the motors. The ESCs vary the voltage supplied to the motor as well as the frequency of the input voltage. The faster the motor needs to spin, the higher the voltage and frequency needs to be.

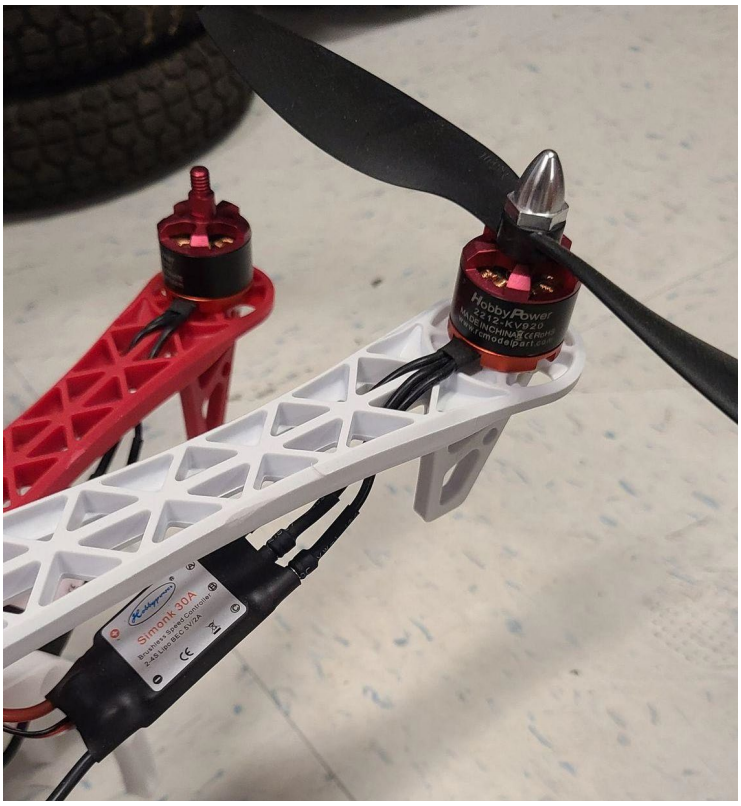

Figure 3. Drone Motors Mounted

For the selection of the motor, the size of the motor should be chosen in accordance with the compatible size of the frame. A 4-digit number notes the size of the motor with the first two numbers describing the diameter of the motor and the last two numbers describe the height of the motor, both in millimeters. Select a motor with the correct sizing and specified for drone applications. Several motor specifications should be noted when deciding on which ESC and propeller to pair with it.

Maximum voltage, maximum current, maximum power, and suggested ESC current help to decide on the ESC specifications. Select an ESC that can handle all of the maximum specifications. Some websites and vendors specify a suggested ESC current which is extremely useful for selecting a compatible ESC. For drone use, there is no need for too many extra features on the ESC. The ESCs do not need features like reversing or power regeneration which are useful for ground vehicles.

For propellers, the motor key type, KV rating, and shaft diameter are specifications for propeller selection. Additionally, ideal propeller specification may be included in the specification of the selected frame. Both the motor key type and shaft diameter ensure physical compatibility of the motor and propeller. Some propellers may specify the motor size that it is designed for. KV rating of the motor describes how fast the motor will spin at a certain voltage without any load. KV is described as RPM/V. For compatible motors with lower KV, it may be a better option to use a higher number of blades for additional lift. Motors with the same physical dimensions, but with different KV differ only in the torque curve. In general, lower KV motors generate more torque than higher KV, however higher KV has the potential to spin faster.

3 Frame

The frame of the drone includes the body, arms, landing gear, mount points, and the battery tray, an example of which is shown in Fig. 4. Various frame models may have additional parts that may not come with other frames. Frame materials vary from manufacturer to manufacturer; however, they consist of high strength, low weight composites. Common materials include carbon composites, glass composites, and even wood for certain types of drones such as fixed wing drones (drones made like airplanes).

Figure 4. Heavy Lift Drone
https://hobbyking.com/en_us/turnigy-h-a-l-heavy-aerial-lift-quadcopter-frame-585mm.html?queryID=fe0abbf40b5c6270810f8d78622f5ddb&objectID=46391&indexName=hbk_live_products_analytics

When considering a frame, find out the physical dimensions of the payload that will be attached to it. The payload should fall within the footprint of the body of drone itself. In addition, the height of the payload should not exceed the height of the landing gear from the body to the ground. If the dimensions exceed these criteria, the possibility of damaging the drone during flights and surveys will increase. The drone may topple when landing if the package is too tall and the handling performance may be negatively affected with too wide of a footprint.

Another factor to consider is the ability to modify the frame. This may be extra screw holes for the mounting of 3D printed parts, simple geometries for easy designing of parts, or extra motor hole sizes to allow bigger motors to be attached. This is important for developing sensor packages as requirements and weights change. When more weight or subsystems are added, larger motors and additional mounting points make it simple to maintain the performance of the drone.

4 Optional Subsystems Distribution Board and Gimbal

Distribution boards: Distribution boards, like the one shown in Fig. 5, are circuit boards designed to connect the battery to the various components of a drone. They are useful for powering subsystems on drones as they contain circuitry that supplies standard voltages to its additional connections. So, instead of having multiple batteries or multiple voltage converters to supply power to subsystems, a distribution board completes this task with a single circuit board. For larger drones, distribution boards may be built into the body, as shown in Fig. 6. For example, the DJI S900 body contains a distribution board which supplies power to the flight controller, gimbal, landing gear, motors, and XT60 connectors for additional subsystems. When deciding on whether to use a distribution board, consider the amount of power needed to power the additional systems. If the additional systems require a significant amount of power, it may be a good idea to separate the systems to prevent a sudden high draw in the subsystem from affecting the rest of the drone.

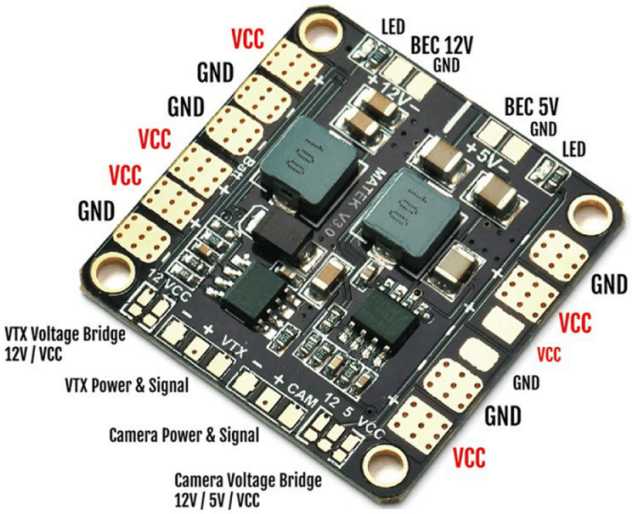

Figure 5. Power Distribution Board with Contact Labels
https://www.aldeid.com/wiki/Category:Drones/Power-Distribution-Board/Matek

Figure 6. Frame Integrated Power Distribution Board from a DJI S900
https://epfilms.tv/review-for%E2%80%AFdji-spreading-wings-s900-hexacopter/

Gimbals: Gimbals, as shown in Fig. 7, are typically mounted on the front or bottom of the drone. They help stabilize image and video capture from the camera. Drone gimbals are typically three axes, which stabilize in the 3 orthogonal rotational axes. In addition to stabilization, it serves as the pan and tilt control for the camera with some models including interface with the camera for zoom and remote capture. Gimbals are extremely useful for survey purposes as the images produced by the system do not have to be adjusted for camera tilt. The drone can move in any fashion while the camera will always be pointed in the direction that it is set at. However, this only works if the gimbal is balanced correctly. Before flying, ensure the gimbal is properly balanced in all three axes. Weights can be added to adjust balance, as well as sliding the arms of the gimbal to the weight of the camera.

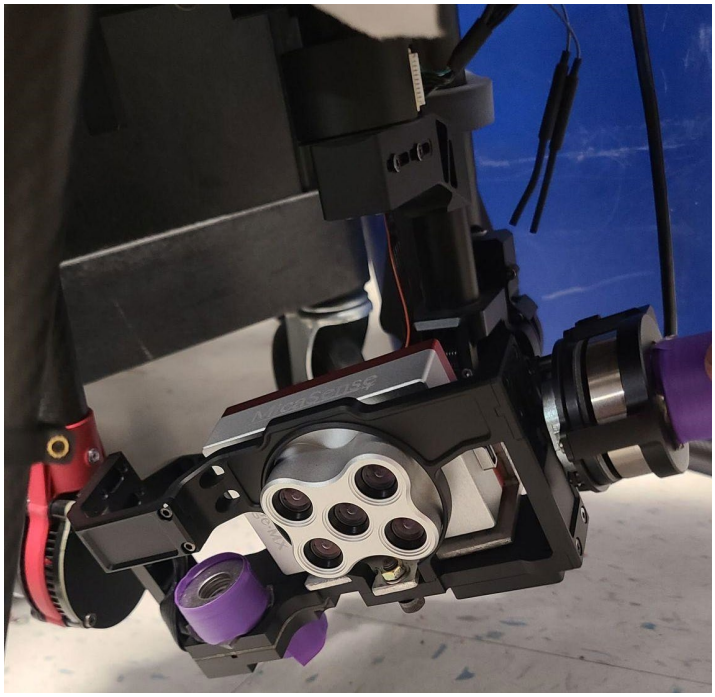

Figure 7. Micasense Rededge Multispectral Camera Mounted on a Gimbal

Appendix B: Custom Lidar Sensor Package

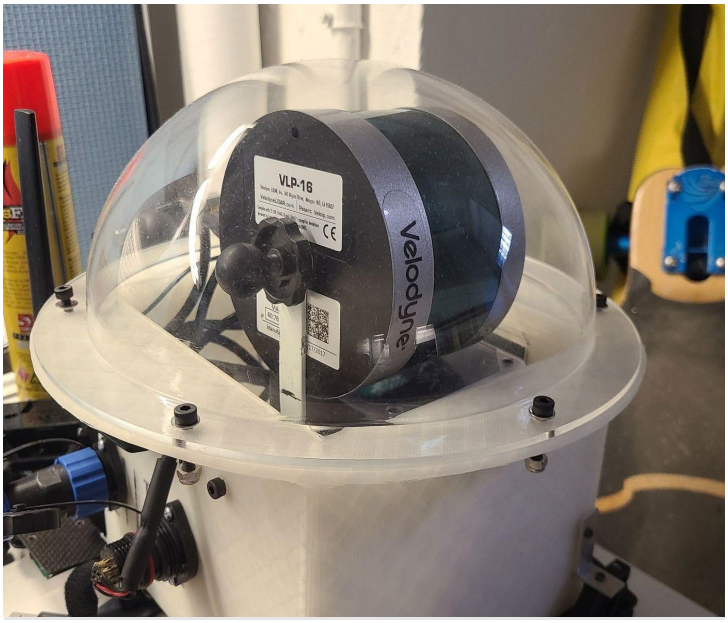

Figure 1. Low-Cost Lidar Package

The custom Lidar package used in this work is shown in Fig. 1. It includes a Raspberry Pi 4, Emlid Reach M+ GPS module, Velodyne VLP-16 Lidar, a dedicated battery and a Pololu MinIMU-9 V5. The Raspberry Pi is running Raspberry Pi OS and all components are integrated together with the Robot Operating System (ROS) Noetic Version[17].

3A.1 Sensor Package Localization

Localization of the sensor package is critical to accurately convert collected Lidar data into a point cloud. Two components are used to localize the sensing package. A high accuracy GPS sensor and an inertial measurement unit (IMU).

- GPS takes signals from satellites to localize itself (and hence the object attached to it) on the Earth's surface. The GPS used in this project is seen in Fig. 2 with an attached long-range radio (LoRa) module. This allows it to connect with a larger "base station" GPS shown in Fig. 3. This "base station" receives GPS corrections over the internet to allow it to have centimeter accuracy. These corrections can then be processed and forwarded to the GPS module on the drone to improve its accuracy.
- The IMU used in this package incorporates an accelerometer, gyroscope, and magnetometer into one single circuit board. By combining the measurements from these three components, an accurate pose (orientation) of the package/robot can be determined.

[17] http://wiki.ros.org/noetic

Figure 2. Emlid Reach M+ GPS Module with Long Range Radio Module Connected
https://blog.emlid.com/lora-radio-reach-m-store/

Figure 3. Emlid Reach RS+ Stationary GPS System

3A.2 Sensor Path Estimation

The raw data from the GPS and IMU give some information about the location of the sensor package, but neither can give the location at any instance in time. The GPS module has excellent accuracy, but it updates at most 14Hz; the IMU does not know the exact global location so eventually a flight path plot based on the IMU will drift away from the real position due to noise as time goes on. The IMU does have a much higher update rate, which gives a lot better kinematic tracking. The disadvantages of the individual sensors can be overcome through the use of a Kalman filter, resulting in a more accurate path plot, as shown in Fig. 4. Note that the Kalman filter utilizes

all sensing data and its uncertainty. Specific details of this method are omitted here, but can be explored at the link in the figure caption.

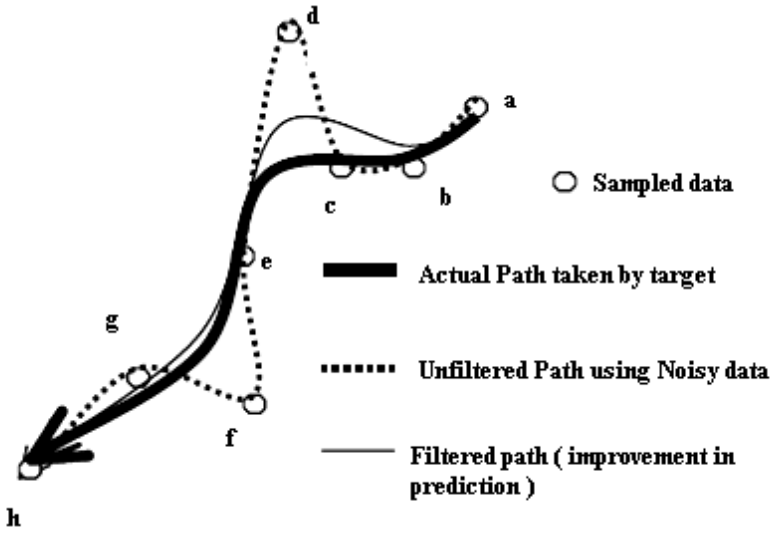

Figure 4. Kalman Filter Diagram Example
https://www.researchgate.net/figure/Target-tracking-by-Kalman-filter-in-WSN_fig1_49612785

Appendix C: Sample Flight Report

Flood Mitigation Solutions

5112001 – VU WO 003

FLIGHT REPORT

Friday, January 14, 2022, and January 21,2022
1:00pm – 4:00pm

I. Attendees

- ❑ Flight Team:
  - Remote Pilot in Command (RPIC) (Kyle Fok)
  - Visual Observer (VO) (Richard Starkey)
  - Visual Observer (VO) (Jessica Erben)

II. Flight Goals

- Collect multispectral data.
- Utilize procedures set from last flight into use.
- Identify issues and shortcomings of procedures.

III. Review of Findings

- **TASK 1: Collect Multispectral Data**
  - Imaging Locations
    - Two locations were identified to be of interest from the flood closures document. These locations were recently closed due to flooding. In addition, the locations provide an excellent line of sight for drone operation. Both places were imaged on the upstream banks.
    - Several vital positions for imaging were identified at each location. For the Old Sumneytown Pike location, the patch of trees along the Long Mill Roadside of the creek was of particular interest due to its relatively low elevation when compared to the opposite bank. For the Garges Road location, the bank opposite Haldeman Road was of particular interest as the washout of that bank can be clearly seen from the vegetation. A short line of vegetation appeared to be flooded and decomposing. A local resident informed us of certain locations that were washed out from previous storms.
- **TASK 2: Utilize Procedures set from last flight into use.**
  - Procedures from the previous drone flight were used in this flight.
    - Lessons learned from the previous drone flight were used to improve the workflow of this drone flight. Although this flight took longer than expected, the workflow was much clearer and easier to follow.
  - Flight Pattern
    - The flight pattern followed the same ideology as the previous drone flight. With the main interest in bank washout and scours, the focus should be on vegetation surrounding the creek. Instead of a "zigzag" style of pattern which would encompass a larger area, a "loop" pattern was used instead. With this method, it is easier to postprocess the images into a continuous picture of the bank.
- **TASK 3: Identify Issues and Shortcomings of Procedures.**
  - Spare Parts

        - Due to an error in landing, the drone toppled while landing during the first flight (January 14th). This destroyed the front two sets of propellers. New parts were requested, along with the tool to replace them. However, due to two seized screws, the team was not able to replace them in the field.
        - Additional propellers should be brought for every drone flight, including new screws and thread locker.
    - Additional Tools
        - With the screws on the motors seized, the Allen key could not provide enough torque to release them. A pair of pliers was used in the lab to remove these screws in addition to the Allen key. A good set of pliers should be brought for each flight.
    - Decide on GPS Modes Before Flight
        - For the second flight, an issue with the GPS flight system caused a brief loss of control in the drone causing a propeller to come into contact with a branch. This broke off the tip of the propeller. Even though the drone was still operational with one of the propellers damaged, the common drone flight procedure for this issue is to replace and discard the damaged propeller.
        - GPS modes should only be changed when clear of any objects. Without a direct reading of GPS data, it is possible for an incorrect reading to eventually correct which may cause unintended movement.
    - Eye Protection
        - For individuals in close proximity to the drone at any point, eye protection is needed. Any propeller contact can launch debris at high speed. Even without contact, a fractured propeller may break at any time which will also launch the propeller pieces at high speed.

Task 3 Executive Summary

This study investigates stormwater inundation of the roadway system impacts the safety, maintenance, operation, and ultimately the overall sustainability of a roadway network. This was accomplished through examining the transportation network response to three characteristic high stream flow events, which impacted the function of the Pennsylvania District 6 transportation network. High flow events, resulting in road closures are common in urban areas, but unfortunately costly. District is bound and bi-sected by the Delaware River, the Schuylkill River, and several small creeks, e.g., the Darby, Cobb, Pennypack, Frankford, and Tacony. The stream responses to different types of wet weather events are reflected differently across the transportation network. The primary objective of task three is to answer the question: what is the system impact of flood inundation to safety and operation from a network perspective? Can priority locations be identified?

This report specifies three subtasks (3a, 3b, 3c) to establish the system impact of flood inundation to safety and function from a network perspective, while identifying priority locations. This has been accomplished through the following tasks:

- Task 3a: Spatial network analysis to assess the impact of flood inundation from a network safety and network flow perspective
- Task 3b: Prioritizing areas of risk based on the network analysis
- Task 3c: Work with PennDOT to identify task priority locations, priority issues, and focuses for recommendations in a final report, aligning with PennDOT's Asset Management Initiatives.

The objectives of these subtasks were completed by conducting a spatial network analysis to assess the impact of flood inundation from a network safety and network flow perspectives. This analysis sought to understand how different sections of the transportation network (e.g., different roadway categories) respond to high stream flow events in terms of congestion and speed reduction, as well as crashes. A spatial analysis of environmental parameters highlighted variables from the physical environment associated with road closures as well as network congestion and spatial temporal speed reduction (Task 3a). This information can be used to identify and prioritize areas of risk through regression to identify the hydrologic drivers of flood and network risk (Task 3b). These findings can be integrated with existing Penn DOT programs and initiatives to support and aid in the advancement of programs for asset management (Task 3c). Ultimately, the findings of this report establish and describe features in the physical environment that can be used to predict bridge closures during different types of high flow events and their influence on roadway networks.

A Workflow Diagram for Task 3

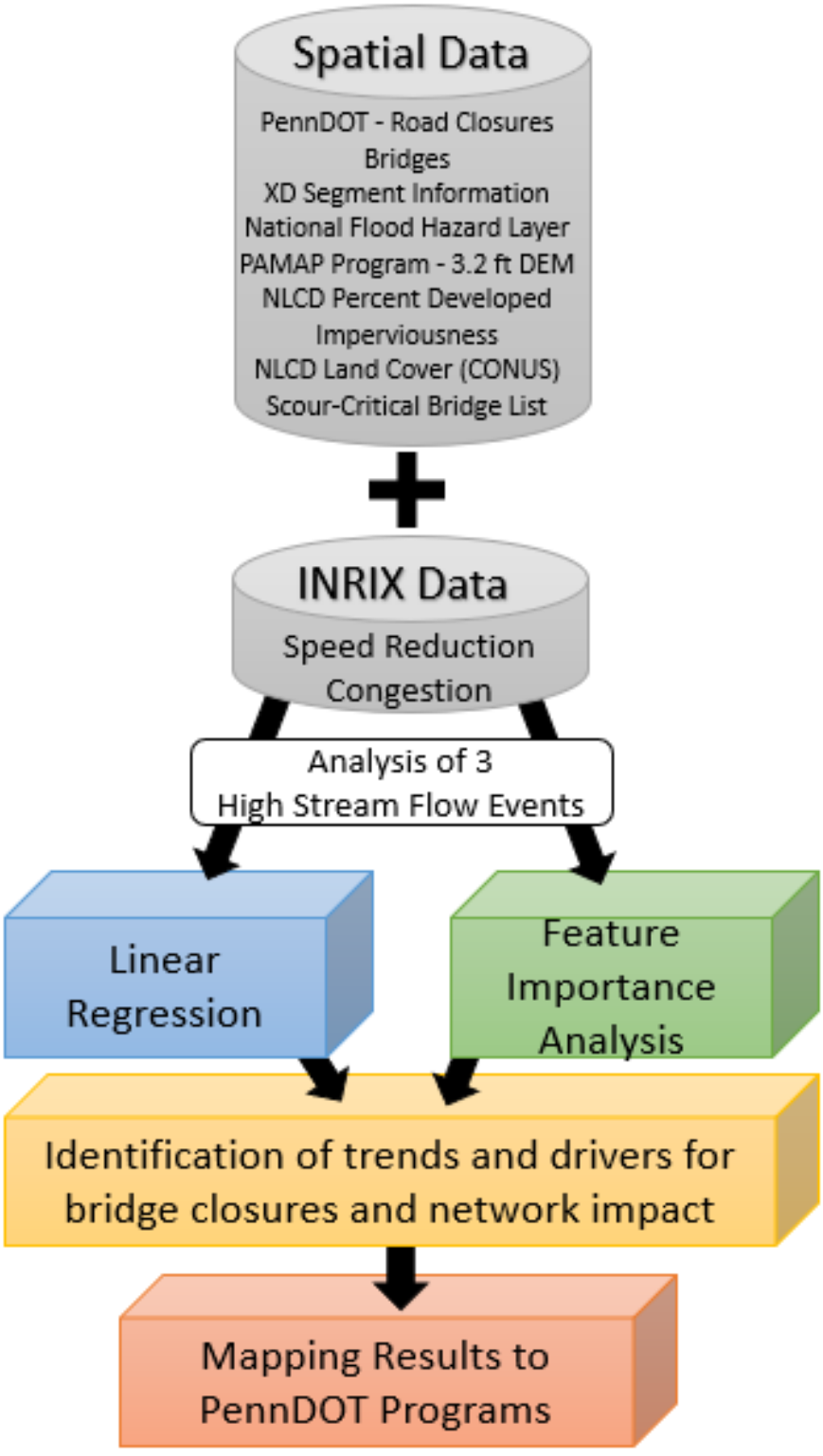

Task 3a: Summary

In this subtask, roadway segment speed values during the selected three severe high stream flow events were obtained through the Regional Integrated Transportation Information System (RITIS) platform to be compared to road closures. The events were chosen as the primary events resulting in road closures over a six-year period of data. RITIS data was collected for all of the events. By analyzing the network impact of these distinct and different high stream flow events reviewed, our goal was to identify any traffic patterns, mainly focusing on the network congestion degree based on speed profiles, that might be relevant to different high stream flow events. This was analyzed relative to five roadway categories along with the two developed congestion indices.

In general, results demonstrated that local roadways exhibit elevated congestion pattern compared to interstates during these events. The two congestion indices were also applied in Task 3b for an in-depth spatial analysis to obtain a further understanding of roadway and bridge closures, due to the high stream flow events, and network performance. Speed data indicated that each storm event had impact on network, but at varying degree depending on the roadway classifications and road closure status.

Task 3a Report

1 Introduction

Ample studies have noted the impacts of severe high stream flow events from various contexts such as economy, infrastructure maintenance and deterioration, and safety (Schinko et al, 2020; M. Allaire 2018; Pregnolato et al, 2017; Zhang et al 2020; Nasr et al, 2021), as described in the Task 1 literature review. While the analyses of post-storm event impacts are evaluated to further prevent such damages, little focus has been centered to identify features (e.g., topography, hydraulic elements, bridge elements, etc.) that play a significant role in roadway closure and subsequently their impact on transportation network performance. This study section aims to review and assess transportation network performance during severe high stream flow events. Results of this section will provide basis in correlating various roadway closure variables presented in Task 1. The study findings will also have the potential to assist in prioritizing the resources for streamlined infrastructure management by providing severe storm event hazard locations (report Task 3b).

2 Data, Methods, and Observations

To assess different impacts of high stream flow events, the team has is located three major high flow events, five years of road closure data (2016-2021), as presented in Task 1. Physical variables were extracted for the drainage area upstream of all of the bridges in the District, and amended to the bridges as metadata (Task 1). To understand their impact on the roadway network, average speed values and two different speed reduction indices were assessed to capture network congestion levels. This subsection illustrates definitions of various network segment classifications, congestion levels, and speed analysis steps. Speed data was obtained from the Regional Integrated Transportation Information System (RITIS) platform, a data-driven platform for transportation analysis, monitoring, and data visualization. Probe vehicle data as well as National Performance Management Research Data Set (NPMRDS), mainly from INRIX a third-party company, are reviewed in this project. Results of this project will identify opportunities to further prepare for the extreme events.

2.1 Roadway Segments/Links

Within the RITIS platform, there are two types of roadway segments of which speed data is obtained. Description of each segment and selection of a particular type, in this case XD segment, are noted below.

TMC Based Segments

RITIS provides roadway linked to the Transportation Management Centers (TMCs). These are coded based on the Traffic Message Channel location tables which are maintained by third party entities. As such, their coverage is limited mainly to major roadways such as interstate freeways.

XD Segments

As illustrated by the Federal Highway Administration (FHWA) roadway functional classifications (FHWA, 2017), different roadways are designed to serve different traffic volumes and speeds. Similar to this roadway concept, a total of five different roadway segments are defined and referred to as XD segments, which delineate specific roadway sections. XD segments are controlled by INRIX, allowing new XD segments to be routinely added as new roadways are constructed. In order to understand how the high stream flow events impacted the traffic network, speed values were pulled from the XD segments that can better present a wide range of roadway functional classification - not limiting to major roadways. Of importance to note is that for some high stream flow events, the XD segments had no data as the corresponding XD segments were added to the network after the date of the storm event. XD segments are coded based on functional road classes (FRC). The FRCs are defined as the class or group of roads to which the road belongs. Table 2.1. below presents five separate FRCs and each class is correlated to PennDOT's Business Plan Network (BPN) organization used for their Pavement Asset Management Systems (PAMS).

Table 2.1. Functional Road Classes (FRC) per XD segment definition

FRC	Road Type	Description	Business Plan Networks (BPN)
1	National highway network	roads allow for high volume, maximum speed traffic movement between and through major metropolitan areas	Interstates
2	State highway network	applied to roads with very few, if any, speed changes. Access to the road is usually controlled. Applied to roads with very few, if any speed changes that allow for high-volume, high-speed traffic movement	National Highway System (NHS) Non-Interstate
3	Interconnecting network	applied to roads which interconnect FRC = 2 roads and provide a high volume of traffic movement at a lower level of mobility than FRC = 2 roads	Non-NHS (> 2,000 ADT)
4	Major connectors	applied to roads that provide for a high volume of traffic movement at moderate speeds between neighborhoods. These roads connect with higher functional class roads to collect and distribute traffic between neighborhoods	Non-NHS (> 2,000 ADT)
5	Minor roads	applied to roads whose volume and traffic movement are below the level of any functional class.	Non-NHS (< 2,000 ADT)

* ADT: Annual Daily Traffic

Details of the XD segments class distribution within this project study site, District 6, is described in Table 2.2 below. As expected, FRC 4 and 5 show the highest distribution rate as it relates to the secondary or local roadways.

Table 2.2. FRC Distribution in District 6 and Speed Finest Sampling Rate

FRC	Number of XD Segments	%	Finest Sampling Rate
1	495	0.87	5 min
2	1,549	2.72	5 min
3	5,158	9.05	10 min
4	21,955	38.54	15 min
5	27,813	48.82	15 min
Total	56,970	100.0	

2.2 Speed Data Collection

As traffic volumes and probe vehicle penetration rate differ per roadway features, different data sampling rate/granularity level is available per XD segment class. For instance, in case of XD FRC 1, as it relates to mainly interstates, there are sufficient probe vehicles traveling to provide speed data. Therefore, the highest data precision level is every 1-minute, meaning for every1-minute speed data is available. Table 2.2 illustrates each FRC's finest available sampling rate. In this project, speed data is retrieved at each possible finest granularity level for each FRC. This will allow capture any dynamic speed fluctuations during the congestion analysis processes. A step-by-step speed data collection process from RITIS platform is presented in Appendix A.

2.3 High stream flow events and Speed Data

As described above, for this study, three high stream flow events were chosen for analysis because these events had the highest number of road closures for the data period. Additionally, these specific events are representative of the three most common storm event types in District 6 of Pennsylvania and had the largest number of road closures during this period of study. The dates and storm characteristics, further described in Task 1, were defined based on the effective roadway closures as shown in Table 2.3.

Table 2.3. Reviewed High stream flow events

High Flow Event	Dates	Description
Rain/snow event	Nov. 24, 2018-Nov. 28, 2018	Beginning early Nov. 2018 District 6 experienced 3 significant high stream flow events, including the snow event analyzed in this study. Prior to the Nov. 24 - Nov. 28 event, a winter storm occurred 15 Nov. - 16 Nov, creating the snow that eventually melted at the same time of the Nov. 24 - Nov. 28 rain event, compounding flooding issues impacting the transportation network. Following the Nov. 24 - Nov. 28 event, another snow event occurred on Dec. 5. The short time period in which these three events occurred in close proximity to each other caused the extensive flooding and road closures examined in this study.
Hurricane Isaias	Aug. 3, 2020-Aug. 6, 2020	Extensive flooding occurred as a result of rainfall from Hurricane Isaias. low lying areas were particularly prone to flash flooding from the Schuylkill river and nearby streams. Septa reported mudslides at various stations and on rail lines. Further exacerbating the problem, downed trees and debris clogged storm drains, preventing runoff from being controlled.
Hurricane Ida	Aug. 31, 2021-Sep. 5, 2021	Historic flooding was observed in the Schuylkill river and nearby smaller streams. The Schuylkill river crested at a height not reached since 1869. Trees downed in severe winds created debris that caused drains to be clogged, and a major pumping station along the Vine Street Expressway to fail. Seven tornadoes were reported between PA and NJ causing further destruction and debris.

Trend Map Analysis and Observations

Using the RITIS platform trend map tool, XD segments per road class were added to the map presented in Appendix A. These maps were created based on the raw speed data recorded during each storm event and the worst-case scenario for each event was captured. This was done by examining the map in hour long increments over the duration of the storm event. The point at which the map contained the most XD segments colored red through orange indicates the point at which these segments experienced the lowest speeds during the storm event, indicating the worst-case scenario. The speed threshold colors were set in increments of 10 mph, with each color indicating a different speed. The darker red through orange indicate areas of concern as this represents when the speed was significantly slowed. Each image shows the period of time during the storm event that produced the most slowdowns resulting in dark red and orange colors on the map.

FRC 1: The FRC 1 roads were most adversely affected by the 2018 snowmelt event which produced significant congestion along I-476 in both the North and South directions. Hurricane Ida in 2021 also produced noticeable speed reductions along I-476, however less than compared to the 2018 snowmelt event. Hurricane Isaias produced the least speed reductions for FRC 1 roads when compared among three high stream flow events considered. Figure 2.1 of Task 3a presents the FRC 1 road worst congestion case of each storm event.

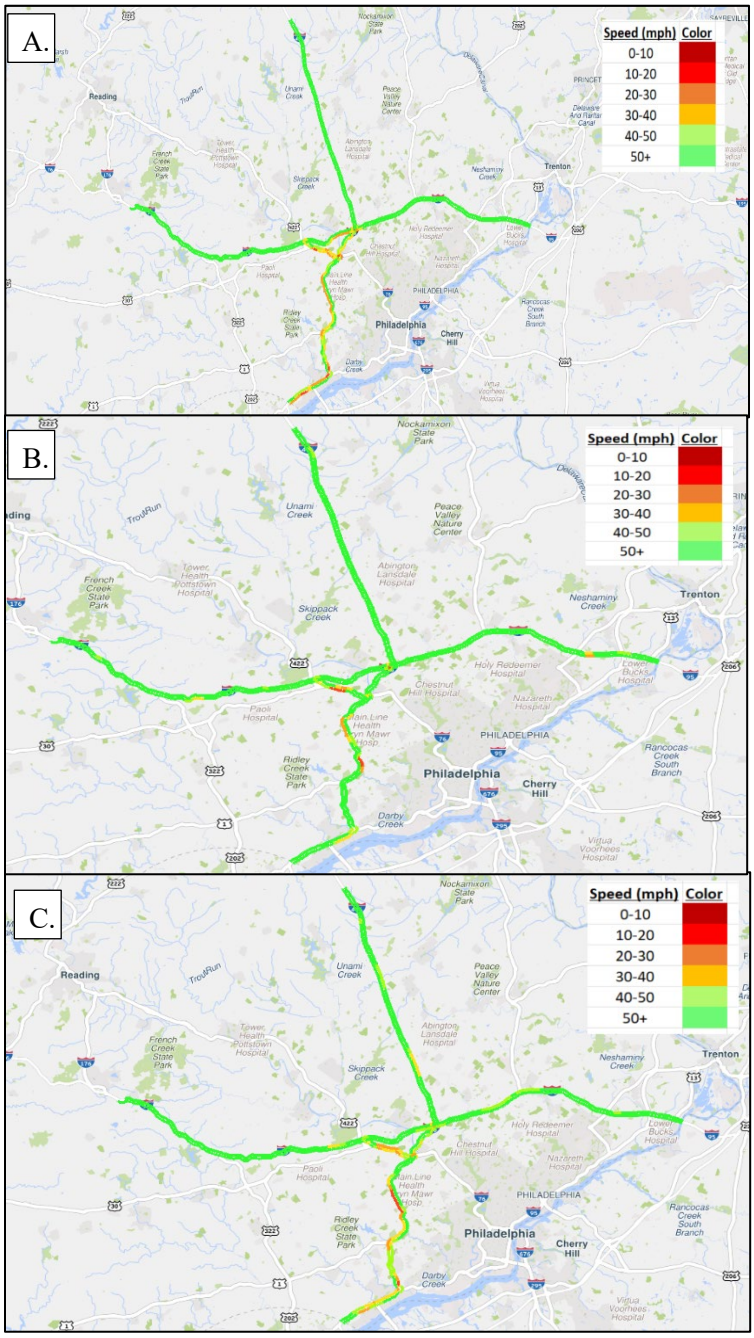

Figure 2.1. FRC 1 Congestion Trend Map. **(A)** Congestion resulting from the rain on snow event, **(B)** Congestion resulting from Hurricane Isaias, **(C)** Congestion resulting from Hurricane Ida.

FRC 2: As presented in Figure 2.2. of Task 3a, FRC 2 roads demonstrated similar speed impact patterns to FRC 1. The 2018 snowmelt event produced the most significant speed reductions, followed by Hurricane Ida in 2021 which also resulted in notable speed reductions. Hurricane Isaias in 2020 caused the least speed reductions in FRC 2 roadways.

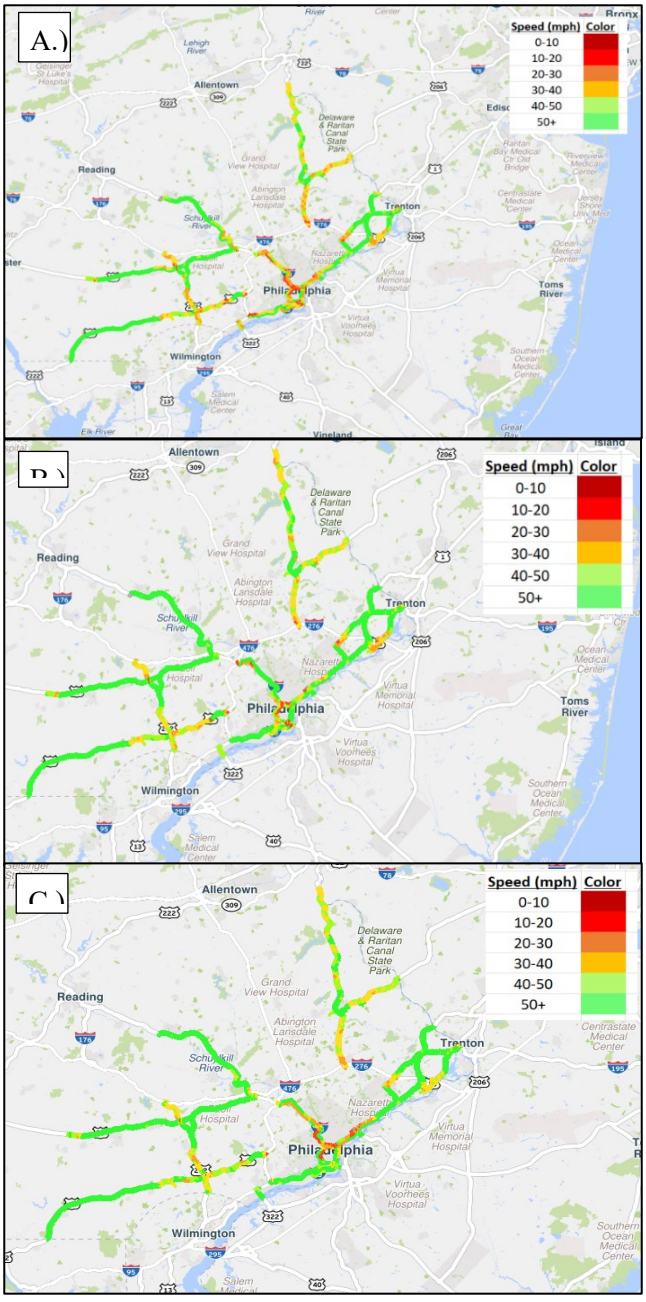

Figure 2.2. FRC 2 Congestion Trend Map **(A)** Congestion resulting from the rain on snow event, **(B)** Congestion resulting from Hurricane Isaias, **(C)** Congestion resulting from Hurricane Ida

FRC 3: The FRC 3 roads were affected similarly across the three high stream flow events. The worst speed reduction of over 80% occurred closest to Philadelphia near Washington Ave, West Allegheny Ave, and W Oregon Ave. The speed reduction became less severe the farther away the FRC 3 road was from center city Philadelphia, showing approximately 10% reduction value.

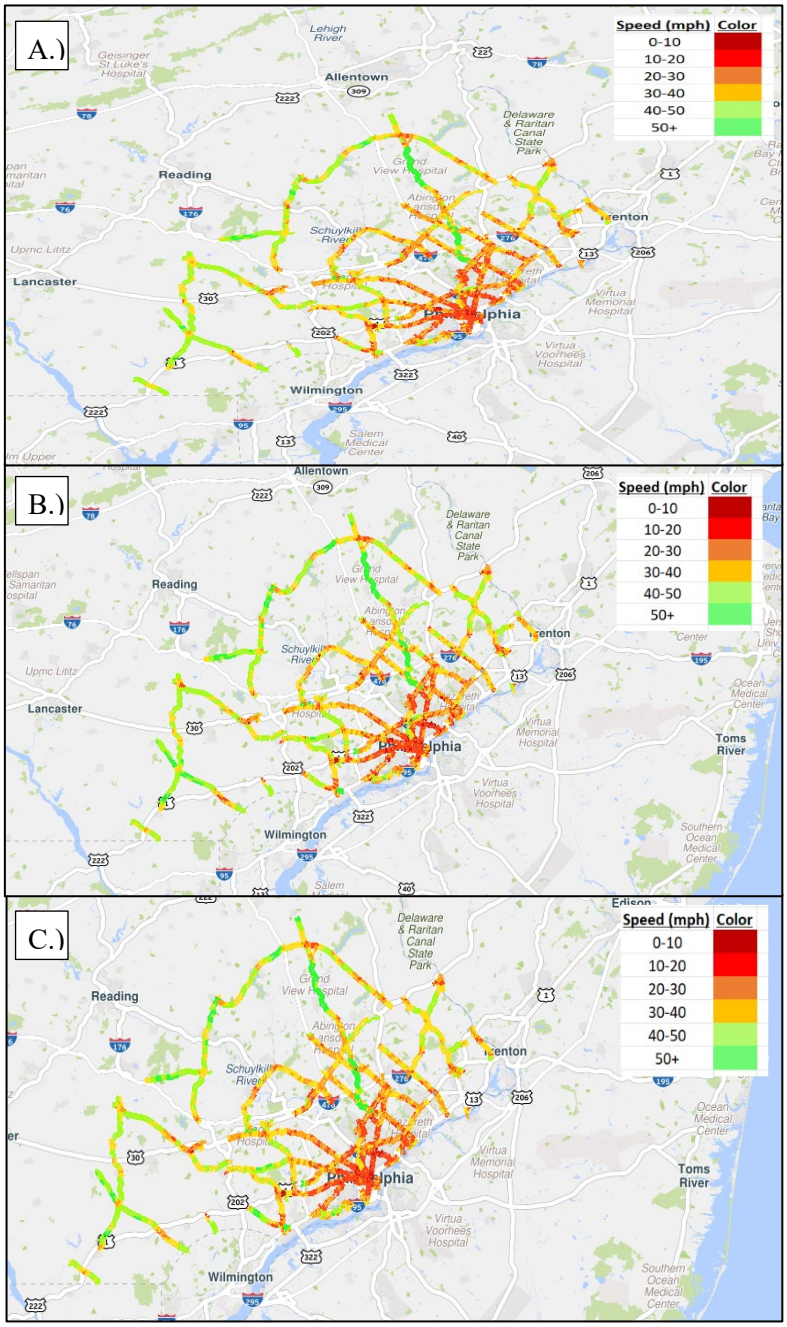

Figure 2.3. FRC 3 Congestion Trend Map. **(A)** Congestion resulting from the rain on snow event, **(B)** Congestion resulting from Hurricane Isaias, **(C)** Congestion resulting from Hurricane Ida

FRC 4: FRC 4 roads were also similarly affected across the various high stream flow events. Specifically, Hurricane Ida showed greater area covering red and orange zones than either the rain/snowmelt event or Hurricane Isaias, indicating significant impact of Ida on FRC 4. Complete figures are presented in Appendix B.

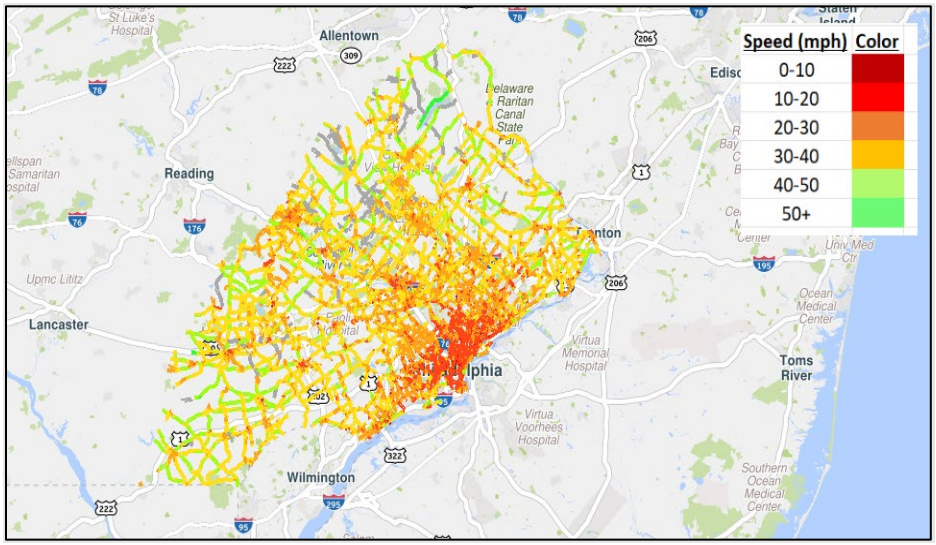

Figure 2.4. FRC 4 Congestion Trend Map. Congestion resulting from Hurricane Ida

FRC 5: In comparison to FRC 1 and FRC 2 roads, FRC 5 roads have displayed significant speed reduction. The majority of FRC 5 roads experienced speed reductions of over 50%, while FRC 1 and FRC 2 roadways experienced more isolated speed reductions, less than 10% speed reduction. Complete figures are presented in Appendix B.

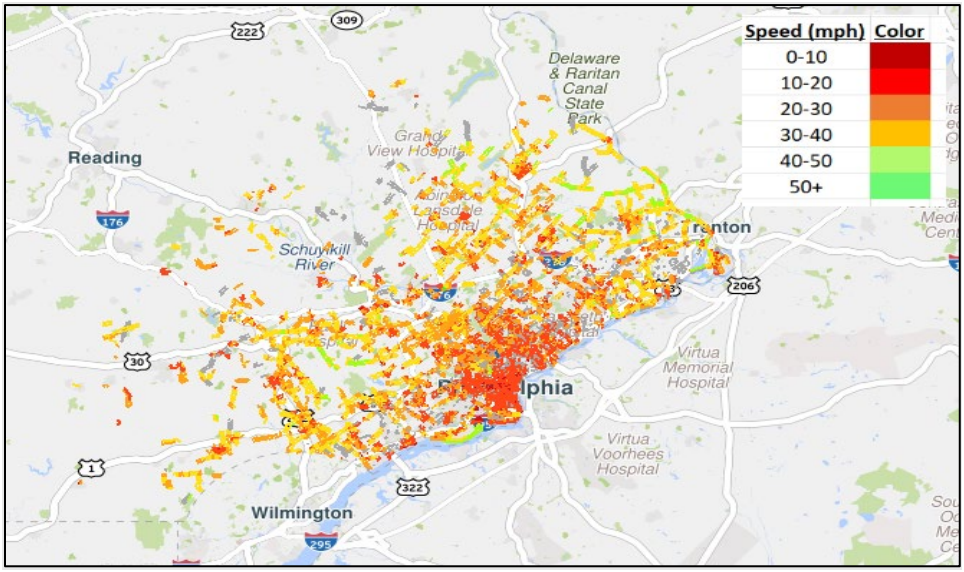

Figure 2.5. FRC 5 Congestion Trend Map. Congestion resulting from Hurricane Ida

2.3.2 Speed Change Observation and Analysis

In addition to examining the high stream flow events through the trend maps, the RITIS platform performance charts tool was used to display speed changes over time for each storm event. The following figures represent speed change over time by high stream flow events and by roadway class. Details of the speed changes are presented in Appendix C.

Daily Speed Change per Storm Event

Snowmelt storm event: The snowmelt event experienced the greatest speed changes over time during the peak hours of day 4 and day 5 of the event. This is when users experienced the most significant delay. The blue and purple drops (Day 3 and 4) in Figure 2.6. represent this speed drop from approximately 30 mph to approximately 25 mph.

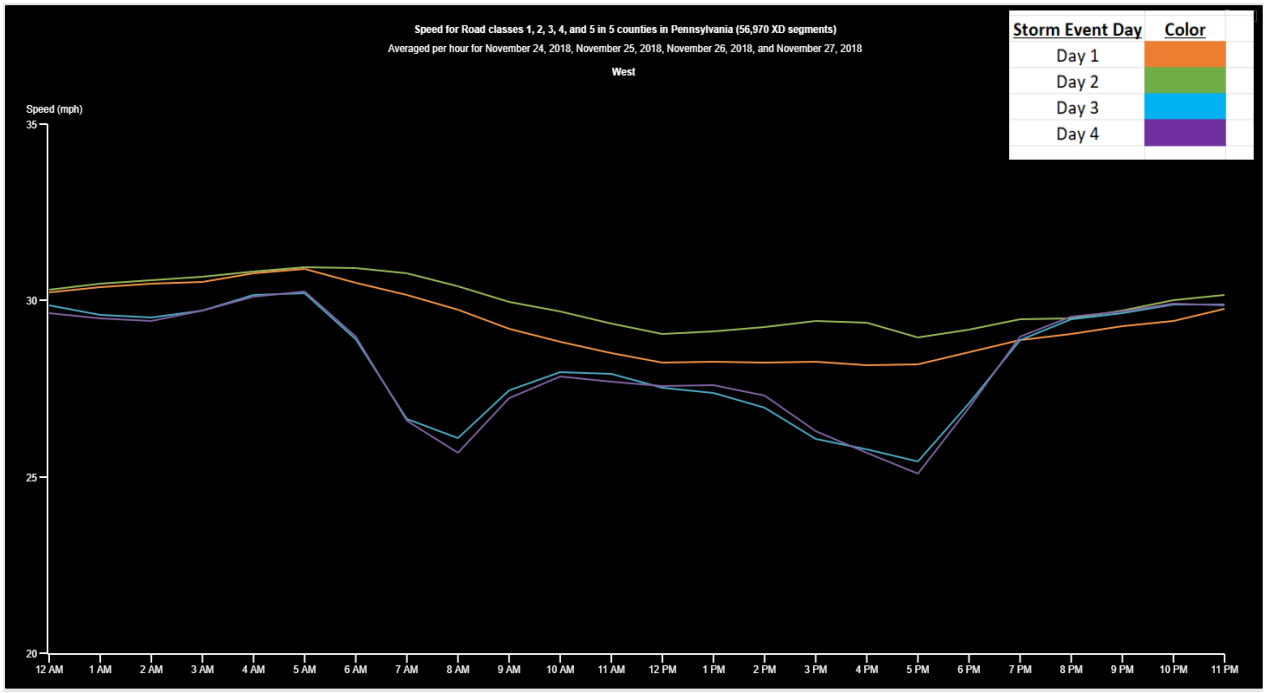

Figure 2.6. Daily Speed Change during Snowmelt Event

The following Figure 2.7 show the road classes individually during the snowmelt event. During the snowmelt storm event, FRC 1 and 2 roads had the largest speed variations across all 4 days of the storm. For each FRC, days 3 and 4 of the event had slower observed speeds than days 1 and 2. The speed reductions during days 3 and 4 were most significant on FRC 2 roads.

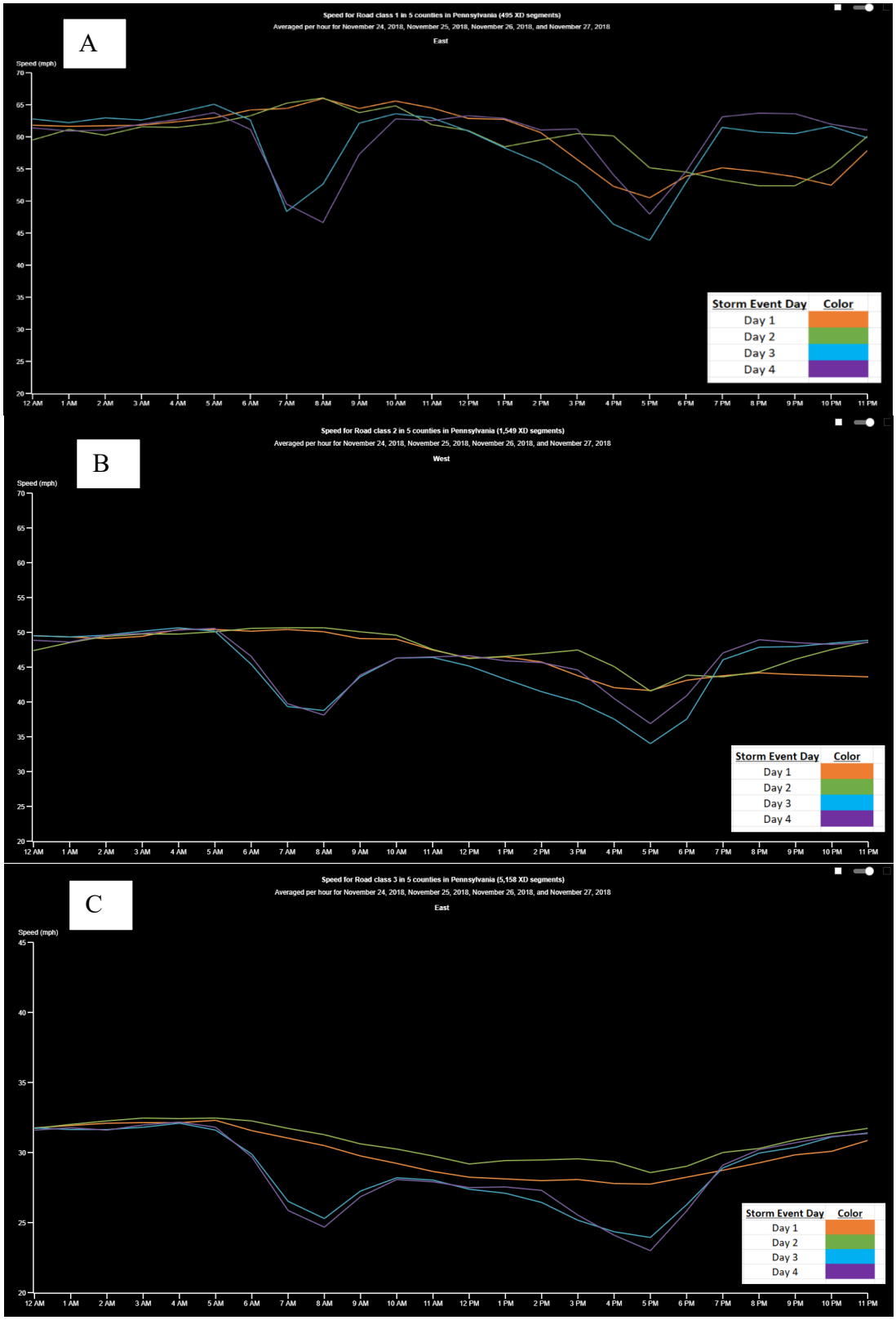
A
Speed for Road class 1 in 5 counties in Pennsylvania (495 XD segments)
Averaged per hour for November 24, 2018, November 25, 2018, November 26, 2018, and November 27, 2018
East
Speed (mph)
70
65
60
55
50
45
40
35
30
25
20
12 AM
1 AM
2 AM
3 AM
4 AM
5 AM
6 AM
7 AM
8 AM
9 AM
10 AM
11 AM
12 PM
1 PM
2 PM
3 PM
4 PM
5 PM
6 PM
7 PM
8 PM
9 PM
10 PM
11 PM
Storm Event Day
Color
Day 1
Day 2
Day 3
Day 4
B
Speed for Road class 2 in 5 counties in Pennsylvania (1,549 XD segments)
Averaged per hour for November 24, 2018, November 25, 2018, November 26, 2018, and November 27, 2018
West
Speed (mph)
70
65
60
55
50
45
40
35
30
25
20
12 AM
1 AM
2 AM
3 AM
4 AM
5 AM
6 AM
7 AM
8 AM
9 AM
10 AM
11 AM
12 PM
1 PM
2 PM
3 PM
4 PM
5 PM
6 PM
7 PM
8 PM
9 PM
10 PM
11 PM
Storm Event Day
Color
Day 1
Day 2
Day 3
Day 4
C
Speed for Road class 3 in 5 counties in Pennsylvania (5,158 XD segments)
Averaged per hour for November 24, 2018, November 25, 2018, November 26, 2018, and November 27, 2018
East
Speed (mph)
45
40
35
30
25
20
12 AM
1 AM
2 AM
3 AM
4 AM
5 AM
6 AM
7 AM
8 AM
9 AM
10 AM
11 AM
12 PM
1 PM
2 PM
3 PM
4 PM
5 PM
6 PM
7 PM
8 PM
9 PM
10 PM
11 PM
Storm Event Day
Color
Day 1
Day 2
Day 3
Day 4

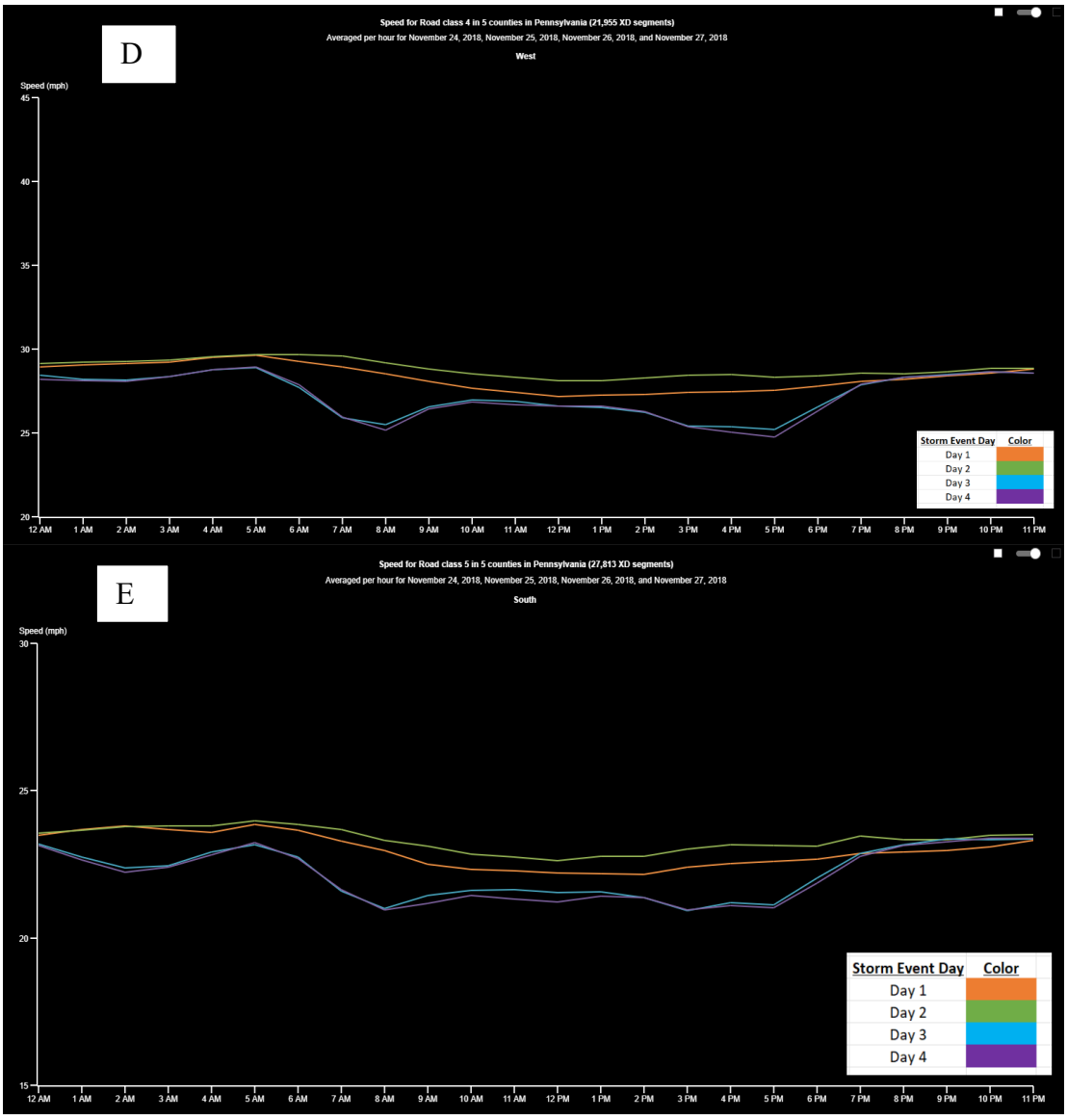

Figure 2.7. Daily Speed Change of all FRCs during Snowmelt Event. **(A)** FRC 1, **(B)** FRC 2, **(C)** FRC 3, **(D)** FRC 4, and **(E)** FRC 5.

Hurricane Isaias: The Isaias storm event experienced the greatest speed reduction during day 2 of the event but overall, the storm event days all followed a similar trend with less variance between individual days of the storm event when compared to the snowmelt event and Hurricane Ida. During Hurricane Isaias, FRC 2 roads experienced the greatest variation in speed. Consistent across all FRCs day 2 of the hurricane had the largest speed reduction from the other storm event days. This was most evident with the FRC 2 roads, where day 2 of the storm event was 20 mph slower than the speed observed on day 1, 3, or 4. Details of the speed change per road class are illustrated in Appendix C.

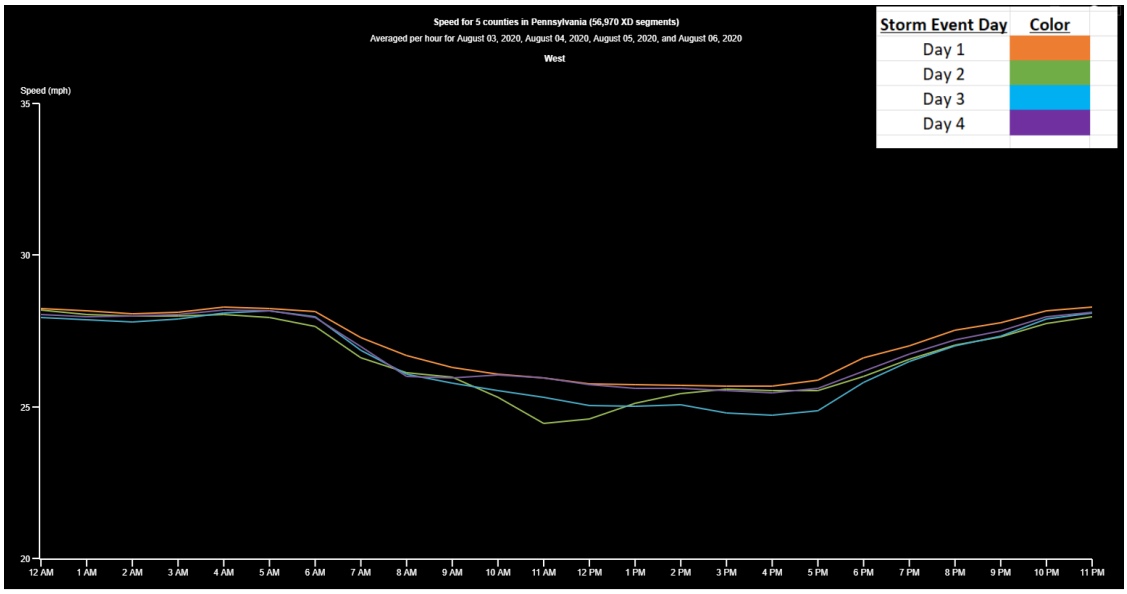

Figure 2.8. Daily Speed Change during Hurricane Isaias

Hurricane Ida: Hurricane Ida was a longer storm event, covering 6 days, compared to the snowmelt event and Hurricane Isaias. Overall, Hurricane Ida had the greatest speed variation across all 6 days when compared to either the snowmelt event or Hurricane Isaias. Hurricane Isaias is also the only event whereby the end of the storm, the roadway network appears to have improved, as days 5 and 6 had consistently higher speeds than the other days of the storm, indicating a return to normal operation of the traffic network. Hurricane Ida experienced the largest variance in speed reduction when compared with the snowmelt event and with Hurricane Isaias. During day 2 and day 3, the greatest reduction in speed occurred. FRC 2 and 3 roads had the largest speed variation across the duration of the event. Details of each road class speed change are presented in Appendix C.

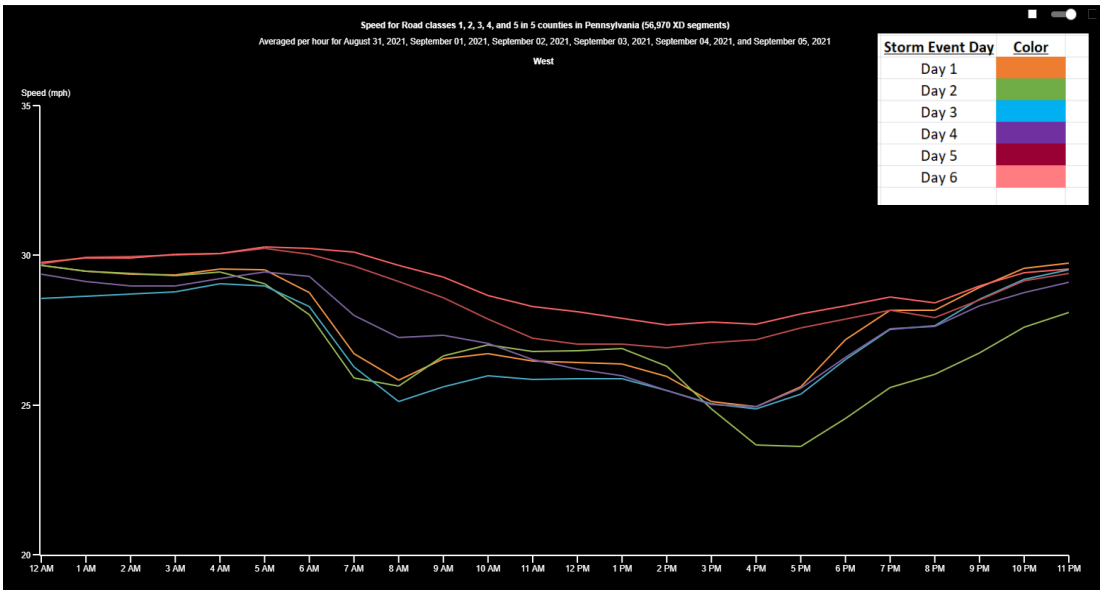

Figure 2.9. Daily Speed Change during Hurricane Ida

Speed Change Comparison per Road Class across High stream flow events

Additionally, to better understand how the three high stream flow events compare to each other across the 5 FRCs, individual charts of speed vs. time were created with the high stream flow events compared to each other per FRC.

FRC 1: FRC 1 roadways were most affected by the snowmelt event especially near AM and PM peak hours. FRC 1 roadways also experienced the greatest variance in speed variance between storm event types, indicating that these events all very differently affect FRC 1 roadways.

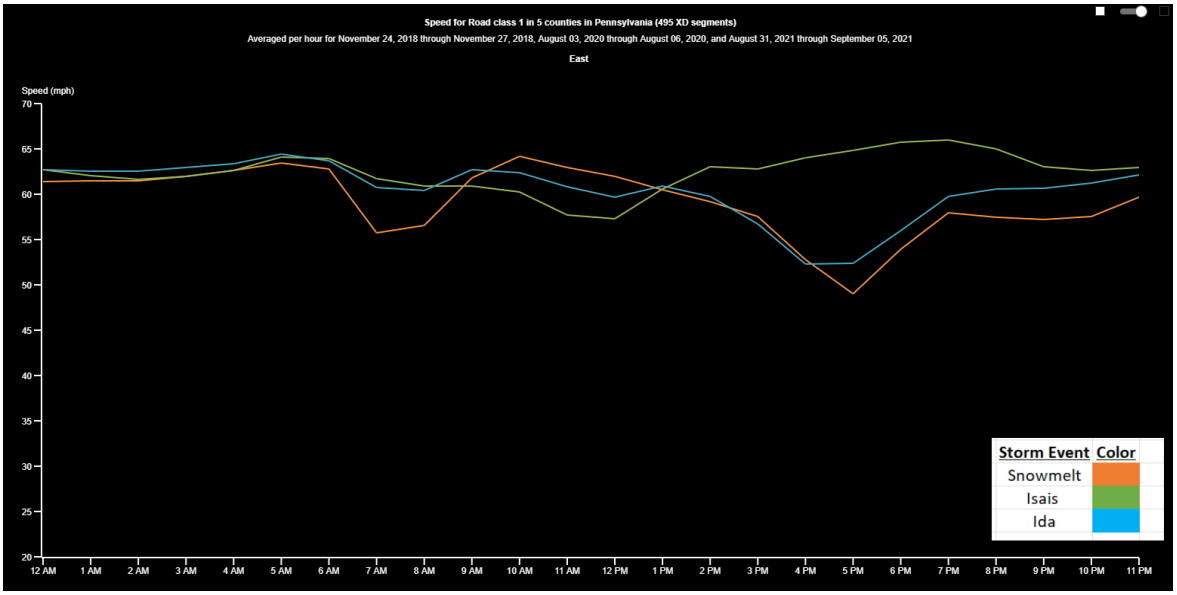

Figure 2.10. FRC1 Speed Change across three high stream flow events

FRC 2: Similar to FRC 1, FRC 2 was most affected by the snowmelt storm event, though with a less significant speed variance between high stream flow events.

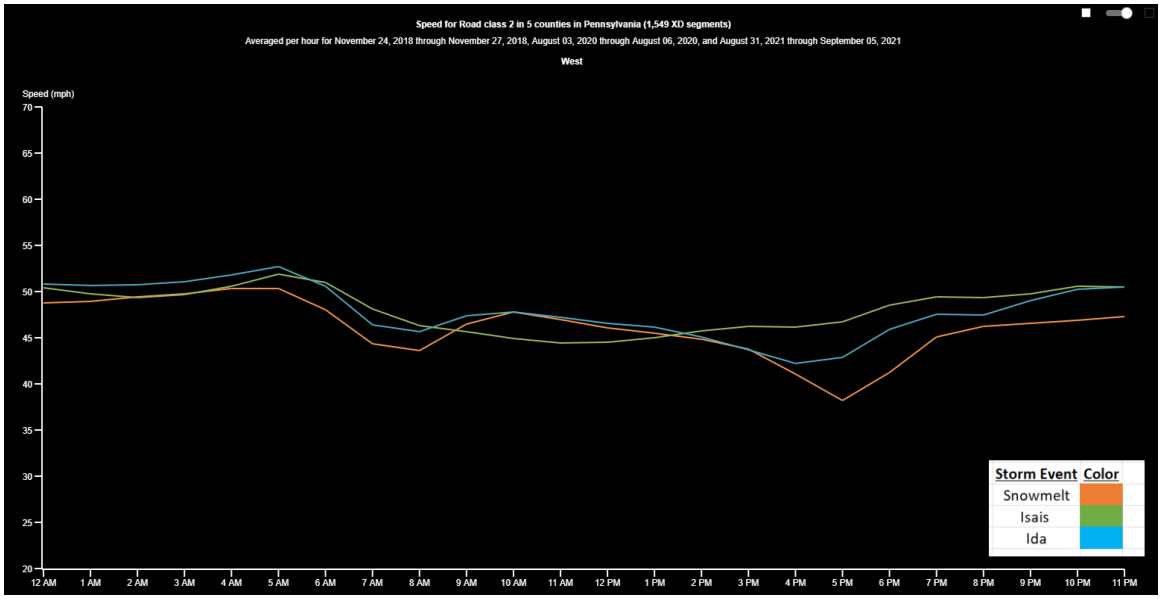

Figure 2.11. FRC2 Speed Change across Three High stream flow events

FRC 3: FRC 3 roadways experience less variation between storm event types (snowmelt, Hurricane Isaias and Hurricane Ida). FRC 3 roadways were most affected by Hurricane Isaias and the snowmelt. The snowmelt produced greater speed variances close to the AM and PM peak hours.

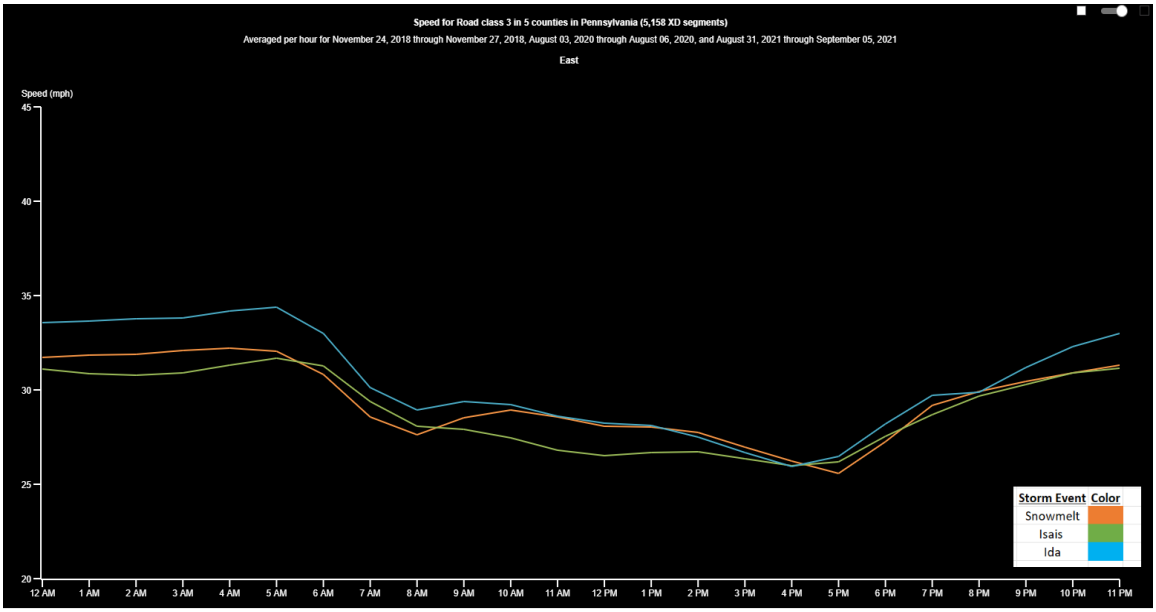

Figure 2.12. FRC3 Speed Change across Three High stream flow events

FRC 4: For FRC 4 roadways, Hurricane Isaias produced the greatest speed variance compared to the snowmelt event and Hurricane Ida. This demonstrates that FRC 4 roadways were most affected by Hurricane Isaias.

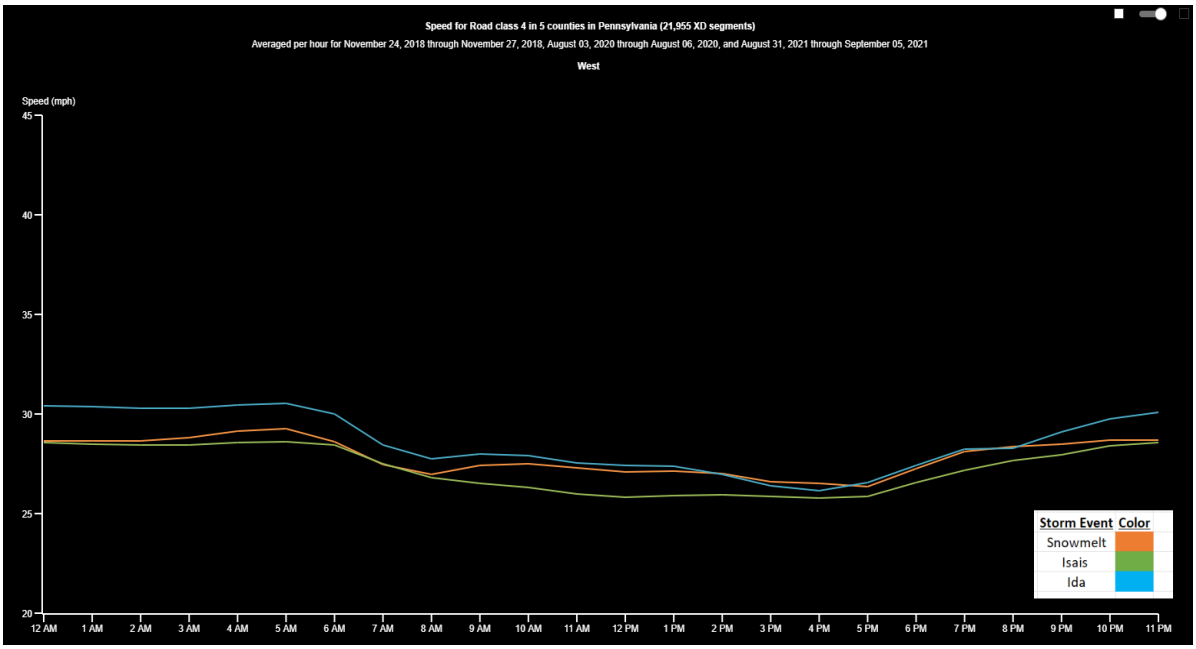

Figure 2.13. FRC4 Speed Change across three high stream flow events

FRC 5: For FRC 5 roadways, Hurricane Isaias produced the greatest variation in speed, demonstrating that high stream flow events similar to this affect FRC 5 roadways the most.

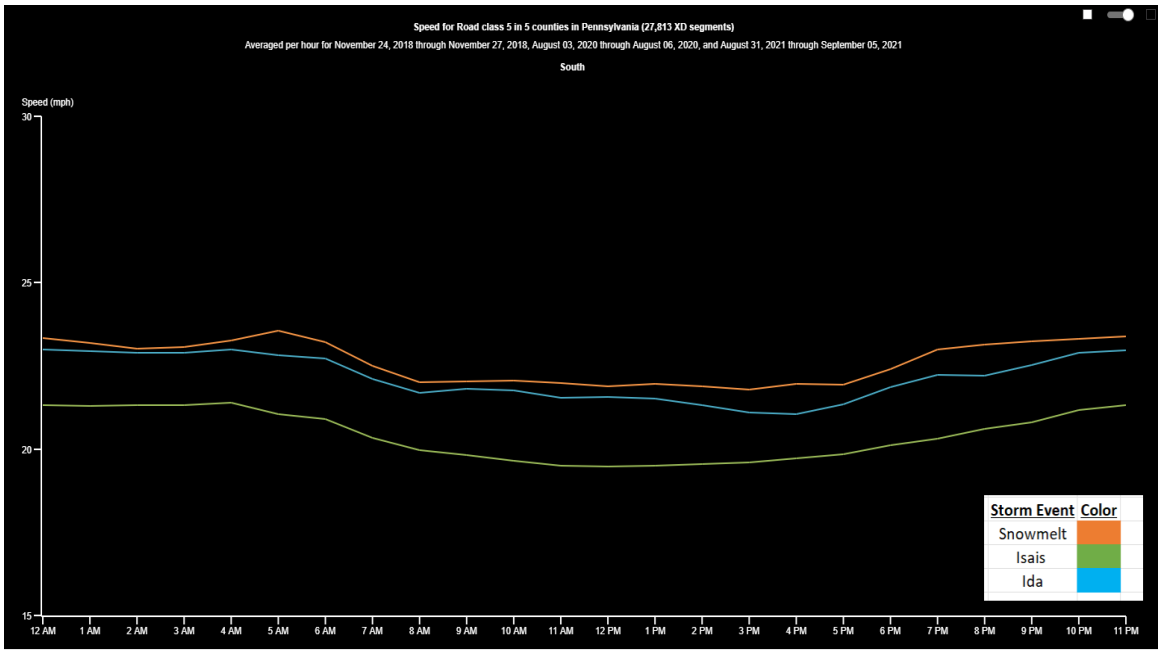

Figure 2.14. FRC5 Speed Change across Three High stream flow events

3 Congestion Level Analysis

There were two methods in assessing roadway congestion levels: 1) free flow speed-based analysis and 2) historic average speed-based analysis. Furthermore, to better identify traffic pattern dynamics during peak and non-peak periods, the analysis timeframes were divided into three categories: AM Peak (7-9 AM), PM Peak (4-6 PM), and non-peak hours that reflect the remaining hours. To define the historic average speed and free flow speed values, 3-week of speed values prior and post of each storm event were applied. For instance, when analyzing 2018 snowmelt storm event (Nov. 24 - Nov. 28), speed data was gathered from Nov. 3, 2018, to Nov. 23, from Nov. 29 to Dec. 22 to capture three weeks prior and post event speed values as well as to calculate historic average speed and free flow speed. This process was repeated for both the Isaias and Ida high stream flow events. Figure 3.1 illustrates the overall congestion analysis process. It should be noted that the final outputs of this section will be used as the inputs in Task 3c for further spatial analyses.

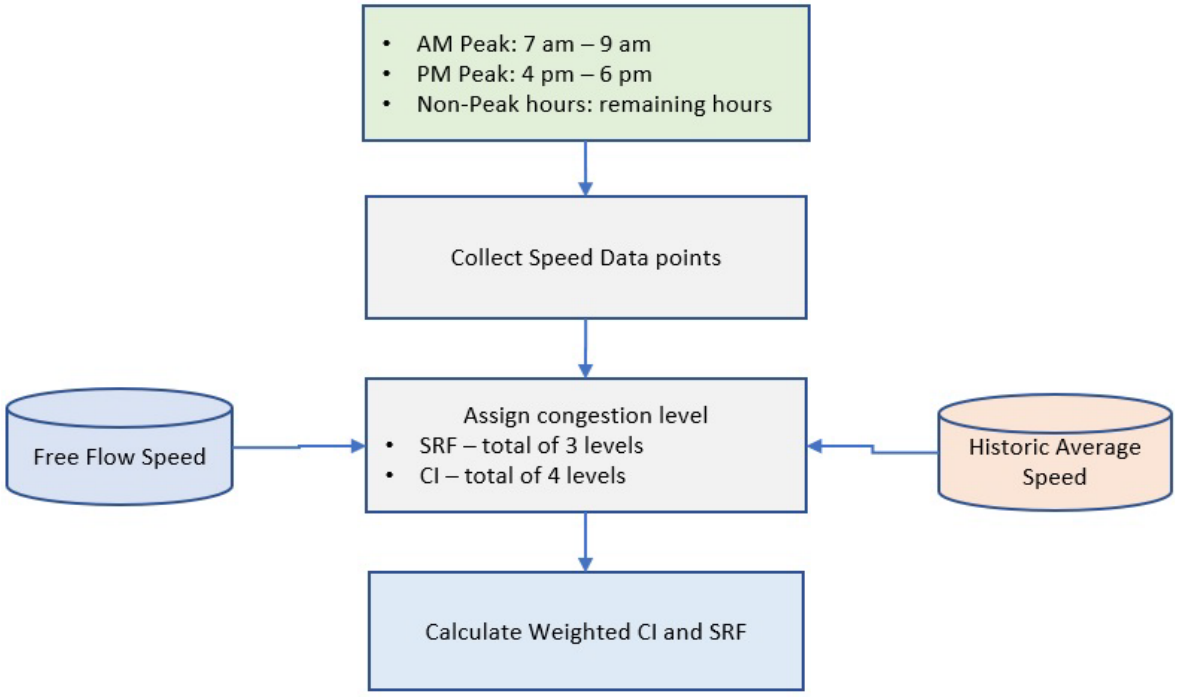

Figure 3.1. Overall Congestion Analysis Process

3.1 Free Flow Speed based Analysis

Congestion levels classification was based on methods described in the 2021 Urban Mobility Report (Schrank et al, 2021). Speed reduction factor (SRF) calculated using the free flow speed, defined as an average speed between 10 PM and 5 AM. As described earlier, 3-week prior and post each storm event speed values were used. The percentage threshold values for each congestion category were set according to the varied speed reduction and roadway speed limit. Equation 3.1 presents the SRF calculation with Table 3.1 threshold values in defining the SRF categories.

$$SRF_j = \left(\frac{Speed_j}{Free\ Flow\ Speed}\right) \times 100 \qquad \textbf{Equation 3.1}$$

- SRF_j: Speed Reduction Factor of XD segment *j* over the analysis period
- $Speed_j$: Observed speed of XD segment *j* during the storm event at its finest speed interval (e.g., for FRC 1 every 5-minute, FRC 5 every 15-minute as presented in Table 2.2)

Table 3.1. Description of SRF Category

SRF Category	Description	FFS ≥ 55 mph	FFS < 55 mph
Level 1	Severe congestion	SRF < 75%	SRF < 65%
Level 2	Moderate Congestion	75% < SRF < 90%	65% < SRF < 80%
Level 3	No to Low congestion	90% < SRF < 100%	80% < SRF < 100%

The final weighted SRF value is calculated by the following four-step process.

Step 1. Collect all observed speed data points: this process involves the gathering of all speed data points for each XD segment. Total observation number will depend on the finest data collection interval level as indicated in Table 2.2.

Step 2. SRF assignment for each speed data point: for each observed data point, SRF category will be assigned based on Equation 3.1.

Step 3. Final SRF for each analysis period: To account for the duration and length of congestion of each XD segment, final SRF for each analysis period was calculated considering the frequency of each SRF category during the corresponding analysis period.

$$Final\ SRF_j = \sum_{i=1}^{3}\left(\left(\frac{Freq_{ij}}{Total\ Freq_j}\right) \times SRF\_C_i\right) \qquad \textbf{Equation 3.2}$$

- Final SRF_j: Final SRF of XD segment *j* over the analysis period
- $Freq_{ij}$: number/frequency of observed data points corresponding to SRF category *i* for XD segment *j* over the analysis period.
- Total $Freq_j$: Total number/frequency of observed data points for XD segment *j* over the analysis period.
- SRF_C_i: Speed Reduction Factor category *i*.

Step 4. Weighted Final SRF: To integrate the different SRFs over three different analysis periods, the team applied a weighted approach. Considering the importance of peak periods' congestion impacts on the network, 40% weight was applied on each peak period while 20% was applied on non-peak period. This weighted final SRF was used in spatial analysis in Task 3b.

$$Weighted\ Final\ SRF_j = \left(0.4 \times SRF_{j\_am}\right) + \left(0.4 \times SRF_{j\_pm}\right) + \left(0.2 \times SRF_{j\_non\ peak}\right)$$

Equation 3.3

3.2 Historic Average Speed based Analysis

Historic speed data was estimated using the speed data pulled for 3 weeks prior and post each storm event. These values were averaged per three analyzed time periods: AM peak, PM peak, and non-peak hours. A total of four different categories were established based on the speed difference percentage between the historic average speed (HAS) and speed during the storm event. It should be noted that different FRC produced different speed granularity levels.

$$CI_j = \left(\frac{Speed_j - HAS_j}{HAS_j}\right) \times 100 \qquad \textbf{Equation 3.4}$$

- CI_j: Congestion Index of XD segment *j* over the analysis period
- $Speed_j$: Observed speed of XD segment *j* during the storm event at its finest speed interval (e.g., for FRC 1 every 5-minute, FRC 5 every 15-minute as presented in Table 2.2)
- HAS*j*: Historic average speed of XD segment *j*

Based on the calculated speed difference percentage, the following four different Congestion Index (CI) categories were developed as shown in Table 3.5.

Table 3.5. Description of Congestion Index (CI) Category

CI Category	Description	Threshold
Level 1	Severe congestion	CI > 80%
Level 2	Moderate Congestion	40 < CI < 80%
Level 3	Mild congestion	15% < CI < 40%
Level 4	Normal/low congestion	CI < 15% or $Speed_j > HAS_j$

As XD segment speed varied over the storm event, the extent of varying congestion levels was captured using the frequency of 4 different CI categories for each XD segment as presented in the following.

Step 1. Collect all observed speed data points: this process involves the gathering of all speed data points for each XD segment. Total observation number will depend on the finest data collection interval level as indicated in Table 2.2.

Step 2. CI assignment for each speed data point: for each observed data point, CI category will be assigned based on Equation 3.4.

Step 3. Final CI for each analysis period: Final CI was calculated considering the frequency of each CI category during the 3 different analysis periods.

$$Final\ CI_j = \sum_{i=1}^{4}\left(\left(\frac{Freq_{ij}}{Total\ Freq_j}\right) \times CI\_C_i\right) \qquad \textbf{Equation 3.5}$$

- Final CI_j: Final CI of XD segment *j* over the analysis period

- $Freq_{ij}$: number/frequency of observed data points corresponding to CI category *i* for XD segment *j* over the analysis period.
- Total $Freq_j$: Total number/frequency of observed data points for XD segment *j* over the analysis period.
- CI_C_i: Congestion Index category *i*.

Step 4. Weighted Final CI: To integrate the different CIs over three different analysis periods, similar approach presented in weighted final SRF section is applied. In addition, this weighted final CI was also used in spatial analysis in Task 3b.

$$Weighted\ Final\ CI_j = \left(0.4 \times CI_{j\_am}\right) + \left(0.4 \times CI_{j\_pm}\right) + \left(0.2 \times CI_{j\_non\ peak}\right)$$

Equation 3.6

An example of the SRF and CI calculator process is presented in Appendix D. Table 3.6 presents the SRF and CI descriptive statistics of each FRC across three high stream flow events while Figures 3.1 and 3.2 visualize the three storm events' resulted CI and SRF distribution over the network. As shown in Table 3.6, while different high stream flow events had different congestion impacts on roadway classes, in general FRC 3, 4 and 5 indicate slightly severe congestion status compared to FRC 1 and 2. This finding support the needs for prioritizing the infrastructure maintenance and preparing for future high stream flow events especially at local agencies levels. In this context, PA's Local Technical Assistance Program (LTAP) would have an important role to bring the awareness of congestion Impacts per different nature of high stream flow events and to assist in planning the proper infrastructure maintenance.

Table 3.6. SRF and CI Distribution across high stream flow events

		Snowmelt Event		Hurricane Isaias		Hurricane Ida	
		Mean	STD	Mean	STD	Mean	STD
SRF	FRC 1	2.22	0.40	2.37	0.39	2.16	0.46
	FRC 2	1.78	0.37	1.89	0.33	1.69	0.35
	FRC 3	1.69	0.38	1.85	0.35	1.34	0.27
	FRC 4	1.58	0.37	1.75	0.38	1.59	0.36
	FRC 5	1.28	0.26	1.61	0.31	1.53	0.34
CI	FRC 1	3.59	0.29	3.56	0.36	3.75	0.25
	FRC 2	3.46	0.52	3.54	0.51	3.50	0.52
	FRC 3	3.11	0.62	3.32	0.61	2.46	0.33
	FRC 4	2.97	0.46	3.19	0.42	3.06	0.37
	FRC 5	3.03	0.67	3.21	0.50	3.00	0.47

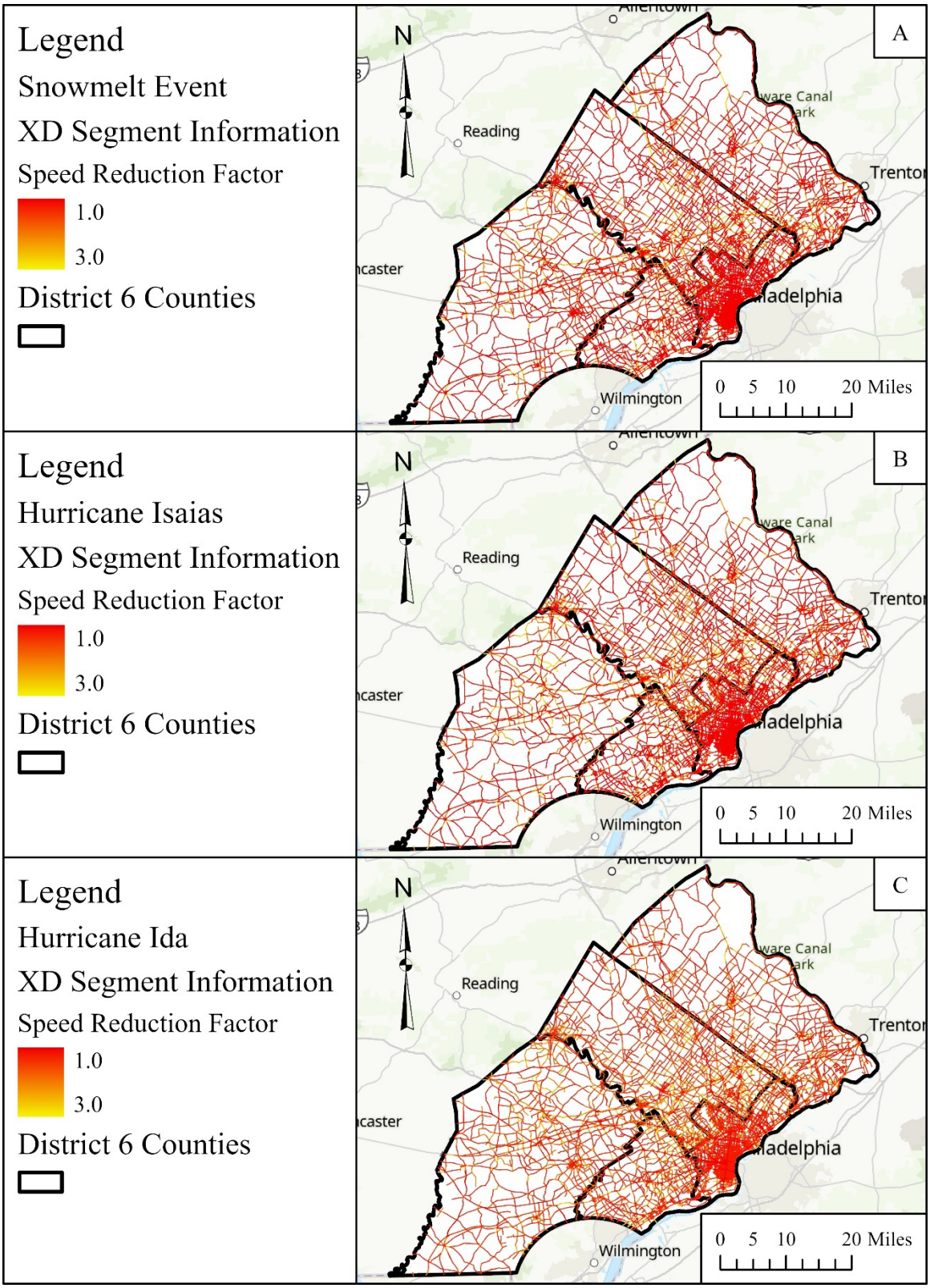

Figure 3.1. Speed Reduction Factor on a 1-3 scale, where 1 is the maximum speed reduction. **(A)** Snowmelt Event. **(B)** Hurricane Isaias. **(C)** Hurricane Ida.

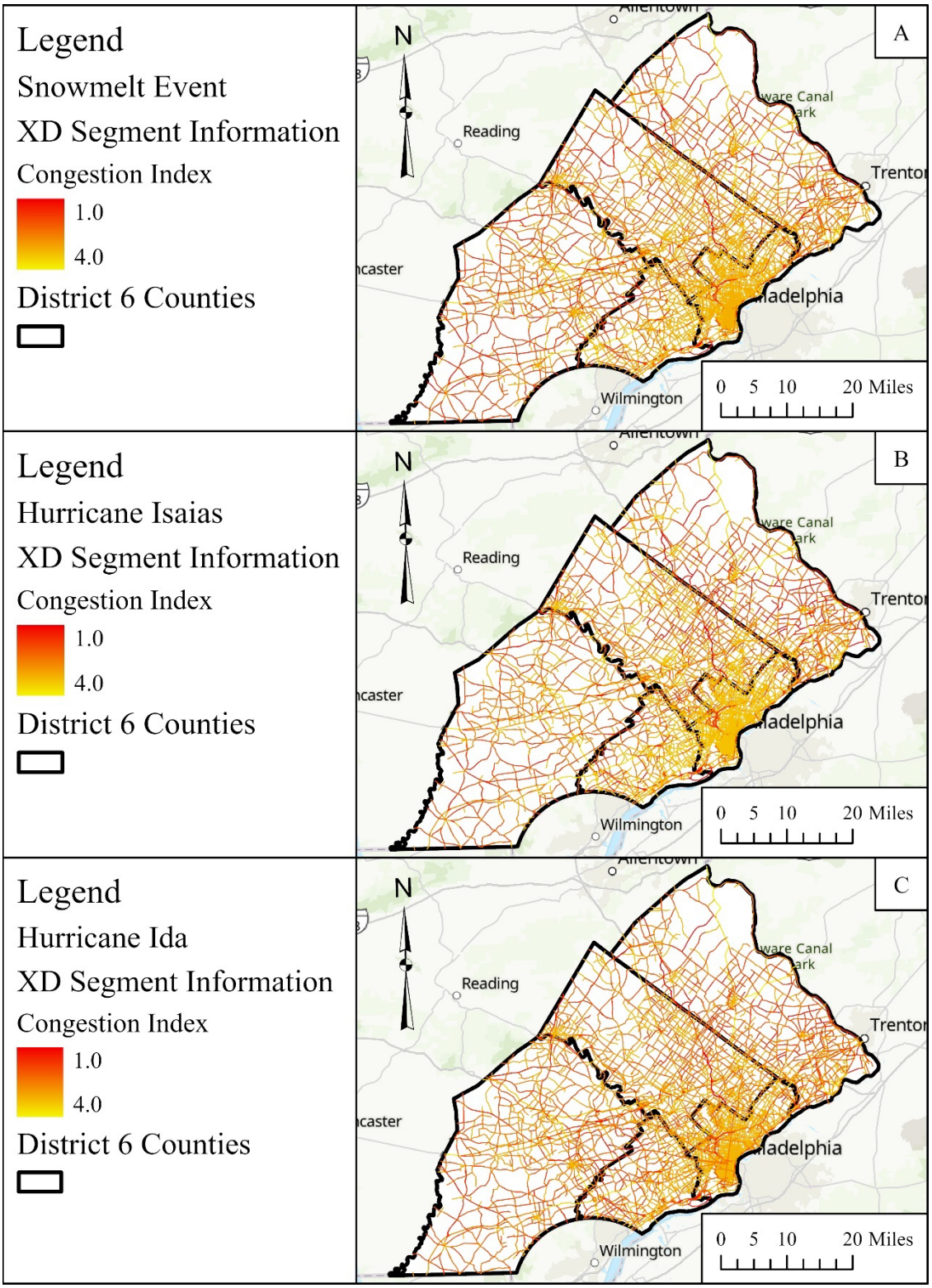

Figure 3.2. Congestion Index on a 1-4 scale, where 1 is the maximum congestion. **(A)** Snowmelt Event. **(B)** Hurricane Isaias. **(C)** Hurricane Ida.

4 Conclusion

This subsection summarized the process of obtaining major traffic parameter, speed, from the RITIS platform to assess the impact of three different severe high flow events on roadway network. Speed data indicated that each storm event had impact on network, but at varying degree depending on the roadway classifications and road closure status. Additionally, there is some spatial variation between high flow events. Different parts of District 6 respond to the different types of high stream flow events. Subbasins within the district vary in their sensitivity to rainfall intensity or volume, which is reflected in the roadway network performance. Although, congestion and speed are not a direct correlation to bridge closures, some parts of the District are subject to more congestion than others under base conditions. However, analyzing the network condition (congestion and speed reduction) provides insight into how the system is functioning spatially relative to bridges.

Speed values and congestion levels per different roadway categories were analyzed as the primary variables in understanding impacts of different severe high flow events road closures. However, there is a need to combine vehicle classification information for capturing more accurate congestion causes in future work, as this information is important in defining roadway pavement integrity and performance. In addition, such information will also provide a better understanding when investigating wet weather impacts on infrastructure. Although outside of the scope of this project, it is an area in need of future investigation.

Two congestion related indices were calculated and to serve as target variables in Section Task 3b. The target variables are used in a regressions and feature importance analysis to identify the watershed and infrastructure parameters linked to road closure and roadway network congestion.

Task 3b: Summary

The hydrology and landscape of a watershed, paired with hydraulic infrastructure parameters have direct impacts on a transportation network through flooding and road closures. As streams rise in response to wet weather events they have the potential to force road/bridge closures in some cases. This in turn impacts the function and flow of the roadway network. However, isolated the parameters (watershed or infrastructure features) which drive road closures can be challenging.

Further, some bridge may closures may not result in major network disruption, while other minor closures can cause intense delays within the network. Additionally, the impacts may differ between types of high stream flow. As urban networks grow in their usage identifying the most susceptible parts of a transportation network is critical. However, that cannot solely be defined by likelihood of inundation, but must also consider the impact to the function of the network. Gaining this understanding, identifying drivers of closures on waterway bridges, during different weather events can provide insight into where efforts and resources should be prioritized.

The watersheds in Pennsylvania District 6 vary substantially in their degree of impervious cover and size. As a result, the streams bisecting the District respond differently to different types of wet weather events. Additionally, different infrastructure features may affect how likely a bridge is to requiring closures. The variations in the physical parameters of these watersheds and infrastructure result in different likelihoods of inundation, and therefore different impacts on the roadway network across the district. Building on the work described in Task 1, here we describe a method for developing a spatial regression analysis for the drainage basin parameters that contribute to downstream road closures.

This analysis was done for the District spanning 6 years, but also investigated how the system response varied across three specific major high stream flow events resulting in many road closures across the District 6 roadway network. The results highlight linkages between physical parameters of a bridge, its drainage area, and the surrounding infrastructure with the likelihood of bridge closure and impact to the transportation network. This was done for road closures, speed reduction, and roadway congestion. Based on this analysis, areas at risk of closure during different types of high stream flow events can be identified.

This report reviews the process of analysis, and the results of the analysis. The driving parameters for predicting road closures, roadway network spatial speed reduction, and spatial congestion for three types of high stream flow events. Findings showed that for the events feature importance varied for different target variable analysis for the snow melt event, this suggest that outside influences, such as ice, might also be impacting road conditions. However, it remained constant for Hurricane Isaias and Hurricane Ida. The most important feature for Ida was drainage area, while the most important for Isaias was impervious area. Therefore, watersheds that are highly developed where more effected by the intensity of Hurricane Isaias (coming up the Atlantic Coast), while watersheds draining large areas were more impacted by the high volume of Hurricane Ida (coming across the US).

Task 3b Report

1 Introduction

The hydrology and watershed landscape have direct impacts on a transportation network through flooding and road closures. However, defining which hydrology drivers most stress on a transportation network becomes a more complex task. Additionally, the impacts may differ between types of weather events. Identifying the most susceptible parts of a transportation network, specifically waterway bridges, during different weather events can provide insight into where efforts and resources should be prioritized.

The watersheds in Pennsylvania District 6 vary substantially in their degree of impervious cover and size. As a result, the streams bi-secting the District respond differently to different types of wet weather events. The variations in the physical parameters of these watersheds result in different likelihoods of flooding, and therefore different impacts on the roadway network across the district. Building on the work described in Task 1, here we describe a method for developing a spatial regression analysis for the drainage basin parameters that contribute to downstream road closures. This analysis was done for the system spanning 6 years, but also investigated how the system response varied across three specific major wet weather events. The results highlight linkages between physical parameters of a bridge's drainage area and the likelihood of bridge closure. Based on this analysis, areas at risk of closure during different types of high stream flow events can be identified.

The goals of this subtask are accomplished through spatial analysis and regression. This study is a continuation of the analysis completed in Task 1c, where a flood risk assessment was completed for bridges that intersect waterways in District 6. Therefore, the hydrological data that is used in this spatial analysis have already been derived. This study focuses on the bridges that intersect waterways of District 6, but it identifies how the hydrological variables impact the transportation variables of the bridges during different weather events.

2 Data and Methods

In this subtask spatial and regression analyses are used in this study to identify the relationships between the hydrology of a landscape during a weather event and a transportation network. Table 2.1 includes a summary of the data used in the analysis. Spatial analysis is completed using Esri ArcGIS Pro. The products of the spatial analysis are different maps displaying the transportation data and compiled tables of hydrological and transportation data. The maps are visually analyzed, aiming to define areas of risk in the transportation network of District 6. The compiled tables of hydrological and transportation data are used in two regressions. The output of the regressions defines which hydrological variables have the greatest correlation to the transportation variables. Crashes were also analyzed, but not as a regression.

Table 2.1. Summary of the data sources used in the spatial and regression analyses.

Data	Creator	Year(s)	Source
Pennsylvania county boundaries	Penn DOT	2022	Pennsylvania Spatial Data Access
PennDOT - Road Closures	Penn DOT	2016-2021	Penn DOT
Bridges	Penn DOT	2022	Pennsylvania Spatial Data Access
XD Segment Information	INRIX	2018-2021	RITIS platform
National Flood Hazard Layer - Berks County	Federal Emergency Management Agency	2018	Pennsylvania Spatial Data Access
National Flood Hazard Layer - Bucks County	Federal Emergency Management Agency	2019	Pennsylvania Spatial Data Access
National Flood Hazard Layer - Carbon County	Federal Emergency Management Agency	2002	Pennsylvania Spatial Data Access
National Flood Hazard Layer - Chester County	Federal Emergency Management Agency	2021	Pennsylvania Spatial Data Access
National Flood Hazard Layer - Delaware County	Federal Emergency Management Agency	2017	Pennsylvania Spatial Data Access
National Flood Hazard Layer - Lancaster County	Federal Emergency Management Agency	2021	Pennsylvania Spatial Data Access
National Flood Hazard Layer - Lebanon County	Federal Emergency Management Agency	2020	Pennsylvania Spatial Data Access
National Flood Hazard Layer - Lehigh County	Federal Emergency Management Agency	2009	Pennsylvania Spatial Data Access
National Flood Hazard Layer - Montgomery County	Federal Emergency Management Agency	2021	Pennsylvania Spatial Data Access
National Flood Hazard Layer - Northampton County	Federal Emergency Management Agency	2020	Pennsylvania Spatial Data Access
National Flood Hazard Layer - Philadelphia County	Federal Emergency Management Agency	2019	Pennsylvania Spatial Data Access
National Flood Hazard Layer - Schuylkill County	Federal Emergency Management Agency	2021	Pennsylvania Spatial Data Access
PAMAP Program - 3.2 ft Digital Elevation Model	DCNR PAMAP Program	2015	Pennsylvania Spatial Data Access
NLCD 2019 Percent Developed Imperviousness	National Land Cover Database	2019	Multi-Resolution Land Characteristics
NLCD Land Cover - All Years	National Land Cover Database	2001-2019	Multi-Resolution Land Characteristics
PennDOT - Scour-Critical Bridge List	Penn DOT	2021	Penn DOT

2.1 Spatial Analysis

There are 3,817 bridges that intersect waterways in District 6. The bridges serve as the data entries for the regression analysis. The analysis will focus on two transportation variables, the speed reduction factor and the congestion index, described in Task 3a. The two variables are geoprocessed coherently but are analyzed independently this data was then joined to spatial variables. The assessment completed in Task 1c produced the hydrological variables that are used in this analysis. The previous assessment joined ten variables to the 3,817 waterway bridges in District 6. The variables considered in this analysis are seen in Table 2.2. An additional detailed summary of the variables can be found in Appendix E. Table 1. Three analyses are completed for each weather event using ArcPro. The congestion index, the speed reduction factor, and the occurrence of road closures due to flooding were extracted for each specific waterway bridge between each respective weather event. These three unique variables need to be joined to the waterway bridges data.

Table 2.2. Summary of the variables included in the analysis.

Transportation Variables		**Source**
y_1	Speed Reduction Factor	RITIS platform
y_2	Congestion Index	RITIS platform
Hydrological Variables		
x_1	Occurrence of Road Closures due to Flooding During Event	Pennsylvania Department of Transportation
x_2	Bridge Age	Pennsylvania Spatial Data Access
x_3	Scour Score	Pennsylvania Department of Transportation
x_4	FEMA Flood Zone Score	Pennsylvania Spatial Data Access
x_5	Upstream Drainage Area	Pennsylvania Spatial Data Access
x_6	Weighted Average of Percent Impervious Area	Multi-Resolution Land Characteristics
x_7	Number of Flood Control Structures in Upstream Drainage Area	Pennsylvania Spatial Data Access
x_8	Number of Flood Obstruction Structures in Upstream Drainage Area	Pennsylvania Spatial Data Access
x_9	Average Slope of Drainage Area	Pennsylvania Spatial Data Access
x_{10}	Percent Change in Land Cover	Multi-Resolution Land Characteristics

The XD Segment Information produced in Task 3a provides a table of roughly 55,000 road segments that include start and end coordinates, the functional road classes of each segment, the weighted final congestion index of each segment per day through the weather event, and the weighted final speed reduction factor of each segment per day through the weather event. There are 4 to 6 days of data per XD segment, depending on the duration of the weather event. Each day contains its own respective row of data for each XD segment defining the congestion index and speed reduction factor during the weather event. The congestion index and speed reduction

factor are averaged, respectively, to summarize the congestion index and speed reduction factor throughout the entirety of the weather event.

Once summarized, the start and end coordinates are used to display the XD Segment Information for each weather event individually in ArcGIS Pro for geoprocessing. The XD segment data for the first weather event is spatially joined to the waterway bridges. This process is repeated for each weather event. There is not XD segment data present for the entirety of District 6. Therefore, there are waterway bridges that do not have XD Segment Information attached. Table 2.3 defined the total number of bridges and the number of bridges that are considered in the remainder of the analysis.

Table 2.3. Number of waterway bridges with joined XD Segment Information.

Weather Event	Total Bridges	Bridges with XD Segment Information
Snowmelt Event	3,817	2,459
Hurricane Isaias	3,817	2,386
Hurricane Ida	3,817	2,459

To identify which road closures due to flooding happened during each weather event, the dataset of all road closures is imported and displayed in ArcGIS Pro. The road closure data is separated and selected by date for each weather event. Table 2.4 includes the dates that road closures due to flooding were recorded by PennDOT during each weather event. Each event is spatially joined to the waterway bridges, determining if road closures due to flooding occurred at each bridge.

Table 2.4. Dates of PennDOT recorded road closures due to flooding in District 6.

Weather Event	Number of Road Closures	Start Date	End Date
Snowmelt Event	13	11/24/2018	11/27/2018
Hurricane Isaias	90	8/4/2020	8/7/2020
Hurricane Ida	137	8/31/2021	9/1/2021

The spatial analysis produces a waterways bridges feature that includes all transportation and hydrological variables. A detailed procedure of the geoprocessing for the XD Segment Information and PennDOT Road Closures due to Flooding Data is included in Appendix F. Additional analyses can be completed with the compiled data, including the creation and visual analysis of maps, and the running of regressions using the exported table from the waterway bridges features.

2.2 Regression Analysis

As stated, the product of the spatial analysis provides the necessary data to run the regressions. The regressions aim to identify which hydrological variables have the strongest correlation with the transportation variables at the bridges that intersect waterways. There are two types of regressions used. The first is linear regression and the second is Machine Learning based regression. Additionally, there are a total of six regressions run for each regression type. Each

weather event has two regressions ran, one solving for the congestion index and one solving for the speed reduction factor. Table 3.2 defines the y and x-variables for the regression analyses. There is only one y-variable used per regression. All x-variables are considered in all regressions.

Linear Regression Analysis

The linear regression is completed using the Regression Tool in the Analysis ToolPak of Microsoft Excel. The built-in regression tool is an easily accessible and simple method for analyzing the relationship between dependent and independent variables using the "least squares" statistical method. Variables with the strongest correlation are determined through outputs from running the regression. The full workflow for this analysis is described in Figure 2.1.

The transportation data joined to the waterway bridges are defined as the dependent variable, y-variable, and the hydrological data inputs are defined as the independent variables, x-variables. As stated, two linear regressions are run for each weather event, first, solving for the congestion index, and second, solving for the speed reduction factor. There are two outputs of the linear regression that summarize the performance if it, which are the R^2 value and the Significance F. The output that determines the correlation of an independent variable is the P-values.

The first output that summarizes the performance of the regression is the Significance F, which defines the statistical significance. If this value is less than 0.001, then the regression can be considered as reliable. The second output used to gauge the performance of the regression is the R^2 value. The R^2 value is the coefficient of determination, defining the correlation of all independent variables to the dependent variable on a scale of 0 to 1, where 0 represents that the independent variables have no correlation to the dependent variable and 1 represents that the independent variables perfectly correlate with the dependent variable.

The output that defines the correlation of a single independent variable is the P-Value. A P-Value is determined for every independent variable when the regression is run. An independent variable with perfect correlation has a P-Value of 0. If the P-Value for an independent variable is greater than 0.05, then the respective independent variable has insufficient correlation and should not be considered in the regression analysis. Therefore, an additional iteration of the linear regression is run, not including the independent variables with P-Values greater 0.05. Once all independent variables have a P-Value less than 0.05, the linear regression is complete.

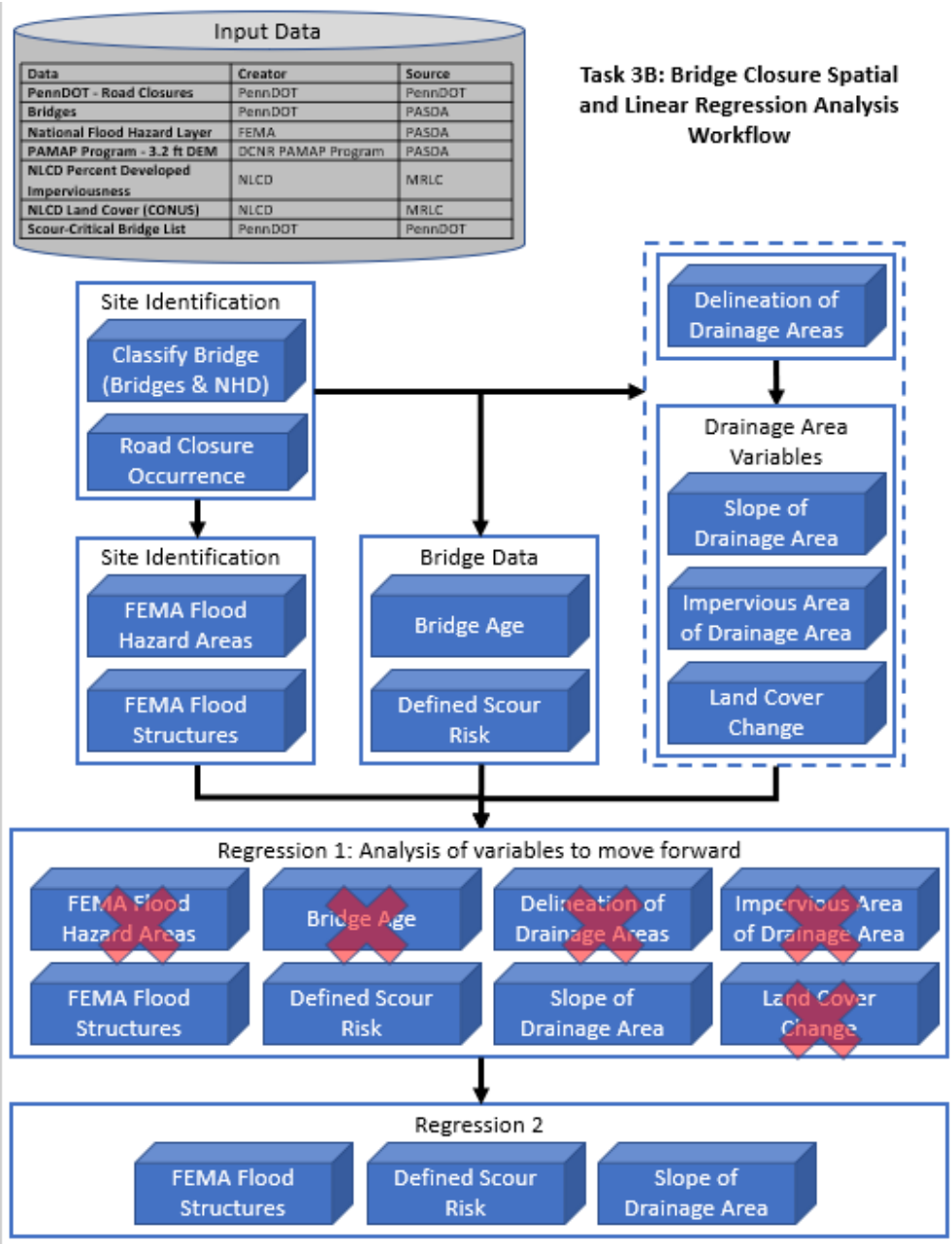

Figure 2.1. A workflow example for linear regression.

Feature Importance with Machine Learning Regression

A feature importance is studied by analyzing Permutation Feature Importance (PFI) technique over the target variable (e.g., road closure, SRF, CI), a method of Machine Learning based feature importance extraction. The PFI is defined to be the decrease in a model score when a single feature value is randomly shuffled 1. This procedure breaks the relationship between the feature and the target, thus the drop in the model score is indicative of how much the model depends on the feature. In PFI, the impact of shuffling the values of a feature (x_m, described in Table 2.2), e.g., impervious area, for a target variable (*y, e, g, SRF*) is quantified. This facilitates

an observation of the response in output variables associated with the change in input variables (x_m). In the PFI technique, a Random Forest (RF) model is run with the values of a specific feature, e.g., impervious areas of the contributing area, as permuted/shuffled keeping the other features constant, while the changes in the values are recorded. The change scores are recorded as an error matrix in the form of the correlation coefficient (R2). The R2 values are obtained from the difference between the series of the target variables after running the RF model with the changed features and the series before running the model. The score of the R2 is derived from the observed and calculated values of the target variable as a result of the shuffle in each of the independent variables. This provides the score of feature importance over the target variables. This process is described in Figure 2.2.

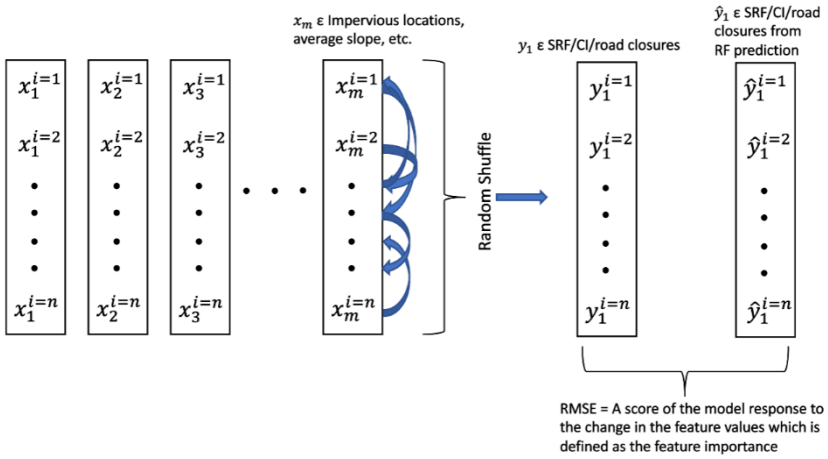

Figure 2.2. Relative Feature Importance analysis.

3 Results

The intention of this study is to define the areas of risk related to flood inundation for a transportation network. This is achieved through spatial and regression analyses. Maps are created to visually analyze the distribution of stress that different weather events put on a network and the regressions aim to identify the variables that affect the magnitude of stress that different weather events put on a network. As stated, the two transportation variables to gauge the stress on a transportation network are the congestion index and the speed reduction factor.

3.1 Analysis of Road Closures due to Flooding

Before the relationship between the hydrological and transportation variables is explored, a regression analysis of the relationship between road closures due to flooding and hydrological variables is completed for each weather event. This analysis follows the same procedure

completed in Task 1c, but it will only use the road closures from flooding during the respective weather event at the waterway bridges. Table 3.1 summarizes the variables used in the regression analysis.

Table 3.1. Summary of variables used in the regression analysis of road closures due to flooding.

Variables	
y_1	Occurrence of Road Closures due to Flooding During Event
x_1	Bridge Age
x_2	Scour Score
x_3	FEMA Flood Zone Score
x_4	Upstream Drainage Area
x_5	Weighted Average of Percent Impervious Area
x_6	Number of Flood Control Structures in Upstream Drainage Area
x_7	Number of Flood Obstruction Structures in Upstream Drainage Area
x_8	Average Slope of Drainage Area
x_9	Percent Change in Land Cover

The results from the regression analysis aim in identify which variables contribute to flooding at bridges during different high stream flow events. The snowmelt event was a product for snowfall from a previous event melting during a rainfall event, generating excessive runoff. Hurricane Isaias was an intense rainstorm event. Hurricane Ida was a weather event that poured large volumes of rainfall across the landscape over a long duration. Each weather event affected the landscape of District 6 differently. Figure 3.1 displays maps of road closures due to flooding during the three weather events. The road closures serve as a proxy for flooding. Therefore, the maps can be used to analyze the distribution of flooding across the District 6 landscape.

3.1.1 Road Closures due to Flooding Spatial Analysis

Figure 4.1 captures the distribution of road closures due to flooding during the three weather events. The road closures serve as a proxy for flooding. Therefore, wherever road closures happened, flooding is considered to have happened at that location. Different types of weather events may affect a landscape differently. Understanding how a landscape will react under given circumstances can allow an agency to better prepare for that type of event.

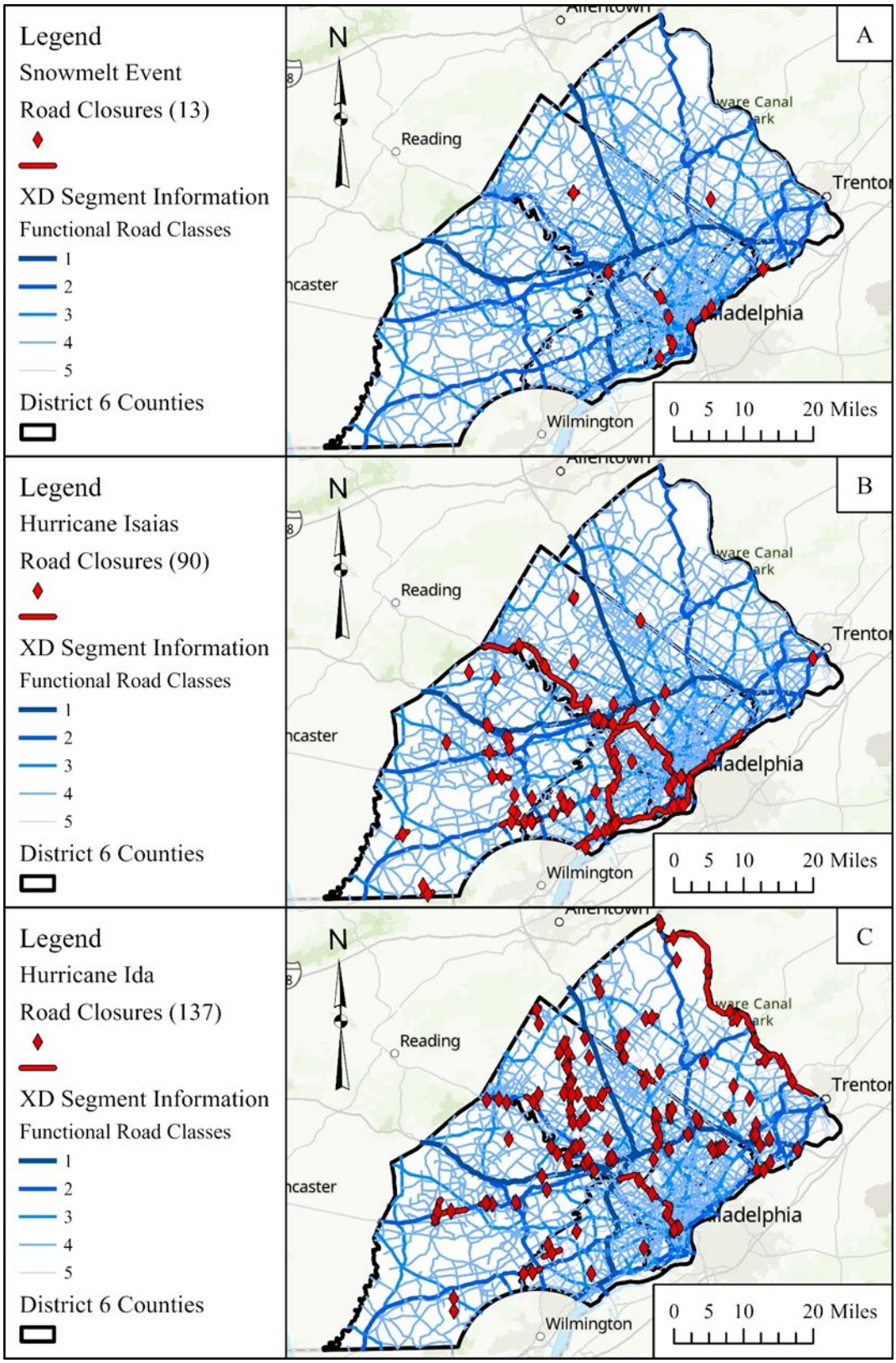

Figure 3.1. The distribution of road closures due to flooding during the **(A)** Snowmelt Event, **(B)** Hurricane Isaias, and **(C)** Hurricane Ida.

The snowmelt event had the least amount of road closures, 13, of the three events. Figure 3.1a displays the road closures during this event. Of the 13 road closures, 11 are focused near the Schuylkill River and Delaware River, which both have a large drainage area. The immense runoff produced during the snowmelt event was a product of a rainfall event happening while snow was melting from a previous snowfall event. This combination pushed a large quantity of runoff across the system since the already saturated landscape could not handle additional precipitation. Therefore, the streams with greater drainage areas were responsible to handle rainfall across the entire landscape that may have infiltrated in the occurrence of different initial conditions.

The results from the regression, supported this concept since the regression analysis identified that the upstream drainage area of the bridges is one of the variables identified as having the greatest correlation with road closures due to flooding occurring at the bridges.

The distribution of road closures that occurred during Hurricane Isaias, seen in Figure 3.1b, is focused on the southwest section of District 6. The southwest section of District 6 is comprised of smaller watersheds, relative to the Schuylkill and Delaware drainage basins. Additionally, the road closures are focused near the draining point of the smaller streams. Therefore, these results suggest that the road closures predominately took place under backwater hydraulic conditions

Of the nine independent variables included in the regression analysis, seven are indicated by the linear regression as having a correlation with the road closures due to flooding occurrence for Hurricane Isaias. Notable variables identified are the weighted average of percent impervious area in the upstream drainage area and the average slope of the upstream drainage area. Since Hurricane Isaias was an extremely intense rainfall event, rainfall would quickly accumulate in the areas with higher percentages of impervious areas. Additionally, the drainage areas with steeper slopes produce more runoff since less time is given for the landscape to allow infiltration, quickly moving excess rainfall across the system.

Hurricane Ida is noted to be a long rainfall event. Rainfall over a long duration caused flooding across the entire landscape, which is reflected in Figure 3.1c. 137 road closures due to flooding occurred throughout the duration of the event. More than half of the road closures took place in the northern section of District 6, which did not see many road closures in the other two weather events. The landscape responded to the weather event with similar effects to the Snowmelt Event, seeing pulses in flow occur further into the event where the saturated landscape could not handle additional precipitation.

There are two notable variables that have the greatest correlation to the road closures occurrence which are the number of flood control structures in the upstream drainage area and the number of flood obstruction structures in the upstream drainage area. Since both of these variables describe the characteristics of the upstream drainage area, there is a direct relationship to how a drainage area responds to a rainfall event since the manmade structures are implemented to help divert, slow, or capture runoff that otherwise travels directly to the local stream networks. Additionally, these variables are identified for the other two weather events.

3.1.2 Regression Analysis of Road Closures due to Flooding

The regression analysis is used to identify the independent variables that have the greatest correlation with the dependent variables. As stated, there are two types of regression analysis types used in this study, linear regression and feature importance analysis. The bridges are analyzed using both types of regression for each weather event. The results from each regression type are compared to see how the outputs differ.

Linear Regression

The same procedure and analysis are completed for all the linear regressions in Task 3b. Examining the results from the regression analysis of the occurrence of road closures due to flooding at the bridges, the performance of the regression is analyzed first. There are two outputs that gauge the performance of the regression, the Significance F and the R^2 value. For the linear regressions to be valid, the Significance F must be less than 0.001. This criterion is satisfied for all three weather events. The R^2 value for the Snowmelt Event, Hurricane Isaias, and Hurricane Ida are 0.0132, 0.064, and 0.029, respectively. While these are low R^2 values, since this is not a predictive model linear regression is a sufficient tool for identifying the correlating variables.

The P-values, defining the correlation of an individual variable, identified the variables with the greatest correlation in the regression. The final variables are identified after two iterations of the linear regression for Hurricane Isaias and Hurricane Ida, and three iterations are needed to identify the variables with greatest correlation for the snowmelt event.

The results from the linear regression analysis of the occurrence of road closures due to flooding is summarized in Table 3.1. An X in the table indicates the variables that have the greatest correlation. The ones without the X indicate the variables that have little to no correlation with the road closures.

For all three events the number of flood control structures and flood obstruction structures is important relative to road closures. The existing infrastructure may suggest that these locations were previously identified as areas of concern. However, changes to the watershed may result in these features no longer providing the same level of insulation to flood events.

Being located in the flood zone was an important feature for the snowmelt event and Isaias, but not Ida. Ida had a much larger volume of water associated with it, causing a different style of flooding.

The average slope within the drainage area was important to both hurricanes. However, only the closures associated with precipitation intense Hurricane Isaias were impacted by bridge age, suggesting that flash flooding may have increased through time associated with watershed development. Scour score was seen as important for Hurricane Ida.

Notably, this is a statical analysis, as opposed to a physics-based model. While these findings are insight, not all findings may be easily linked to the on the ground scenario.

Table 3.1. Variables with the greatest correlation to the road closure due to flooding occurrence for all three weather events.

High Stream Flow Event			Snowmelt Event	Hurricane Isaias	Hurricane Ida
Solving for	y	Road Closures Occurrence			
Input Parameters (x_n)	x_1	Bridge Age		**X**	
	x_2	Scour Score			**X**
	x_3	FEMA Flood Zone Score		**X**	
	x_4	Upstream Drainage Area	**X**	**X**	
	x_5	Weighted Average of Percent Impervious Area		**X**	
	x_6	Number of Flood Control Structures in Upstream Drainage Area	**X**	**X**	**X**
	x_7	Number of Flood Obstruction Structures in Upstream Drainage Area	**X**	**X**	**X**
	x_8	Average Slope of Drainage Area		**X**	**X**
	x_9	Percent Change in Land Cover			

Feature Importance Analysis

The results of the PFI analysis for road closures assess the relative values of a range of variables (described in Table 3.1) and their influence on road closures. Figure 3.2 shows the feature importance for each feature assessed for the three high flow events assessed (A. snowmelt, B. Hurricane Isaias, and C. Hurricane Ida). As can be seen from these figures the importance of features varies by event. The most important features were uniformly, bridge age, drainage area, land cover change, and impervious area, as well as slope. This aligns somewhat with the linear regression, as the features vary in their importance. The most important feature for Ida was drainage area, while the most important for Isaias was impervious area. The most important feature for the snow melt event was land cover change.

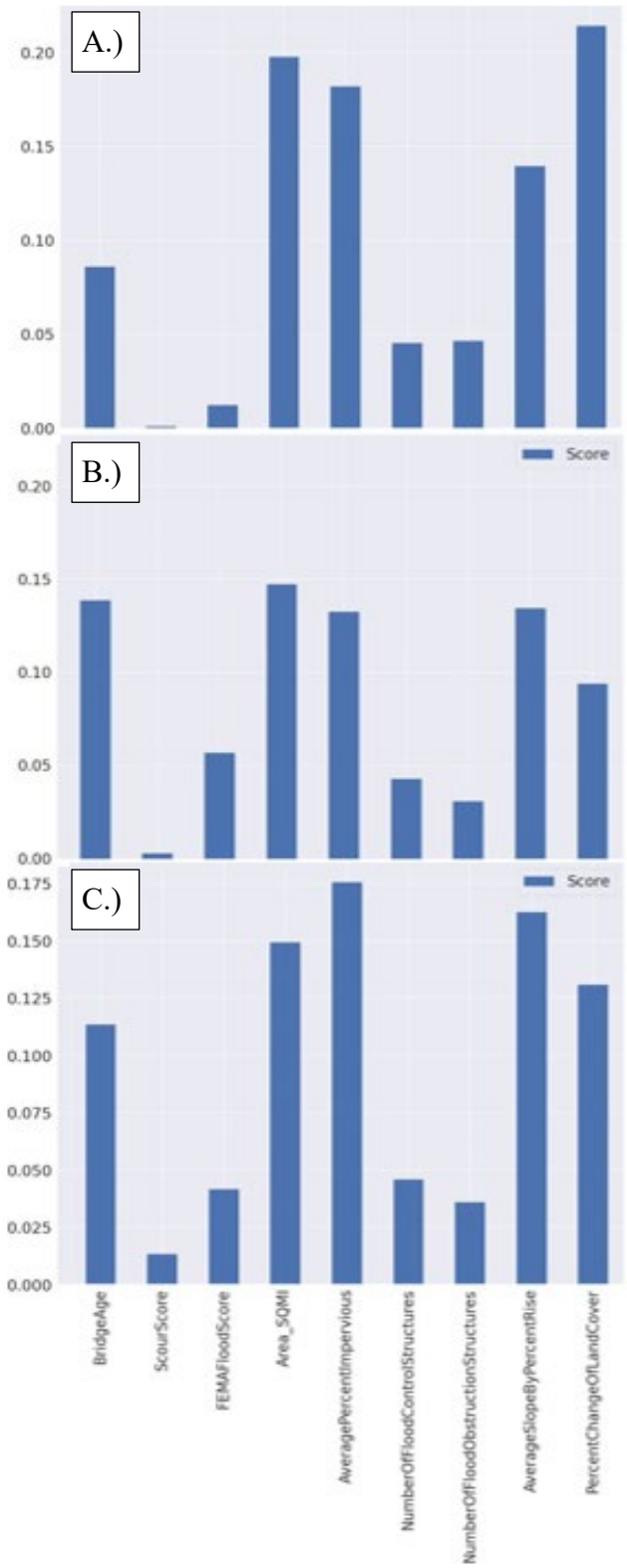

Figure 3.2. The distribution feature importance based on the RF analysis of road closures due to flooding during the **(A)** Snowmelt Event, **(B)** Hurricane Isaias, and **(C)** Hurricane Ida.

3.2 Speed Reduction Factor Analysis

Flooding can put stress on a transportation network, affecting its functionality. The effects can reach past the immediate area flooding is happening, leaking into surrounding areas and networks. This section of the analysis explores the effects of different variables on the speed reduction factor of bridges.

3.2.1 Speed Reduction Factor Spatial Analysis

Maps provide insight into a dataset, enabling the identification of patterns and trends in the distribution of data. Through spatial analysis, the XD Segment Information and the additional hydrological data are joined to the waterway bridges. Using ArcGIS Pro, maps are created to display the transportation data at the waterway bridges. Additional data is represented in the map to address possible correlations in the data.

The speed reduction factor of the bridges is represented in Figure 3.3. The speed reduction factor is the first method to represent the congestion level of District 6 through the three weather events. The maps included in Figure 3.3 display the bridges as circles with a color scale indicating the level of congestion. A value of 1, represented as green, indicates severe congestion, while a value of 3, represented as yellow, indicates little to no congestion.

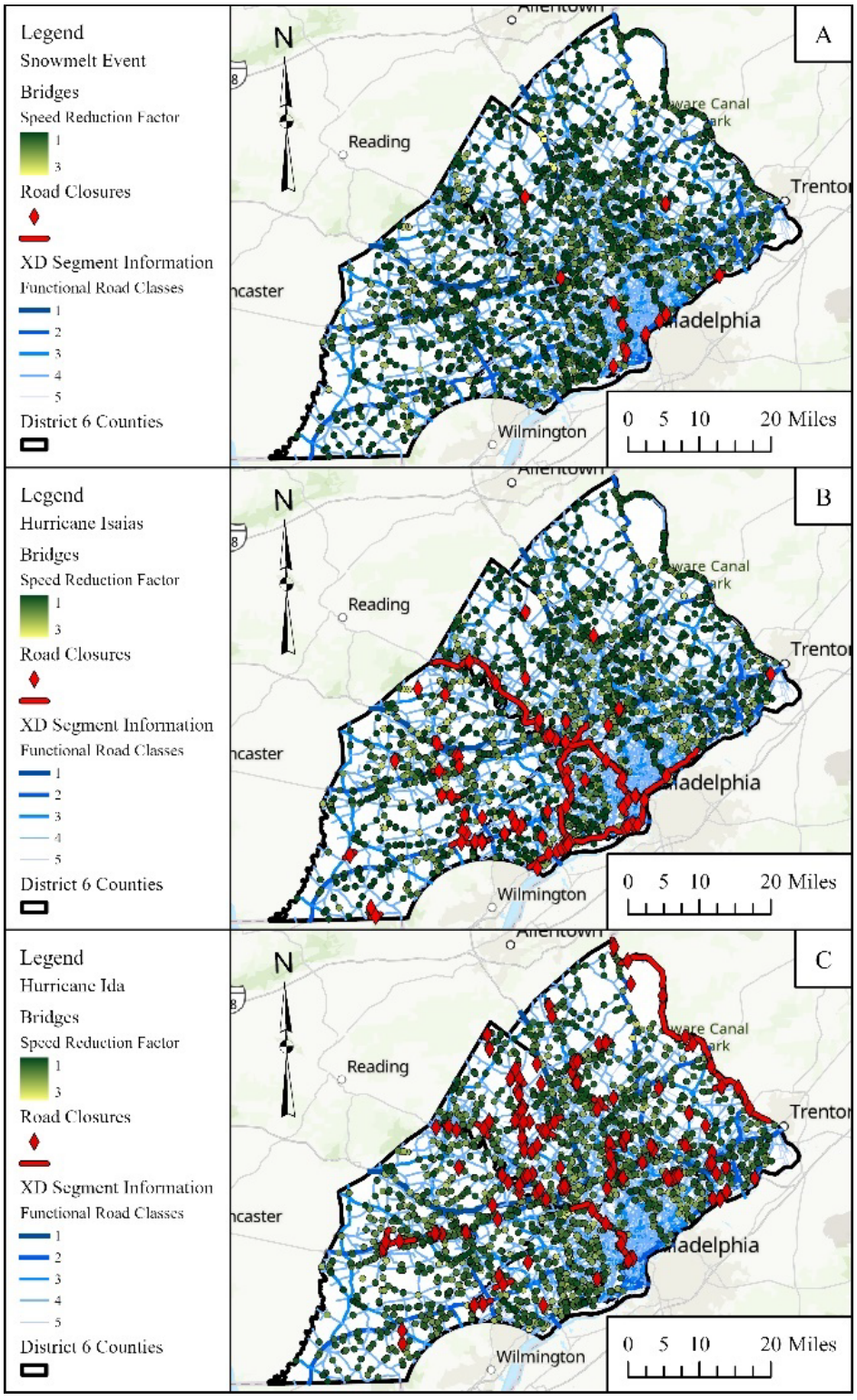

Figure 3.3. Speed Reduction Factor of bridges in District 6 for the **(A)** Snowmelt Event, **(B)** Hurricane Isaias, and **(C)** Hurricane Ida. The SRF ranges from 1 to 3, where 1 is greatest reduction in speed.

Using the speed reduction factor method to represent the congestion level, the map of the Snowmelt Event suggests there was severe congestions throughout the entirety of District 6. As seen in Figure 3.2a, few of the bridges experienced little congestion. Considering the circumstances of the event, having a snowfall event cover the landscape in snow followed by a rainfall event, road conditions could have been immensely worsened from slush making the road slippery.

There is no clear correlation between road closures influencing the congestion level since all of District 6 appears to have reduced speed. This is supported by the results from the regression (seen in the next section) where road closure occurrences are not found as a variable with correlation too the speed reduction factor. However, the weighted average of percent impervious area in the upstream drainage area does have an importance in the regression. Areas with higher percentage of impervious area provide more space for the snow/rain to accumulate during the event. These effects can last past the date of the weather event given the colder conditions, having a lack energy to evaporate the areas with accumulated runoff. Additionally, if the runoff remains on impervious area following the event, freezing can provoke icy roadways.

The speed reduction factor of the bridges during Hurricane Isaias has more concentrated areas with heavy congestion, seen in Figure 3.2b. Bridge closures appear to have a greater significance on the speed reduction factor. The results from the linear regression support this, seeing road closure occurrence at the bridges as a variable with importance.

Hurricane Ida has the least amount of congestion across District 6 compared to the other weather events, seen in Figure 3.2c. The long nature of the event could have aided in reducing the congestion level, since there was not sustained intense rainfall which traditionally reduces speed of vehicles. Similar to Hurricane Isaias, bridge closures appear to affect the congestion levels throughout District 6. The results from the linear regression support this claim.

3.2.2 Speed Reduction Factor Regression Analysis

Linear Regression Analysis

Gauging the performance of the linear regression for the speed reduction factor, the Significance F is below the threshold value of 0.001 for the three weather events. The R2 values are 0.034, 0.063, and 0.017 for the Snowmelt Event, Hurricane Isaias, and Hurricane Ida, respectively. Two iterations are needed for the three weather events to narrow down the variables that have the greatest correlation with the speed reduction factor.

The results for the linear regression of the speed reduction factor are summarized in Table 3.2. For all three events the most import factors contributing to speed reduction includes the amount of impervious area and the average drainage area slope. It is important to note that while this study focuses on fluvial flooding, these factors may be more indicative of pluvial flooding. These attributes may be representative of the general area, as opposed to the bridge. During both Hurricanes, Isaias and Ida, there was a strong linkage to road closures suggesting, that the speed reduction is closely tied to road closures. This was not the case for the snowmelt event

Hurricane Ida showed a linkage to drainage area was particularly important. This is because the slow-moving, high-volume storm impacting areas with larger drainage basins. Bridge age is important for the high intensity Hurricane Isaias, suggesting that the bridges now be undersized for that level of intense precipitation combined with impervious area. Notably, during the snowmelt event the significantly important features are bridge age and if the bridge in a flood zone.

Table 3.2. Variables with the greatest correlation to the speed reduction factor for all three weather events.

Weather Event			**Snowmelt Event**	**Hurricane Isaias**	**Hurricane Ida**
Solving for	y	Speed Reduction Factor			
Input Parameters (x_n)	x_1	Road Closures Occurrence		**X**	**X**
	x_2	Bridge Age	**X**	**X**	
	x_3	Scour Score			
	x_4	FEMA Flood Zone Score	**X**		
	x_5	Upstream Drainage Area			
	x_6	Weighted Average of Percent Impervious Area	**X**	**X**	**X**
	x_7	Number of Flood Control Structures in Upstream Drainage Area			
	x_8	Number of Flood Obstruction Structures in Upstream Drainage Area			
	x_9	Average Slope of Drainage Area	**X**	**X**	**X**
	x_{10}	Percent Change in Land Cover			

Feature Importance Analysis

The results of the PFI analysis for road closures assesses the relative values of a range of variables (described in Table 3.2) and their influence on SRF. Figure 3.4 shows the feature importance for each feature assessed for the three high flow events assessed (A. snowmelt, B. Hurricane Isaias, and C. Hurricane Ida). As can be seen from these figures the importance of features varies by events. Similar to the road closure analysis, the most important features were uniformly, bridge age, drainage area, land cover change, and impervious area, as well as slope. The most important feature for Ida was drainage area, while the most important for Isaias was impervious area. The most important feature for the snow melt event was drainage area.

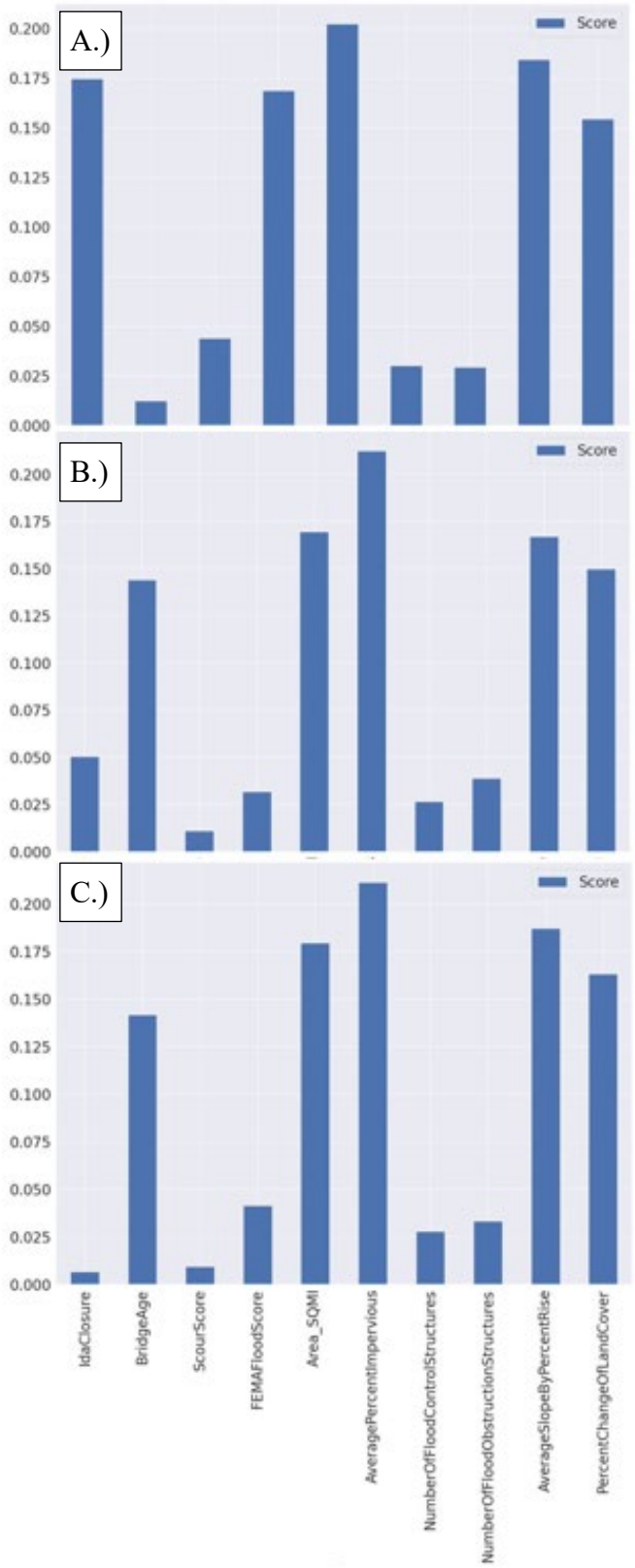

Figure 3.4. The distribution feature importance based on the SRF analysis of road closures due to flooding during the **(A)** Snowmelt Event, **(B)** Hurricane Isaias, and **(C)** Hurricane Ida.

3.3 Congestion Index Analysis

The second method for identifying the level of congestion of roadways is the congestion index. To capture the effects that the explored variables have on the congestion index, a map of the congestion index of the bridges for each event and a linear regression is utilized. Identifying the variables that make the transportation network susceptible to congestion can improve the preparation an agency can make, knowing where to tackle.

Congestion Index Maps

The congestion maps, shown in Figure 3.5, show road closures and relative congestion based on the INRIX data (described in report 3a, section 3). The three events analyzed, a rain on snow event, Hurricane Ida, and Hurricane Isais, caused bridge closures in different parts of the District 6. The flow events all resulted in high flows, however, those flows varied depending on watershed characteristics (section 3.2.2), as well as storm characteristics. The flood pulses associated with the events varied based on event intensity and duration.

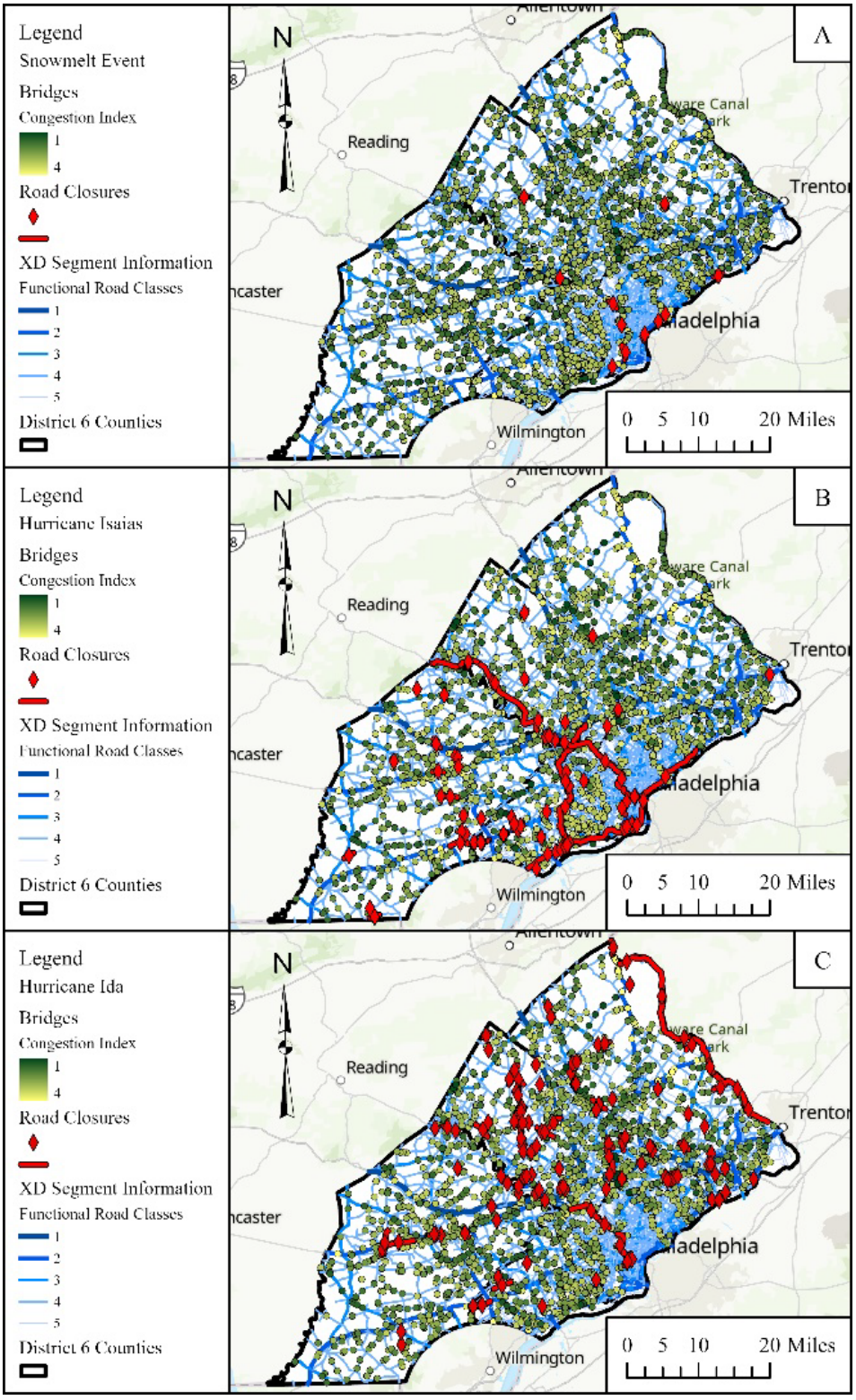

Figure 3.5. Congestion Index of bridges in District 6 for the **(A)** Snowmelt Event, **(B)** Hurricane Isaias, and **(C)** Hurricane Ida. The CI ranges from 1 to 4, where 1 is greatest congestion.

The congestion index is represented at each bridge on a scale from 1 to 4. A value of 1 indicates the most severe congestion while a value of 4 represent little to no congestion. Each bridge is represented as a circle with a color classify the severity. Green is on the severe side, representing an extremely congested bridge with a value of 1, and yellow is on the opposite side of the scale, representing no congestion with a value of 4.

The rain on snow event caused high flows, but there were relatively few bridge closures compared to larger hurricanes (e.g., Isaias and Ida). However, due to the pre-existing winter conditions congestions were elevated across the city. This does not appear to be exclusively driven by the bridge closures.

Hurricane Isaias came up the coast with a high velocity and high rainfall intensity, resulting in flooding and congestion (Fig. 3.3). The Hurricane precipitated a lot of water with a high intensity but moved on relatively quickly compared to Hurricane Ida. Hurricane Ida slowly moved across District, delivery a high volume of water over a large area, but not with the same intensity as Hurricane Isais. As a result, the road closures associated with Hurricane Isaias located primarily in smaller highly urban watersheds towards the southern portion of the district (e.g., those bridges crossing Cobb and Darby Creeks). These flood pulses passed relatively quickly. Larger basins were able to mute the flood pulse because not much water was contributed outside of District 6.

In the Hurricane Ida (Fig. 3.5), water from surrounding drainage areas drained into District 6 resulted in flooding and closures along the main branches of the Schuylkill and Delaware Rivers. This water slowly collected in the river network, resulting in a peak flow twelve hours after the storm began. Smaller watersheds were able to easily drain, but large drainage basins, such as the Schuylkill and Delaware were overwhelmed by the drainage from all the upstream contributing area.

3.3.2 Regression Analysis

Linear Regression Analysis

The results from the linear regression of the congestion index provided a sufficient Significance F, less than 0.001. for the three weather events. The R^2 values for the Snowmelt Event, Hurricane Isaias, and Hurricane Ida are 0.073, 0.088, and 0.027, respectively. Only two iterations of the linear regression analysis are needed to produce the remaining variables that correlate most with the congestion index.

Table 3.3 includes a summary of the results from the linear regression of the congestion index for the three weather events. Similar to the results seen in the speed reduction factor linear regression, the weighted average of percent impervious area of the upstream drainage area and the average slope of the upstream drainage area are recognized as being important factors all weather events. Additionally, the number of flood control structure in the upstream drainage area of the bridges is identified for the three events while the number of flood obstruction structures in the upstream drainage area are for Hurricane Isaias, and Hurricane Ida.

Table 3.3. Variables with the greatest correlation to the congestion index for all three weather events.

Weather Event			Snowmelt Event	Hurricane Isaias	Hurricane Ida
Solving for	y	Congestion Index			
Input Parameters (x_n)	x_1	Road Closures Occurrence		**X**	
	x_2	Bridge Age			
	x_3	Scour Score			
	x_4	FEMA Flood Zone Score		**X**	
	x_5	Upstream Drainage Area			
	x_6	Weighted Average of Percent Impervious Area	**X**	**X**	**X**
	x_7	Number of Flood Control Structures in Upstream Drainage Area	**X**	**X**	**X**
	x_8	Number of Flood Obstruction Structures in Upstream Drainage Area		**X**	**X**
	x_9	Average Slope of Drainage Area	**X**	**X**	**X**
	x_{10}	Percent Change in Land Cover			

Feature Importance Analysis

The results of the PFI analysis for road closures assess the relative values of a range of variables (described in Table 3.3) and their influence on CI. Figure 3.6 shows the feature importance for each feature assessed for the three high flow events assessed (A. snowmelt, B. Hurricane Isaias, and C. Hurricane Ida). As can be seen from these figures the importance of features varies by events. Similar to the road closure analysis, the most important features were uniformly, bridge age, drainage area, land cover change, and impervious area, as well as slope. The most important feature for Ida was drainage area, while the most important for Isaias was impervious area. The most important feature for the snow melt event was impervious area.

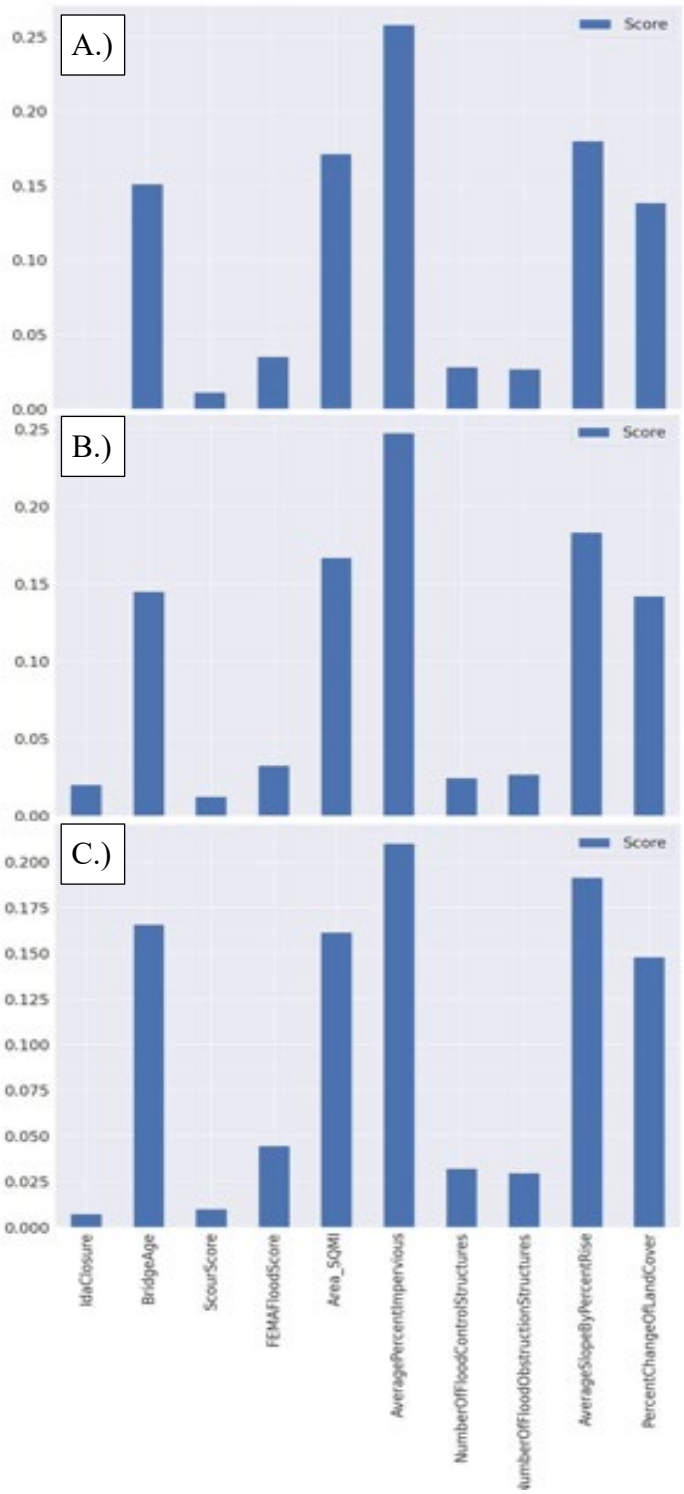

Figure 3.6: The distribution feature importance based on the RF analysis of road closures due to flooding during the **(A)** Snowmelt Event, **(B)** Hurricane Isaias, and **(C)** Hurricane Ida.

4 Impact on Safety

This section describes the crash distribution during two high stream flow events: Snowmelt event of November 2018 and Hurricane Isaias during August 2020. There was no crash data available for Hurricane Ida (2021) at the time of this report production. Overall, with high traffic volume surrounding the city of Philadelphia, higher crash frequency was observed nearby the City network for both events. Crash Record Number (CRN) served as the main point in connecting various types of open-source crash data files (e.g., crash file, person file, vehicle file, etc.). The process of integrating open-source crash datasets with crash date, bridge and roadway closure information is fully presented in Appendix G. Key crash features reviewed include collision type and injury severity degree as well as crash location. These features were spatially joined with road and bridge closure information to better visualize any potential correlation among above mentioned crash attributes. However, there is not a strong correlation between crashes and road closures associated with flooding.

This analysis was completed from the snowmelt high flow event and Hurricane Isaias. Hurricane Ida was not included due to data unavailability.

4.1. Snowmelt Event

For the snowmelt storm event, a total of 112 crashes were recorded during the storm period, shown in Figure 4.1. The most highly observed crash collision type was "*hit fixed objects*" along FRC 1 as well as the FRCs within the City. This is expected as roadway friction is a function of pavement surface and weather condition, especially the wet event. And lower roadway friction will result in a more challenging braking or negotiating roadway curvature that could increase crash likelihood. No fatal crash was observed while the unknown injury was the most identified crash severity level followed by the minor injury. When comparing the congestion levels of XD segments associated with the crash to the XD segments of overall network, FRC 3 associated with crash location demonstrated slightly higher congestion values than the overall FRC 3, while other FRCs showed similar congestion degree to the overall FRCs. As expected, the crash counts of pre and post storm event showed lower occurrence when compared to the value during the event, suggesting the adverse impact of severe weather on network safety.

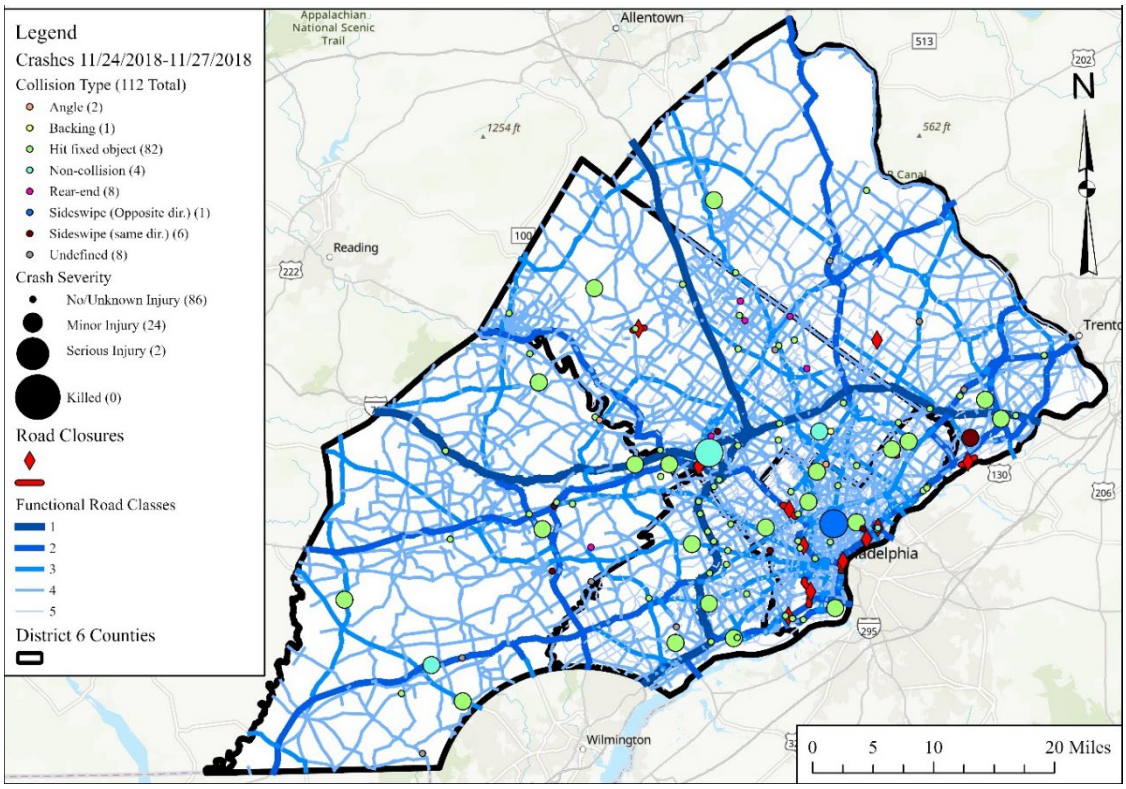

Figure 4.1. Crash Distribution during the snowmelt event across District 6.

4.2. Hurricane Isaias

During Hurricane Isaias, which had the same closure duration as the 2018 snowmelt event, there were a total of 109 crashes, shown in Figure 4.2. Two fatal crashes were observed at the proximity of FRC 4. As the roadway closure was concentrated along major interstates, crash distribution displayed a more spread-out pattern compared to the snowmelt case. For the collision type, "*hit fixed objects*" was the most observed one (72 counts, 66%) followed by the "*sideswipe"* type. Overall FRCs 1 and 2 with crash experienced higher congestion levels when compared to the overall network FRC 1 and 2 congestion levels. This might be due to the fact that the roadway closure was mostly along interstates, and congestion of crash locations at the proximity of roadway closure got exacerbated due to the closure. When compared to pre and post storm event period for the same storm duration (4 days), the data shows indeed higher crash frequency during the storm event.

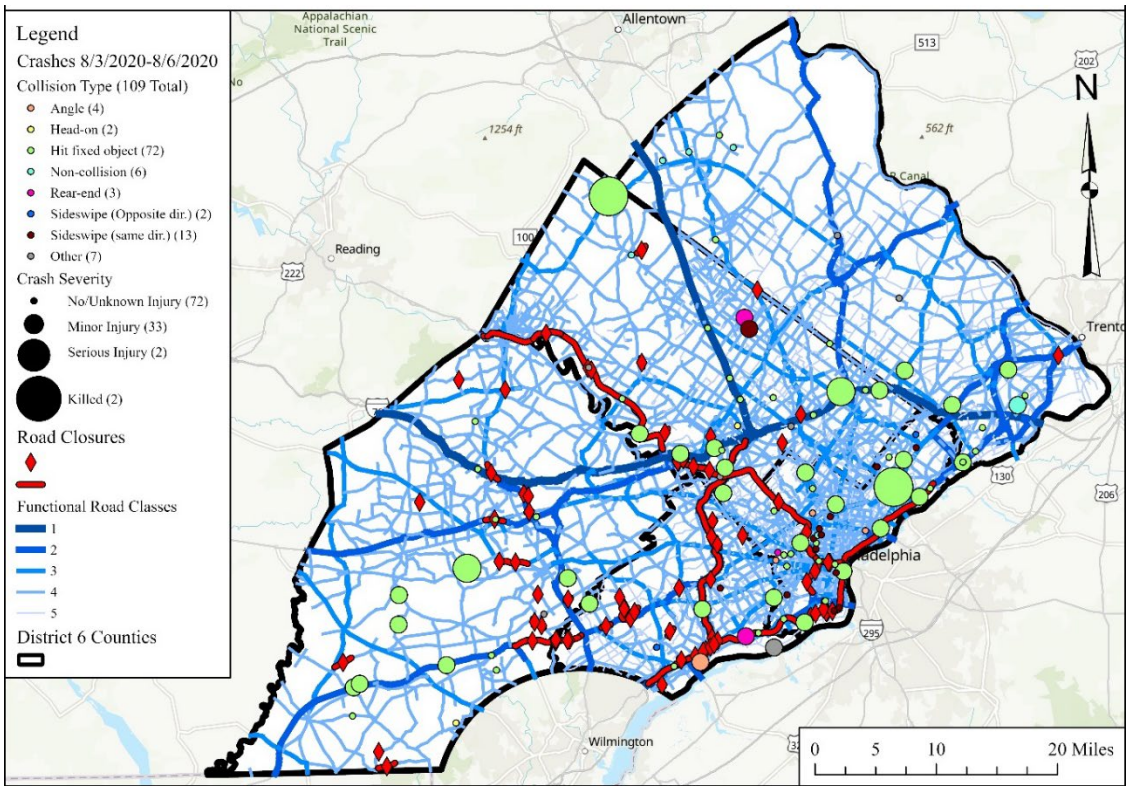

Figure 4.2. Crash Distribution during Hurricane Isaias across District 6.

5 Conclusion

As noted in Task 1c, the linear regression analysis includes criteria that explore the effects that a bridge's attributes, urbanization, stormwater management practices, field-collected data, and natural topography on the associated flooding at bridges. The criteria analyzed included bridges' attributes such as (i) the bridge age and (iii) the location of the bridge within FEMA flood zones. The criteria that summarize the effects of urbanization are (vii) the weighted average of the percent impervious area of the upstream drainage area and (viii) the percent change in land cover of the upstream drainage area. The criteria that summarize the effects of stormwater management practices are (iv) the number of flood control structures within the upstream drainage area and (v) the number of flood obstruction structures within the upstream drainage area, (ix) the scour grade. The criteria that summarize the effects of natural topography are (ii) the upstream drainage area of the bridge and (vi) the average slope of the upstream drainage area. These attributes were joined to each stream bridge feature.

The distribution of road closures that occurred during the three events are shown in Figure 3.1, while the results of the linear correlation is shown in Table 3.1 and the feature importance in Figure 3.2. From this analysis resulted in the following conclusions:

- Of the nine independent variables included in the regression analysis, seven are indicated by the linear regression as having a correlation with the road closures due to flooding occurrence for Hurricane Isaias and Ida. Notable variables identified are percent impervious area in the upstream drainage area and the average slope of the upstream drainage area.
- Hurricane Isaias was an extremely intense rainfall event, causing rainfall to quickly accumulate in areas with higher percentages of impervious areas. Additionally, the drainage areas with steeper slopes produce more runoff since less time is given for the landscape to allow infiltration, quickly moving excess rainfall across the system.
- For all three events the number of flood control structures and flood obstruction structures is important relative to road closures. The existing infrastructure may suggest that these locations were previously identified as areas of concern. However, changes to the watershed may result in these features no longer providing the same level of insulation to flood events.
- Being located in the flood zone was an important feature for the snowmelt event and Isaias, but not Ida. Ida had a much larger volume of water associated with it, causing a different style of flooding.
- The average slope within the drainage area was important to both hurricanes, which saw substantial and more rapid runoff than the snowmelt event. However, only the closures associated with precipitation intense Hurricane Isaias were impacted by bridge age, suggesting that flash flooding may have increased through time associated with watershed development.
- While this describes the response in analysis of the road closures, the response was somewhat consistent across the other target variables, speed reduction factor and congestion index. Where differences occurred it is likely due to an issue in the general area of the bridge, as opposed to at the bridge itself.
- In the feature importance analysis, the most important features were uniformly, bridge age, drainage area, land cover change, and impervious area, as well as slope. This remained constant for all of the target variables analyzed. This aligns somewhat with the linear regression, but the features vary in their importance.
- Feature importance varied for different target variable analysis for the snow melt event, this suggest that outside influences, such as ice, might also be impacting road conditions. However, it remained constant for Hurricane Isaias and Hurricane Ida. The most important feature for Ida was drainage area, while the most important for Isaias was impervious area. Therefore, watersheds that are highly developed where more effected by the intensity of Hurricane Isaias (coming up the Atlantic Coast), while watersheds draining large areas were more impacted by the high volume of Hurricane Ida (coming across the US).

- Notably, this is a statical analysis, as opposed to a physics-based model. While these findings are insight, not all findings may be easily linked to the on the ground scenario.

Task 3c: Summary

This subsection presents an overview of various PennDOT efforts toward the asset management related to this study. Connection to each task of this study is illustrated in a tabulated form to better provide study findings. The identification of hydraulic and environmental variables that impact roadway and bridge closures is critical in understanding network performance congestion levels. Furthermore, Task 2 results provided an example of latest sensor technology application in detecting and monitoring infrastructure changes. Hence, in this subtask, the study contributions are highlighted in the context of various PennDOT's programs and initiatives.

Task 3c Report

1 Introduction

In this subtask, various PennDOT's initiatives, programs, interactive platforms, and studies were reviewed to identify relevance to this study's findings and where the findings of this study could contribute. It should be noted that this subtask is a dynamic section that can expand to respond to the growing number of studies focusing on extreme events and infrastructure/network resiliency.

2 Project Relevance Review

According to the American Association of State Highway and Transportation Officials (AASHTO), transportation asset management (TAM) is defined as a "*strategic and systematic process of operating, maintaining, upgrading, and expanding physical assets effectively throughout their life cycle. TAM focuses on business and engineering practices for resource allocation and utilization, with the objective of better decision-making based on quality information and well-defined objectives*." In this context, TAM includes various activities that are interconnected for monitoring and managing the risks, optimizing the infrastructure maintenance, and distributing limited resources by prioritizing work to meet both short- and long-term state goals. Other tangential programs support these principles. Table 2.1 of task 3c presents significance and findings of this study and their relevance to reviewed PennDOT's efforts toward asset management. Furthermore, the findings described in Task 2 can be leveraged to apply the latest sensors to better monitor and assess the flooding extent, which is an essential step for flood and asset management.

Table 2.1. PennDOT Asset Management Efforts

PennDOT Initiatives/ Studies/ Programs	Description	Relevance to proposed study
Transportation Asset Management Plan (TAMP)	With four major objectives, PennDOT's TAMP presents an overall approach of PennDOT's asset management. Roadway pavement and bridges are main focal points of TAMP.	Task 3b findings can assist better identify congestion prone locations within District 6. Also, since the land surface is dynamics hydrologic drivers can ultimately help develop an informed resiliency rating system.
Pavement Asset Management Systems (PAMS)	PennDOT's PAMS is a predictive approach and strategic framework for managing transportation infrastructure, aligning resource allocation to maintain and/or improve the system to a specific level.	Considering that roadway congestion and inundation degree are major factors in pavement deterioration, information from Task 3a and 3b, about the congestion level per FRC, can provide further insights in estimating the impact of high stream flow events on pavement performance. Furthermore, through this study, a more informed decision in prioritization of the pavement maintenance scheduling can be achieved. In addition, the application of various sensors, as described in the Task 2 report, will contribute an accurate pavement inspection.
Bridge Asset Management System (BAMS)	Penn DOT's BAMS is a predictive approach and strategic framework for managing bridges. PennDOT's Asset Management released its custom BAMS, labeled BridgeCare, as a software to assists both engineers and planners by providing a recommended list of projects, based on individual or regional input and needs, in accordance with federally mandated lowest life cycle cost (LLCC) methodology.	The findings of this study will help identify bridges at risk of closure in District 6. Further, this study identifies features that often lead to bridge closures which may help identify problems early. And, by linking the bridge closures to congestions and speed reduction values we can identify the bridges that are the highest risk for the network.
PennDOT Local Technical Assistance Program	LTAP's main objective is to provide technical information and proven technologies associated with roadway maintenance and safety approaches to meet the growing needs of local governments.	The study findings will help disseminate information about the roadways and bridges prone to the closure for a better understanding of the flood impacts. In addition, by gaining a better understanding of the storm impacts on roadways, a proactive maintenance scheduling and evaluation system of roadway condition for resiliency can be established. Furthermore, local agency engineers can develop easy tracking system to record flooding hot spots integrated with the safety data

PennDOT Transportation Systems Management and Operations (TSMO)	TSMO aims to address reliability, mobility, and congestion by utilizing various strategies.	Identifying attributes that are significant in bridge and roadway closure as well as understanding congestion level at different roadway categories will be useful in developing informed and efficient detour routes. Furthermore, in the event of evacuation due to the severe high stream flow events, this study findings provide critical information that could integrate adjustability toward optimal evacuation routes.
Local Scour Critical Bridges	Platform that illustrates identifies and locates scour critical bridges owned by Pennsylvania local government agencies	As bridge scour is also a function of severe high stream flow events, by identifying closure prone bridge locations through this study will help better be prepared for future severe high stream flow events. Additionally, the bridges likely to be repetitively impaired may be in danger of scour.
PA Flood Risk Map	This platform provides an interactive and user-friendly web map application with map features connected to geospatial databases. The percentage of annual Chance Flood Hazard. to discern the effective flood hazard zones	Task 1 results are directly related to this interactive platform and can provide hydrologic drivers to identify features that are linked to flooding and roadway closure.
PennDOT Extreme Weather Vulnerability Study	Focusing on the state-owned roadways, this vulnerability study investigated flooding vulnerabilities and risks.	Task 3 findings can further complement the vulnerability study by providing other FRC information as well as roadway closure relevant environmental attributes. With the review of three different severe high stream flow events and its impacts on network, specific linkages between the hydrologic features driving bridge closures and network congestion the study findings. This can provide further helpful insight understanding of the potential impacts of weather.

Task 3 References

Thomas Schinko *et al* 2020 *Environ. Res. Commun.* 2 015002

Maura Allaire, Socio-economic impacts of flooding: A review of the empirical literature, Water Security, Volume 3, 2018, Pages 18-26, ISSN 2468-3124, https://doi.org/10.1016/j.wasec.2018.09.002.

Maria Pregnolato, Alistair Ford, Sean M. Wilkinson, Richard J. Dawson, The impact of flooding on road transport: A depth-disruption function, Transportation Research Part D: Transport and Environment, Volume 55, 2017, Pages 67-81, ISSN 1361-9209.

Ning Zhang, Alice Alipour, Multi-scale robustness model for highway networks under flood events, Transportation Research Part D: Transport and Environment, Volume 83, 2020, 102281, ISSN 1361-9209

Amro Nasr, I. Björnsson, D. Honfi, O. Larsson Ivanov, J. Johansson & E. Kjellström (2021) A review of the potential impacts of climate change on the safety and performance of bridges, Sustainable and Resilient Infrastructure, 6:3-4, 192-212, DOI: 10.1080/23789689.2019.1593003

"Highway Functional Classification Concepts, Criteria and Procedures", Federal Highway Administration, 2017, https://www.fhwa.dot.gov/planning/processes/statewide/related/highway_functional_classifications/section03.cfm

David Schrank, Luke Albert, Bill Eisele, & Tim Lomax (2021) Urban Mobility Report, https://mobility.tamu.edu/umr/report/

Task 3 Appendix List

Appendix A: RITIS User Manual

Appendix B: Congestion Maps

Appendix C: Speed Analysis Graphs

Appendix D: SRF and CI Calculation Example

Appendix E: Regression Analysis Variable Definitions

Appendix F: XD Segment Information and Bridge Closure Spatial Analysis

Appendix G: Crash Data Spatial Analysis

Appendix H: Maps from Analysis

Appendix A: RITIS User Manual

RITIS User Manual

To access RITIS

Once on the RITIS platform, the home screen will be visible

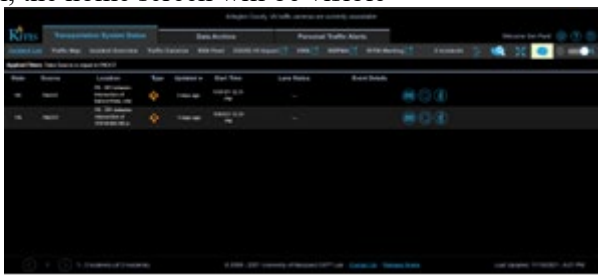

The default screen shows a current incident list of traffic events that updates when you open the platform

To specify data for and create a congestion map

1. From RITIS platform home screen navigate to the second tab next to "Transportation System Status" labeled "Data Archive" this will bring you to the screen shown below

2. From this screen click on the subtab labeled "Probe Analytics"

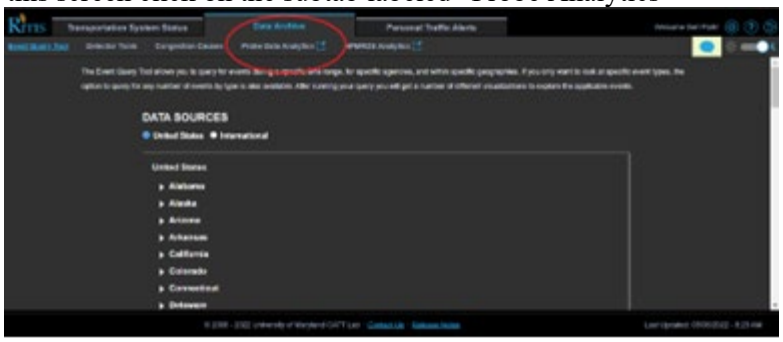

3. Now click on the tab labeled "Trend Map"

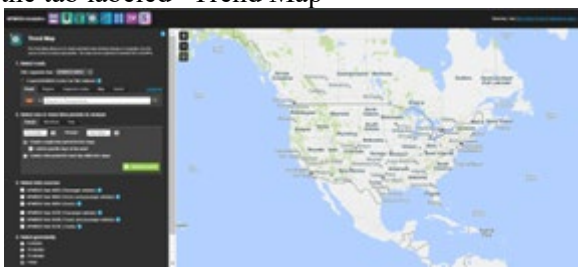

4. To retrieve INRIX data specify it as the desired segment from INRIX using the drop-down tab by choosing “XD” or “TMC”. This will change how segments are defined.

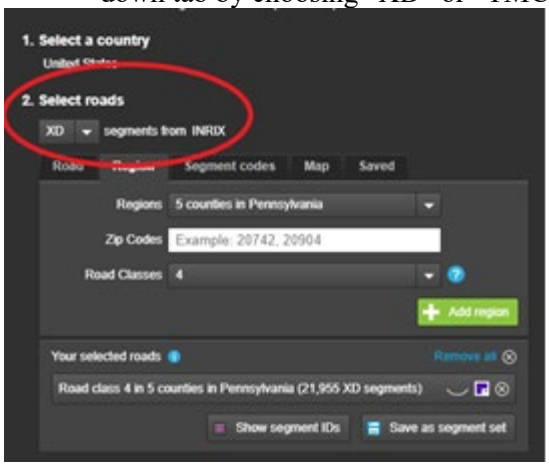

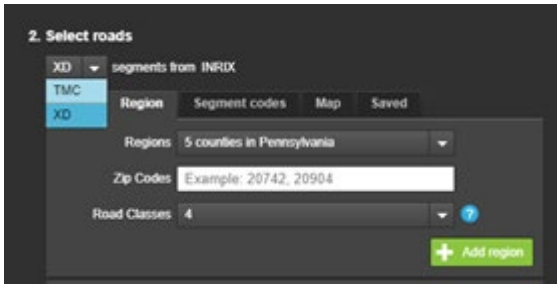

5. Under step 2 after specifying “XD” or “TMC” segments from INRIX source choose the segments to include. This can be done using any of the five tabs listed: Road, Region, Segment codes, Map, or saved. Once the desired segments are shown on the map, the green button “Add Region” must be clicked

   a. Road: If using the Road option first choose the state of interest using the drop-down list with the orange icon to the left. Then type in the roadway name into the search bar to the right. Depending on the roadway chosen, a variety of options will be shown corresponding to different roadway intersections located on the chosen roadway.

From this drop down selected the intersections of interest. They will then be added to the blank map to the right of the screen.

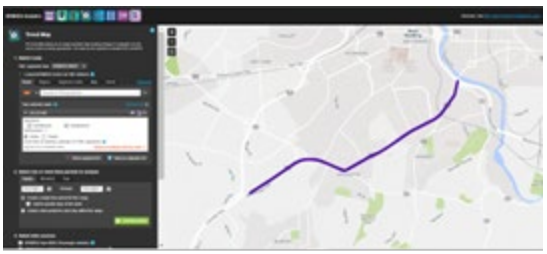

b. Region: If using the Region option, click the tab next to “Road” labeled “Region”

From here you can specify which specific counties of interest you want shown by hovering over the dropdown next to the state you selected

Direction, zip code, and road class can also be specified according to the dropdown lists shown below, multiple directions and road classes can be chosen at the same time

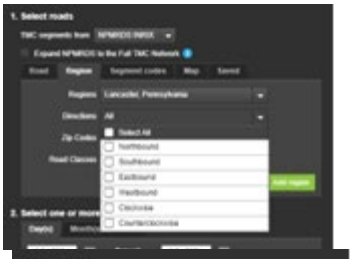

Direction

Road Classes

The type of road class options shown will differ for XD segments and for TMC segments. XD segments are coded based on the Functional Road Classes, defined below.

Value	Road Type
1	National highway network
2	State highway network
3	Interconnecting network
4	Major connectors
5	Minor roads

The current option for XD FRC's This column contains the FRC's for the given value

Functional Class = 1 roads allow for high volume, maximum speed traffic movement between and through major metropolitan areas.
Functional Class = 1 is applied to roads with very few, if any, speed changes. Access to the road is usually controlled.

Functional Class = 2 roads are used to channel traffic to Functional Class = 1 roads for travel between and through cities in the shortest amount of time.
Functional Class = 2 is applied to roads with very few, if any speed changes that allow for high volume, high speed traffic movement.

Functional Class = 3 is applied to roads which interconnect Functional Class = 2 roads and provide a high volume of traffic movement at a lower level of mobility than Functional Class = 2 roads.

Functional Class = 4 is applied to roads that provide for a high volume of traffic movement at moderate speeds between neighbourhoods. These roads connect with higher functional class roads to collect and distribute traffic between neighborhoods.

Functional Class = 5 is applied to roads whose volume and traffic movement are below the level of any functional class. In addition, walkways, truck only roads, bus only roads, and emergency vehicle only roads receive Functional Class = 5.

For TMC segments, the road class options can be selected as the following:

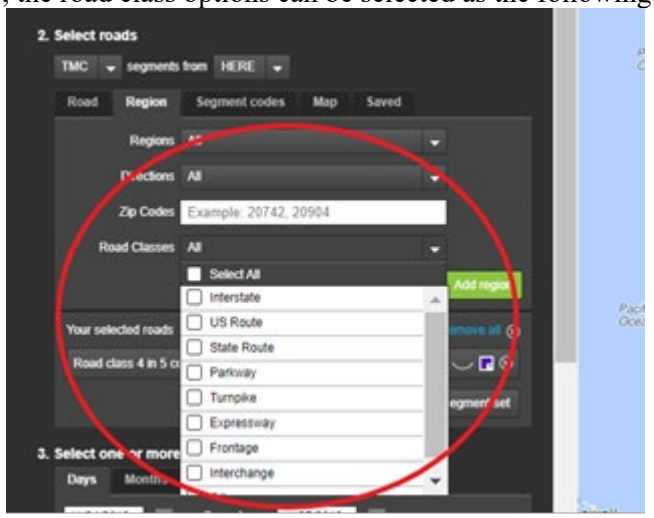

Once the fields have been filled the map to the right of the screen will populate with the chosen segments selected as described above.

c. Segment: If using the segment option enter the TMC or XD codes corresponding to the segment in the blank textbox to the right of the screen that you wish to analyze if multiple segments are to be analyzed enter them separated with a comma.

Once entered the TMC/XD codes will populate the map to the right of the screen

d. Map: If using the map option, the State of interest can be specified with the Region tab as shown below

Road class can also be specified according to the dropdowns below (multiple road classes can be chosen at once). The road class options will vary based on the type of segments chosen as described under the "Region" option above.

XD segments are classified according to the Functional Road Classes defined below:

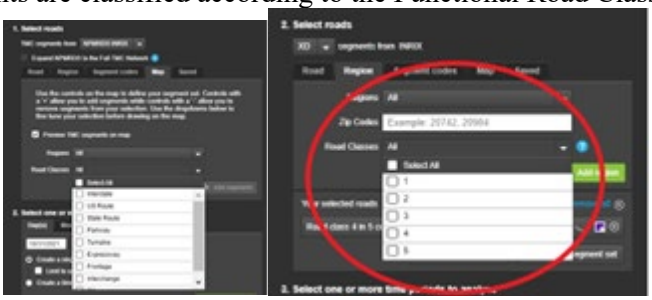

Once these are specified the drawing tools shown in the red circle below can be used to specify an area on the map, from the drawn shape roadway segments that fall within the drawn shape will populate the map.

If unwanted segments are inadvertently selected as falling within the shape, any of the shape icons with a (-) symbol can be used to remove these segments which will be highlighted in red, while remaining segments will be highlighted in green. An example is shown below.

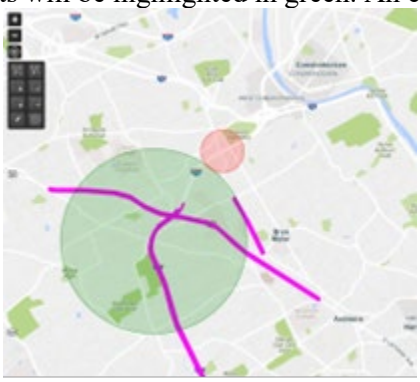

e. Saved: The saved tab can be used if any specific segment selections have been previously selected and saved as a grouped selection when using the trend map tool

6. Once the desired segments are shown on the map to the right, the green button “Add Segments” must be clicked

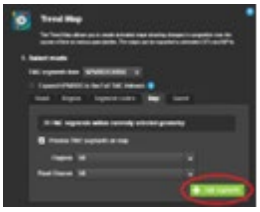

7. Part 2 requires the desired time period to be entered, this can be done for a specific day, a range of days, a month, or a year.

The time period chosen can also be specified as a singular time period, wherein specific days of the week can also be specified, or a time period for each day within the range can be specified. Once the desired time period has been entered, the green button “Add time period” must be clicked

8. The desired data source must then be specified. This must match the selection that was made in step 4. Data can be specified as for passenger vehicles, Trucks and passenger vehicles, or Trucks. (Multiple options may be selected at once).

9. The granularity must now be specified. Periods of 5 minutes, 10 minutes, 15 minutes, or 1 hour may be selected.

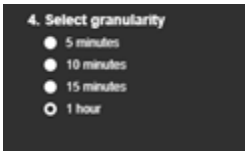

10. After all the above information has been entered, the blue "submit" button at the bottom of the right-hand panel can be selected to create the trend map visualization of the data.

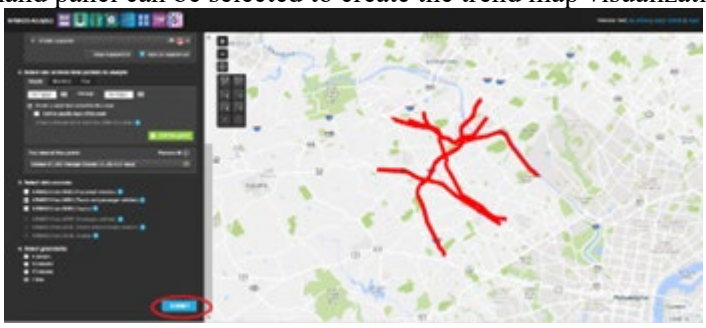

11. A new browser tab will then be opened for the trend map to be displayed and loaded. Depending on the number of segments and the granularity, size of the data will vary and may take a few minutes to load. The loaded trend map will load as shown below.

12. The display shown can be changed to indicate speed, historic average congestion, comparative speed, congestion, travel time index, buffer index, and planning time index using the display dropdown menu.

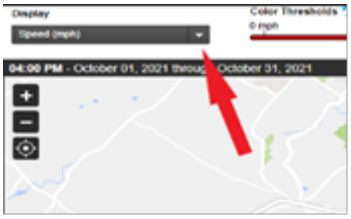

13. Once the desired display has been chosen, the color threshold can be adjusted by value using the sliders at the top of the screen (indicated with the red arrow below).

14. The timeline displayed can also be adjusted using the black slider at the bottom of the screen in intervals according to the granularity chosen. (An example is shown below).

15. If multiple days were selected for analysis, the display can be rearranged according to preference, using the display options tab at the top right hand of the screen.

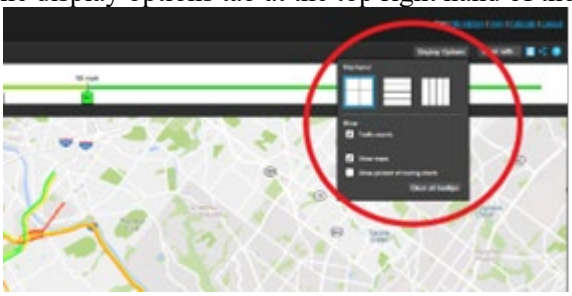

16. The data can then be downloaded for further analysis outside of the site using the left most blue icon at the right-hand side of the screen.

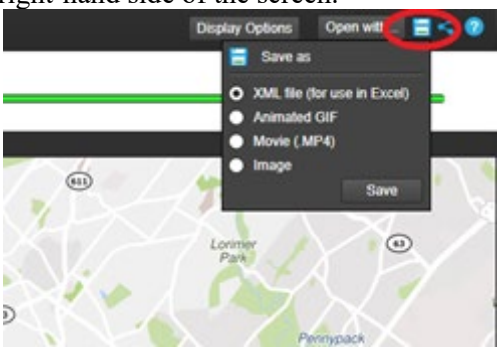

The animated GIF and movie (.MP4) files will save as videos that can be played according to the time period specified in Step 7. The image option will only save the current view that you have displayed on the screen. The XML file will download as a .xml file that must be viewed and opened in excel.

The color coding will correspond to the values set in Step 13, and the location data is coded based on the TMC segment code selected in Step 5.
Each sheet in the excel will correspond to a different direction of travel. This data can then be used for offline analysis.

Page Break

To access latitude and longitude information corresponding to XD or TMC segment Codes

1. From RITIS platform home screen navigate to data archive tab (Step 1 above).
2. Following this, click on the "Probe Analytics" tab (Step 2 above).
3. Click on the icon labeled "Massive Data Downloader"

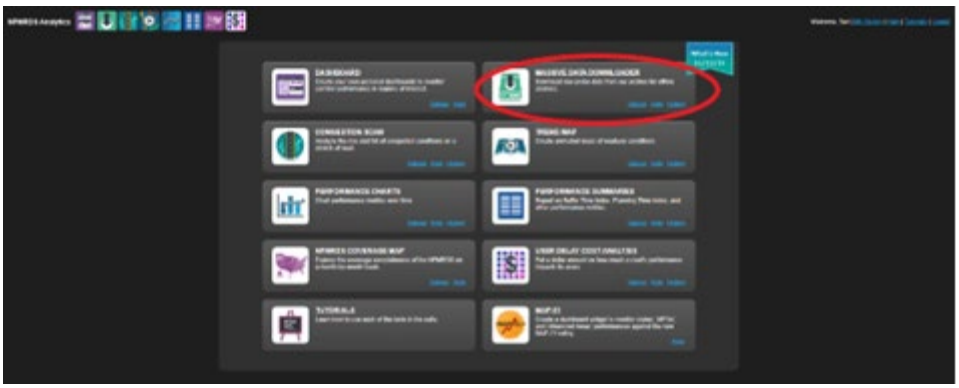

4. This tool will bring up the screen shown below, similar to the screen presented with the Trend Map tool.

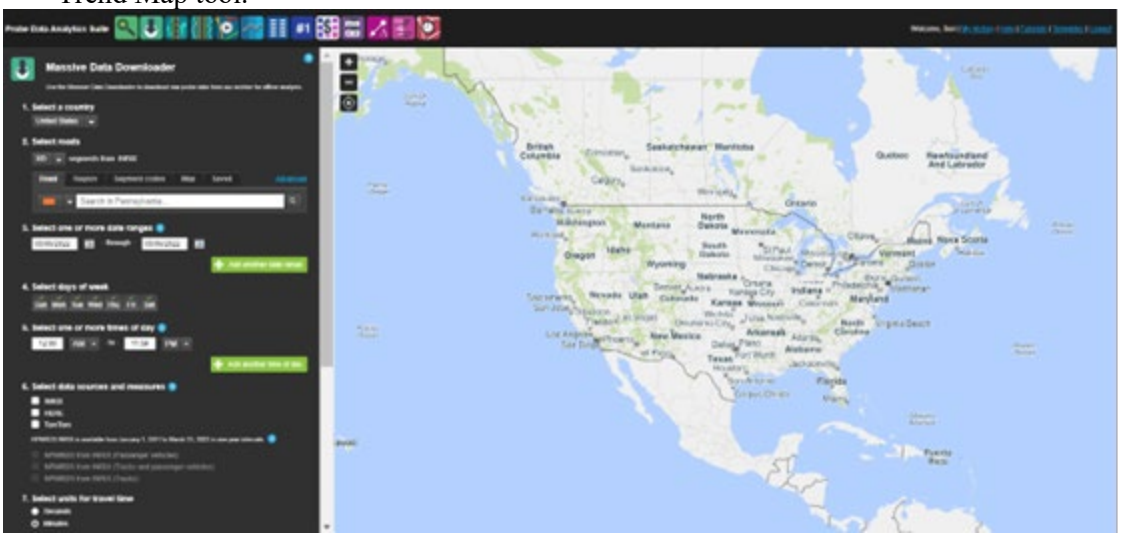

5. Using the left-hand side panel navigated through inputs #1-#8 as with the trend map tool use above. Ensure that the "Selected Roads" match exactly what was input with the trend map tool in order to obtain latitude and longitude data for these segments. Be sure to specify either XD or TMC segments as done above.

6. Enter a title for the data set in the text box for #9.

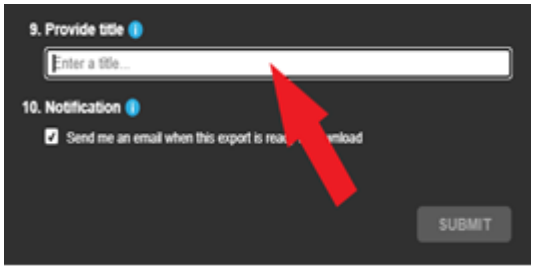

7. Ensure for #10 the box is checked to be sent an email when the export is ready to be downloaded

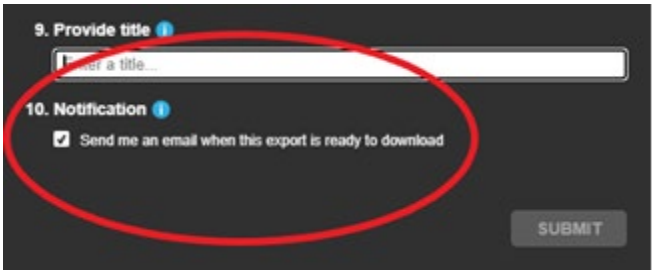

To access Historic Average Speed Data

1. Open RITIS platform as done above
2. Select "Data Archive" and "Probe Analytics" repeating steps 1. and 2. under "***To specify data for and create a congestion map"*** above
3. Select performance charts tool under probe analytics suite

4. Select Roads, Time Period(s), and Data Source, and granularity as with steps 1. – 9.
5. Select submit

6. Once submitted a new window will open showing the following

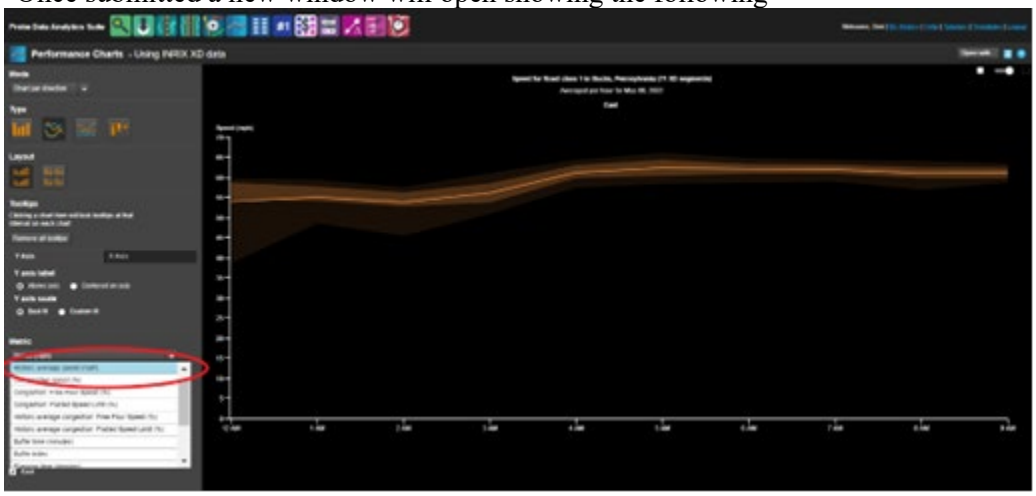

7. Select Historic Average Speed
    a. This will update the chart shown and data can be downloaded as excel file
    b. Click “save as” blue icon

ii. Select XML file
iii. Data will then download and can be opened in excel

Appendix B: Congestion Maps

Snowmelt Event FRC 4

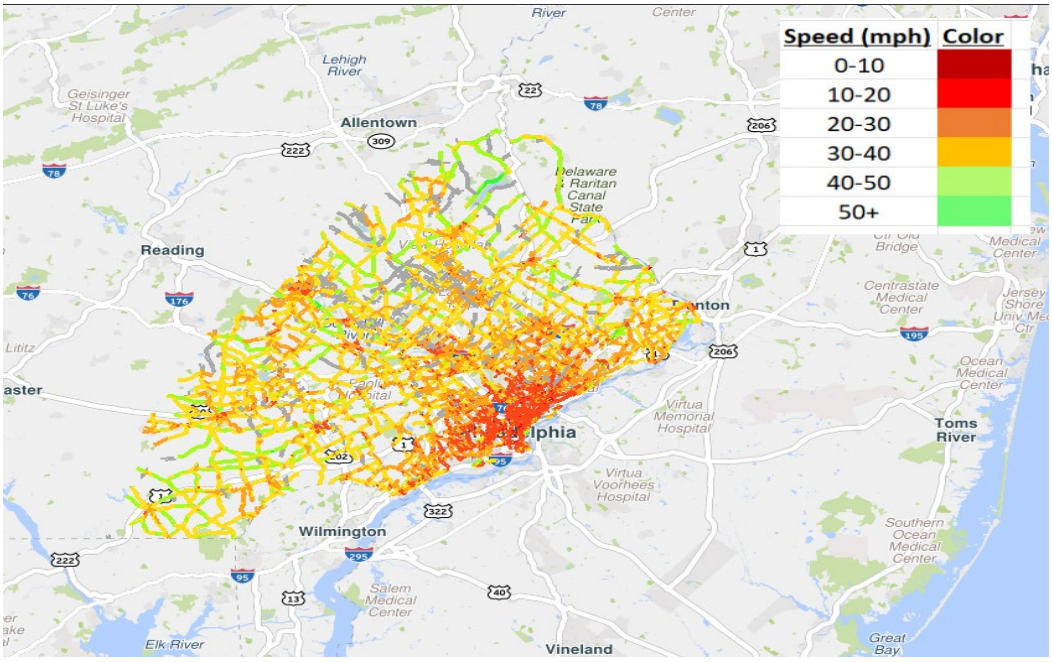

Snowmelt Event FRC 5

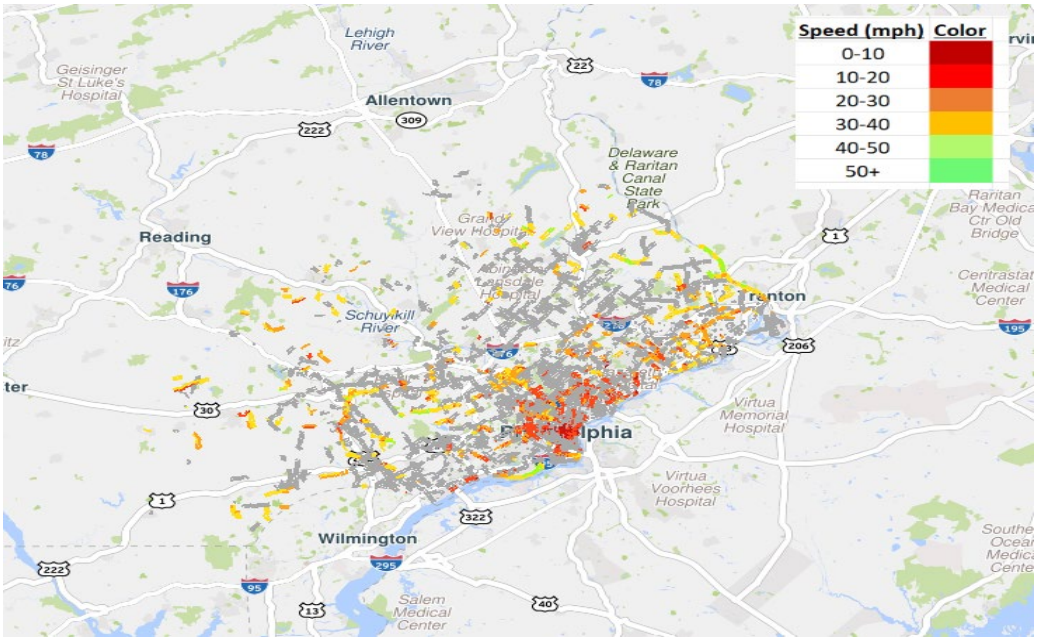

Hurricane Isaias FRC 4

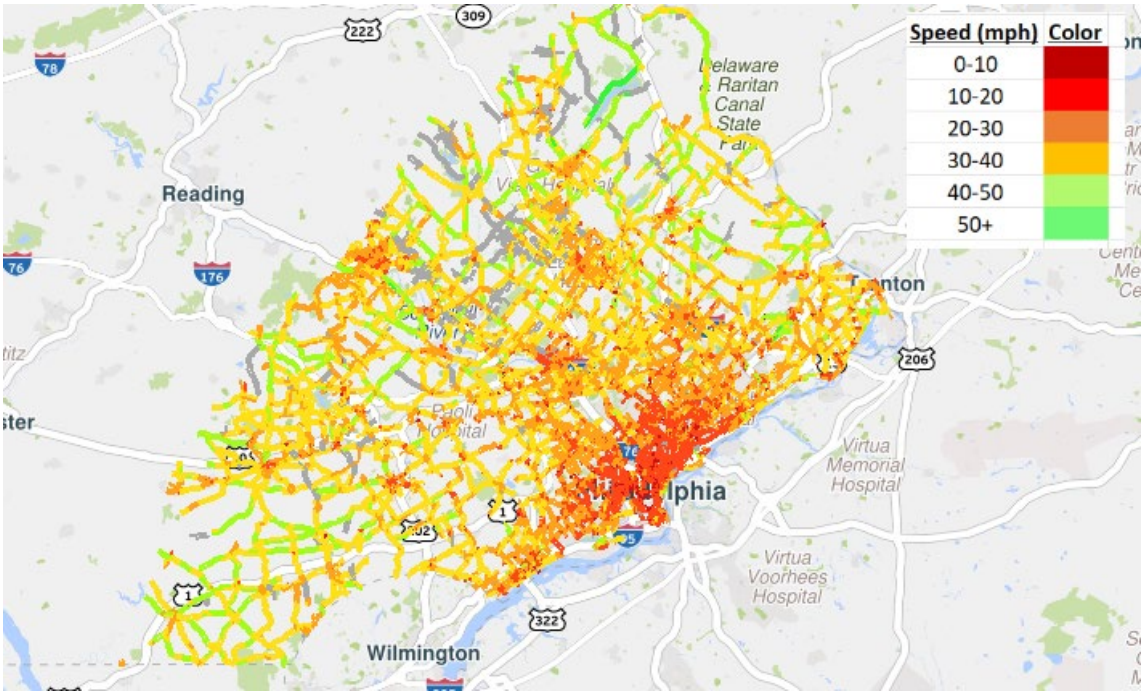

Hurricane Isaias FRC 5

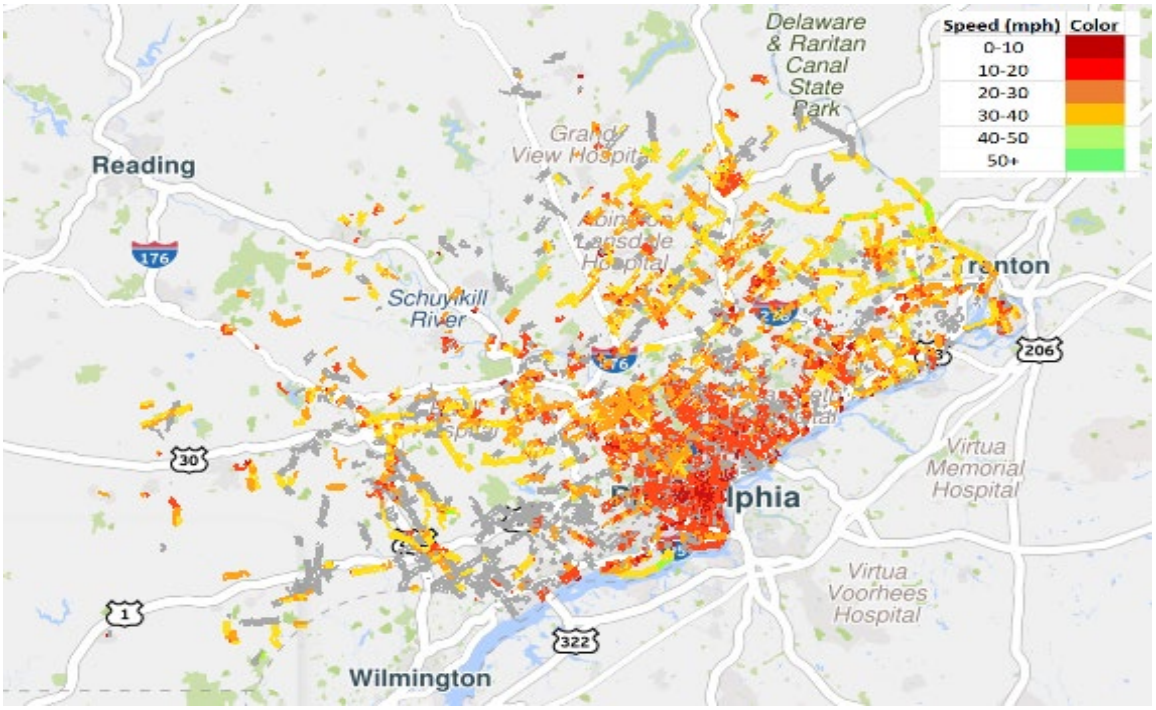

Hurricane Ida FRC 4

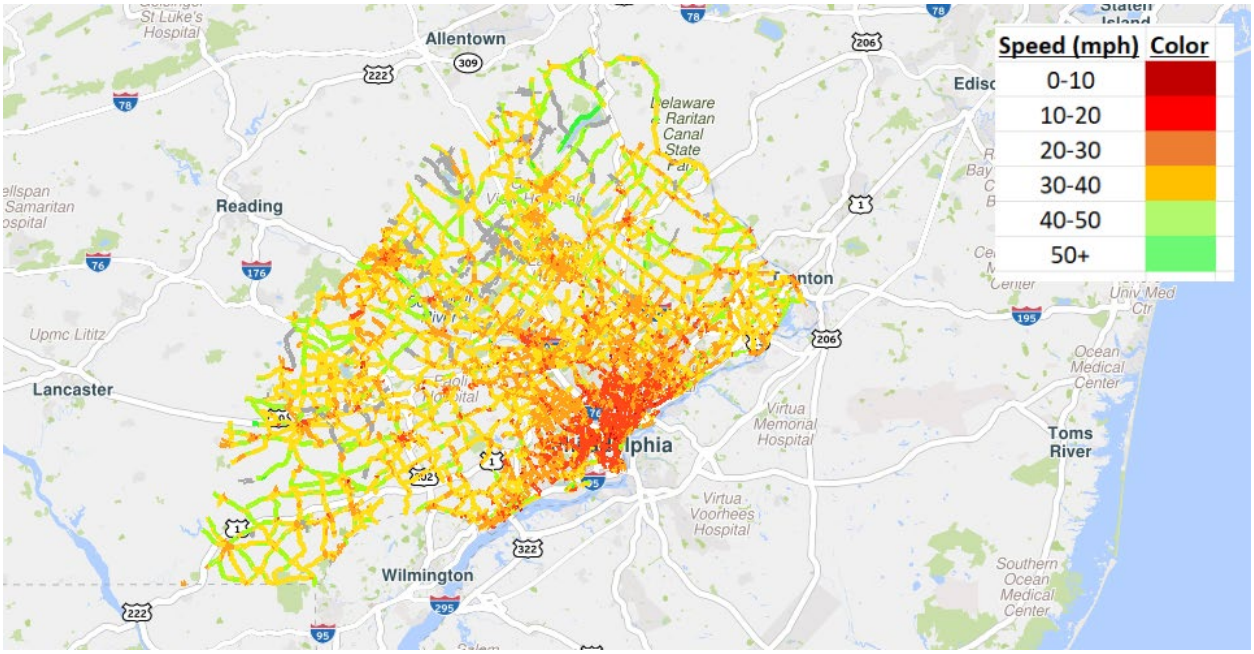

Hurricane Ida Class 5

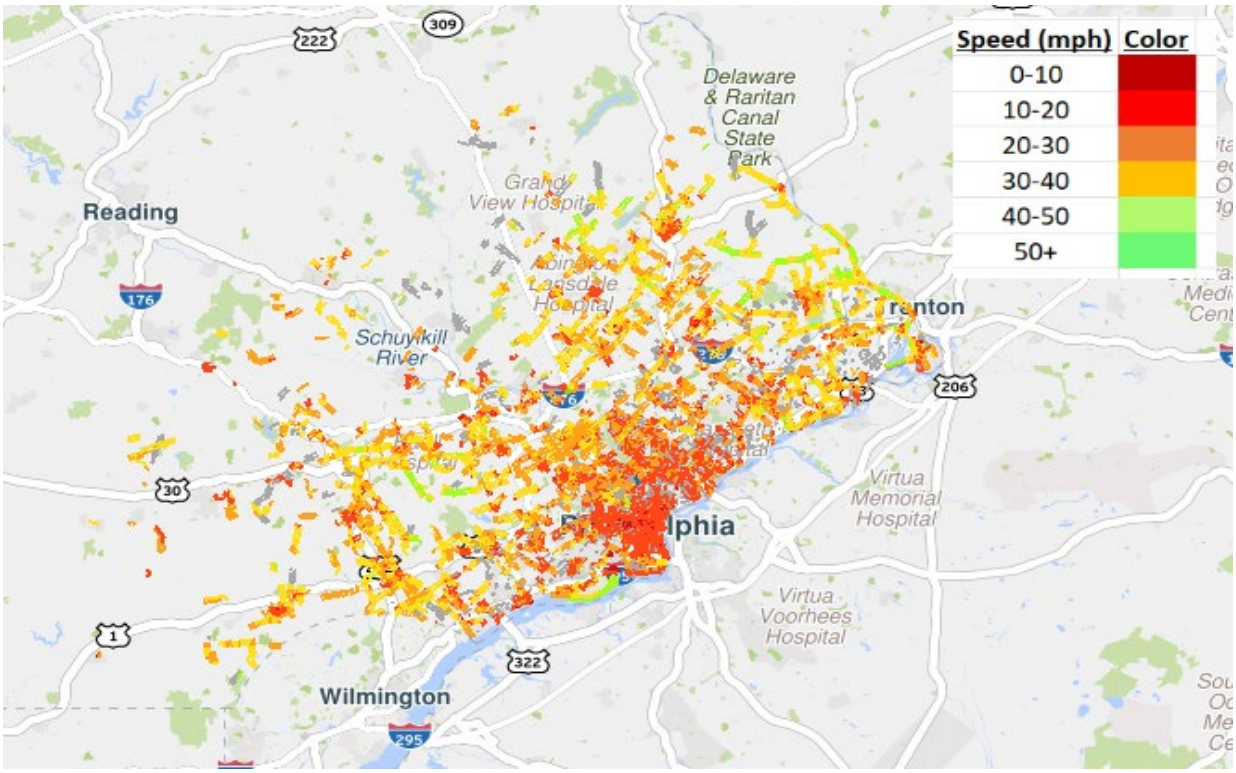

Appendix C: Speed Analysis Graphs

Speed vs. Time All Road Classes

Snowmelt

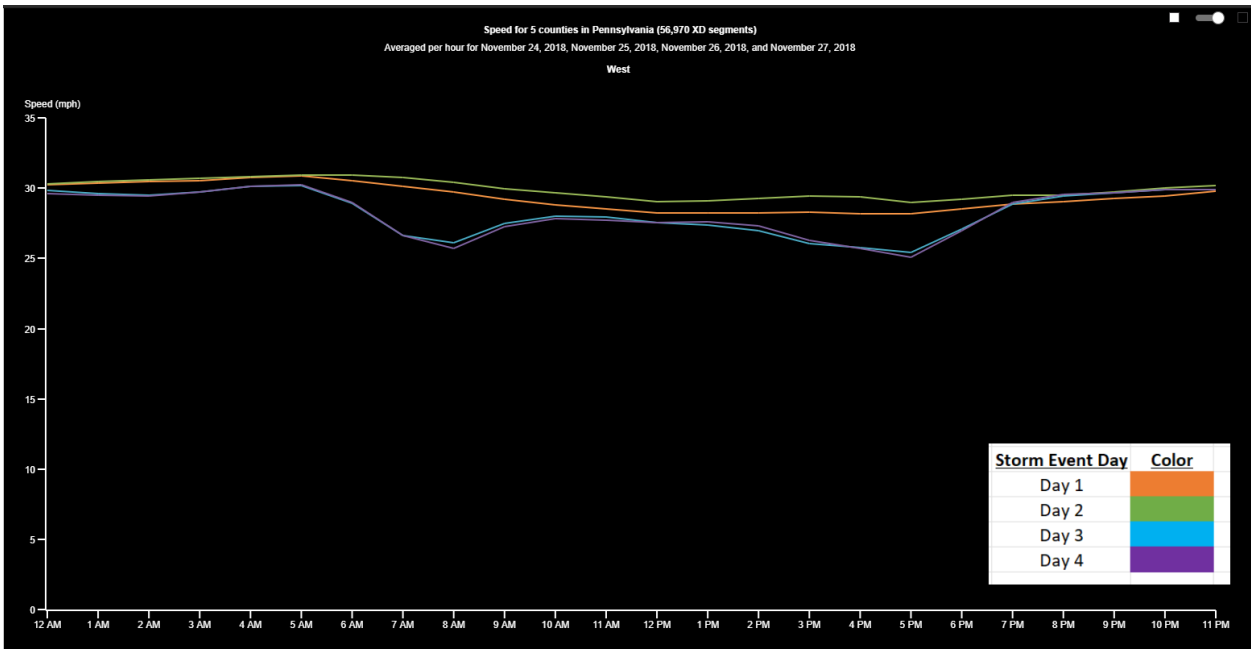

Isaias

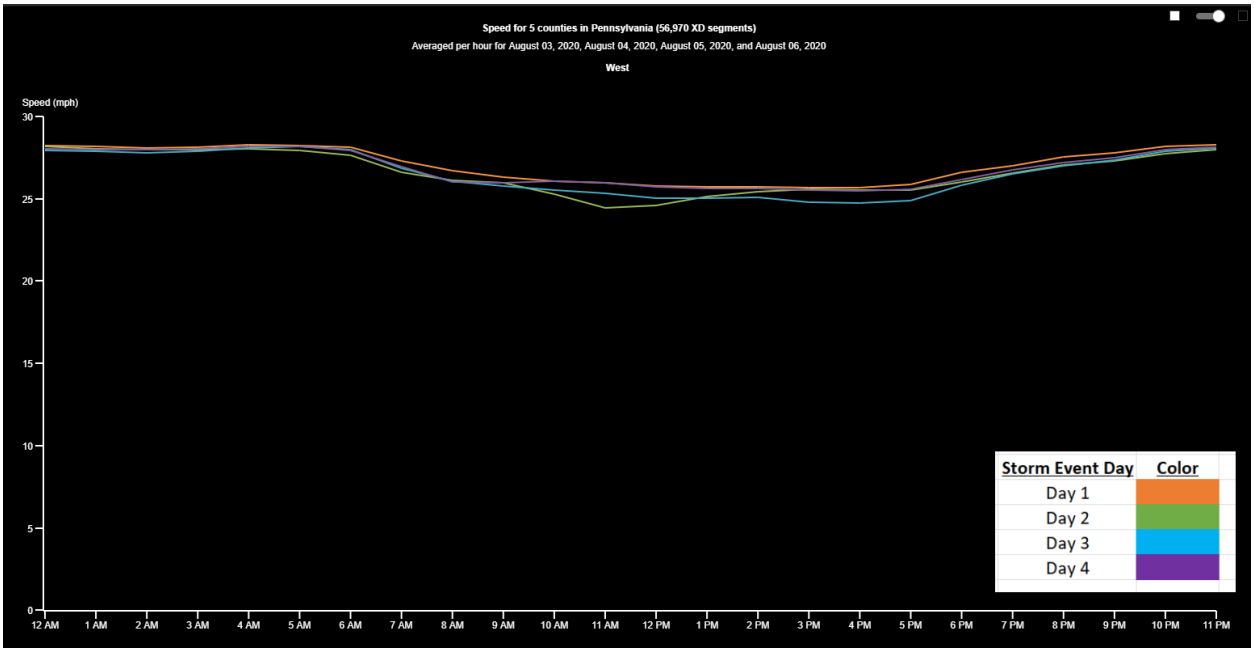

Ida

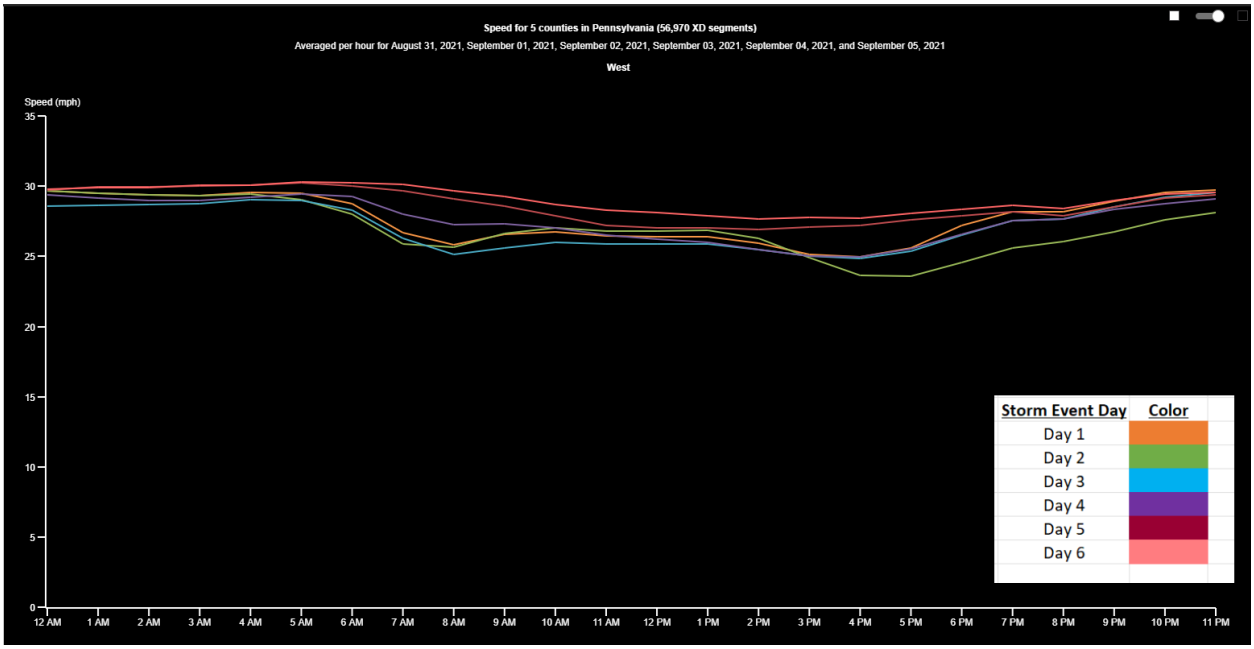

Speed vs. Time per event per Class

Snowmelt FRC 1

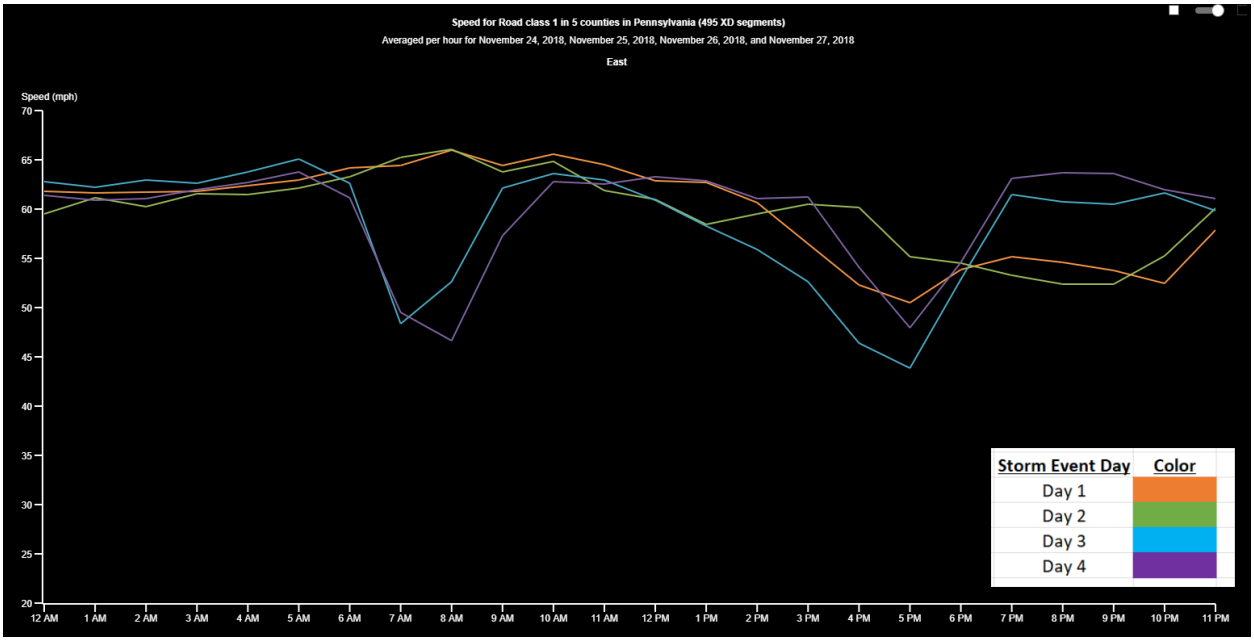

Snowmelt FRC 2

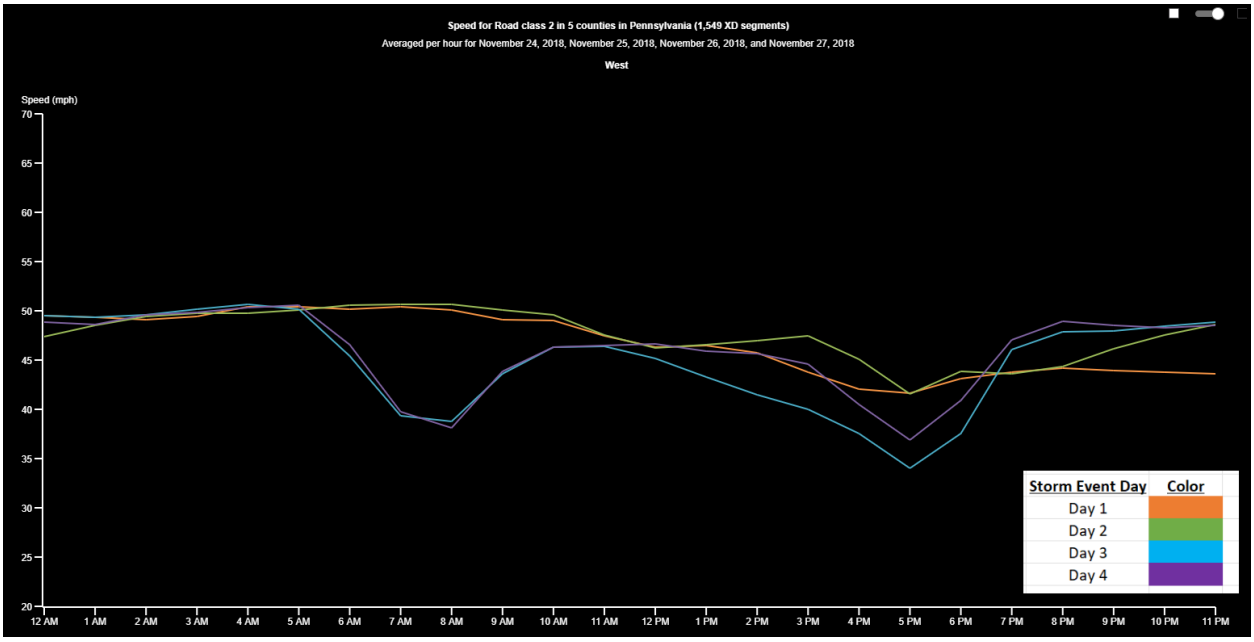

Snowmelt FRC 3

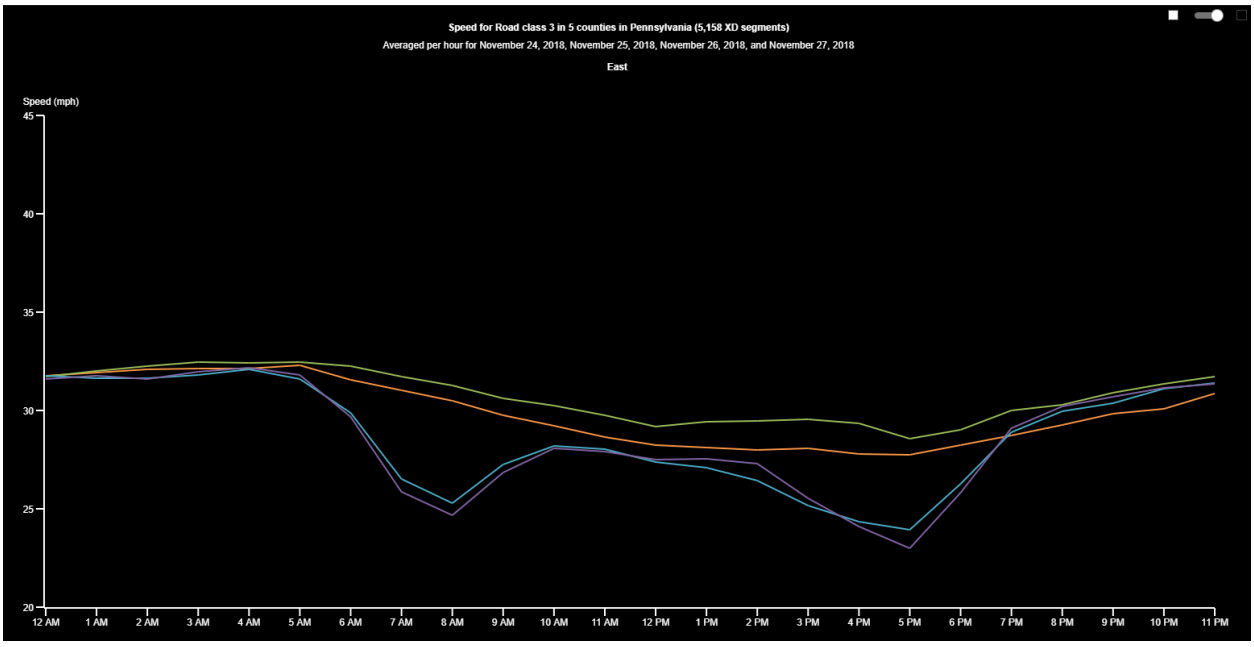

Snowmelt FRC 4

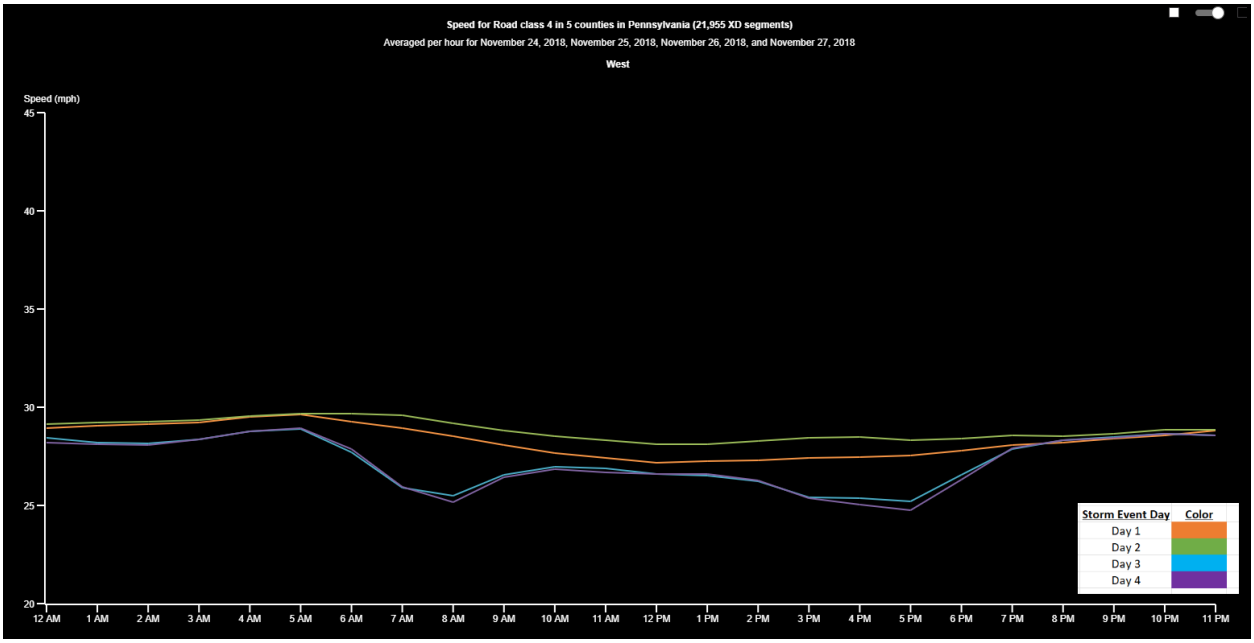

Snowmelt FRC 5

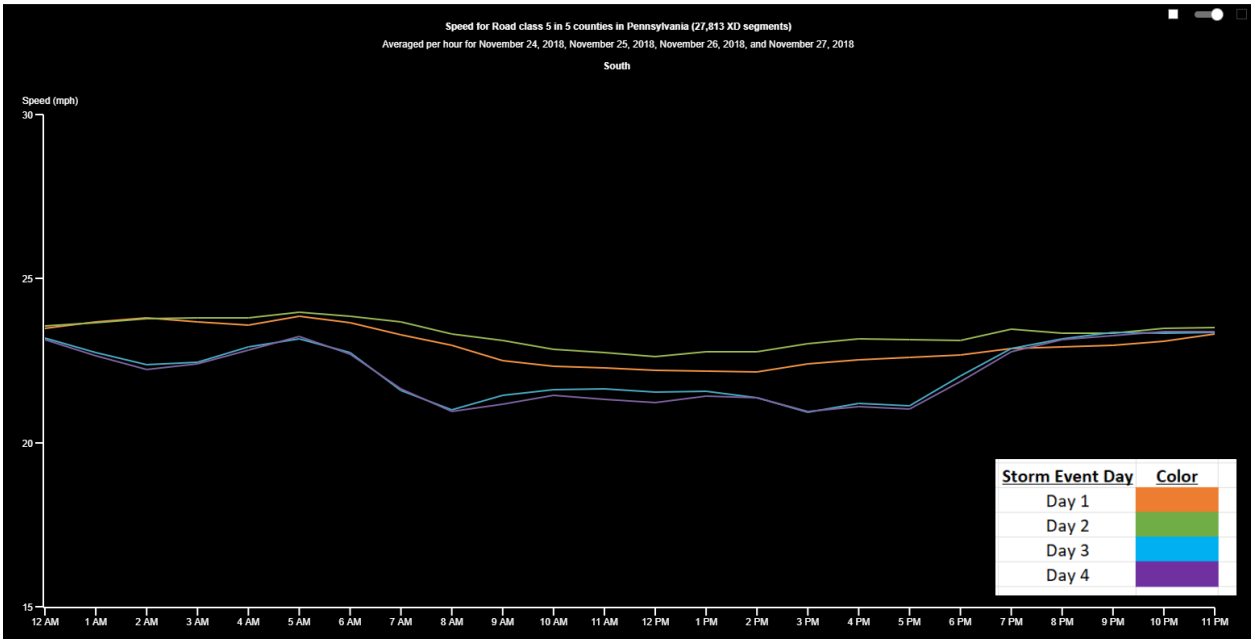

Isaias FRC 1

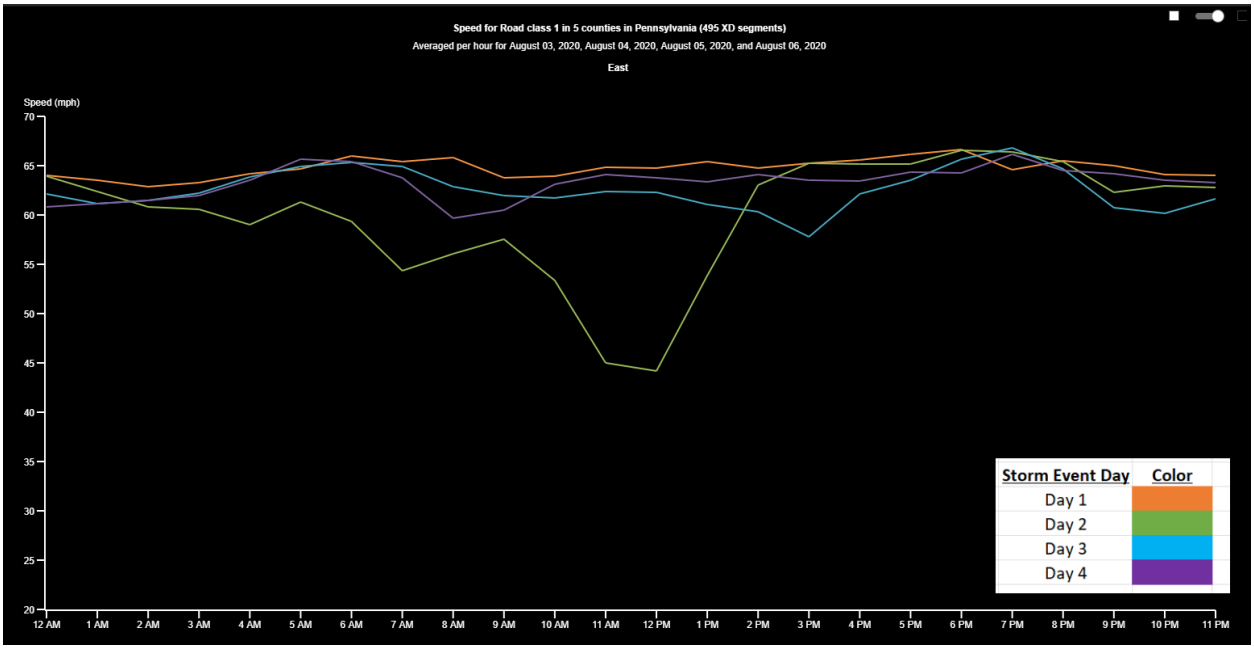

Isaias FRC 2

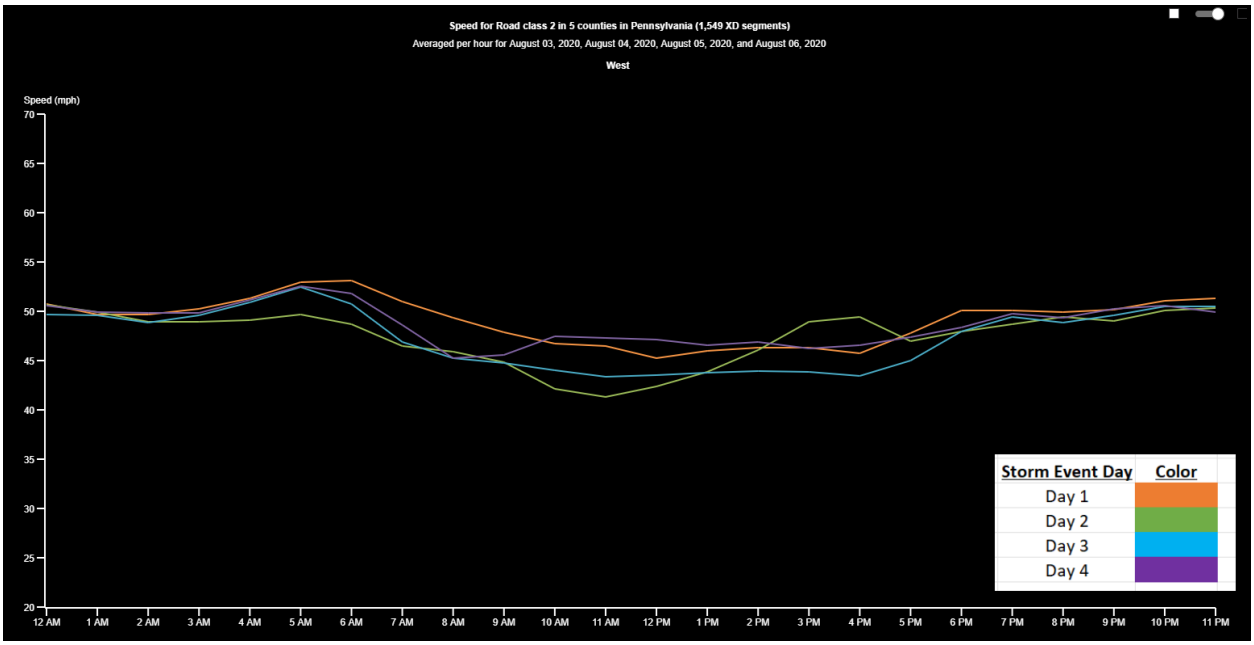

Isaias FRC 3

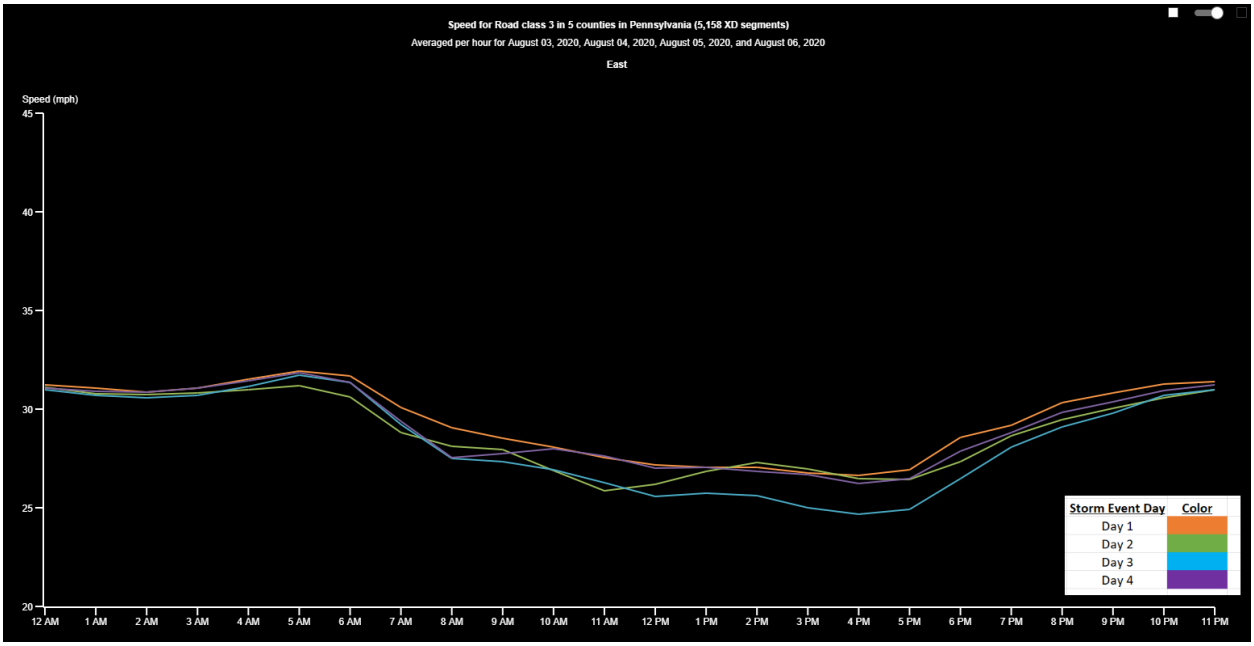

Isaias FRC 4

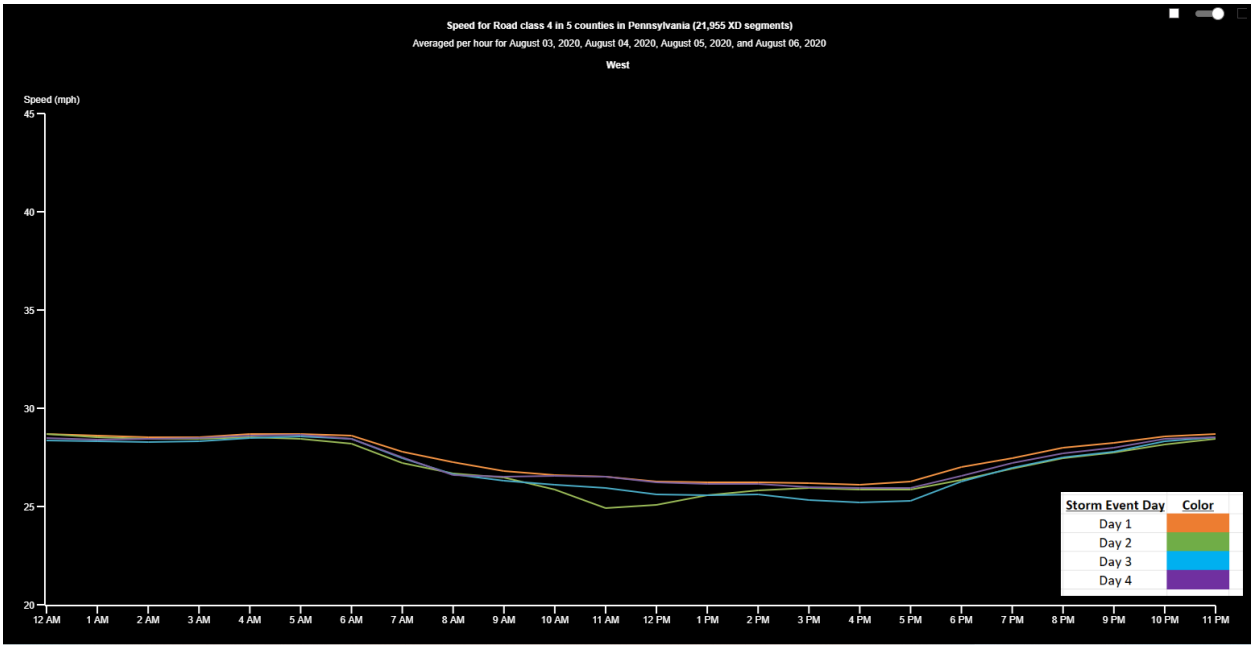

Isaias FRC 5

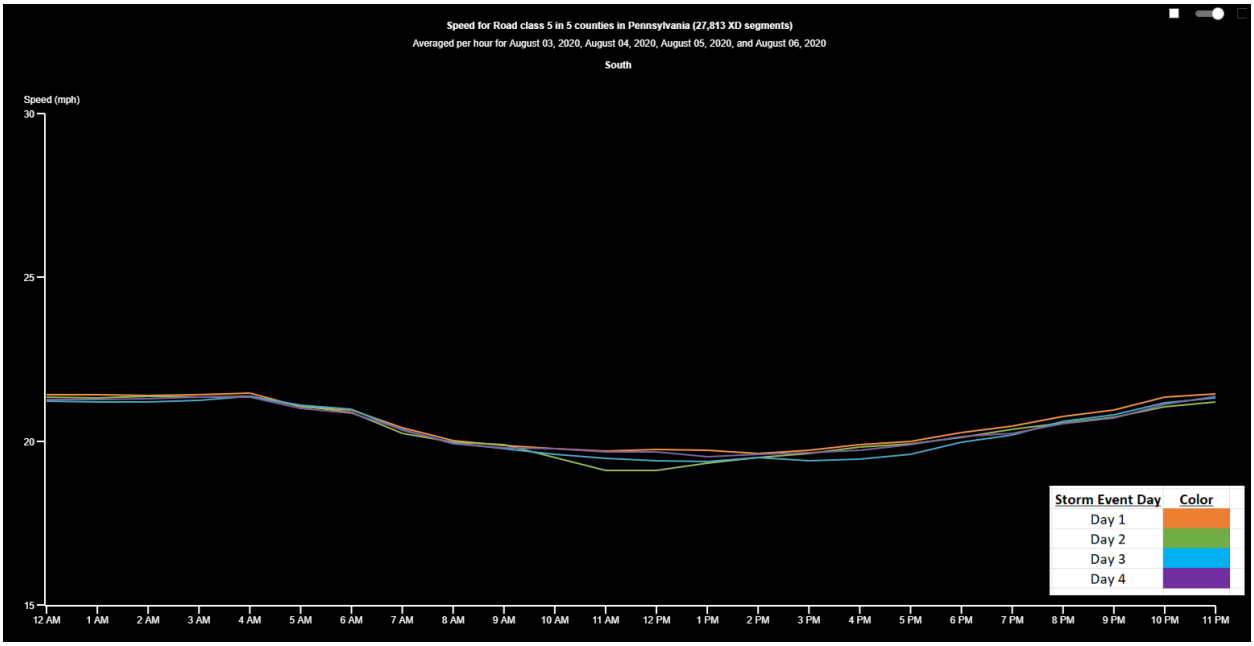

Ida FRC 1

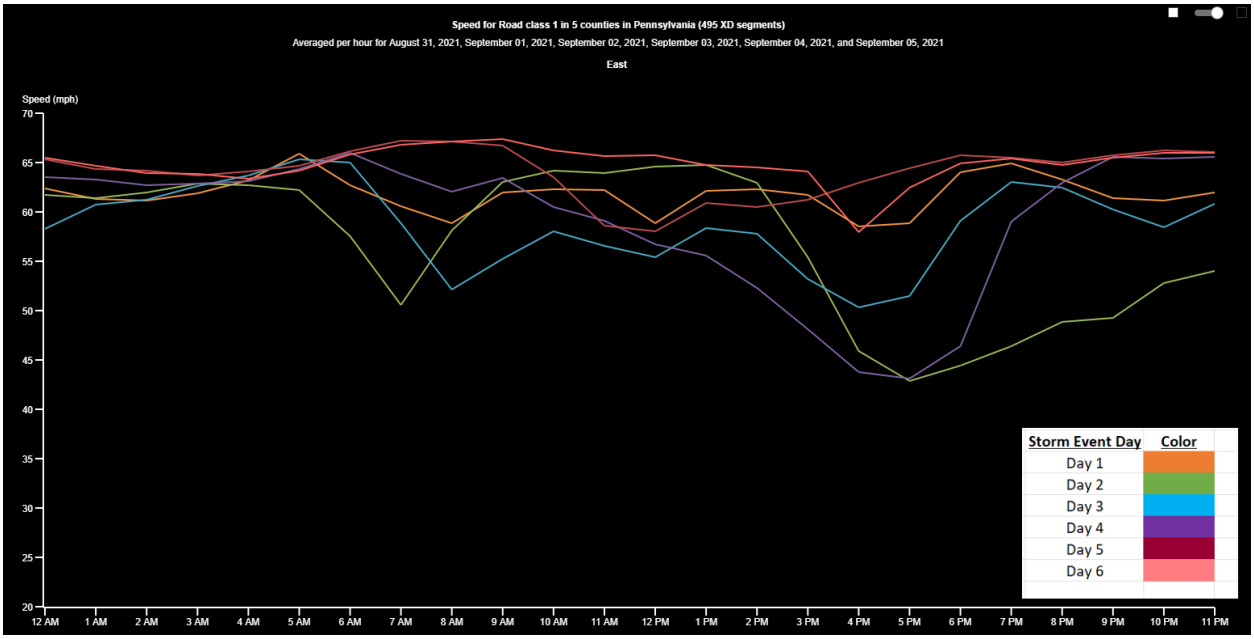

Ida FRC 2

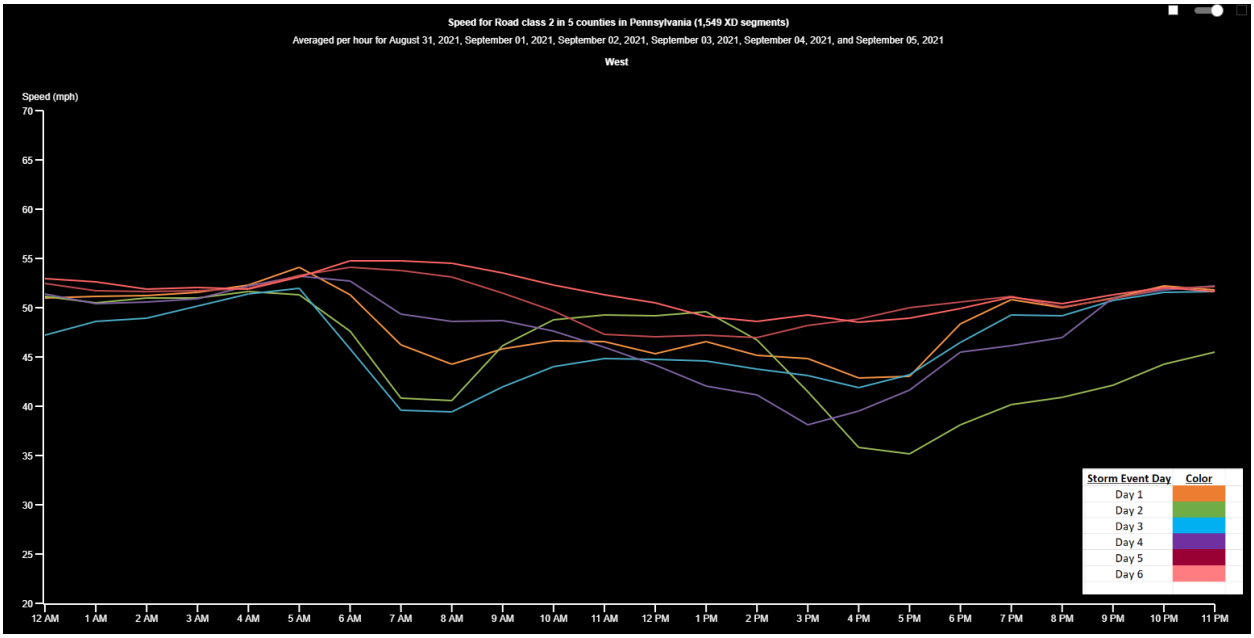

Ida FRC 3

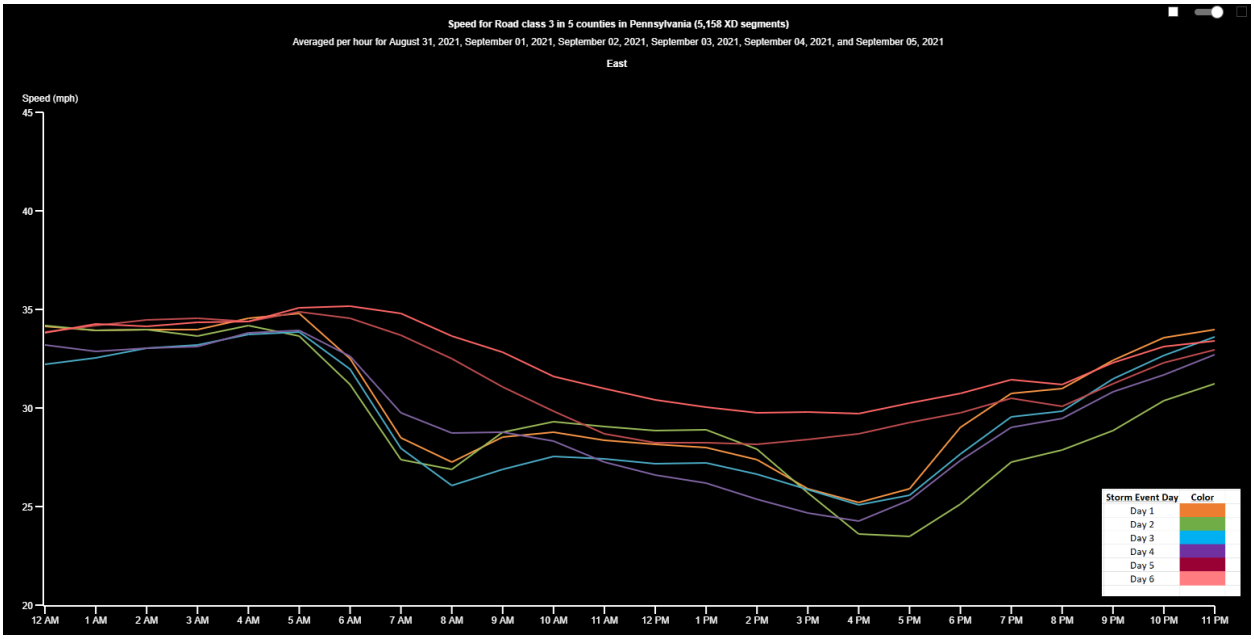

Ida FRC 4

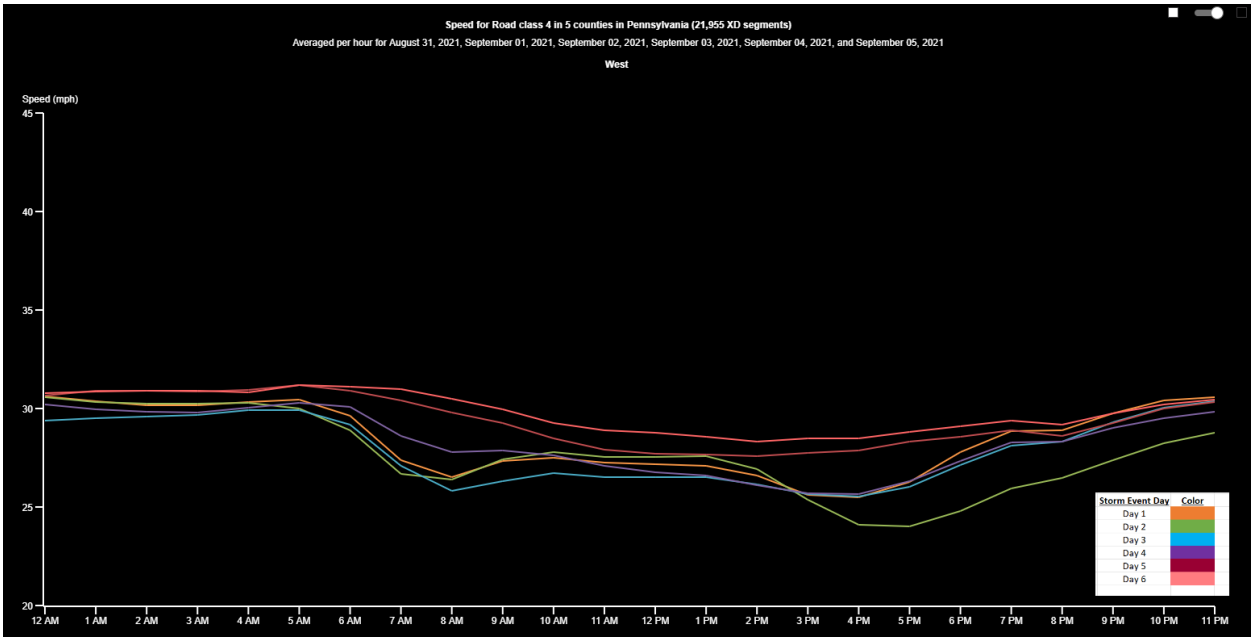

Ida FRC 5

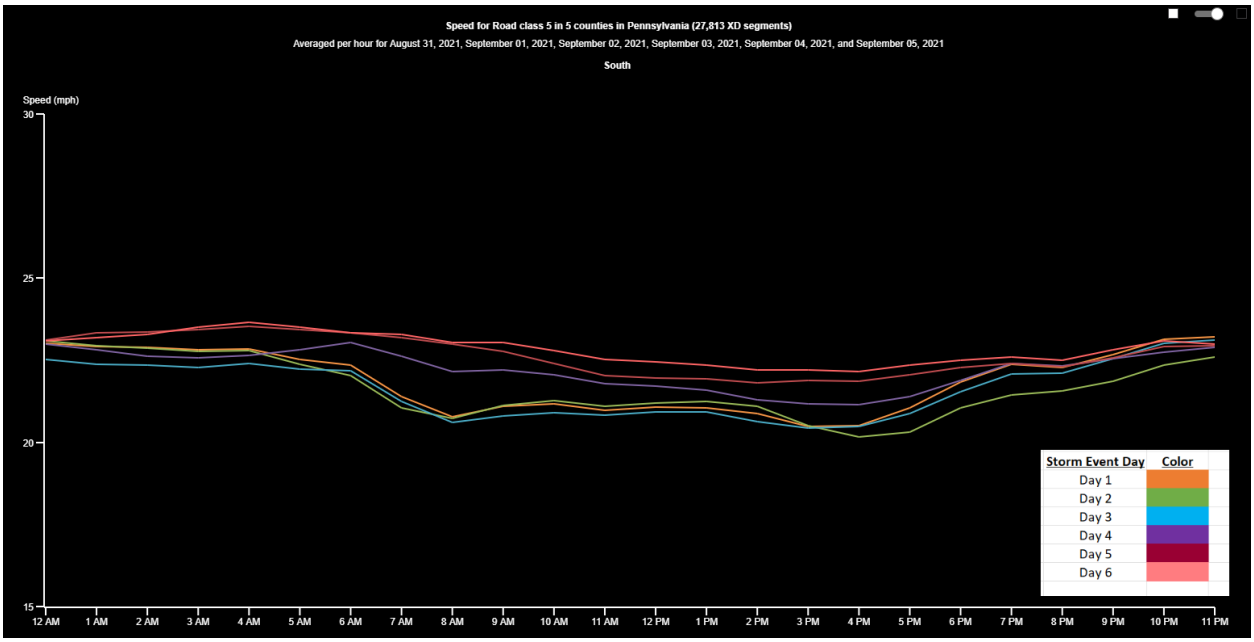

Speed vs. Time Graphs per Road Class

FRC 1

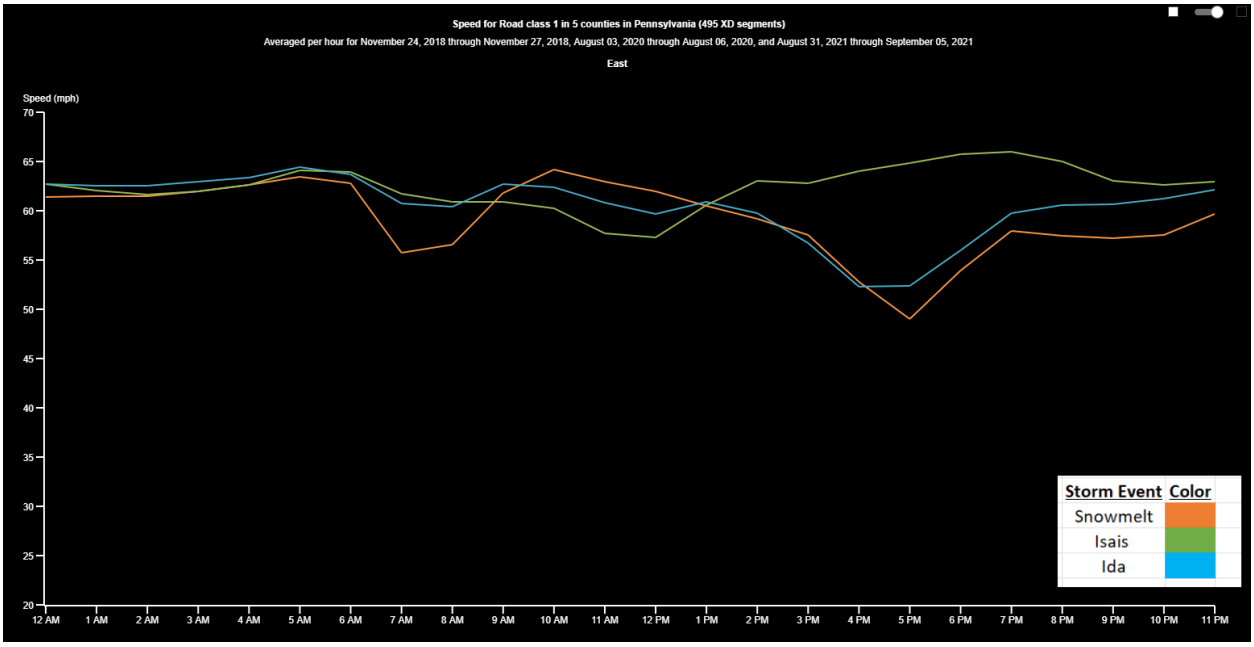

FRC 2

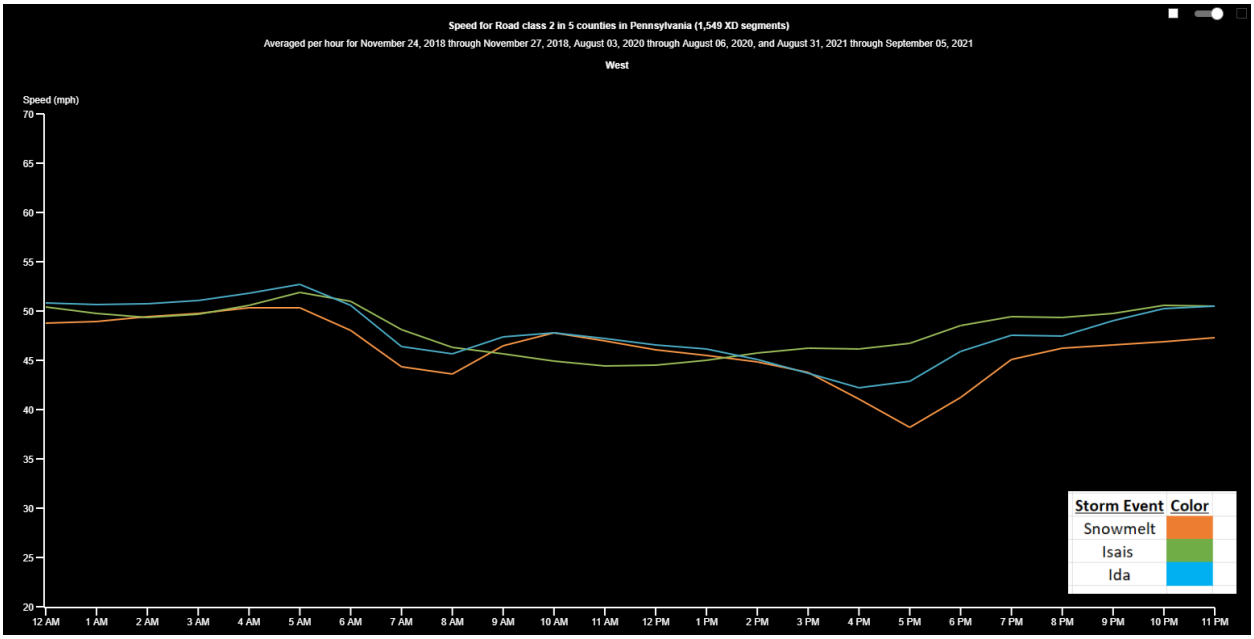

FRC 3

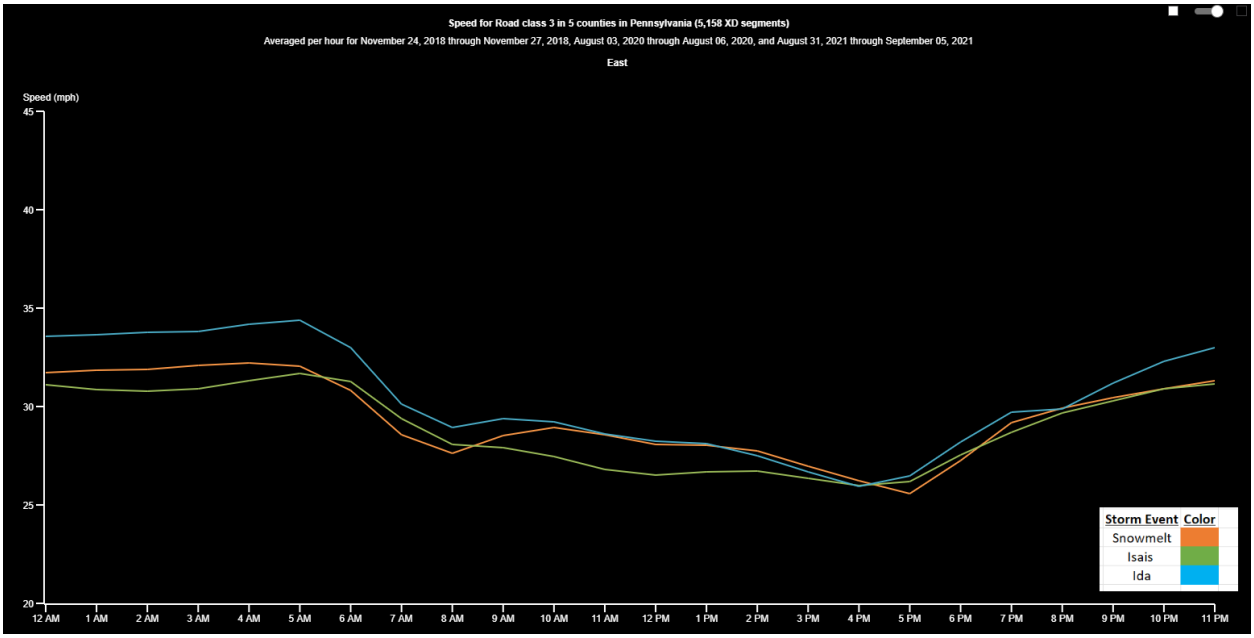
Speed for Road class 3 in 5 counties in Pennsylvania (5,158 XD segments)
Averaged per hour for November 24, 2018 through November 27, 2018, August 03, 2020 through August 06, 2020, and August 31, 2021 through September 05, 2021
East
Speed (mph)
45
40
35
30
25
20
12 AM
1 AM
2 AM
3 AM
4 AM
5 AM
6 AM
7 AM
8 AM
9 AM
10 AM
11 AM
12 PM
1 PM
2 PM
3 PM
4 PM
5 PM
6 PM
7 PM
8 PM
9 PM
10 PM
11 PM
Storm Event Color
Snowmelt
Isais
Ida

FRC 4

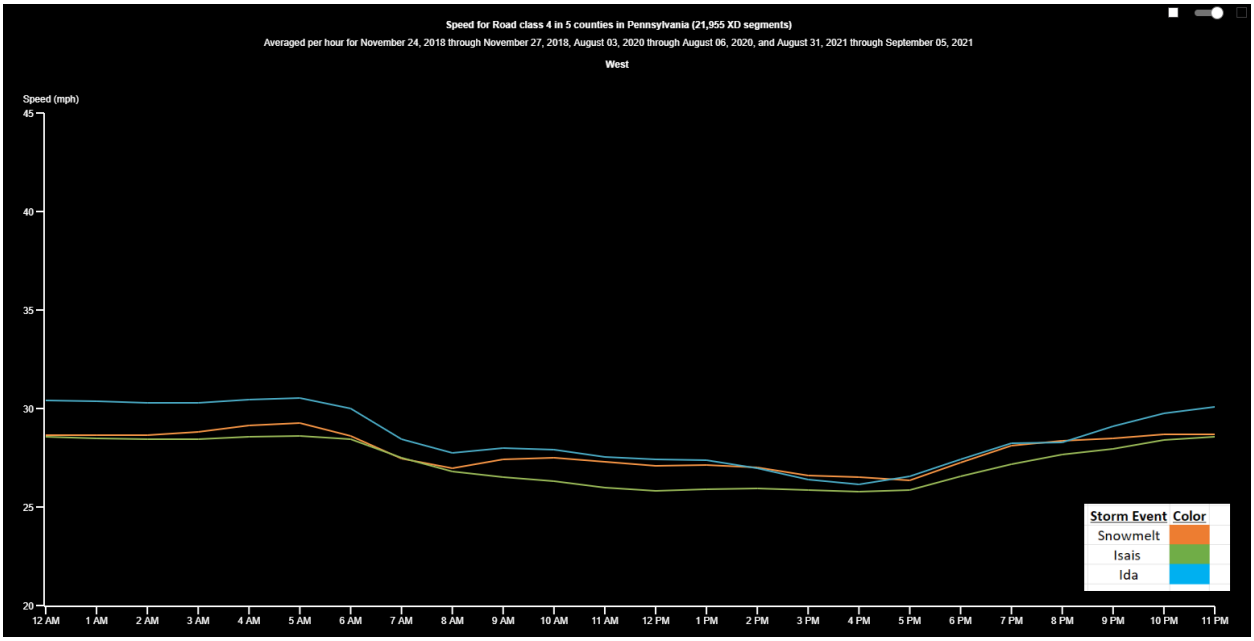
Speed for Road class 4 in 5 counties in Pennsylvania (21,955 XD segments)
Averaged per hour for November 24, 2018 through November 27, 2018, August 03, 2020 through August 06, 2020, and August 31, 2021 through September 05, 2021
West
Speed (mph)
45
40
35
30
25
20
12 AM
1 AM
2 AM
3 AM
4 AM
5 AM
6 AM
7 AM
8 AM
9 AM
10 AM
11 AM
12 PM
1 PM
2 PM
3 PM
4 PM
5 PM
6 PM
7 PM
8 PM
9 PM
10 PM
11 PM
Storm Event Color
Snowmelt
Isais
Ida

FRC 5

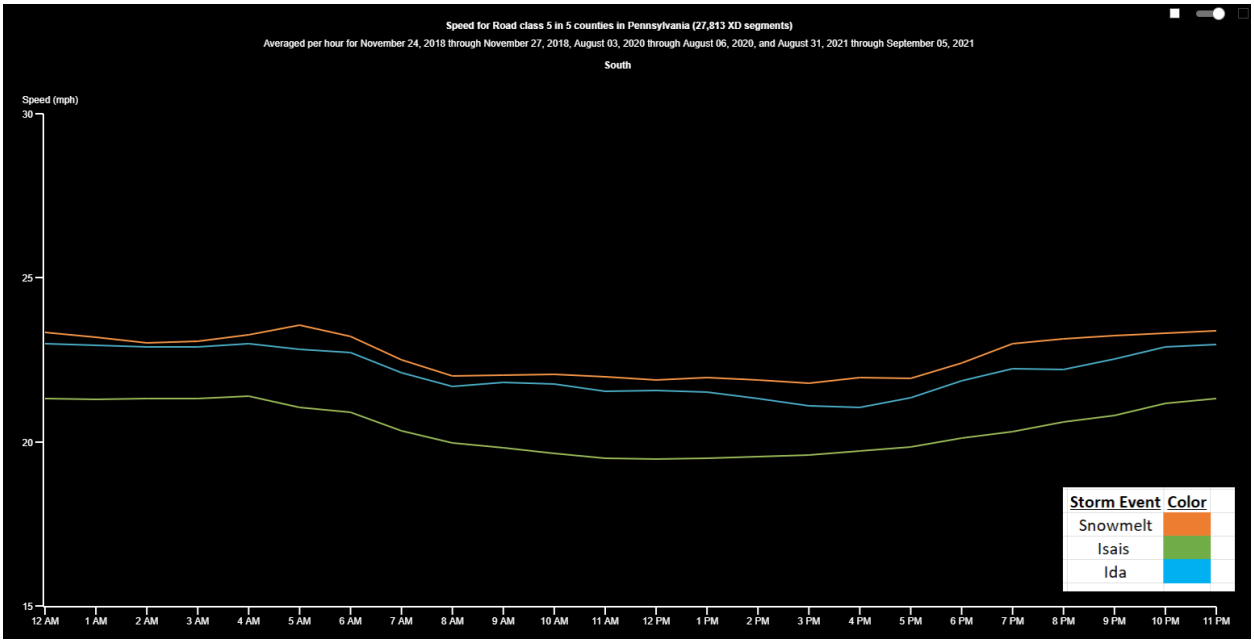
Speed for Road class 5 in 5 counties in Pennsylvania (27,813 XD segments)
Averaged per hour for November 24, 2018 through November 27, 2018, August 03, 2020 through August 06, 2020, and August 31, 2021 through September 05, 2021
South
Speed (mph)
30
25
20
15
12 AM
1 AM
2 AM
3 AM
4 AM
5 AM
6 AM
7 AM
8 AM
9 AM
10 AM
11 AM
12 PM
1 PM
2 PM
3 PM
4 PM
5 PM
6 PM
7 PM
8 PM
9 PM
10 PM
11 PM
Storm Event
Color
Snowmelt
Isais
Ida

Appendix D: SRF and CI Calculation Example

This document presents an example of SRF and CI estimation. Assume that an FRC 5 XD segment is examined during Hurricane Isaias. The following processes were considered for CI and SRF calculations.

Step 1. Collect all observed speed data points

Total observed speed data points: 384 points. The finest speed interval for FRC 5 is 15-minute as noted in Table 2.2. The storm event was 4-day long. Therefore, a total of 384 speed data points were extracted from RITIS (= 4 x 24 x 4). Of these 384 points, AM peak and PM peak had 48 points respectively while the remaining 288 points represent nonpeak hour period.

Step 2. SRF and CI assignment for each speed data point

When the CI and SRF distributions for this FRC 5 XD segment during AM peak are as below, then final CI and SRF for AM peak are calculated by weighing the percentage of each CI category frequency.

SRF Category (total of 3 categories)	1	2	3	
SRF Frequency	24	10	14	
CI category (total of 4 categories)	1	2	3	4
CI Frequency	14	14	12	8

Step 3. Final SRF and CI for each analysis period

Final SRF of AM Peak = [(24/48) x 1] + [(10/48) x 2] + [(14/48) x 3] = 1.8. Therefore SRF 1.8 is assigned for this XD segment during AM peak.

Final CI of AM Peak = [(14/48) x 1] + [(14/48) x 2] + [(12/48) x 3] + [(8/48) x 4] = 2.3. Therefore CI 2.3 is assigned for this XD segment during AM peak.

Step 4. Weighted Final SR and CI

If PM peak CI and non-peak period SRF are 1.7 and 2.2 respectively, the weighted final SRF for this XD segment is calculated as below:

Weighted Final SRF

= (40% weight x AM Peak SRF) + (40% weight x PM Peak SRF) + (20% weight x nonpeak SRF) = (0.4 x 1.8) + (0.4 x 1.7) + (0.2 x 2.2) = 1.8

If PM peak CI and non-peak period CI are 2.5 and 3.6 respectively, the weighted final CI for this XD segment is calculated as below:

Weighted Final CI

= (40% weight x AM Peak CI) + (40% weight x PM Peak CI) + (20% weight x nonpeak CI)

= (0.4 x 2.3) + (0.4 x 2.5) + (0.2 x 3.6) = 2.6

Appendix E: Regression Analysis Variable Definitions

Table 1. Detailed summary of the variables used in the regression analysis.

	Variable		Definition
Input Parameters (x_n)	x_1	Road Closures Occurrence	Defines if a bridge experienced a road closure throughout the duration of the event through binary, 1 – closure, 0 – no closure
	x_2	Bridge Age	The duration of time in years for when the bridge was constructed or reconstructed
	x_3	Scour Score*	A score is assigned to each bridge depending on if it was on PennDOT Scour list (the list is generated from inspections)
	x_4	FEMA Flood Zone Score*	A score is assigned to each bridge depending on its relative location in the FEMA Flood Hazard Map
	x_5	Upstream Drainage Area	The upstream drainage area of the stream that intersects the bridge in square miles
	x_6	Weighted Average of Percent Impervious Area	The weighted average of percent impervious area in the upstream drainage area of the bridge.
	x_7	Number of Flood Control Structures in Upstream Drainage Area*	The number of flood control structures in the upstream drainage area. This data is obtained from FEMA. The type of structures that fall within control structures are listed in the additional detail section.
	x_8	Number of Flood Obstruction Structures in Upstream Drainage Area*	The number of flood obstruction structures in the upstream drainage area. This data is obtained from FEMA. The type of structures that fall within obstruction structures are listed in the additional detail section.
	x_9	Average Slope of Drainage Area	The average slope of the upstream drainage area of the bridges in the units of percent rise.
	x_{10}	Percent Change in Land Cover	The number of 30 m by 30 m cells that changed within the upstream drainage area of the bridges from 2016-2019.

*See for additional information.

Scour Score:

Table 2. Scour grades reclass values.

Scour Category	Reclass Value
A	1
B	0.67
C	0.33
D/ Not included on list	0

Category A: Inspect all bridges for flood damage where a significant flooding event was experienced. Bridges in this category that have been closed due to approach roadway or bridge overtopping or pressure flow must be inspected for flood damage before reopening to traffic. Inspect once every 4 hours.
Category B and C: Inspect all bridges for flood damage where a significant flooding event was experienced or if the bridge has been closed due to either approach roadway or bridge overtopping or pressure flow must be inspected for flood damage before reopening to traffic. B - Inspect once every 12 hours. C - Inspect once every 24 hours
Category D: Inspect for flood damage after each significant flooding event or if the bridge has been closed due to overtopping or pressure flow.

FEMA Flood Score:

Table 3. FEMA Flood Zone reclass values.

Flood Zone	Reclass Value
Floodway	1
1% annual chance flood hazard	0.67
0.2% annual chance flood hazard	0.33
Area of minimal flood hazard	0

Number of Flood Control Structures in Upstream Drainage:

Table 4. Types of flood control structures:

Flood Control Structures
0.2 PCT Annual Chance Flood Discharge Contained in Structure
1 PCT Annual Chance Flood Discharge Contained in Structure
Control Structure
Dam
Floodway Contained in Structure
Weir

Number of Flood Obstruction Structures in Upstream Drainage Area:

Table 3. Types of flood obstruction structures:

Flood Obstruction Structures
Obstruction
Canal
Channel
Culvert
Side Weir Structure
Wing Wall

Appendix F: XD Segment Information and Bridge Closure Spatial Analysis

Detailed Procedure for Geoprocessing INRIX XD Segment Information and Road Closures Due to Flooding Data.

1. Open the INRIX XD Segment data for each event in Excel. There are two tables per event that include a congestion interval and speed reduction factor.
2. Use the Pivot Table Tool to average the CI and SRF values across the x number of days for each weather event.
    a. There are 4 days of data for the Snowmelt Event.
    b. There are 4 days of data for Hurricane Isaias.
    c. There are 6 days of data for Hurricane Ida.
3. Import the summarized XD Segment data for each event and each congestion level.
4. Use the XY to Line Tool to create a polyline feature of the segments.
    a. Using the start longitude, start latitude, end longitude, and end latitude using the GCS WGS 1984.
5. Use the Project Tool to project the INRIX Segments polyline feature to the project PCS, NAD 1983 StatePlane Pennsylvania South FIPS 3702 (US Feet).
6. Import the PennDOT District 6 Bridges point feature from Task 1 into the project.
    a. The bridges included in the analysis are of the bridges that intersect the NHD Flowlines.
    b. The bridges shapefile included all variables used in the analysis in Task 1.
7. Use the Spatial Join Tool to add the INRIX Segment data to the PennDOT District 6 Bridges point feature.
    a. The columns that are included in the join are the Total_CI/Total_SRF and Functional Road Classes.
    b. The closest segment within 100 meters is joined to the bridges.
8. Import the PennDOT District 6 Road Closures due to Flooding point and polyline features from Task 1 into the project.
    a. Create 3 features selecting the road closures that took place during the duration of each weather event.
9. Use the Spatial Join Tool to determine if there is a recorded PennDOT District 6 Road Closures due to Flooding (point or polyline feature) at each bridge.
    a. A search of 50 feet is used to account for spatial tolerance in the coordinates.
    b. A binary classification is used to identify if a bridge closure occurred.
        i. 1 – a road closure happened during the event
        ii. 0 – a road closure did not happen during the event
10. Use the Table to Excel Tool to export the table from the bridge's shapefile with the joined data from INRIX XD Segments data and PennDOT District 6 Road Closures data.
    a. The regression analysis is completed using the table produced in this step.

Appendix G: Crash Data Spatial Analysis

Detailed Procedure for Geoprocessing Crash Data.

1. Import PennDOT District 6 Crash Data into ArcGIS Pro for the following events:
    a. Snowmelt Event: 11/24/2018 – 11/27/2018
    b. Hurricane Isaias: 8/3/2022 – 8/6/2022
2. Clean and tidy the tables, leaving only the columns focused on in the analysis.
    a. The columns used in this analysis include:
        i. CRN
        ii. CRASH_DATE
        iii. DEC_LAT
        iv. DEC_LONG
        v. COLLISION_TYPE
        vi. MAX_SEVERITY_LEVEL
3. Use the XY to Point Tool to display the crashes as a point feature using the DEC_LAT and DEC_LONG columns with a GCS of WGS 1984.
4. Use the Project Tool to project the point features to the project PCS, NAD 1983 StatePlane Pennsylvania South FIPS 3702 (US Feet).
5. Use the Calculate Field Tool to reclass the data within the following columns using the PennDOT Crash Data Dictionary:
    a. COLLISION_TYPE
        i. 0 – Non-collision
        ii. 1 – Rear-end
        iii. 2 – Head-on
        iv. 3 – Backing
        v. 4 – Angle
        vi. 5 – Sideswipe (same dir.)
        vii. 6 – Sideswipe (Opposite dir.)
        viii. 7 – Hit fixed object
        ix. 8 – Hit pedestrian
        x. 9 – Undefined
        xi. 98 – Other
        xii. 99 - Unknown
    b. MAX_SEVERITY_LEVEL (a value is assigned depending on severity of injury)
        i. 0 - Not injured (severity value 1)
        ii. 1 – Killed (severity value 4)
        iii. 2 – Suspected Serious injury (severity value 3)
        iv. 3 – Suspected Minor injury (severity value 2)
        v. 4 – Possible Injury (severity value 2)
        vi. 8 - Injury/ Unknown Severity (severity value 2)
        vii. 9 - Unknown if Injured (severity value 1)
6. A map is created displaying the distribution of crashes and bridge closures for each event.
    a. The color of the shape specifies the collision type.
    b. The size of the shape specifies the severity of the collision.

Appendix H: Maps from Analysis

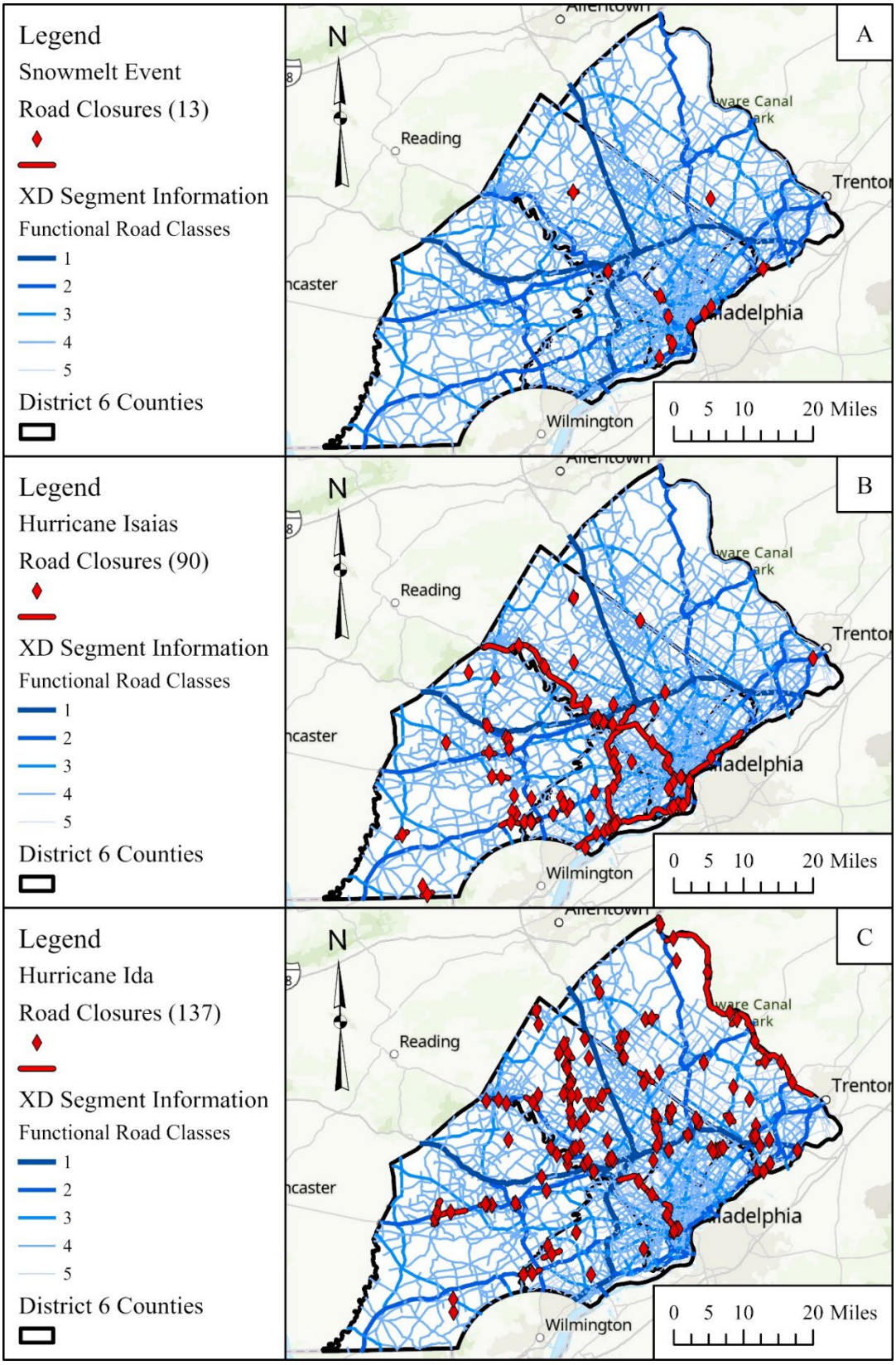

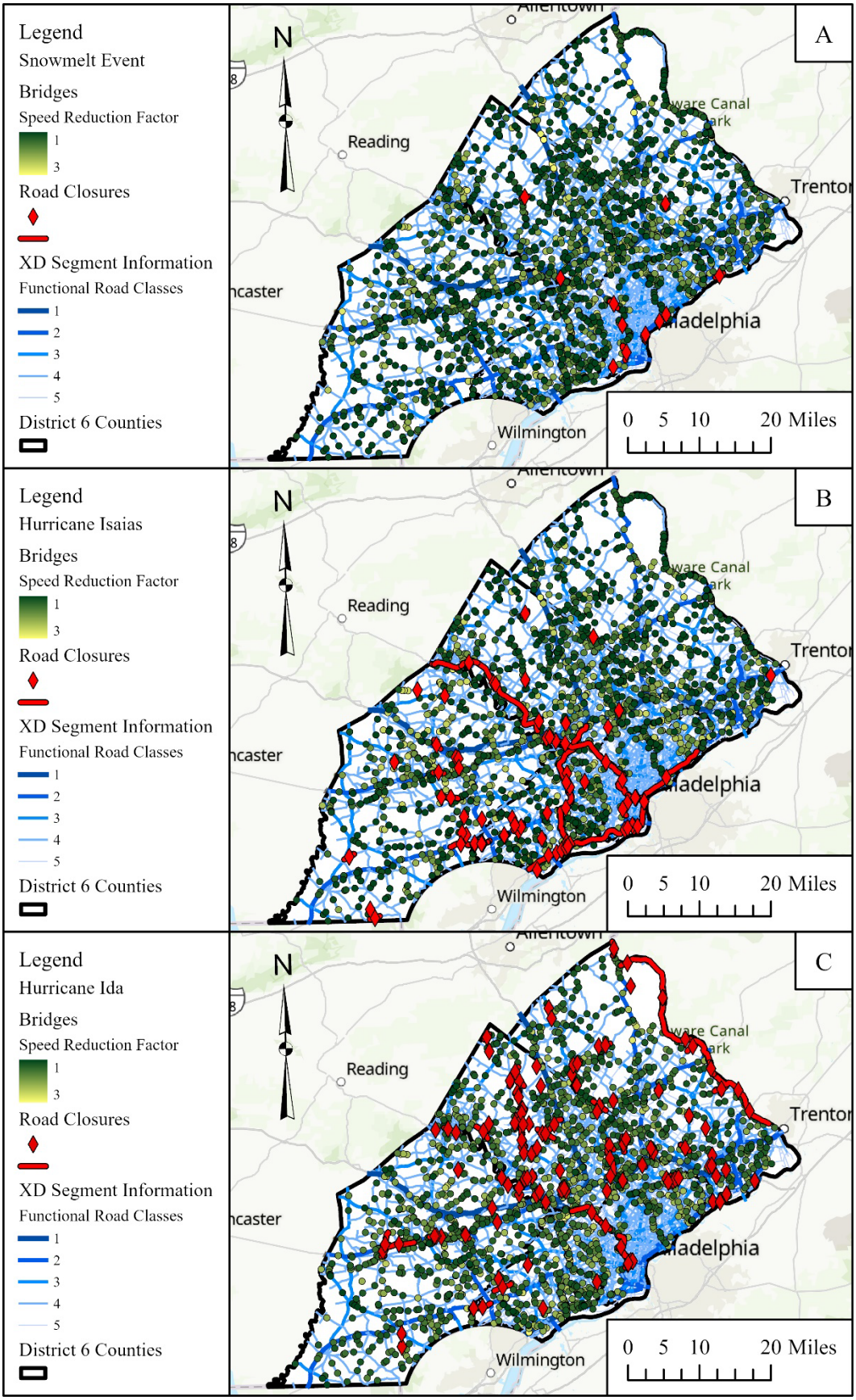
Legend
Snowmelt Event
Bridges
Speed Reduction Factor
1
3
Road Closures
XD Segment Information
Functional Road Classes
1
2
3
4
5
District 6 Counties
N
A
Reading
Trenton
Wilmington
0 5 10 20 Miles
Legend
Hurricane Isaias
Bridges
Speed Reduction Factor
1
3
Road Closures
XD Segment Information
Functional Road Classes
1
2
3
4
5
District 6 Counties
N
B
Reading
Trenton
Wilmington
0 5 10 20 Miles
Legend
Hurricane Ida
Bridges
Speed Reduction Factor
1
3
Road Closures
XD Segment Information
Functional Road Classes
1
2
3
4
5
District 6 Counties
N
C
Reading
Trenton
Wilmington
0 5 10 20 Miles

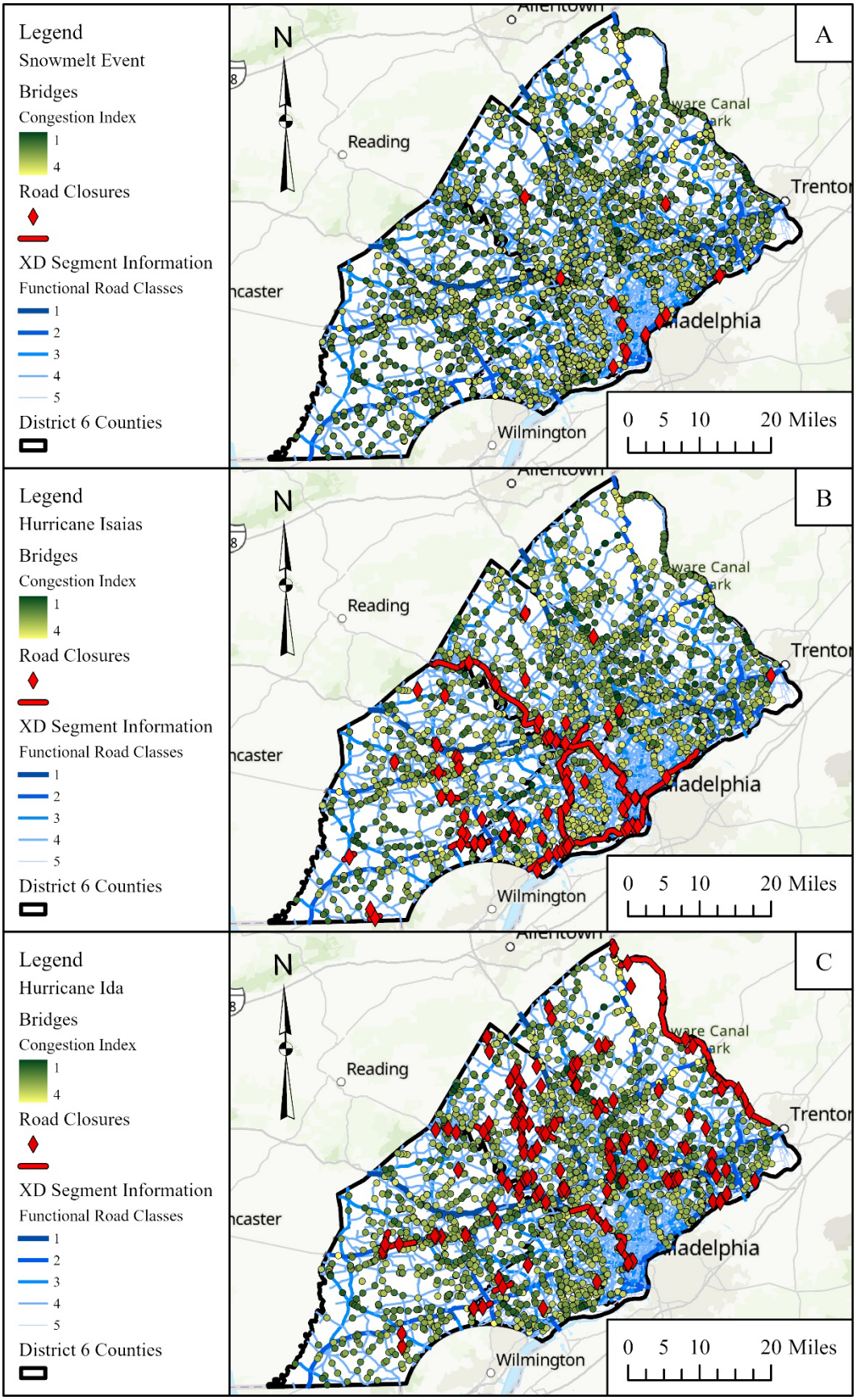
Legend
Snowmelt Event
Bridges
Congestion Index
1
4
Road Closures
XD Segment Information
Functional Road Classes
1
2
3
4
5
District 6 Counties
N
A
Reading
Wilmington
0 5 10 20 Miles
Legend
Hurricane Isaias
Bridges
Congestion Index
1
4
Road Closures
XD Segment Information
Functional Road Classes
1
2
3
4
5
District 6 Counties
N
B
Reading
Wilmington
0 5 10 20 Miles
Legend
Hurricane Ida
Bridges
Congestion Index
1
4
Road Closures
XD Segment Information
Functional Road Classes
1
2
3
4
5
District 6 Counties
N
C
Reading
Wilmington
0 5 10 20 Miles

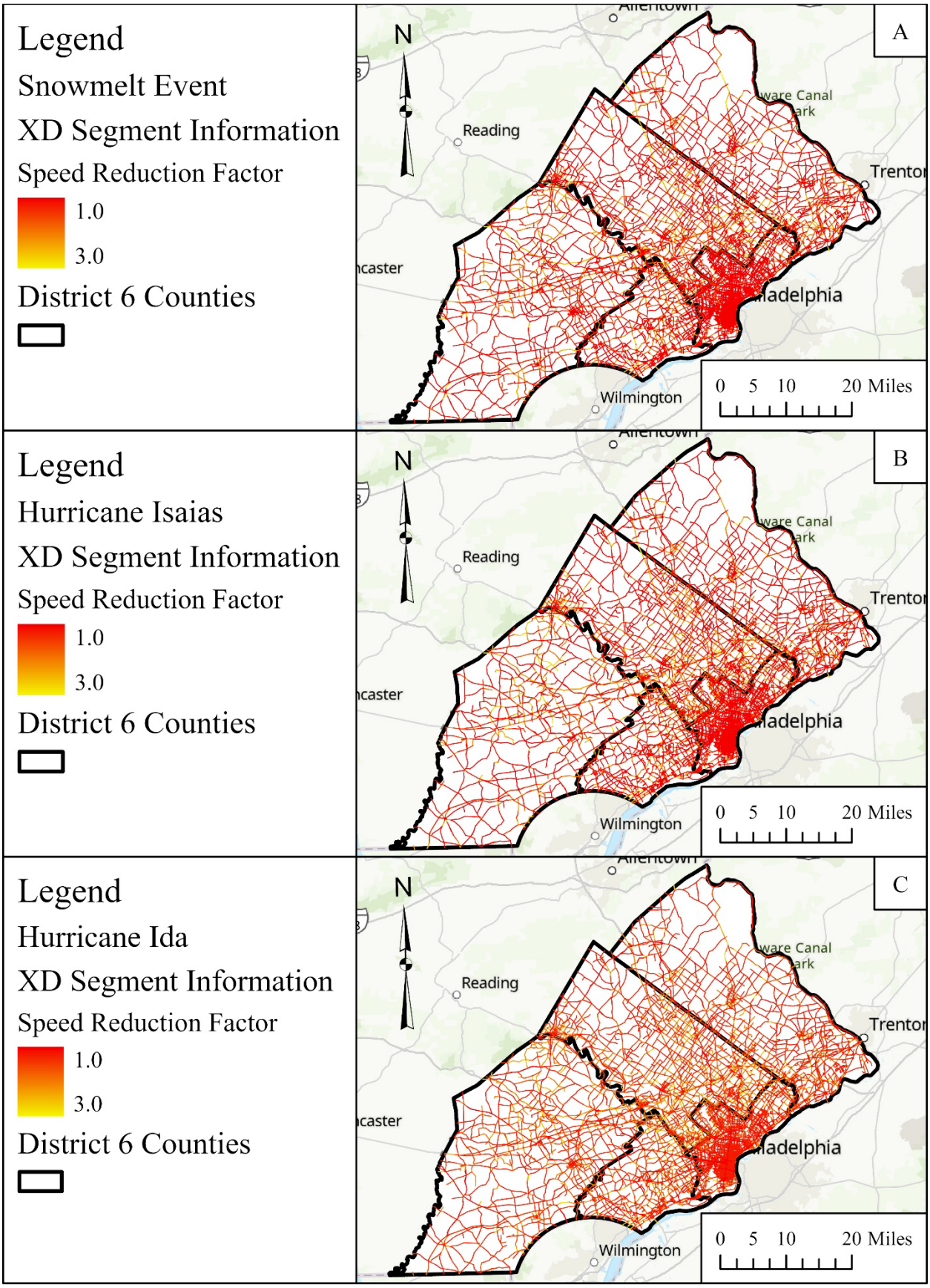
Legend
Snowmelt Event
XD Segment Information
Speed Reduction Factor
1.0
3.0
District 6 Counties
N
Reading
Wilmington
A
0 5 10 20 Miles
Legend
Hurricane Isaias
XD Segment Information
Speed Reduction Factor
1.0
3.0
District 6 Counties
N
Reading
Wilmington
B
0 5 10 20 Miles
Legend
Hurricane Ida
XD Segment Information
Speed Reduction Factor
1.0
3.0
District 6 Counties
N
Reading
Wilmington
C
0 5 10 20 Miles

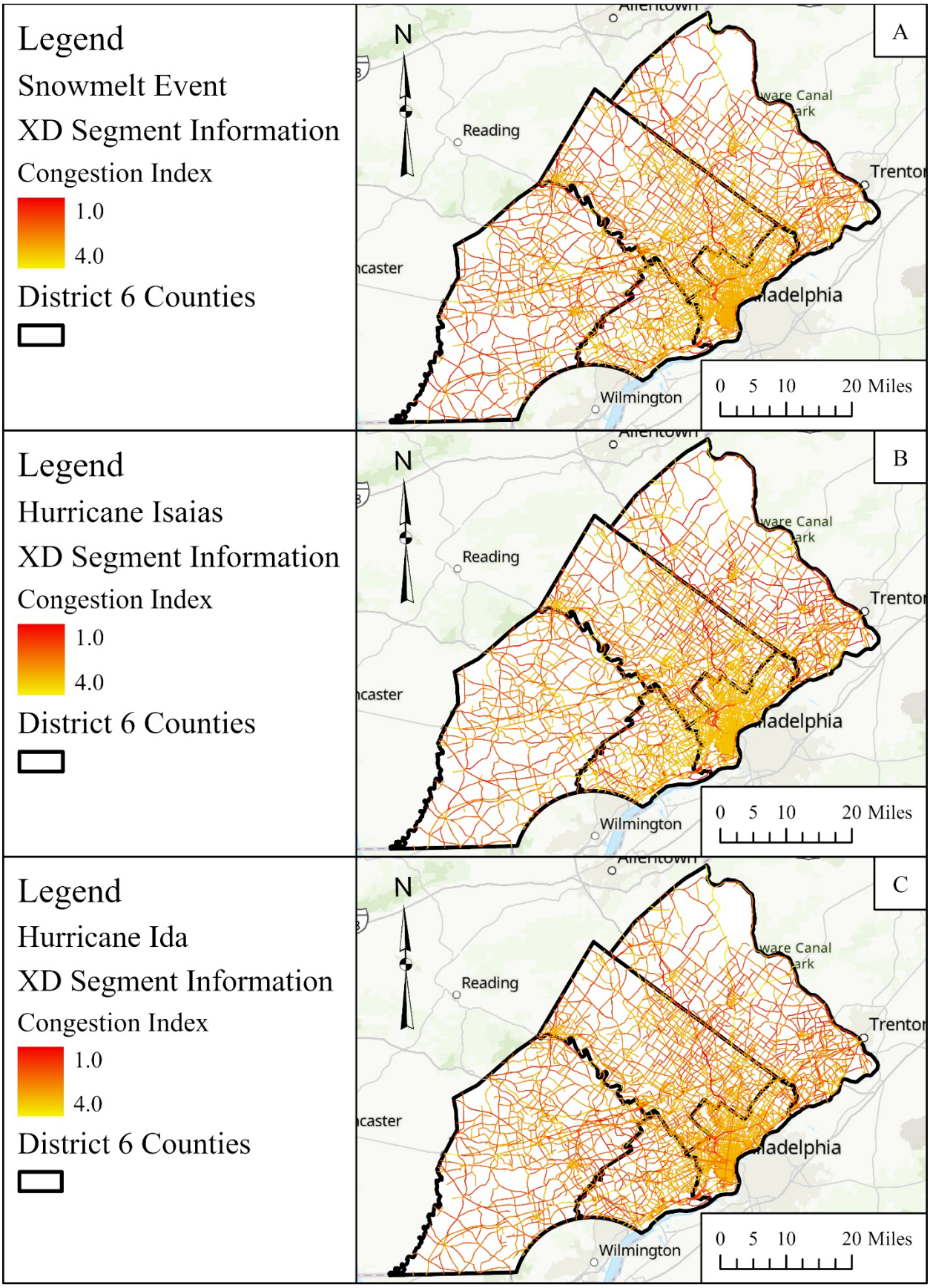
Legend
Snowmelt Event
XD Segment Information
Congestion Index
1.0
4.0
District 6 Counties
N
Reading
Wilmington
A
0 5 10 20 Miles
Legend
Hurricane Isaias
XD Segment Information
Congestion Index
1.0
4.0
District 6 Counties
N
Reading
Wilmington
B
0 5 10 20 Miles
Legend
Hurricane Ida
XD Segment Information
Congestion Index
1.0
4.0
District 6 Counties
N
Reading
Wilmington
C
0 5 10 20 Miles

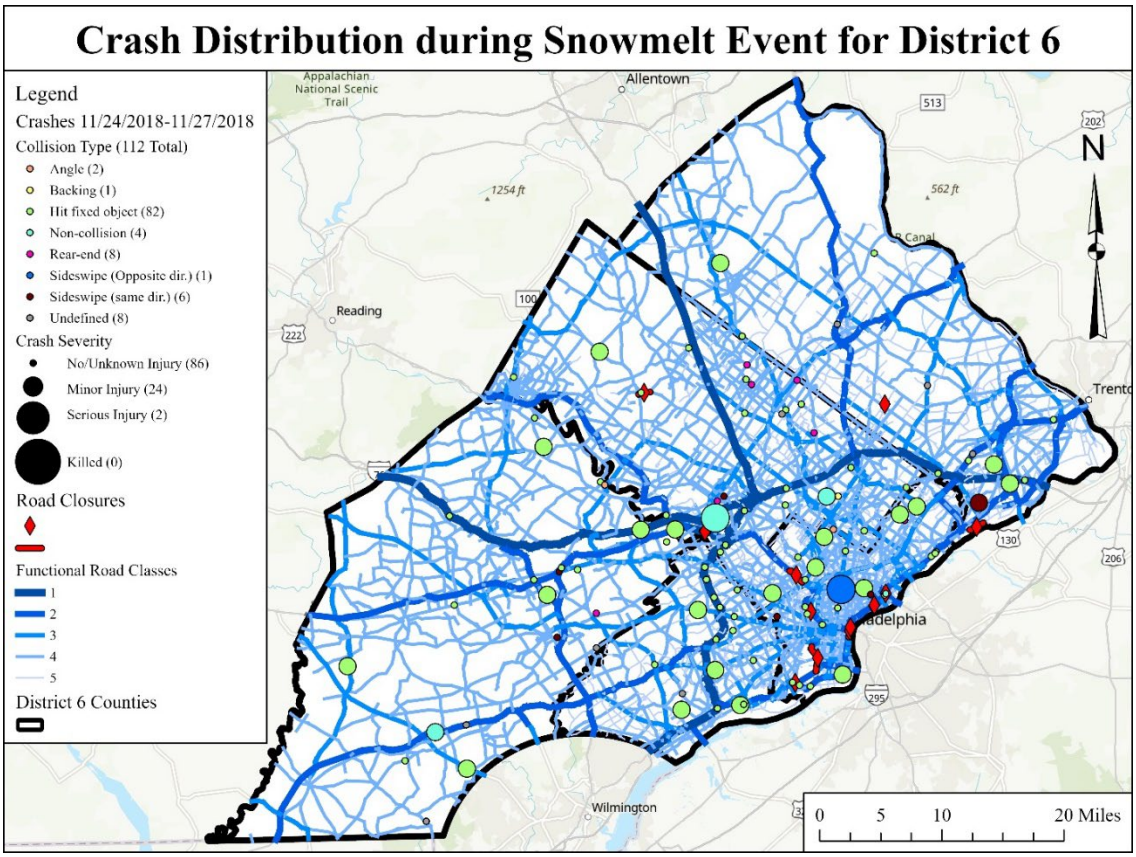
Crash Distribution during Snowmelt Event for District 6
Legend
Crashes 11/24/2018-11/27/2018
Collision Type (112 Total)
Angle (2)
Backing (1)
Hit fixed object (82)
Non-collision (4)
Rear-end (8)
Sideswipe (Opposite dir.) (1)
Sideswipe (same dir.) (6)
Undefined (8)
Crash Severity
No/Unknown Injury (86)
Minor Injury (24)
Serious Injury (2)
Killed (0)
Road Closures
Functional Road Classes
1
2
3
4
5
District 6 Counties
Appalachian National Scenic Trail
Allentown
Reading
Wilmington
1254 ft
562 ft
N
0 5 10 20 Miles

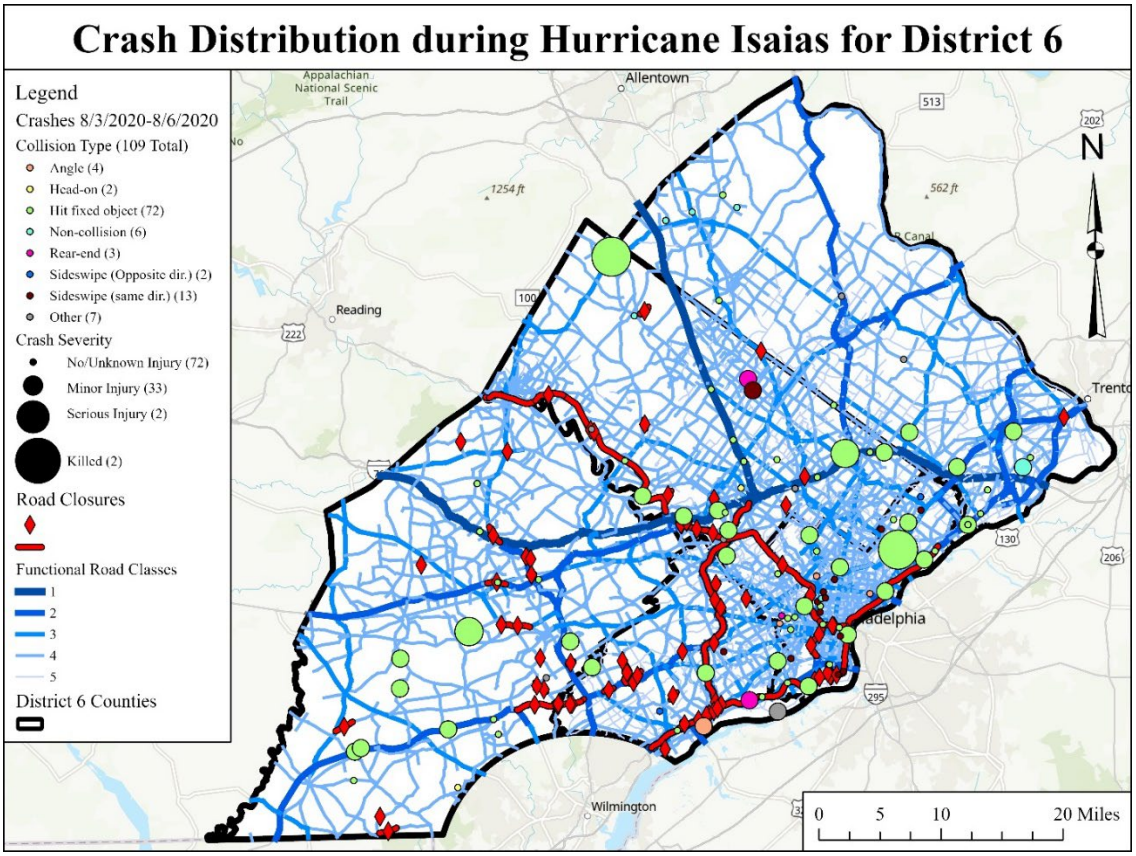
Crash Distribution during Hurricane Isaias for District 6
Legend
Crashes 8/3/2020-8/6/2020
Collision Type (109 Total)
Angle (4)
Head-on (2)
Hit fixed object (72)
Non-collision (6)
Rear-end (3)
Sideswipe (Opposite dir.) (2)
Sideswipe (same dir.) (13)
Other (7)
Crash Severity
No/Unknown Injury (72)
Minor Injury (33)
Serious Injury (2)
Killed (2)
Road Closures
Functional Road Classes
1
2
3
4
5
District 6 Counties
Appalachian National Scenic Trail
Allentown
Reading
Wilmington
1254 ft
562 ft
N
0 5 10 20 Miles

Task 4 Report

This task summarizes an Implementation Plan and a roadmap to guide the implementation that provides detail on the broader use of the results of this project. This roadmap aligns Table 2.2 from Task 3 with the outcomes of each Task within the report to delineate how the results of each task could be applied to existing PennDOT programs for implementation.

Table 1: A roadmap for implementation to PennDOT programs.

Report Outcome	Potential Avenue for Implementation
Task 1a: Created a baseline of analysis techniques used in the field through an extensive review of the literature of DOT flood management processes across the U.S..	The PennDOT PAMS program would benefit from the application of Task 1a by comparing current practices and developments across the US.
Task 1b: A holistic spatial analysis based on flood inundation data to identify flood inundation-prone locations within PennDOT District 6.	The data collected and integrated in this section of the report can be used by PAMS to identify past areas of concern regarding flooding. Additionally, the PA Flood Risk Map would benefit from the analysis of features contributing to flooding and roadway closure.
Task 2a: A literature review of drone systems, multispectral cameras, and Lidar is presented.	The PennDOT PAMS program would benefit from the application of Task 2a by comparing current practices and applications of drones, cameras, and lidar for asset management for flooding. This may also be beneficial for the BAMS program.
Task 2b: An overview of workflow practices for drone flights is provided, with a simple guide which can be applied to any type of drone survey.	The PennDOT PAMS program would benefit from the application of various sensors, as described in the Task 2b report, will contribute an accurate pavement inspection. TSMO and Emergency Planning would also benefit from being able to identifying attributes when making decisions concerning bridge and roadway closure.
Task 1c and 3a: Spatial network analysis to assess the impact of flood inundation from a network safety and network flow perspective.	BAMS and PAMS could benefit from the findings of these studies to help identify bridges at risk of closure in District 6. Further, this study identifies features that often lead to bridge closures which may help identify problems early. And, by linking the bridge closures to congestions and speed reduction values we can identify the bridges that are the highest risk for the network.
Task 3b: Prioritizing areas of risk based on the network analysis.	PAMS Considering that roadway congestion and inundation degree are major factors in pavement deterioration, information from Task 3a and 3b, about the congestion level per FRC, can provide further

	insights in estimating the impact of high stream flow events on pavement performance, potentially aiding the PAMS program. TAMPS Task 3b findings can assist better identify congestion prone locations within District 6, potentially aiding the TAMPS program. Also, since the land surface is dynamics hydrologic drivers can ultimately help develop an informed resiliency rating of transportation system.
Task 3c: Work with PennDOT to identify task priority locations, priority issues, and focuses for recommendations in a final report, aligning with PennDOT's Asset Management Initiatives.	The findings of this study will help identify bridges at risk of closure in District 6, aiding the BAMS. Further, this study identifies features that often lead to bridge closures which may help identify problems early. And, by linking the bridge closures to congestions and speed reduction values we can identify the bridges that are the highest risk for the network. The findings have applications for the PennDOT Local Technical Assistance Program as these results could provide useful information about the roadways and bridges (and their features) that are prone to the closure for a better understanding and preparation of the flood impacts. In addition, by gaining a better understanding of the storm impacts on roadways, a proactive maintenance scheduling and evaluation system of roadway condition for resiliency can be established. Furthermore, local agency engineers can develop easy tracking system to record flooding hot spots integrated with the safety data. PennDOT Extreme Weather Vulnerability Study can further complement the vulnerability study by providing other FRC information as well as roadway closure relevant environmental attributes. With the review of three different severe high stream flow events and its impacts on network, specific linkages between the hydrologic features driving bridge closures and network congestion the study findings. This can provide further helpful insight understanding of the potential impacts of weather. TSMO By identifying closure prone bridge locations through this study has to potential to aide TSMO to better prepare and plan for future severe high stream flow events. Additionally, the bridges likely to be repetitively impaired may be in danger of scour. These results also provide insight to congestion level at different roadway categories, which will be useful for developing informed and efficient detour routes. Furthermore, in the event of evacuation due to the severe high stream flow events, this study findings provide critical information that could integrate adjustability toward optimal evacuation routes. The findings of this report also aide in identifying bridges for consideration by Local Scour Critical Bridges. The bridges identified experience high flows and are at a greater risk of scour or damaged due to repetitive inundation. By identifying closure prone bridge locations through this study will help better be prepared for future severe high stream flow events.